UNIVERSIDAD DE SALAMANCA

PROGRAMA DE DOCTORADO FORMACIÓN EN LA SOCIEDAD DEL CONOCIMIENTO

VNiVERSiDAD D SALAMANCA

CAMPUS DE EXCELENCIA INTERNACIONAL

DESARROLLO DE NUEVAS FÉRULAS DE INMOVILIZACIÓN SENSORIZADAS, PARA LA GENERACIÓN DE INFORMACIÓN CLÍNICA

TESIS DOCTORAL PRESENTADA POR

José María de Agustín del Burgo

BAJO LA DIRECCIÓN DE LOS DOCTORES:

Juan Antonio Juanes Méndez

Fernando Blaya Haro

Salamanca, España 2021

PROGRAMA DE DOCTORADO FORMACIÓN EN LA SOCIEDAD DEL CONOCIMIENTO

VNiVERSiDAD D SALAMANCA
CAMPUS DE EXCELENCIA INTERNACIONAL

TESIS DOCTORAL

DESARROLLO DE NUEVAS FÉRULAS DE INMOVILIZACIÓN SENSORIZADAS, PARA LA GENERACIÓN DE INFORMACIÓN CLÍNICA

Autor:

José María de Agustín del Burgo

Salamanca, España

2021

JOSÉ MARÍA DE AGUSTÍN DEL BURGO

D. JUAN ANTONIO JUANES MÉNDEZ, DOCTOR EN MEDICINA Y CIRUGÍA, PROFESOR DEL DEPARTAMENTO DE ANATOMÍA E HISTOLOGÍA HUMANAS DE LA UNIVERSIDAD DE SALAMANCA y **D. FERNANDO BLAYA HARO,** DOCTOR POR LA UNIVERSIDAD AUTÓNOMA DE MADRID EN EL PROGRAMA MEDICINA Y CIRURGÍA, Y PROFESOR DE LA UNIVERSIDAD POLITÉCNICA DE MADRID.

CERTIFICAMOS:

Que el trabajo titulado "DESARROLLO DE NUEVAS FÉRULAS DE INMOVILIZACIÓN SENSORIZADAS, PARA LA GENERACIÓN DE INFORMACIÓN CLÍNICA" ha sido realizado por. D *José María de Agustín del Burgo,* bajo nuestra dirección; reuniendo, a nuestro juicio, los requisitos y méritos suficientes para que la autora de este pueda optar al Grado de Doctor por la Universidad de Salamanca.

Y para que así conste, firmamos la presente certificación en Salamanca a trece de septiembre de dos mil veintiuno.

Fdo.: Juan Antonio Juanes Méndez

Fdo.: Fernando Blaya Haro

JOSÉ MARÍA DE AGUSTÍN DEL BURGO

JOSÉ MARÍA DE AGUSTÍN DEL BURGO

DECLARACIÓN DE AUTORÍA

Declaro que he redactado el trabajo titulado: "DESARROLLO DE NUEVAS FÉRULAS DE INMOVILIZACIÓN SENSORIZADAS, PARA LA GENERACIÓN DE INFORMACIÓN CLÍNICA" para la obtención del Grado de Doctor por la Universidad de Salamanca. Ha sido realizado, de forma autónoma, con la ayuda de mis directores, siguiendo las directrices del artículo 14.1 en su capítulo II del Reglamento de Doctorado de la Universidad de Salamanca, sobre la elaboración y defensa de la Tesis Doctoral.

Los resultados de este trabajo han sido publicados en diferentes revistas a nivel internacional, con un nivel de impacto del primer cuartil.

En Salamanca, 13 de septiembre de dos mil veintiuno.

Fdo.: José María de Agustín del Burgo

JOSÉ MARÍA DE AGUSTÍN DEL BURGO

JOSÉ MARÍA DE AGUSTÍN DEL BURGO

AGRADECIMIENTOS

Quiero expresar mi más sincero agradecimiento a mis tutores D. Juan Antonio Juanes Méndez y a D. Fernando Blaya Haro, por su aceptación en la dirección de esta Tesis Doctoral, seguimiento, y las facilidades prestadas en todo el transcurso de este trabajo. Sin su gran esfuerzo y acierto en la ejecución de este proyecto de Tesis Doctoral este trabajo no hubiera sido posible. También al profesor Roberto D'Amato, quien me ha aconsejado y ayudado durante todo el proceso.

Especial mención y agradecimiento al Departamento de Ingeniería Mecánica y Química y Diseño Industrial, de la Universidad Politécnica de Madrid, y a D. Fernando Blaya por brindarme todos los recursos y herramientas que fueron necesarios para llevar a cabo el proceso de investigación, y haberme aconsejado y ayudado desde que terminé mis estudios como Ingeniero Técnico Industrial. No hubiese podido alcanzar estos resultados de no haber sido por su incondicional ayuda.

Quiero agradecer igualmente a todos aquellos que en los momentos de desaliento han estado acompañándome en todo el proceso de trabajo de este trabajo. En especial, quiero mencionar a mi hermana y a mis padres, que siempre me apoyaron a conseguir mis objetivos, y que con su trabajo y esfuerzo han hecho posible que me forme desde pequeño y llegue hasta este día de presentación de mi propia Tesis Doctoral. También a mi pareja, que me ha apoyado y ayudado a invertir todo mi esfuerzo y tiempo en lograr este objetivo.

A todos mis amigos que, de alguna manera, me alentaron y se interesaron para que esta Tesis fuera terminada.

A todos, muchas gracias.

JOSÉ MARÍA DE AGUSTÍN DEL BURGO

CONTENIDO

1. INTRODUCCIÓN

Es un hecho que la impresión 3D se está posicionando como el proceso de fabricación del siglo XXI. En particular, la fabricación por deposición de filamento (FDM) se ha extendido más que ninguna otra gracias a la gran comunidad de desarrolladores que se han interesado en esta técnica. Esto ha llevado a un aumento en la oferta disponible en el mercado, ha generado una bajada drástica de precios y ha ampliado la variedad de materiales con los que se pueden fabricar; por ejemplo, filamentos conductores de electricidad, biodegradables, resistentes o biocompatibles.

La inclusión de este tipo de materiales, con una técnica de fabricación totalmente novedosa, abre un inmenso campo de posibilidades, permitiendo llevar a cabo desarrollos nunca vistos hasta ahora, de una forma sencilla y con coste reducido.

Ejemplos claros de utilización de estos materiales es la creación de piezas dentales utilizando la técnica SLM (fusión por láser selectiva) [1] o la fabricación de prótesis ortopédicas [2], [3] utilizando la técnica FDM. En este caso, el proceso consiste en el escaneado de la extremidad del paciente y tras el procesado correspondiente, es posible fabricar una férula a medida [4]. Aprovechando las nuevas técnicas de fabricación y las novedosas tecnologías en sensores y electrónica, se propone llevar la reinterpretación de esta técnica desde el siglo X hasta la actualidad, mediante el uso de nuevas tecnologías sensoriales y electrónicas [5], [6] y el uso del concepto IoT (Internet of Things) [7], [8], orientado a aplicaciones médicas. Será posible desarrollar férulas inteligentes diseñadas de acuerdo con la lesión y morfología del paciente. La férula se diseñará exclusivamente para cada individuo, y es posible que se preparen férulas antes de la lesión, especialmente en atletas de alto nivel. Esto permitiría modificar los tratamientos de rehabilitación con los datos adquiridos por los sensores durante el proceso [9]. En este estudio se presentarán los pasos para fabricar una férula inteligente con tecnología FDM desde la digitalización de la extremidad hasta la inmovilización. Además, como objetivo futuro, hay diferentes líneas de investigación donde la impresión 3D permite el diseño y creación de tejidos y órganos con materia orgánica [10]–[12].

Sin embargo, no hay que olvidar que el aumento en la fabricación a un nivel particular y profesional requiere un aumento en la calidad de impresión, una reducción en los costos de la máquina y un aumento en el conocimiento de la comunidad científica [13]–[15]. Al realizar impresiones tridimensionales por adición de material, es necesario controlar varios parámetros para lograr un producto final óptimo. En muchos casos, es necesario supervisar el proceso en persona cuando es la primera vez que desea fabricar un objeto, ya que la tasa de falla es

relativamente alta en el FDM. Esto cobra especial importancia en caso de emplear materiales biocompatibles, ya que sus propiedades podrían llegar a verse deterioradas [16]–[18].

Durante el proceso de deposición, muchas de las variables que contribuyen a mejorar o empeorar el resultado final están sujetas a perturbaciones que provienen del propio sistema y de fuera de la máquina. Este tipo de desviaciones son difíciles de controlar, como sucede con la variabilidad del material, las variaciones en la temperatura exterior e interior de la máquina, la humedad o las desviaciones en el área de impresión [19]. Actualmente, el proceso de sensorizado y de control de fabricación aditiva, se presenta como una evolución de los métodos, categorizados como sensorizados y control de las variables y control de atributos de fabricación [20]. El control y la optimización de las operaciones de producción de filamentos contribuyen a obtener una mejor calidad del filamento, pero aún alcanza grandes tolerancias [21]–[24].

Como desarrollo y conjunción de estas ideas previas, el objetivo de este estudio es plantear el diseño de un nuevo sistema de férulas "inteligentes" personalizadas según la morfología y patología del individuo. Estas férulas serán fabricadas con materiales biocompatibles, garantizando las condiciones de producción e inalterabilidad de propiedades. Incluirán sensores para monitorizar la evolución de la lesión desde un dispositivo móvil cercano o de forma telemática, gestión de la información recogida, y además permitirán aplicar terapias ambulatorias de tratamiento incompatibles con la metodología clásica basada en férulas de yeso [25]. Todo ello, manteniendo la premisa de coste reducido gracias a las nuevas técnicas de fabricación.

Como resultado de este estudio, se han realizado las siguientes publicaciones en revistas internacionales y libros, y que pueden ser encontradas en los Anexos:

Revista: Sensors, Journal Rank: JCR - Q1 (*Instruments & Instrumentation*) / CiteScore - Q1 (*Instrumentation*):

- Filament advance detection sensor for fused deposition modelling 3D printers. DOI: 10.3390/s18051495
- Development of a Smart Splint to Monitor Different Parameters during the Treatment. DOI: 10.3390/s20154207
- Development of a Smart Leg Splint by Using New Sensor Technologies and New Therapy Possibilities. DOI: 10.3390/s21155252

Revista: Journal of Medical Systems, Impact factor 4.460:

- Monitoring an Analysis of Perturbations in Fusion Deposition Modelling (FDM) Processes for the Use of Biomaterials. DOI: 10.1007/s10916-019-1236-2

Además, se encuentra actualmente en revisión para publicación los siguientes trabajos:

Libro: Technological Adoption and Trends in Health Sciences Teaching, Learning, and Practice, Impact factor 1.213

- New technologies for diagnosis during initial stages of the treatment applied to Splints. New therapies possibilities.

Artículo en proceso:

- Fused deposition manufacturing for biocompatible materials certification.

Por último, se han participado en los siguientes congresos internacionales:

- TEEM 2019 Real time analysis of the filament for FDM 3D printers
- TEEM 2020 Smart Splint for diagnosis during initial stage of treatment.

  En este ultimo congreso se obtuvo el **reconocimiento de mejor paper de su catergoría:** "Best paper in the category of State-of-the-art technologies at the service of medical training and practice to foster Digital Health Ecosystems"

2. JUSTIFICACIÓN DEL TRABAJO Y PLANTEAMIENTO: OBJETIVOS

Es conocido que el origen de las escayolas y férulas para inmovilizar con yeso se atribuye a los persas, en el siglo X. Desde entonces, la evolución ha sido escasa, y se sigue empleando la misma técnica para inmovilizar miembros lesionados. Este tipo de técnica, aunque válida, no permite aplicar ciertos tratamientos o airear la zona de la piel cubierta, entre otras cosas. Es por esto que, aprovechando las nuevas técnicas de fabricación y las nuevas tecnologías en sensores y electrónica, se plantea la reinterpretación de esta técnica del siglo X para traerla a nuestra época actual.

Desarrollo de férulas inteligentes diseñadas según la lesión y morfología del paciente, que permitan una monitorización en tiempo real de la evolución y la aplicación de nuevos tratamientos.

Objetivo principal:

El objetivo principal de esta tesis es desarrollar un nuevo sistema de férulas totalmente novedoso, que permita aplicar un tratamiento más efectivo a lesiones principalmente de las extremidades. Este nuevo sistema de férulas inteligentes podría llegar a ser revolucionario en lesiones musculares, óseas, de fibras o de tendones; ya que no hay ningún desarrollo previo de bajo coste que monitorice la evolución de la lesión, especialmente en las primeras horas de producirse. El sistema permitirá detectar cambios de presión, temperatura, humedad y color de la piel en la zona de la lesión.

La férula será diseñada exclusivamente para cada individuo, y podría contemplarse el tener férulas preparadas previamente a producirse una lesión, especialmente en deportistas de alto nivel. Esto aplicando la metodología tradicional es totalmente impensable ya que se construyen directamente sobre el paciente.

Las tecnologías de sensorizado se presentarán para la adquisición de datos que faciliten información sobre el estado de salud, basándose en el concepto IoT (Internet of Things). Los parámetros que se controlarán son la temperatura, la humedad, la presión y el color de la piel, así como una colocación correcta de la férula. La combinación de estos puede indicar diferentes problemas que pueden estar sufriendo los pacientes, como la inflamación. Para obtener el prototipo de la férula se considerarán las ventanas para el alojamiento de las terapias rehabilitadoras y el tipo de tratamiento. De hecho, la aplicación de tratamientos en la fase de inmovilización tiene una influencia sustancial en la evolución de la lesión y en la rehabilitación de la movilidad del miembro.

Además, las férulas contemplarán la aplicación de nuevos tratamientos en la fase de inmovilización por ser sumergibles en medio acuoso, y permitirán el acceso visual a través de ventanas de trabajo y el contacto directo con la piel. Los tratamientos que se plantean son:

1. Cura para el caso de simultaneidad con heridas, patologías dermatológicas o cirugías.
2. Drenaje Linfático
3. Iontoforesis
4. Ultrasonidos
5. Láser
6. Electroestimulación

Objetivos secundarios:

Como parte del proceso, los objetivos secundarios que se irán contemplando durante el proceso y desarrollo del estudio son:

1. Estudio de diferentes materiales biocompatibles y propiedades.
2. Desarrollo de sistema que permita certificar las condiciones en las que la férula ha sido producida, garantizando la que no se han alterado sus propiedades materiales, así como sus características mecánicas.
3. Ensayos para la caracterización de diferentes materiales biocompatibles.
4. Desarrollo del protocolo de escaneado, mallado, diseño y producción de la férula.
5. Acceso de manera telemática a los datos desde dispositivo conectado a internet.
6. Implementación de algoritmo para detección de inflamaciones mediante cambios de presión, temperatura o color de la zona afectada.
7. Estudio de la medición de los sensores en la cara interna de la férula, según discusión de conveniencia que se hará más adelante en el trabajo.

3. METODOLOGÍA

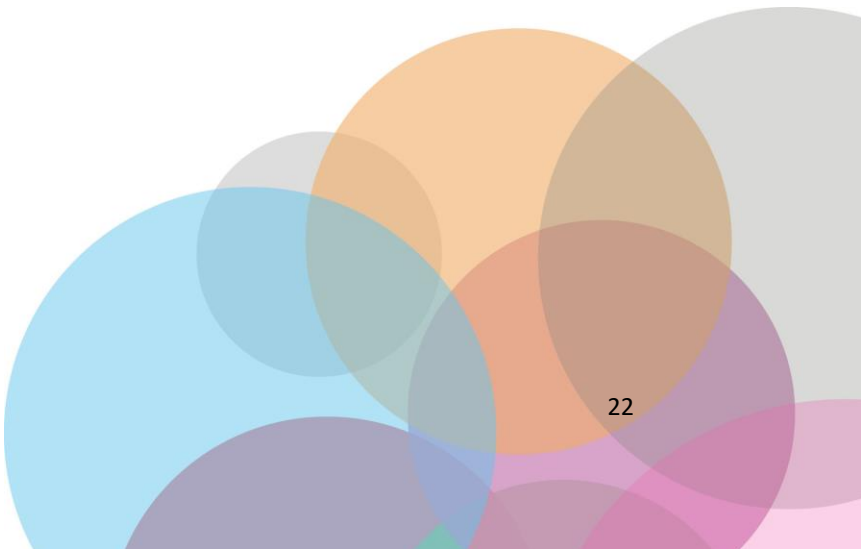

En este capítulo se exponen los métodos y técnicas empleados en la fabricación de los modelos 3D y el posterior desarrollo para la implementación de los sistemas electrónicos, así como los datos que han sido recogidos en las publicaciones y artículos que generan esta Tesis Doctoral.

Terapias consideradas en el estudio

Drenaje linfático:

El sistema linfático se ha identificado tarde en la historia. Probablemente esto se deba a que no es posible verlo a simple vista. Sin embargo, las técnicas manuales para el sistema linfático se han utilizado desde finales del siglo XIX. El terapeuta Emil Vodder, desarrolló un enfoque innovador que permitió mejorar manualmente el flujo linfático del cuerpo. Hoy en día, los terapeutas manuales utilizan la fisioterapia descongestiva combinada (CDP) para el linfo-edema. La CDP es uno de los tratamientos no invasivos que se eligen para el linfo-edema [26]. Consta de muchos componentes como la práctica, el cuidado de la piel, la terapia de drenaje linfático manual (MLDT), las compresiones externas, etc. La base del MLDT es crear diferentes vías a través de las cuales puede fluir el fluido linfático [27], [28].

Iontoforesis:

La iontoforesis es una de las técnicas más utilizadas durante el tratamiento de rehabilitación para la administración de medicamentos antiinflamatorios y analgésicos en las partes del cuerpo humano afectadas por procesos inflamatorios del sistema musculoesquelético [29]–[31]. De esta forma, algunos medicamentos son capaces de atravesar la piel y producir su efecto, eludiendo el tracto digestivo y sin necesidad de que se administren por inyección [32]–[34]. La explicación del modo de trabajo es que las sustancias iónicas tienen carga eléctrica, por lo que tienden a moverse hacia el polo del signo opuesto. Es en ese punto donde se absorben a través de la piel. De esta forma, algunos medicamentos consiguen atravesar la piel y surtir su efecto, evitando pasar por el tracto digestivo y sin necesidad de administrarlos por inyección.

Ultrasonidos:

La técnica de ultrasonidos terapéuticos se considera un tratamiento eficaz para la rehabilitación de afecciones musculoesqueléticas debidas a contracturas, dolores y espasmos musculares o lesiones articulares. Mejora la elasticidad de los tejidos, y tiene efecto mecánico, antiálgico y circulatorio [35], [36]. Este tratamiento promueve la liberación de calor a tejidos como tendones, músculos y articulaciones, reduciendo los síntomas de inflamación y promoviendo la regeneración tisular [37]–[39]. Este tratamiento no es doloroso, no tiene efectos secundarios y se realiza mediante un transductor capaz de generar corrientes eléctricas de frecuencia alterna y capaz de penetrar en el tejido y estimular el flujo sanguíneo en la zona. El ultrasonido también se puede utilizar en modo subacuático o con gel.

Las ondas sonoras liberadas a través del transductor penetran en el tejido según el tipo de medio utilizado, es decir, gel o loción, calidad del transductor, superficie de tratamiento y tipo de lesión a tratar. Normalmente los huesos y la zona de conexión del tendón tienen baja capacidad de absorción, siendo recomendable realizar otro tipo de tratamiento o utilizar una frecuencia más baja de ultrasonidos [40], [41].

Láser:

La terapia con láser acelera el metabolismo energético y la síntesis de tejidos. Hay muchos estudios que concluyen que el láser terapéutico puede ser potencialmente efectivo en el tratamiento de la tendinopatía cuando se utilizan las dosis recomendadas [42], [43].

Se considera que la terapia con láser de bajo nivel actúa a través de la absorción de luz por fotorreceptores, que estimulan las células y modulan los procesos inflamatorios [44]–[46]. Diferentes estudios realizados en una variedad de condiciones patológicas como tendones lesionados. Los tendones se trataron diariamente durante 3 a 21 días. Se observaron cambios histopatológicos en los tendones que estaban recibiendo tratamiento con láser, como un incremento de la producción de colágeno, una mejor organización del haz de colágeno y también un incremento del número de vasos sanguíneos [38], [47]–[49]. Además, algunos estudios han investigado el efecto de la terapia con láser dentro de las primeras 24 h después de una inflamación aguda. Se encontró que después de la inflamación seguida de solo tres o cuatro sesiones, las concentraciones de células y marcadores inflamatorios se habían reducido en comparación con los controles sin tratamiento [37], [50].

Electroestimulación:

La aplicación de la electricidad para el tratamiento del dolor se remonta a miles de años antes de Cristo. Los antiguos egipcios y más tarde los griegos y los romanos reconocieron que los peces eléctricos son capaces de generar descargas eléctricas para aliviar el dolor [51]. Las terapias modernas de electroterapia para el dolor neuromuscular-esquelético de leve a moderado se basan en la estimulación nerviosa eléctrica transcutánea (TENS) y la estimulación nerviosa eléctrica percutánea (PENS) [52]. También existen diferentes estudios sobre los efectos de la electroestimulación sobre el dolor, la fuerza muscular y la capacidad funcional en pacientes con artrosis de rodilla [53].

Para la terapia de electroestimulación se requiere un dispositivo simple que tenga al menos un circuito con un par de electrodos. Se pueden seleccionar diferentes curvas y frecuencias. La electroestimulación muscular en el músculo gastrocnemio tiene efecto antiálgico y antiinflamatorio, las corrientes analgésicas de baja frecuencia y las corrientes farádicas producen retardo de la atrofia muscular en el músculo de la pantorrilla, y las corrientes estimulantes en el gastrocnemio y los músculos intrínsecos de la suela, producen respuestas motoras [54].

Estas técnicas son solo algunos ejemplos considerados en este estudio, que pueden aplicarse por ejemplo, a lesiones en brazos [55], rodillas [56], codos [57] o tendón de Aquiles [58]. Sin embargo, mediante el uso de férulas 3D, también podría ser posible aplicar otras terapias, consideradas por un especialista [59]).

Según estudios previos [25], es posible ver las mejoras de evolución al aplicar algunas de estas terapias. Las férulas tradicionales no permiten la aplicación de técnicas de fisioterapia hasta que se retira el dispositivo. Sin embargo, al usar nuevas férulas inteligentes, es posible aplicar los tratamientos tan pronto como ocurra la lesión. Es posible ver las nuevas posibilidades de sincronización (en color azul), en comparación con la programación tradicional (en negro) en la Figura 1.

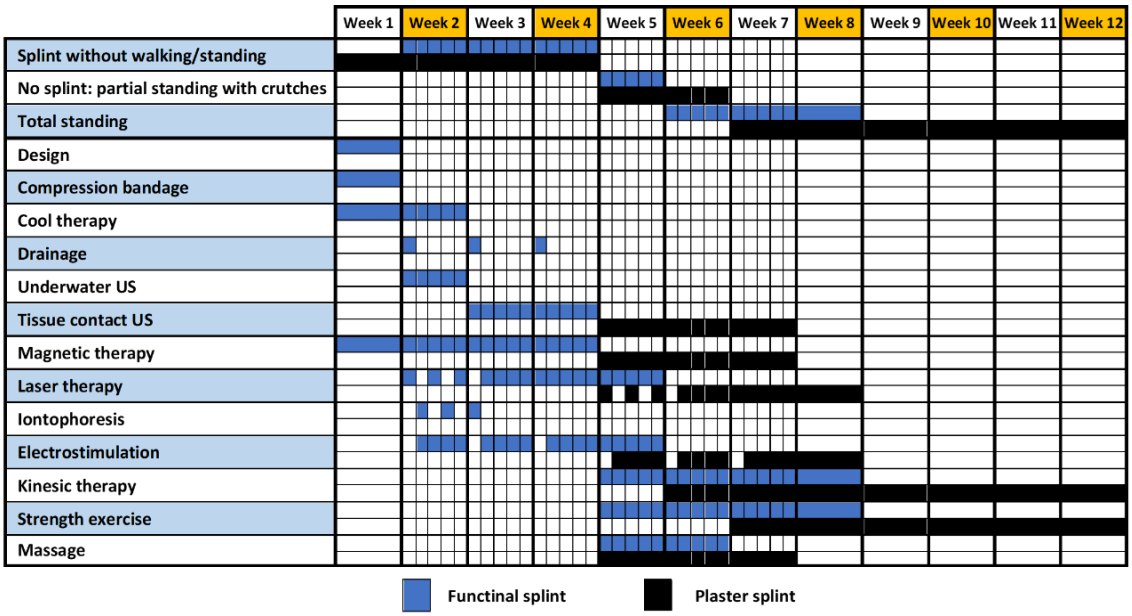

Figura 1. Cronograma de rehabilitación cuando se aplican nuevas terapias, no compatibles con las férulas tradicionales [25]

Como se aprecia, la aplicación de estas terapias implica al menos la reducción del 30% del período de tratamiento. Además, la aplicación de técnicas de fisioterapia durante la fase de inmovilización contribuye a la prevención de complicaciones articulares, musculares y vasculares, derivadas de la aplicación de dispositivos de retención en la fase inicial del tratamiento.

Sensores para la recogida de datos

Como se detalla en los objetivos principales del presente estudio, es requisito indispensable el poder "**detectar cambios de presión, temperatura y color de la piel en la zona de la lesión**" para considerar realmente una férula como "inteligente".

Cuando ocurre una lesión, pueden aparecer signos inflamatorios normales como variaciones de la temperatura, cambios en el color de la piel, aumento de la sudoración o edemas. Estos síntomas pueden aparecer debido a diferentes problemas que pueda estar sufriendo el paciente [60], [61].

Los sensores implementados serán los encargados de monitorizar algunos parámetros para realizar un diagnóstico. Los parámetros considerados son presión, temperatura, humedad y color de piel. Los datos obtenidos se combinan para determinar si existe alguna señal de evolución inesperada durante el tratamiento. La información registrada por estos sensores se combina para

determinar si existe algún tipo de evolución inesperada del tratamiento. En total, los sensores implementados son: dos sensores de temperatura DS18B20 [62] en contacto con la piel, un sensor de temperatura y humedad entre la piel y la férula (DHT22) [63], dos sensores de presión DF9-40 [64] colocado en dos ejes diferentes de la férula (X, Y), un sensor de color TCS34725 [65], y un sensor de presencia infrarrojo CNY70 [66]. Los golpes y vibraciones que puede producir el cuerpo humano no son fundamentales para el rendimiento y la durabilidad de estos sensores. Además, cuando se trata una lesión de estas características, se debe la exigencia de inmovilización. Por tanto, los golpes y las vibraciones son controlados. Los detalles de estos sensores se muestran en la Tabla 1.

Tabla 1. Especificaciones de los sensores seleccionados

Modelo de sensor	DS18B20	DHT22	DF9-40	CNY70	TCS34725
Dimensiones (*mm*)	6 x 6 x 50	15 x 7.7 x 20	40 x 20 x 0,25	7 x 7 x 6	25 x 20 x 1.5
Voltaje (*V*)	3,0 - 5,5	3.3 – 6	5	5	5
Rango de trabajo	-55 *°C* a 125 *°C*	-40 *°C* a 80 *°C* 0 to 100% *RH*	0-500 *g*	0 a 10 *mm*	-
Resolución	± 0,0625 *°C*	0.1 *°C*, 0.1% *RH*	14.5 *g*	-	-

Los sensores DS18B20 son sensores de temperatura digitales en bus. La salida la da directamente en grados Celsius, con una precisión de 9 a 12 bits. Cada sensor tiene un número de serie único de 64 bits grabado en él, lo que permite utilizar una gran cantidad de sensores en un bus de datos.

El sensor DHT22 utiliza una técnica exclusiva de recolección de señales digitales y tecnología de detección de humedad. Realiza la medida, y comunica la humedad relativa y la temperatura al microprocesador.

El sensor DF9-40 está compuesto por una película de presión basada en tecnología de detección de presión flexible (FSR). Al aplicar una fuerza, la resistencia cambia (Figura 2a), generando variaciones en el voltaje leído desde el microprocesador. Para medir la fuerza aplicada con un microporcesador, será necesario construir un circuito divisor de tensión. Este circuito crea una salida de voltaje variable que puede ser leída por la entrada ADC (convertidor analógico a digital) del microcontrolador. Significa que, para una conversión simple de presión a voltaje, el

dispositivo de resistencia de detección de fuerza (RFSR) está conectado a una resistencia de medición (RM) en un divisor de voltaje (Figura 2b). En este caso, se utilizará una resistencia de 10kΩ. El voltaje de salida (Vout) que es posible medir con el Arduino se describe mediante la siguiente ecuación:

$$V_{out} = \frac{V_{cc} \cdot \mathrm{R}}{\mathrm{R} + \mathrm{R}_{FSR}}$$

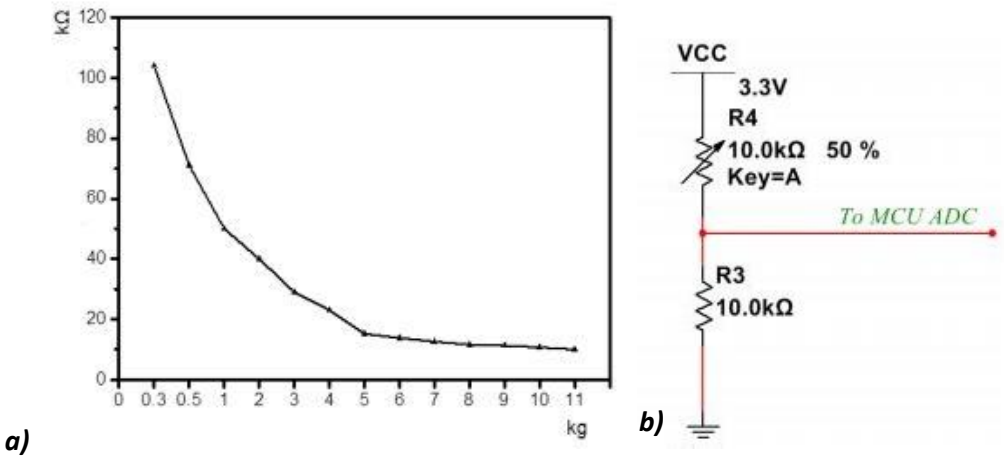

Figura 2. Variación de resistencia con la carga (a) y esquema de divisor de tensión (b)

Analizando el circuito es posible ver que la medida del voltaje de salida es la caída de voltaje a través de la resistencia del sensor. Cuando no se aplica fuerza, la resistencia RFSR será realmente alta, por ejemplo, 10 MΩ, y por tanto, el voltaje muy bajo. El uso de una resistencia pull-down de 10kΩ y un Vcc de 5V, da como resultado la salida cuando no se aplica fuerza VOUT = 0.005V. En cambio, cuando se presiona el FSR, la resistencia baja a aproximadamente 200 Ω. Esto da como resultado un voltaje de salida VOUT = 4.9V. Se han realizado desarrollos similares en otros estudios para otras aplicaciones médicas [26].

El sensor CNY70 es un sensor de reflexión que incluye un emisor de infrarrojos y un fototransistor en un paquete, junto a un filtro de bloqueo de la luz solar. Este sensor puede detectar la cantidad de luz reflejada en una superficie en función de la distancia. Por otro lado, si establecemos una distancia fija, es posible detectar diferentes colores en función de la luz infrarroja absorbida por ese color. Para utilizar este sensor, es necesario construir un circuito

divisor de voltaje con una resistencia pull-down como en el caso del sensor de presión. En este caso, se utiliza un valor de 39kΩ.

El sensor TCS3472 proporciona un valor de retorno digital de los tres componentes de la luz (rojo, verde y azul). Incluye un filtro de bloqueo de infrarrojos, que minimiza el componente espectral de infrarrojos de la luz, lo que permite mediciones precisas del color sobre la piel, donde no hay luz externa. La figura 3 muestra gráficos de la respuesta específica de este sensor a la luz. Como muestra la Figura 3a, el sensor puede detectar diferentes longitudes de onda utilizando un fotodiodo espectral. De esta forma, comprende la cantidad de luz de cada longitud de onda que rebota en una superficie. La Figura 3b ilustra que la mayor capacidad de respuesta del sensor está en la dirección perpendicular de la superficie del fotodiodo. Esto debe tenerse en cuenta cuando se diseña la carcasa del sensor. Este sensor es una solución ideal para diferentes condiciones de iluminación y materiales, debido a su sensibilidad, el amplio rango dinámico y el filtro de bloqueo de infrarrojos. Los datos se transfieren a través de un bus I2C, utilizando los contactos SDA y SCL.

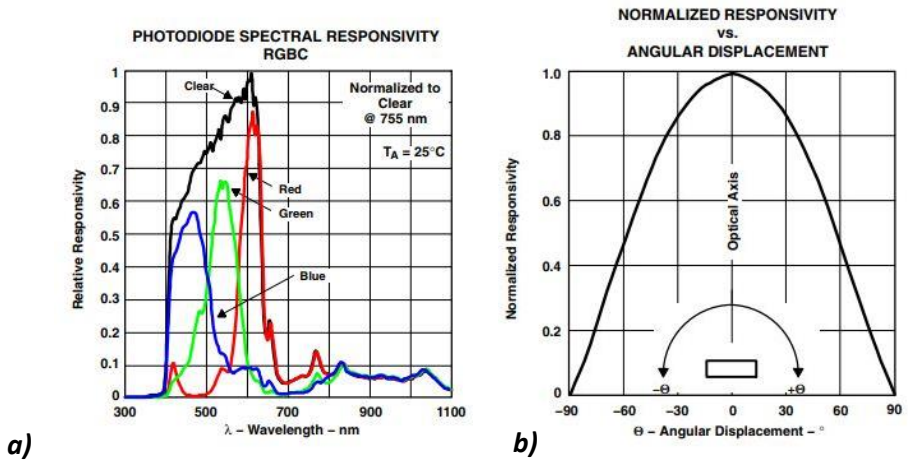

Figura 3. Gráficos de respuesta del sensor TCS3472

Durante el proceso de curación, un hematoma generalmente tendrá diferentes colores (Figura 4). A menudo comienza en rojo porque la sangre fresca rica en oxígeno se ha acumulado debajo de la piel. Después de aproximadamente 1 a 2 días, la sangre comienza a perder oxígeno y cambiar de color. Un hematoma que tiene unos pocos días a menudo se verá azul, morado o incluso negro. En aproximadamente 5 a 10 días, se vuelve de color amarillo o verde. Estos colores provienen de compuestos llamados biliverdina y bilirrubina que el cuerpo produce cuando descompone la hemoglobina. Después de 10 a 14 días, cambiará a un tono de marrón amarillento o marrón claro [67], [68].

Figura 4. Diferentes colores de moretón, según la etapa de evolución. Inmediato (a), 2-5 días (b) ,5-10 días (c), 10-14 días (d)

Estudios anteriores muestran la idoneidad del uso de diferentes canales RGB y sus diferencias para la detección de hematomas o equimosis [69], [70]. El sensor de color detecta los colores cambiantes de la piel, durante la etapa de inflamación inicial, debido a la equimosis [71], que se produce aproximadamente en los primeros seis días [72], [73]. El objetivo principal de utilizar un sensor RGB es detectar la variación en los componentes rojo, verde y azul de la luz. El dispositivo, incorpora un emisor de luz blanca, que rebota en la piel y vuelve al receptor. El sensor lee la variación de los tres componentes, en comparación con la luz blanca original. De esta forma es posible saber qué componente se absorbe y, por tanto, el color de la piel. No es necesario modificar el valor de ganancia ni otros parámetros, ya que el sensor ya está configurado. Además, dado que el estadio inicial de la lesión que se debe monitorizar tiene una duración de una semana, la durabilidad no es un parámetro crítico. El sensor lee los valores en términos de RGB (rojo, verde y azul) entre 1 y 256.

Proceso de obtención del modelo digital y diseño de la férula

Tal y como se explica en los objetivos, "**La férula será diseñada exclusivamente para cada individuo, y podría contemplarse el tener férulas preparadas previamente a producirse una lesión**". Para este primer objetivo, necesario e indispensable para continuar con el estudio, se procede a seguir el método de ingeniería inversa [74] (Figura 5). Por este proceso, se parte de un modelo real, del que se obtiene una nube de puntos. Una vez obtenida dicha nube, se prosigue con una serie de pasos para llegar a obtener el modelo CAD.

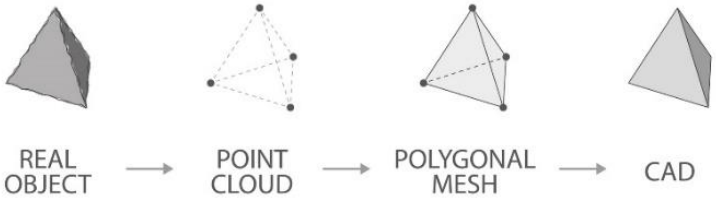

Figura 5. Ingeniería inversa 3D [75]

En este caso se ha empleado un Escáner 3D de láser infrarrojo tipo Sense (Figura 6):

- Volumen de escaneo: 0.2x0.2x0.2m hasta 2x2x2m
- Campo de visión de trabajo: 45° horizontal, 57.5° vertical, 69° Diagonal
- Distancia de escaneo: 0.2m hasta 1.6m
- Resolución en 0.5m: x/y 0.9mm – Profundidad resolución 1mm

Figura 6. Escáner de mano Sense 3D Systems. Fuente: Elaboración propia

Se trata de un escáner de bajo peso, que da una nube de puntos con una resolución suficiente para la labor que necesitamos desempeñar. Además, el volumen de trabajo, hasta 2m3, es suficiente para el escaneo de una zona o articulación.

Una vez obtenida la nube de puntos, y poder abordar también parte de los objetivos secundarios **"Desarrollo del protocolo de escaneado, mallado, diseño y producción de la férula"**, es necesario realizar una serie de procesos para producir un modelo sólido sobre el que poder trabajar introduciendo los alojamientos para los sensores, así como las ventanas para los posibles tratamientos; y por último para que pueda ser fabricado en una máquina de impresión 3D. Durante el proceso, se han empleado dos técnicas con diferentes softwares.

Para ello, los softwares empleados han sido:

- Sense 2 (3D Systems, Inc., United States):

Este software es el indicado para ser utilizado con el escáner elegido y producir la nube de puntos. Esta nube de puntos deberá ser procesada en otros softwares.

- 3D CAD software Geomagic FreeForm y 3D CAD Geomagic Design X™ Software (3D Systems, Inc., United States).

La nube de puntos se editó con los softwares tipo CAD (Computer Aided Design). Estos softwares permiten convertir los datos del escáner 3D en modelos CAD con manteniendo una gran calidad dimensional, ya que combinan la extracción de modelos de una manera automática, así como de una forma guiada de edición de mallas y procesamiento de nubes de puntos. También permite realizar una limpieza de posibles puntos o ruido que se hayan creado debido a brillos u otros factores, durante el escaneado. Es posible suavizar superficies, eliminar y unir puntos, y obtener un diseño más homogéneo, pudiendo finalmente construir un sólido de mayor calidad y preparado para una mejor definición al ser producido por impresora 3D.

- Inventor Professional 2020 (Autodesk, United States) y CATIA™ 3DEXPERIENCE®3D Software (Dassault Systèmes®, France)

Una vez obtenido el modelo sólido a partir de la nube de puntos, se podría haber continuado trabajando con el software Geomagic para realizar los alojamientos de los sensores, así como las ventanas de los tratamientos, parte del objetivo principal de este estudio. Sin embargo, se ha decidido pasar a trabajar con un software de diseño 3D paramétrico. Se ha elegido este tipo de software ya que permite parametrizar fácilmente el tipo de huecos a crear en la estructura con medidas precisas, así como realizar secciones. Además, ofrece la posibilidad de modificar las operaciones de diseño gracias al proceso estructurado tipo árbol que emplea este tipo de software.

Desarrollo de férula para brazo

En un primer desarrollo, se procede a realizar un modelo de férula para brazo. Se ha empleado la extremidad de un sujeto de 29 años, sin ningún tipo de lesión, pero que será la base para el desarrollo del modelo 3D y la generación de la férula en la que se ensamblarán colocarán los sensores, para la recogida de datos.

Es posible escanear la zona completa de una sola vez, o también realizar diferentes escaneados para después unir las diferentes nubes de puntos. Este proceso, vendrá determinado por las limitaciones debidas a la lesión en concreto. Esta etapa es mostrada en la Figura 7.

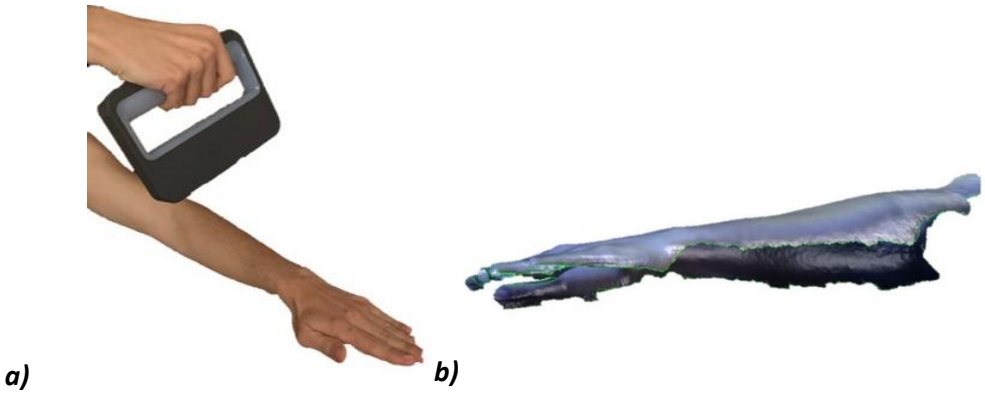

Figura 7. Proceso de escaneado del brazo para obtener el modelo digital (a) y nube de puntos (b). Fuente: Elaboración propia

Una vez obtenida la nube de puntos, se pasa a trabajar con un software CAD que permita manejar el modelo 3D. En este caso se emplea Geomagic FreeForm (3D Systems, Inc., United States). Este software permite limpiar las nubes de puntos, de posibles errores debidos a reflejos u otros motivos [76], [77], así como rellenar espacios vacíos. Tras esto, se añade un offset de 0.5mm que permita acomodar correctamente la férula sobre el miembro. La Figura 8 muestra el proceso de trabajo con el modelo digital del brazo:

Figura 8. Modelo digital del brazo (a) modelo limpio sobre el que trabajar (b) y sólido con offset inicio del diseño de la férula (c)

En este caso, para un primer prototipo, y teniendo en cuenta las propiedades del PLA, se dota a la férula de un espesor de 5mm [78]. Este sólido 3D, se divide en dos partes, para poder ensamblarlo después correctamente sobre el brazo. Las dos partes se ensamblarán gracias a unos tetones que se han insertado en el diseño. Llegados a este punto, y de acuerdo con el objetivo **"las férulas contemplarán la aplicación de nuevos tratamientos en la fase de inmovilización por ser sumergibles en medio acuoso, y permitirán el acceso visual a través de ventanas de trabajo y el contacto directo con la piel"** se procede a realizar una serie de ventanas o huecos que permitan la aplicación de diferentes tratamientos, así como de alojamientos para los sensores. En este primer desarrollo, se realizan una serie de ventanas a modo de prueba, y será en el diseño que se muestra después, donde realmente se aplicarán ventanas de acuerdo con los tratamientos elegidos. La Figura 9 muestra este proceso.

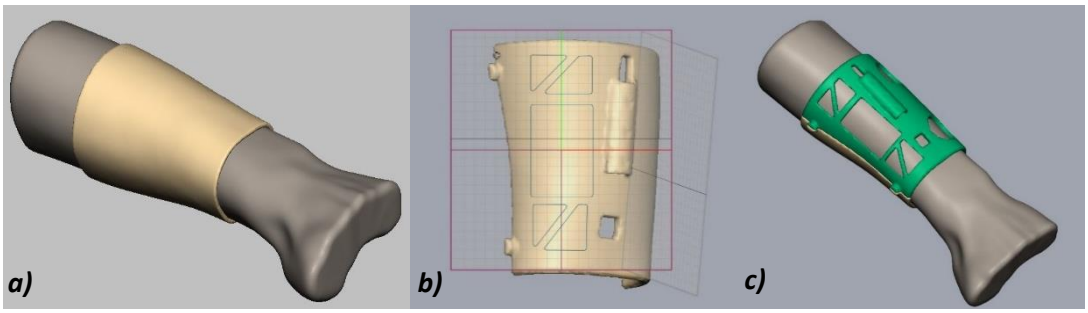

Figura 9. Modelo inicial sobre el brazo (a), diseño de ventanas y alojamientos (b) y modelo final virtual (c)

Desarrollo de férula para pierna

En un segundo desarrollo, se plantea un diseño equivalente, para pierna. Además, se procederá al uso de programas paramétricos, que permitan realizar modificaciones rápidamente en el diseño, así como parametrizar algunos de los parámetros. Esto, supone un salto importante, ya que podría realizarse una base de datos que relacione determinadas formas o dimensiones de una extremidad, con otras. Se ha empleado la pierna de un sujeto de 29 años, sin ningún tipo de lesión, pero que será la base para el desarrollo del modelo 3D y la generación de la férula en la que se colocarán los sensores para la recogida de datos.

En este caso, el proceso de escaneado se realiza de forma similar, en única toma y manteniendo la pierna en posición vertical suspendida. Durante la primera etapa, se obtiene la nube de puntos (Figura 10), que es procesada con el software CAD Geomagic Freeform Software. En este caso, trabajamos con la malla generada desde la nube de puntos, y del mismo modo que en el caso del brazo, se aplica un offset de 0.5mm. Sin embargo, en esta ocasión,tras haber realizado anteriormente el modelo del brazo y en aras de optimizar al máximo el modelo, se pasa a aplicar un espesor de 3.7mm [74], [78].

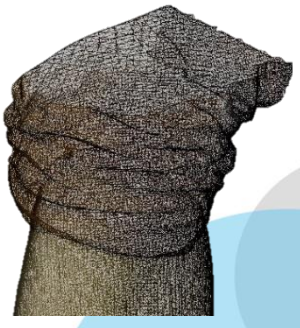

Figura 10. Nube de puntos

Para poder diseñar fácilmente las modificaciones para los tratamientos y sensores, es necesario crear un cuerpo sólido a partir de esta superficie de malla. De esta forma, será posible importar el modelo digital a un programa CAD paramétrico para manipularlo correctamente. Este objetivo no es trivial, ya que la metodología del modelado paramétrico y los programas de modelado no paramétrico (programas de modelado orgánico) son completamente opuestos. El modelado paramétrico es un enfoque de CAD en 3D en el que captura la intención del diseño utilizando características y restricciones, lo que permite a los usuarios automatizar cambios repetitivos, como los que se encuentran en familias de piezas de productos. Estas capacidades son ideales para tareas de diseño que involucran requisitos precisos y criterios de fabricación. Por ejemplo, esto se usa normalmente cuando se fabrican familias de productos que incluyen ligeras variaciones de un diseño central. Esto admite diseños que necesitarán ser modificados o iterados de forma regular y crea modelos con características individuales, como agujeros y chaflanes, que pueden modificarse o cambiarse. Primeramente, se reduce la malla para poder manipularla fácilmente. Es importante reducir el número de triángulos, pero también mantener las dimensiones y formas originales. Después, la malla se envía al software 3D CAD Geomagic Design X ™ (3D Systems, Inc., Estados Unidos). Con este programa es posible completar la malla y reducir el número de superficies. La Figura 11 muestra un total de 67,376 triángulos, y después de aplicar la herramienta, estos triángulos se reducen a 10,820. Esta reducción del 84% de la malla mantiene el diseño original con un tamaño de archivo mucho más pequeño.

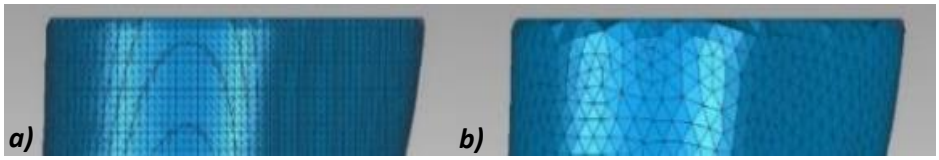

Figura 11. Malla original (a) vs reducida (b)

En este punto, tendríamos generada la malla completa para ser convertida a sólido en un programa CAD paramétrico, habiendo partido del modelo inicial de la nube de puntos (Figura 12). En este caso, el software elegido es CATIA™ 3DEXPERIENCE® 3D Software (Dassault Systèmes®, Francia)

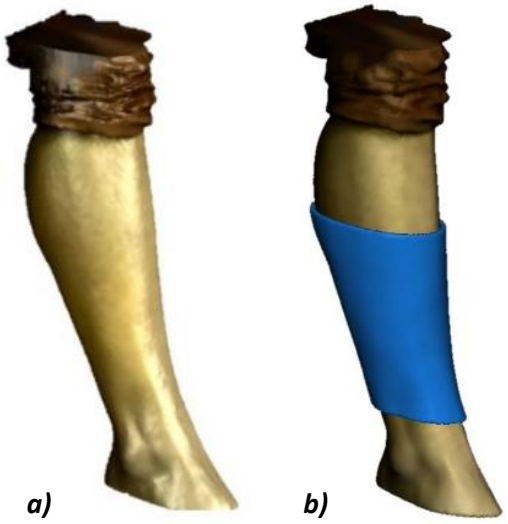

Figura 12. Nube de puntos inicial (a) y malla creada a partir de la nube de puntos (b)

El proceso de conversión resulta bastante tedioso. Además, es imprescindible hacerlo bien para evitar posteriores errores en el diseño, que pudiesen resultar en roces o molestias sobre la piel una vez obtenido el modelo físico. La malla reducida se importa mediante el módulo Diseño de ensamblajes. Después de esto, la malla se convierte a un archivo de extensión *".model*" usando el módulo DMU Optimizer con la herramienta de aplicar un desplazamiento 0 a la malla. El archivo generado se abre y el árbol del diseño debe copiarse y pegarse en una nueva parte del módulo Generative Shape Design. Con este módulo, es posible utilizar la herramienta "Unión" para crear una malla única y compleja. Finalmente, esta malla se abre mediante el módulo de Diseño de Pieza y se aplica la herramienta "Cerrar Superficie" para crear el cuerpo sólido de la férula. Después de este procedimiento, la malla original se convierte en un cuerpo sólido. Gracias a este proceso, ahora es posible abrir el archivo con un software de modelado paramétrico. En este caso, se utilizará Inventor Professional 2020 (Autodesk, Estados Unidos). Tal y como se puede apreciar en la Figura 13, el modelo ha mantenido el espesor correctamente. Esto indica que el proceso no ha modificado las dimensiones en comparación con el offset original que se estableció, por lo que el proceso es válido y no ha modificado la morfología ni las dimensiones originales.

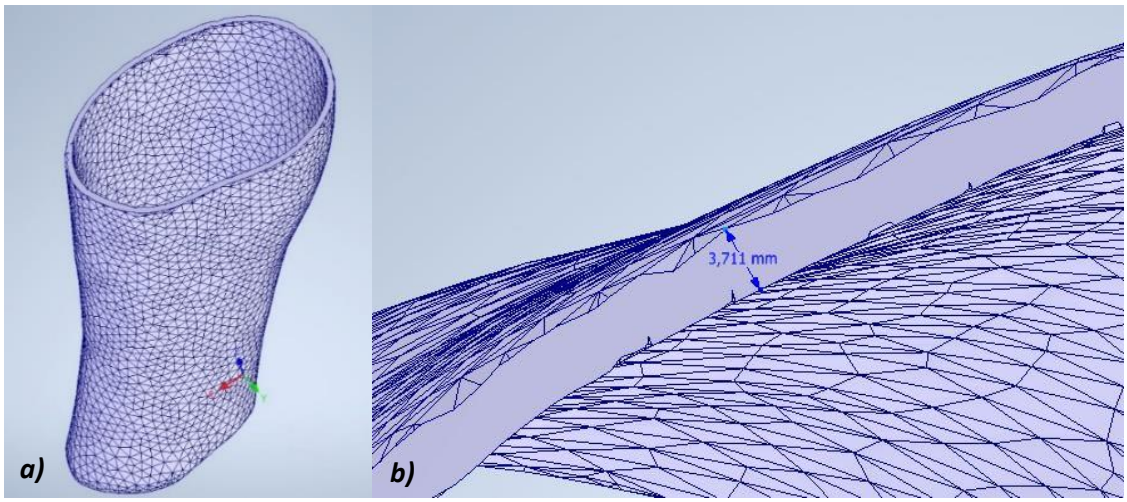

Figura 13. Modelo digital en Inventor Autodesk (a) y comprobación de espesor (b)

Llegados a este punto, se procede a realizar una serie de modificaciones que permitan aplicar diferentes tratamientos, así como alojar diferentes sensores en la férula. También, se ha de tener en cuenta que, para montar la férula sobre el miembro, se ha de dividir en dos partes que después se unirán. Para ello, en este caso se emplearán 24 imanes de neodimio de 3mm (Figura 14). Sin embargo, otros métodos pueden ser empleados.

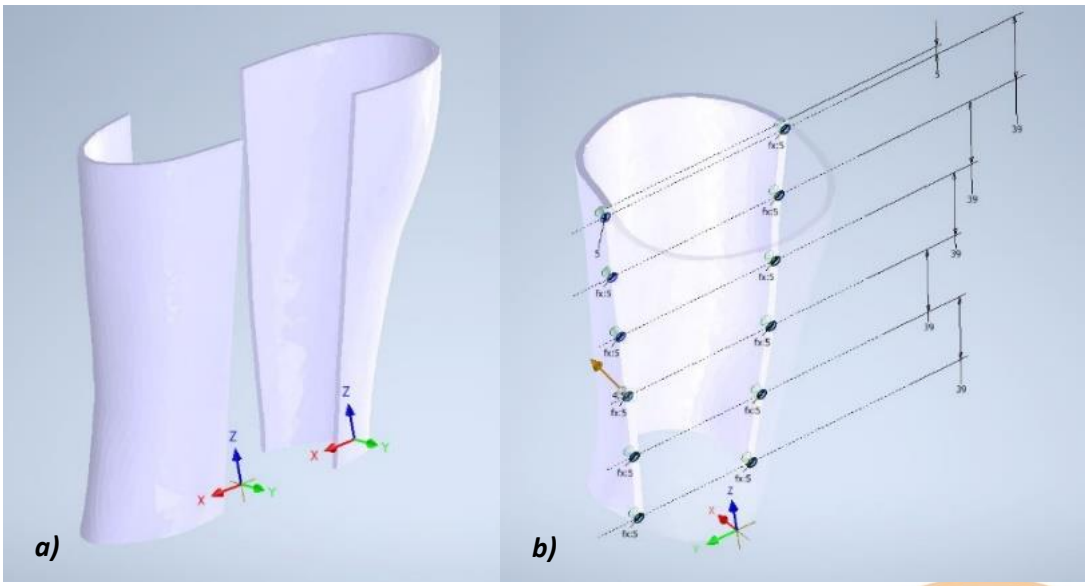

Figura 14. División de férula (a) y diseño del sistema de fijación

En este punto, es necesario introducir en la férula las diferentes carcasas para los sensores, así como las ventanas para los diferentes tratamientos propuestos en el apartado 2.2. En la Figura 15 se muestran las zonas donde se aplicarán los tratamientos de terapia rehabilitadora, según la morfología del miembro a inmovilizar y estudios previos [32], [38].

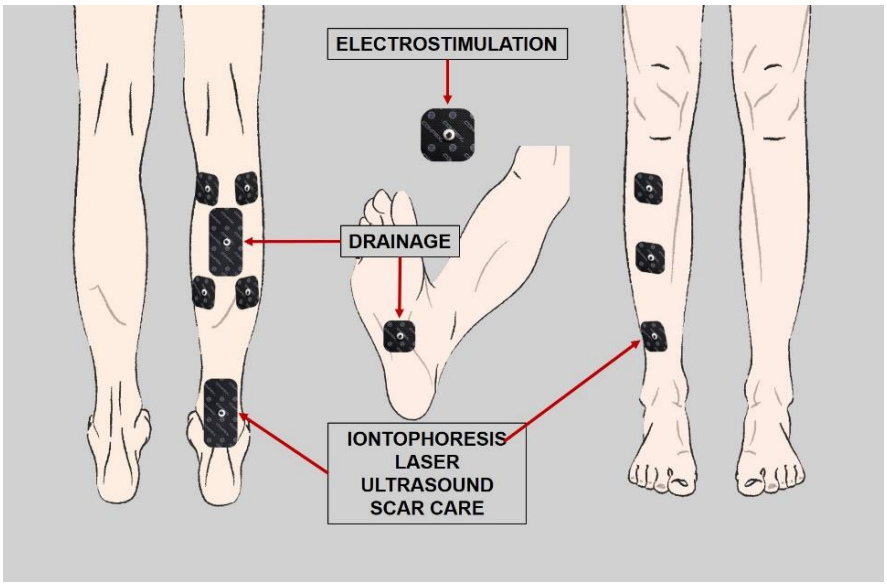

Figura 15. Zona de ventanas para los tratamientos

Teniendo en cuenta esta información, se diseñan las diferentes ventanas. Para la electroestimulación se fabrican ventanas de 30x30mm, mientras que, para drenaje, iontoforesis, láser y ultrasonidos, las ventanas tienen un tamaño de 30x40mm. Además, se consideran diferentes alojamientos para los sensores y el cableado. La Figura 16 muestra tanto la parte trasera como la delantera después del proceso de diseño. Finalmente, se abre el modelo diseñado sobre la malla original de la pierna, obtenida al inicio de este proceso, para confirmar que encaja perfectamente (Figura 16d).

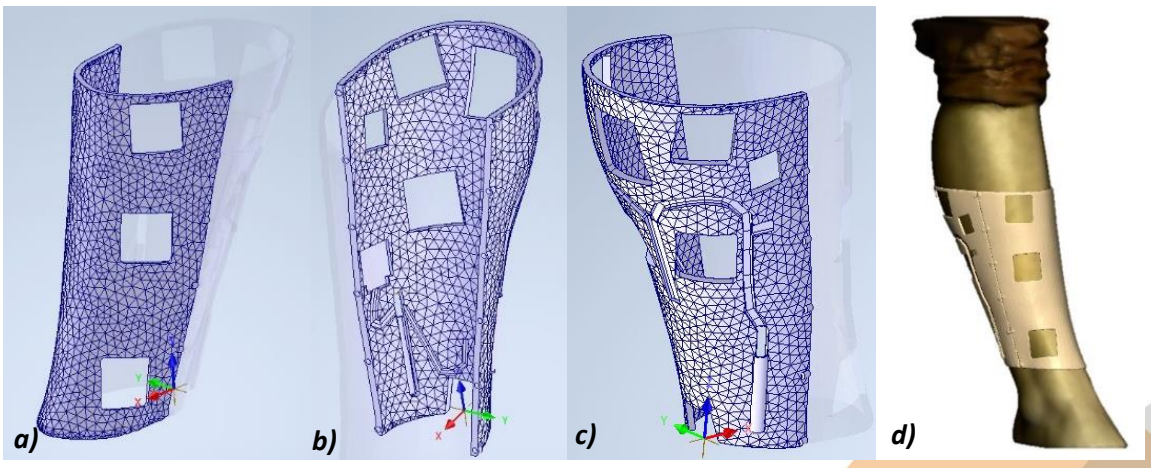

Figura 16.Vista de la férula: parte delantera (a), interior (a) exterior (b) desde la parte trasera de la férula. (d) férula diseñada sobre el modelo escaneado

Proceso de fabricación de las férulas. Máquina y materiales.

Una vez obtenido el modelo CAD final, el diseño se envía a una impresora 3D para la obtención del modelo real. Para ello, se convierte el archivo CAD a formato STL que será leído por el software de laminado 3D para convertir en comandos G-Code que serán después interpretados por la impresora. Para ello, el software empleado es el siguiente:

- Software Cura (Ultimaker, Países Bajos)

Se ha seleccionado este software, por ser gratuito, de fácil manejo, y muy configurable. Además, es compatible con el Firmware de la impresora que se emplea en el proceso.

Por otro lado, y puesto que se está tratando de sistemas para uso médico, es necesario considerar el material usado durante la fabricación, así como el proceso de producción, y las características del producto. Primeramente, será necesario realizar un estudio de diferentes materiales biocompatibles, de acuerdo con el objetivo "**Estudio de diferentes materiales biocompatibles y propiedades**". Tras esto, se ha de analizar con detenimiento el proceso de fabricación y las condiciones en las que el producto se obtiene. Para ello, se ha elegido la Máquina de impresión 3D sensorizada Total Printer (Figura 17) de diseño propio, que permita lograr el objetivo secundario **"certificar las condiciones en las que la férula ha sido producida, garantizando la que no se han alterado sus propiedades materiales, así como sus características mecánicas"** [79], [80]**.** Además, se deberán realizar diferentes ensayos, abordando de este modo otro de los objetivos secundarios **"Ensayos para la caracterización de diferentes materiales biocompatibles".**

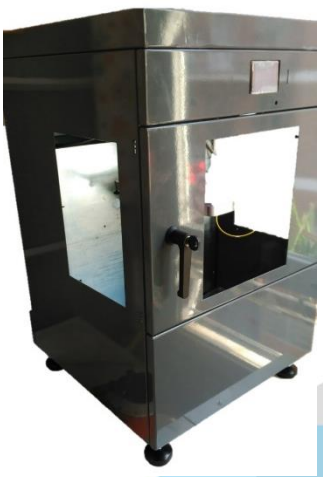

Figura 17. Máquina Total Printer. Fuente: Elaboración propia.

Por último, se ha contado con el Laboratorio de Fabricación aditiva y digitalización industrial de la ETSIDI (Escuela Técnica Superior de Ingeniería y Diseño Industrial) de la Universidad Politécnica de Madrid. Laboratorio nº 425 de la red de Laboratorios Madri+d de la Comunidad de Madrid, así como el Laboratorio de plásticos de la ETSIDI (UPM), para la producción de los diferentes prototipos y pruebas, y posteriormente llevar a cabo las mismas.

Evolución de la máquina de FDM para garantizar las condiciones de producción

Aunque los fabricantes e investigadores mejoran constantemente el proceso de fabricación de polímeros, el bobinado de filamentos y el moldeo por inyección; la calidad del producto y la eficiencia de producción están influenciados por múltiples parámetros debidos tanto al procesamiento como al propio material, como el diámetro nominal y el acumulado, la temperatura del proceso o la extrusión: mecanismos que actualmente no están completamente controlados. La supervisión y optimización de este tipo de operaciones contribuyen a acercarnos cada vez más al tamaño nominal del filamento, pero todavía se encuentran fabricantes con tolerancias bastante grandes [21], [23]. En la Figura 18, es posible para ver las imperfecciones que se pueden encontrar en un filamento nuevo.

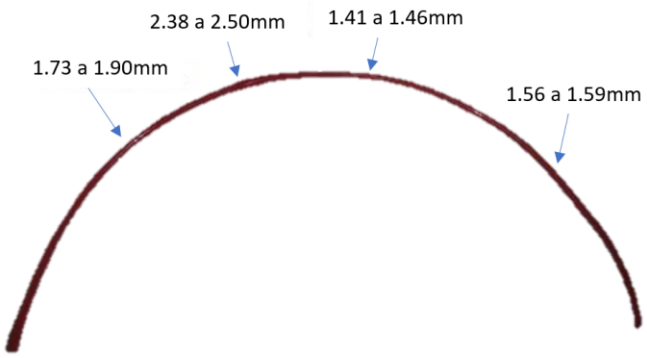

Figura 18. Variación de diámetro en una muestra de filamento

Durante el proceso de estudio, se tomó una muestra de 300cm de diferentes fabricantes de filamento, y se realizó una medida a través de un sensor de diámetro con una resolución de 0.01mm. La Figura 19 muestra las medidas registradas con el sensor:

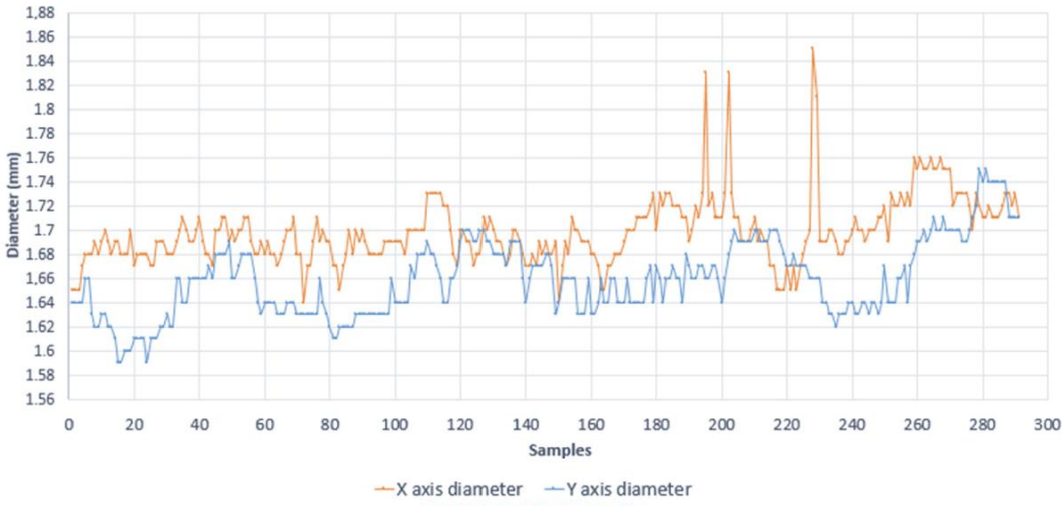

Filament provider A

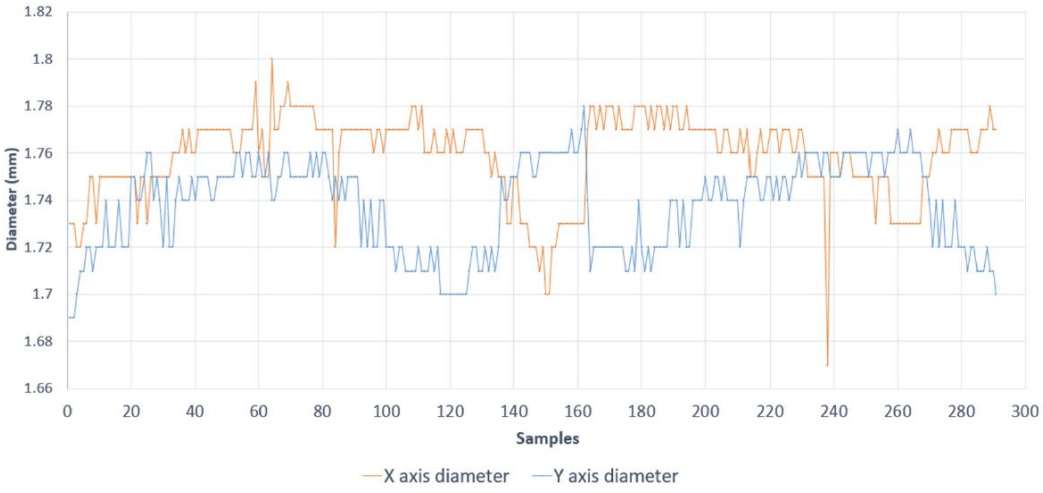

Filament provider B

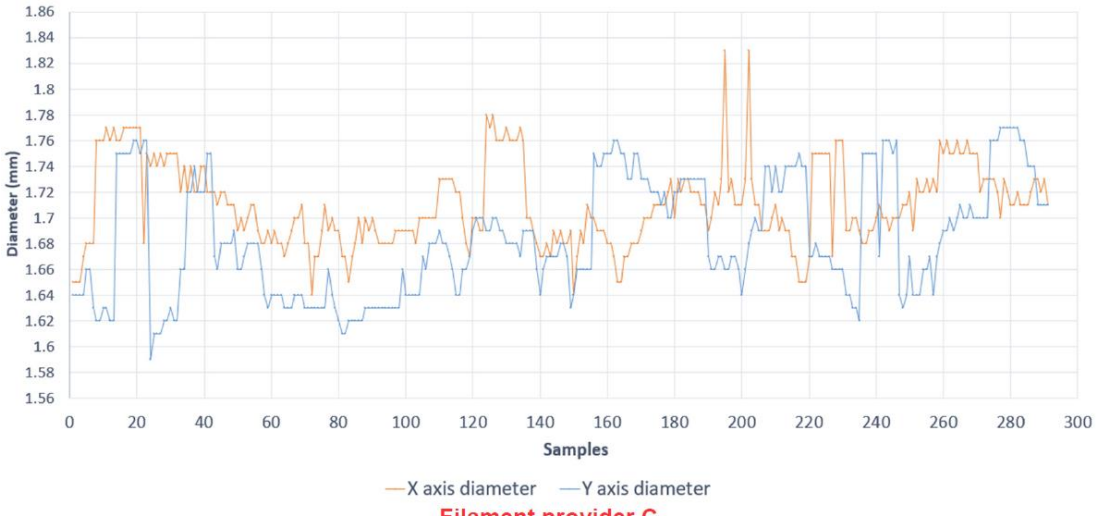

Filament provider C

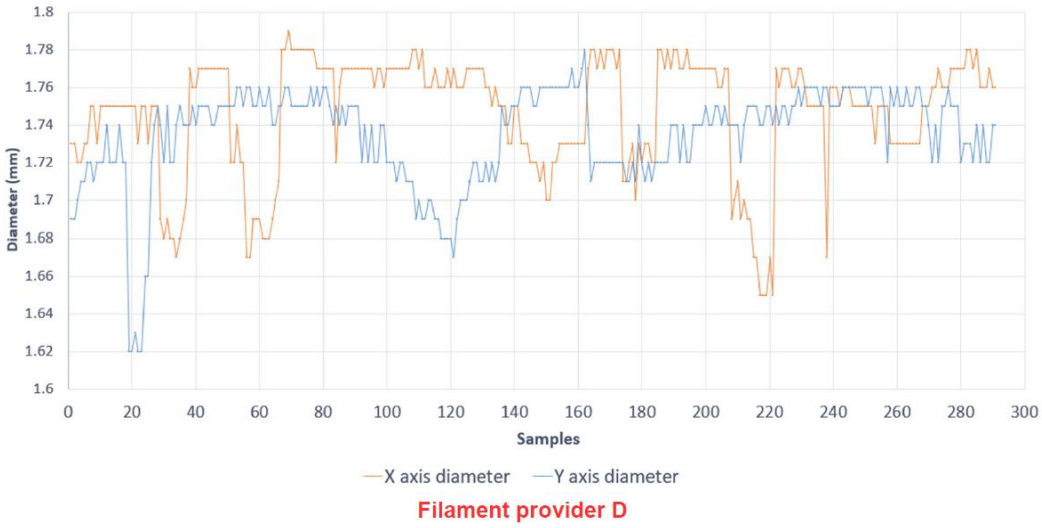

Figura 19. Variaciones de diámetro de cuatro fabricantes diferentes

Al analizar estas muestras (ver Tabla 2), es posible ver que el diámetro varía de 1,56 mm hasta 1,85mm. Esta es la razón principal de las obstrucciones del extrusor, un fallo típico en el método de fabricación por deposición fundida.

Tabla 2. Diámetro máximo, mínimo y medio de los filamentos analizados

Fabricante	D máximo (mm)	D mínimo (mm)	Media (mm)
A	1.85	1.59	1.68
B	1.80	1.67	1.75
C	1.84	1.56	1.75
D	1.83	1.59	1.78

Cualquiera de estos fallos supone perder la pieza que se está creando, lo que requiere que el proceso comience de nuevo. Además, al continuar imprimiendo sin plástico extruido, la máquina consume energía y produce un desperdicio innecesario. Debido a esta razón, el operador debe estar atento a la máquina mientras esté en funcionamiento, asegurándose de que el plástico fluye sin problema, lo que es especialmente difícil cuando la pieza tarda varias horas en producirse.

Otro de los problemas derivados de esto, es que el volumen de material depositado no es constante. Esto crea diferencias entre el espesor diseñado y el obtenido, lo que puede generar roces en caso de depositar demasiado material, o debilidades estructurales en caso de depositar menos material del necesario.

Estas alteraciones, junto con otras características como la temperatura o la humedad de la cámara de impresión, son extremadamente importantes en caso de utilizar materiales

biocompatibles. El uso de este tipo de materiales en ambiente no controlado puede ocasionar que se modifiquen o pierdan sus propiedades, lo que inutilizará el producto. Por todo esto, es necesario contar con una máquina que permita supervisar el proceso productivo. El seguimiento de todos estos datos permitirá conocer las condiciones a las que estuvo expuesto el producto durante el proceso. De esta forma podrá verificar la validez del producto final. Los parámetros elegidos para monitorizar son: diámetro del filamento, temperatura en la boquilla de extrusión, temperatura ambiente en cámara cerrada, humedad ambiental en cámara cerrada y velocidad de deposición de material.

El procedimiento se basará en sensores instalados en la electrónica de una máquina de fabricación que se encargarán de recoger los parámetros relevantes, en este caso la humedad, la temperatura ambiente en varios puntos, el diámetro real del filamento y la velocidad de entrada del filamento [81]. Adicionalmente, la impresora se comunicará con el sistema a través de SPI para suministrar de forma complementaria los datos de altura del eje Z y la temperatura de la extrusora.

Tras esto, es necesario programar un algoritmo de comunicación entre la placa controladora de los sensores y la impresora para coordinar la impresión con la recolección de datos además de extraer los datos directamente de los parámetros de la máquina.

La etapa final será recopilar vía puerto serie toda esta información de cada proceso de impresión y elaborar informes en los que se pueda ver en detalle si se han mantenido los estándares de calidad durante todo el proceso. Si no se ha mantenido, también será posible localizar el punto exacto de la pieza donde no se cumplió e incluso predecir futuras fallas estructurales.

Con todo ello, se pretende demostrar que se pueden fabricar objetos mediante deposición por fusión con estándares de calidad. La Tabla 3 muestra las especificaciones de los sensores.

Tabla 3. Sensores usados

Sensor	Medida	Precisión	Rango	Frecuencia
DHT11	Humedad	+-5% HR	20%-90%	500Hz-2kHz
LM35	Temperatura	+-0.5ºC	-55ºC-150ºC	-
NTC	Temperatura	+-0.5ºC	-55ºC-280ºC	-
DS18B20	Temperatura	+-2ºC	-55ºC-125ºC	-
TSL1401CL	Diámetro	1%	0.2V-2.4V	8MHz
Encóder HC020K	Velocidad	0,01mm/s	-	100kHz

- El sensor de humedad elegido es el DHT11 es un sensor previamente calibrado con una señal de salida digital.

- En cuanto a temperatura, se han utilizado dos sensores LM35, ya que es el que tiene más precisión y rango de temperatura entre los analizados. Este dispositivo es un sensor de temperatura lineal que consta de un circuito integrado y un encapsulado. Genera una tensión de salida proporcional a la temperatura de 10mV / ° C [82]. Las funciones que relacionan la temperatura y el voltaje de salida son:

$$T = 100 \cdot Vout$$

Y como el convertidor analógico - digital del microcontrolador tiene una resolución de 10 bits con un voltaje de referencia de 5 V:

$$T = 100 \cdot Ain \frac{Vref}{2^{10}}$$

Donde T = temperatura medida, Vref = 5V y Ain = señal leída por la placa.

- El encóder HC020K se utilizará para medir la velocidad de alimentación filamento en la entrada de la extrusora. Un encóder óptico consta de un foto interruptor y una rueda con muescas que lo activan y desactivan. En la figura 20 es posible ver un ejemplo de cómo funciona un codificador.

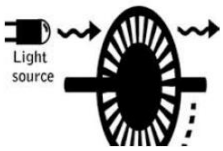

Figura 20. Encóder óptico

El movimiento lineal del filamento es transformado por un eje dentado [83] en un movimiento de rotación que es medido por el codificador contando los pulsos de luz. Se pretende obtener la velocidad y distancia recorrida del material a la entrada de la extrusora. Para obtener la distancia utilizamos la siguiente ecuación:

$$X = X_0 + \frac{n \cdot \pi \cdot D}{N}$$

Donde x = distancia total, x0 = distancia medida anterior, n = pulsos detectados, D = diámetro del eje dentado, N = 20 (muescas de la rueda). Para medir la velocidad,

simplemente sería necesario dividir la distancia medida desde la última muestra entre el tiempo de muestreo. En la Figura 21 se muestra el encapsulado diseñado para alojar el encóder óptico.

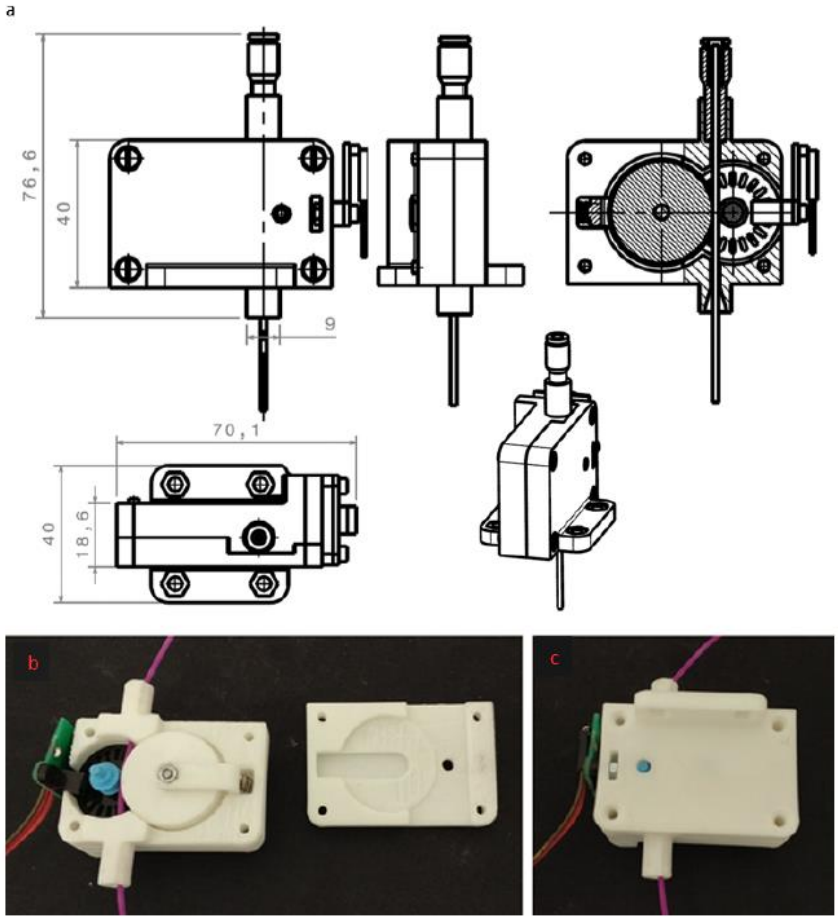

Figura 21. Encapsulado diseñado para medir la velocidad de entrada de material con dimensiones en mm (a) y modelo real abierto (b) y cerrado (c)

- El sensor de diámetro elegido es el 3D V3.2 diseñado por JasonKits [84]. Su componente principal es el TSL1401CL, un sensor de matriz de fotodiodos de 128 bits dispuesto en línea. Por medio de una electrónica de control, la sombra proyectada por el filamento sobre el sensor de fotodiodo se pasa a una tensión de salida correspondiente al diámetro en milímetros. De esta forma una proyección de 1,75 mm de espesor genera a la placa una salida de 1,75V. Esta señal es recogida por el convertidor analógico - digital del microcontrolador.

Mediante la combinación de sensor de avance y sensor de diámetro podemos obtener la medición en tiempo real del flujo de material que ingresa al extrusor:

$$\bar{Q} = \bar{v} \cdot A = \bar{v} \cdot \pi \cdot \frac{D^2}{4}$$

Donde Q = flujo, v = velocidad del filamento, A = área de la sección y D = diámetro del filamento.

Con todos estos datos, será posible realizar un informe para cada proceso de fabricación, según las condiciones en las que se ha llevado a cabo el proceso.

Estudio de materiales

Como se ha explicado anteriormente, la evolución de los materiales para FDM ha crecido exponencialmente en los últimos años. Dependiendo del uso que se vaya a dar al producto real, así como del proceso de fabricación, será necesario emplear uno u otro material. Como es lógico, cada material tiene sus propias características mecánicas (en la Tabla 4 se pueden ver las propiedades mecánicas del PLA). Es por esto que, se hace necesario el estudio de diferentes materiales biocompatibles, para comparar entre las diferentes opciones y poder encontrar el material idóneo. Además, se deberán tener en cuenta las restricciones de la máquina, para el proceso de fabricación. El material y el proceso deben seguirse cuidadosamente para evitar problemas de biocompatibilidad [17], [18].

Tabla 4. Propiedades mecánicas del PLA

Propiedad	Unidades	Valor
ρ (Densidad)	g/cm3	1.21–1.25
σ (Resistencia a la extensión)	MPa	21.0–60.0
E (Módulo de Young)	GPa	0.35–3.50
ε (Tensión de rotura)	%	2.50–6.00
σ* (Resistencia a la extensión específica)	Nm/g	16.8–48.0
E* (Módulo de Young específico)	kNm/g	0.28–2.80
Tg (Temperatura transición vítrea)	°C	45–60
Tm (Temperatura de fusión)	°C	150–162

Se propone para este estudio, el análisis de diferentes materiales biocompatibles, que serán analizados en detalle. En la Tabla 5 se muestran los materiales seleccionados junto a las características de impresión.

Tabla 5. Materiales seleccionados y características de impresión

Filamento	Diámetro	Temperatura de fusión	Base calefactada
ABS Smartfil Medical [85]	1.75mm	240ºC	90ºC
PETG Smartfil sterilizable [86]	1.75mm	240ºC	No necesaria
PLA Smartfil Antibacterial [87], [88]	1.75mm	220ºC	No necesaria
PLA 3D870 [89]	1.75mm	220ºC	No necesaria
NYLON Smartfil Nylstrong [90]	1.75mm	260ºC	90ºC
PLA 3D850 [91]	1.75mm	220ºC	No necesaria

Es importante señalar que uno de los materiales seleccionados, ABS Smartfil Medical, ha sido diseñado para fines médicos y cuenta con las certificaciones USP Clase VI e ISO 10993-1[92], [93]. En la tabla 6 se muestran los resultados según diferentes ensayos de este material específico.

Tabla 6. Características mecánicas del ABS Smartfil según diferentes ISO [94]

Características	Resultado	Tipo de ensayo
Resistencia al impacto	124KJ/m2	ISO 179
Módulo de flexión	2600 MPa	ISO 178
Resistencia a la flexión	75 MPa	ISO 178
Impacto Izod	15 kJ/m2	ISO 180
Dureza	106Mpa	ISO 2039-1
Densidad	1.05g/cm3	ISO 1183
Resistencia a la tracción	36.5 MPa	ISO 527
Módulo de tracción	2550 MPa	ISO 527
Resistencia térmica	101ºC	ISO 306

Los ensayos que se realizan son:

- Ensayo de tracción

  Se realizan una serie de probetas para ensayar, según la norma Norma UNE Fabricación Aditiva-UNE_116005_2012. En la Figura 22 se muestra el plano de la probeta, y la preparación del G-Code para imprimir dichas probetas. La colocación elegida ha sido en vertical, para poder evaluar la adhesión entre capas de los diferentes filamentos, dado que las férulas se producen en la misma posición.

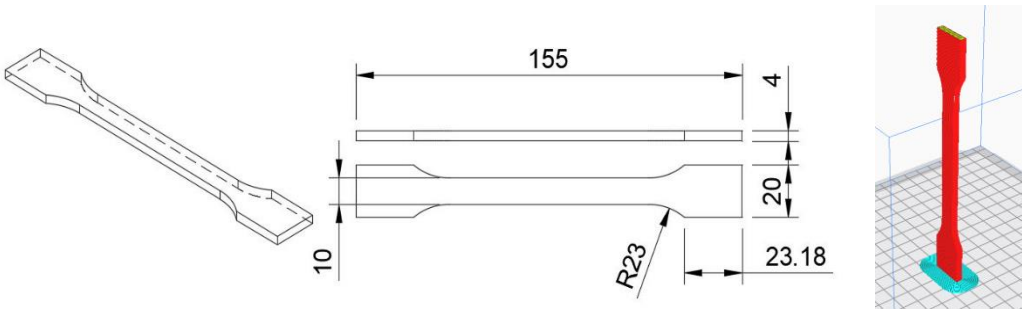

Figura 22. Cotas en mm de la probeta para el ensayo de tracción (a) y preparación del G-Code (b)

- Test de Izod

Se realizan una serie de probetas para ensayar, según la norma Norma UNE Fabricación Aditiva-UNE_116005_2012. En la Figura 23 se muestra el plano de la probeta, y la preparación del G-Code para imprimir dichas probetas. La colocación elegida ha sido en vertical, para poder evaluar la resistencia al corte entre capas de los diferentes filamentos, dado que las férulas se producen en la misma posición.

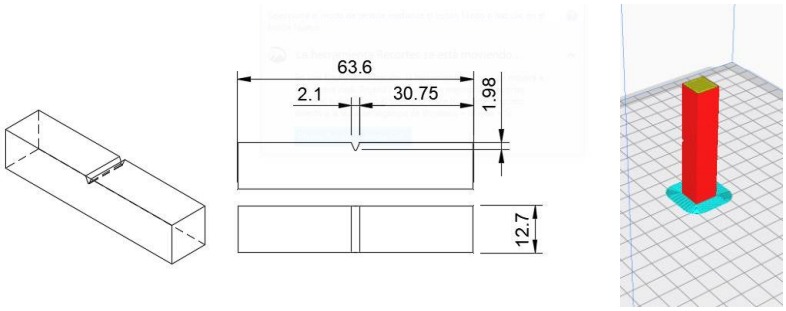

Figura 23. Cotas en mm de la probeta para la prueba de Izod (a) y preparación del G-Code (b)

- Calorimetría

Para el análisis por calorimetría se ha empleado una muestra de 5mm de cada uno de los filamentos.

Desarrollo software y hardware

Durante el desarrollo de la presente tesis, se han desarrollado dos sistemas independientes. En un primer prototipo, se contó con una placa de desarrollo, que ha de contar con conexión cableada a un equipo para registrar los datos, para después pasar a una placa totalmente autónoma, con batería, módulo wifi, bluetooth y pantalla incorporadas.

- Software de programación Arduino (Arduino, Italia)

Arduino es una empresa de hardware y software de código abierto, para proyectos y usuarios que diseñan y fabrican microcontroladores de placa única y kits de microcontroladores para la construcción de dispositivos digitales. Sus productos de hardware tienen una licencia CC-BY-SA, mientras que el software tiene la licencia GNU Lesser General Public License (LGPL) o la GNU General Public License (GPL), que permite la fabricación de placas Arduino y la distribución de software.

En el artículo ***"Development of a Smart Splint to monitor different parameters during the treatment process"*** [74] se usa un Arduino UNO para realizar el primer prototipo, y comprobar la viabilidad del sistema. Una vez comprobado esto, se pasa a usar una segunda plataforma, "ESP32 TTGO OLED and battery board". Esta nueva plataforma se emplea en el desarrollo del artículo ***"Development of a smart leg splint by using new sensors technologies and new therapies possibilities"*** [95]. Se elige esta plataforma para poder llevar a cabo los objetivos secundarios **"Acceso de manera telemática a los datos desde dispositivo conectado a internet"** e **"Implementación de algoritmo para detección de inflamaciones mediante cambios de presión, temperatura o color de la zona afectada"** consiguiendo un dispositivo autónomo, compatible con el software de programación Arduino.

El equipamiento electrónico, tal y como se ha adelantado en el punto anterior ha sido:

- Microcontrolador ATmega328, a 16MHz (Figura 24)

- Velocidad de reloj: 16MHz
- Salida máxima de 150 mA
- Peso inferior a 2 gramos
- Entrada DC 5V hasta 12V
- Leds de encendido y de estado integrados
- Puertos analógicos: 8
- Puertos digitales I/O: 14

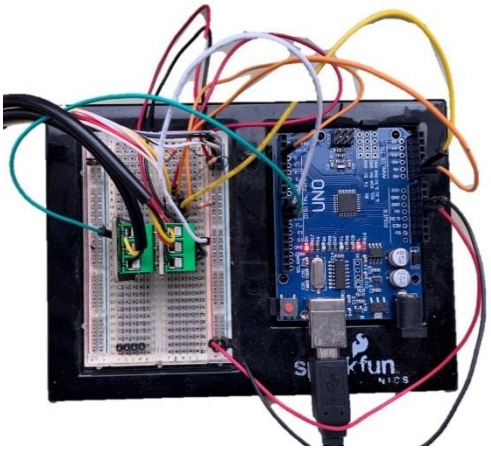

Figura 24. Montaje electrónica Arduino UNO. Fuente: Elaboración propia

- ESP32 TTGO OLED and battery board (Figura 25)
  - Chip Wi-Fi ESP32 @ 80 MHz - 802.11 b/g/n
  - ESP-WROOM-32 Module, con conectividad Wi-Fi y Bluetooth
  - Circuito de carga de batería incluido, para poder recargar el sistema con un cargador micro USB
  - Pantalla OLED

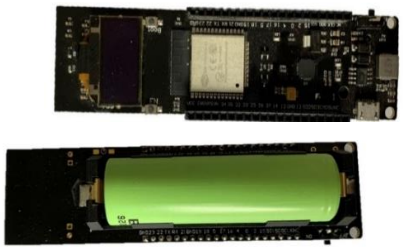

Figura 25. ESP32 TTGO OLED and battery board. Fuente: Elaboración propia

Para leer correctamente los datos de los sensores, es necesario desarrollar una placa electrónica que permita conectar todo fácilmente. Es importante centrarse en un diseño duradero, ligero y de dimensiones reducidas. Teniendo en cuenta estos propósitos principales, se diseña una placa que se instalará directamente en el módulo de batería y pantalla OLED TTGO, que se muestra en la Figura 25. Esta placa tiene dos convertidores de analógico a digital (ADC1 y ADC2). La resolución de estos convertidores es de 12 bits. Un ADC de 12 bits significa que puede leer 2 ^ 12 valores entre 0 y 5v. Por tanto, serían un total de 4096 valores, permitiendo detectar cambios de 1,22mv, que es suficiente para lo requerido por los sensores seleccionados. El ADC1 se utiliza para los sensores, mientras que el ADC2 se utiliza para la comunicación entre el microprocesador y el módulo Wi-Fi, que se utilizará para crear el servidor web [96].

Es necesario instalar diferentes componentes pasivos, así como terminales para conectar correctamente cada sensor. Es posible ver el diseño y montaje en las Figuras 26a y 26b. El conjunto electrónico final se muestra en la Figura 26c.

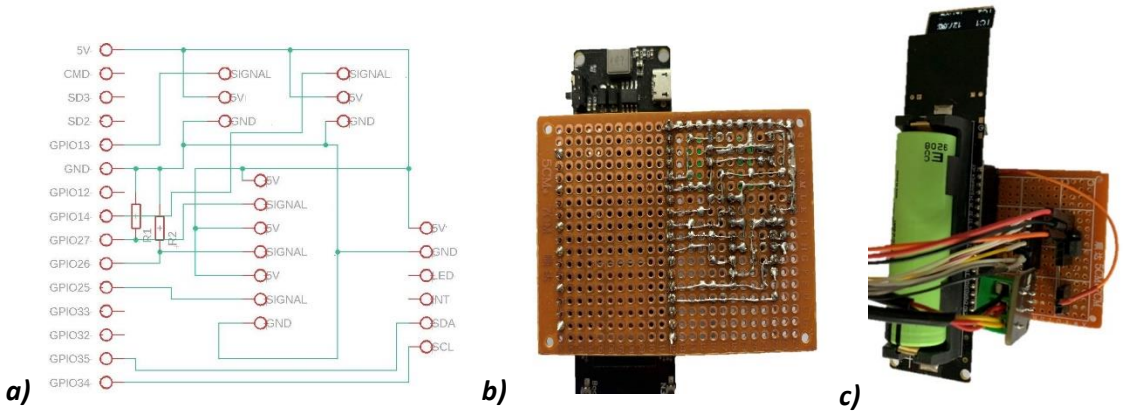

Figura 26. Diseño esquemático del circuito (a), proceso de soldadura (b) y electrónica ensamblada (c)

La placa elegida, como se explicó anteriormente, permite ser accedida desde otros dispositivos a través de diferentes formas y protocolos. Tiene una pantalla OLED que puede mostrar los datos adquiridos (presiones, temperaturas, humedad y detección de cambio de color). Además, es posible crear una conexión Bluetooth con un teléfono móvil o dispositivo similar. Sin embargo, en este caso, se seleccionará la opción de crear un servidor web. De esta forma, la información puede ser consultada desde cualquier dispositivo conectado a Internet, en cualquier parte del mundo. El gran beneficio de esto es que un médico puede ver los datos y seguir el tratamiento en tiempo real desde su lugar de trabajo.

El consumo real total de la placa electrónica y el sistema de detección es de 84,66mA. Debido a que la batería tiene una capacidad de 12210mAH, la autonomía del sistema ronda las 144h. Esto significa que el sistema es capaz de recolectar datos durante seis días sin cargar la batería, lo que es muy significativo porque la primera semana después de ocurrida la lesión, es el período más importante para analizar. Cuando la autonomía se agota, es posible reemplazar o cargar la batería.

4. RESULTADOS

En este capítulo se exponen los resultados según las técnicas y procedimientos expuestos en el capítulo anterior, en la fabricación de los modelos 3D y el posterior desarrollo para la implementación de los sistemas electrónicos, así como los datos que han sido recogidos en las publicaciones y artículos que generan esta Tesis Doctoral.

Ensayo de los diferentes materiales

En el artículo ***"Filament advance detection sensor for fused deposition modelling 3d printers" (Sensors, 2018)*** se estudian las características de diferentes filamentos de fabricación por deposición fundida. Es posible ver que las máquinas sencillas no permiten un control correcto de diferentes parámetros que afectan a la calidad del producto final. Se realiza un estudio del diámetro del material de diferentes fabricantes, encontrando diferencias de calidad considerables.

Tras esto, en los artículos ***"Monitoring of the additive manufacturing process for the use of biomaterials in medical" (TEEM 2018)*** y ***"Monitoring an Analysis of Perturbations in Fusion Deposition" (JOURNAL OF MEDICAL SYSTEMS 2019)*** se pasan a analizar los diferentes parámetros que afectan al proceso de fabricación, especialmente para el uso de materiales biocompatibles.

En el artículo ***"Real time analysis of the filament for FDM 3D printers" (TEEM 2019)*** se emplea dicha máquina para producir una serie de probetas, provocando variaciones en los parámetros, para posteriormente analizar mecánicamente dichas probetas.

Una vez comprobadas las características que afectan a la calidad dimensional y mecánica de las piezas producidas, se pasa a realizar el estudio con diferentes materiales biocompatibles. En el artículo ***"Fused deposition manufacturing for biocompatible materials certification"*** **(que se encuentra actualmente en edición para ser publicado)** se recogen diferentes materiales biocompatibles que hay actualmente en el mercado.

Para las pruebas de los diferentes materiales, se han producido un total de 6 probetas por ensayo con cada uno de los materiales. En la Tabla 7 se muestran los parámetros de impresión.

Tabla 7. Parámetros de impresión

Altura de capa [mm]	**0.2**
Diámetro de extrusor [mm]	0.4
Densidad interior [%]	40
Espesor de perímetro [mm]	1
Velocidad de impresión [mm/s]	60

En las Figuras 27 y 28 se muestra una unidad de cada probeta y material.

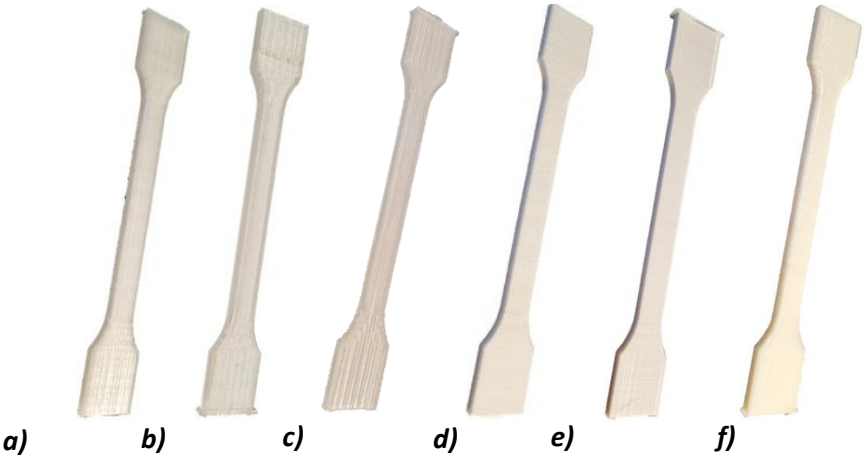

Figura 27. Probetas para tracción de los diferentes materiales. 3D870 (a), 3D850(b), PETG (c), Nylstrong (d), Antibacterial (e), Medical (f)

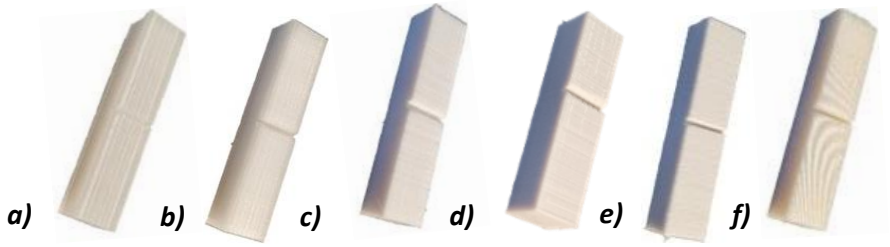

Figura 28. Probetas para test de Izod de los diferentes materiales. 3D870 (a), 3D850(b), PETG (c), Nylstrong (d), Antibacterial (e), Medical (f)

Análisis dimensional

Primeramente, se realiza un análisis dimensional de cada una de las probetas obtenidas. Hay que remarcar, que en el caso de las probetas para Izod de Nylstrong, la medida longitudinal, se perdió debido a un fallo durante el proceso de producción. No obstante, como dicha dimensión no interfiere en la correcta realización del ensayo, se dio por válida la producción. En la tabla 8, se muestran las medias de las diferentes medidas tomadas a las probetas. Las cotas para las probetas de tracción son A=20mm, B=4mm, C=10mm. Para las de Izod, las cotas son A=12.7mm, B=12,7mm, C=63,6mm.

Tabla 8. Dimensiones medias en mm de las probetas

Probetas para Tracción	Cota A	Cota B	Cota C
PLA 3D870	20,34	4,41	10,22
PLA 3D850	20,22	4,37	10,16
Sterilizable PETG	19,96	4,43	10,13
Nylstrong	20,38	4,66	10,28
Antibacterial PLA	20,44	4,48	10,28
Medical ABS	20,07	4,62	10,26

Probetas para Izod	Cota A	Cota B	Cota C
PLA 3D870	13,26	13,17	63,41
PLA 3D850	13,20	13,21	63,59
Sterilizable PETG	13,09	12,98	63,58
Nylstrong	13,22	13,13	63,59
Antibacterial PLA	13,28	13,20	-
Medical ABS	13,17	13,09	63,45

Los errores dimensionales se muestran en la Figura 29:

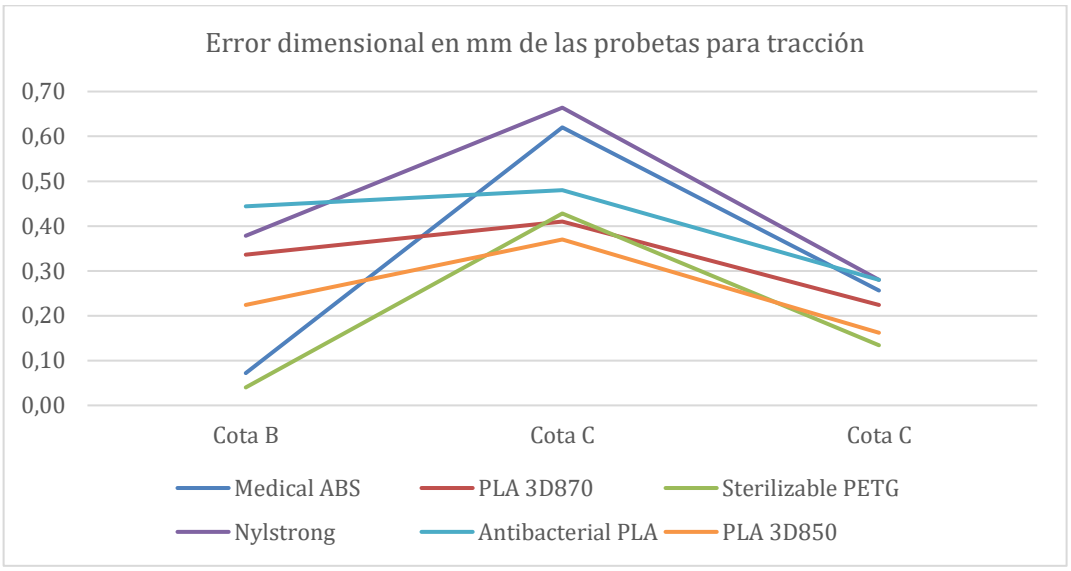

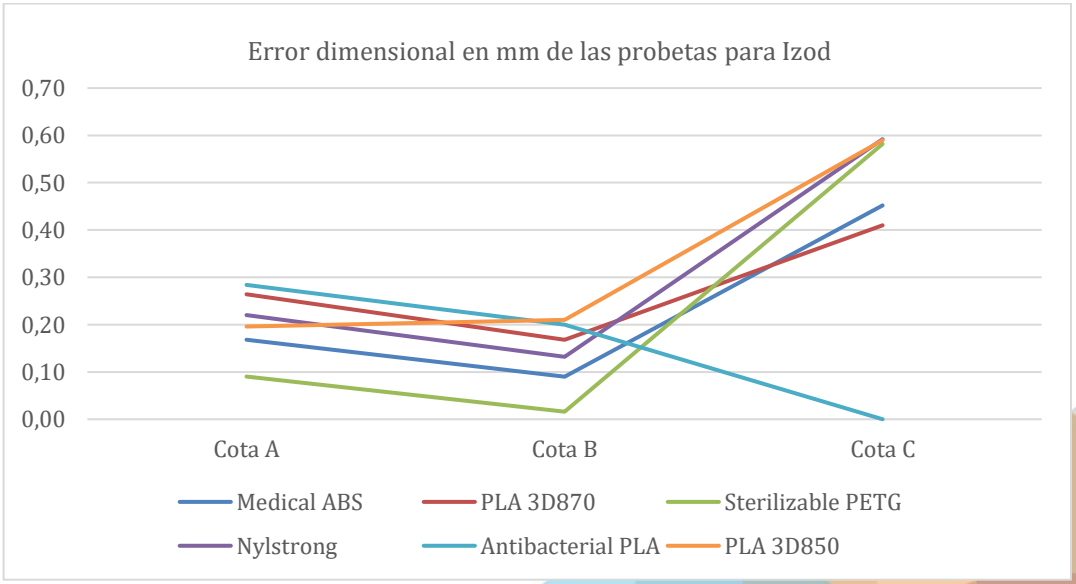

Figura 29. Error dimensional medio en mm de las diferentes probetas

Es posible observar que todos los materiales se expanden en el plano horizontal, siendo el PETG esterilizable el que mejor se comporta. Además, se aprecia que todos se expanden en el eje normal al plano de las capas una media de 0.5mm. Es curioso ver que el mayor error lo encontramos en la Cota C en todas las probetas de tracción. Esto podría deberse a algún error de precisión de la máquina en ese eje.

Calorimetría

Para el ensayo de calorimetría, se toman muestras de cada uno de los filamentos, y se emplea el equipo SDT Q600 cuyas características se muestran en la tabla 9:

Tabla 9. Especificaciones técnicas del equipo SDT Q600

System Design	Horizontal Balance & Furnace
Balance Design	Dual Beam (growth compensated)
Sample Capacity	200 mg (350 mg including sample holder)
Balance Sensitivity	0.1 µg
Furnace Type	Bifilar Wound
Temperature Range	Ambient to 1500°C
Heating rate – Ambient to 1000 °C	0.1 to 100 °C/min
Heating rate – Ambient to 1500 °C	0.1 to 25 °C/min
Furnace Cooling	Forced Air: 1500 to 50 °C in < 30 min 1000 to 100°C in < 20 min
Thermocouples	Platinum/Platinum Rhodium (T pe RI)
Temperature Calibration	Curie Point or Metal Standards (1 to 5 Points)
DTA Sensitivity	0.001 ‘C
Calorimetric Accuracy/Precision	±2% (based on metal standards)
Mass Flow Controller with Automatic Gas Switching	
Vacuum	to 7 Pa 10.05 torr)
Reactive Gas Capability	Included – separate gas tube
Dual Sample TGA	Included
Auto-Stepwise TGA	Included
Sample Pans	Platinum: 40 µL, 110µL Aluminia: 40µL, 90µL

Los resultados de los ensayos se pueden ver en las Figuras 30, 31 y 32.

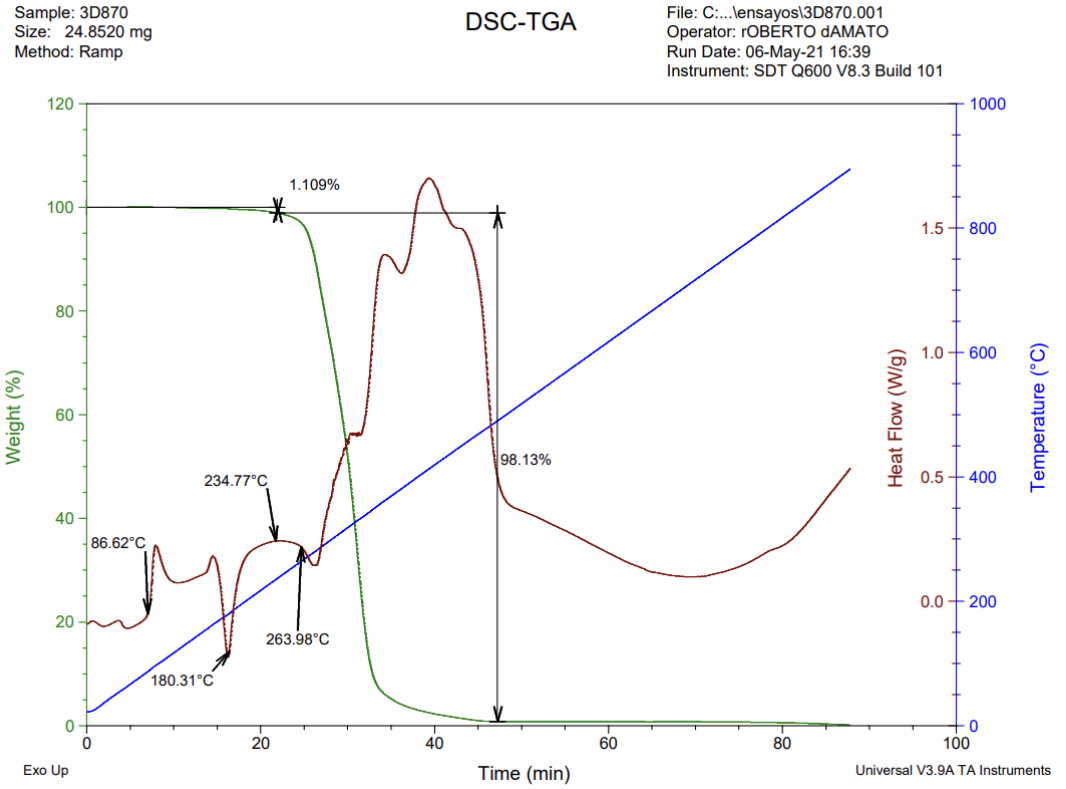

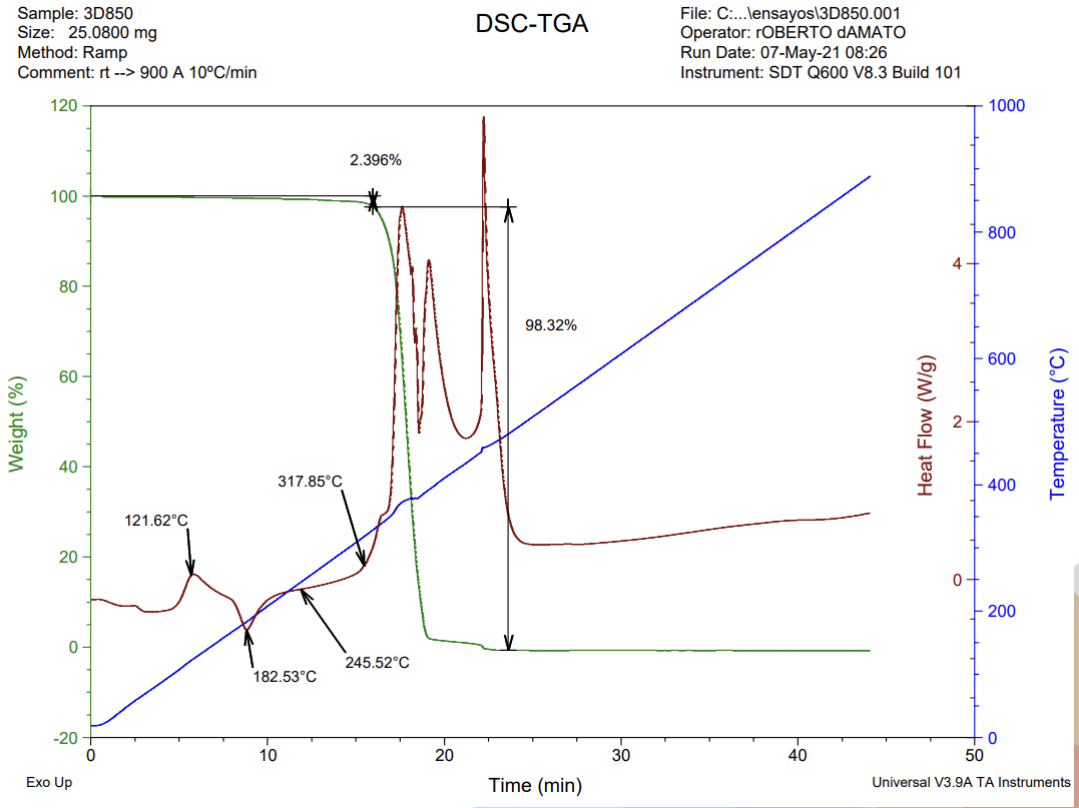

Figura 30. Resultados ensayo calorimetría de los materiales 3D870 y 3D850

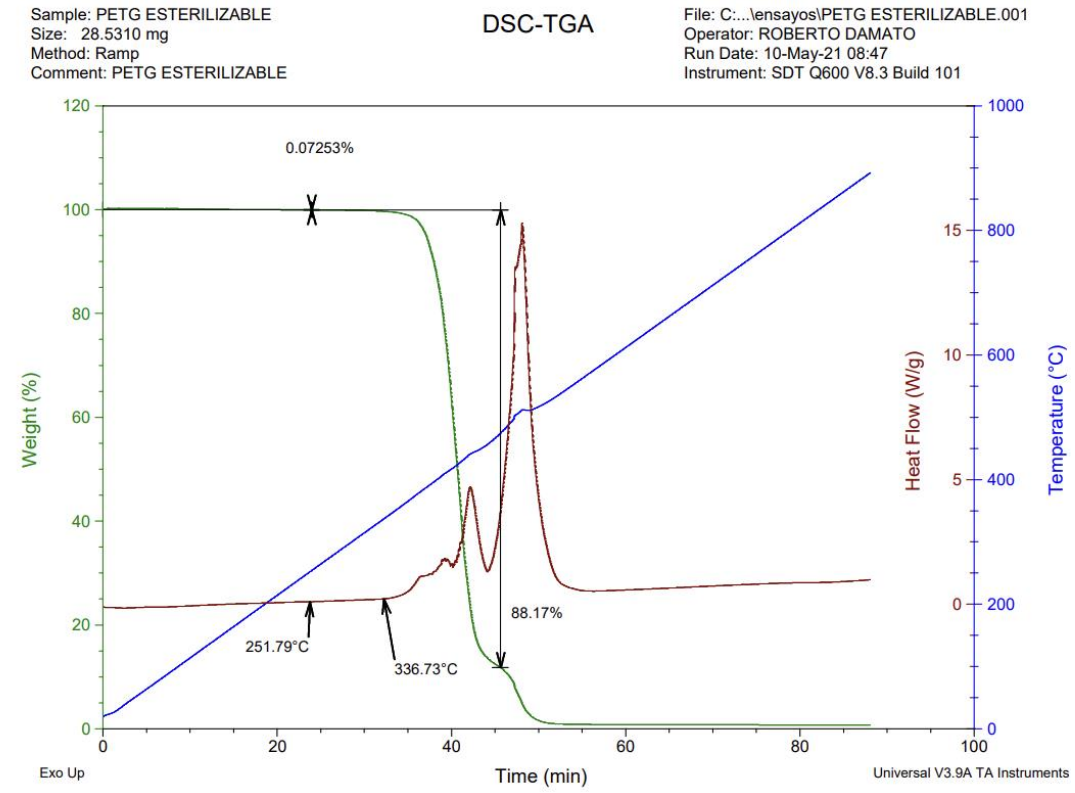

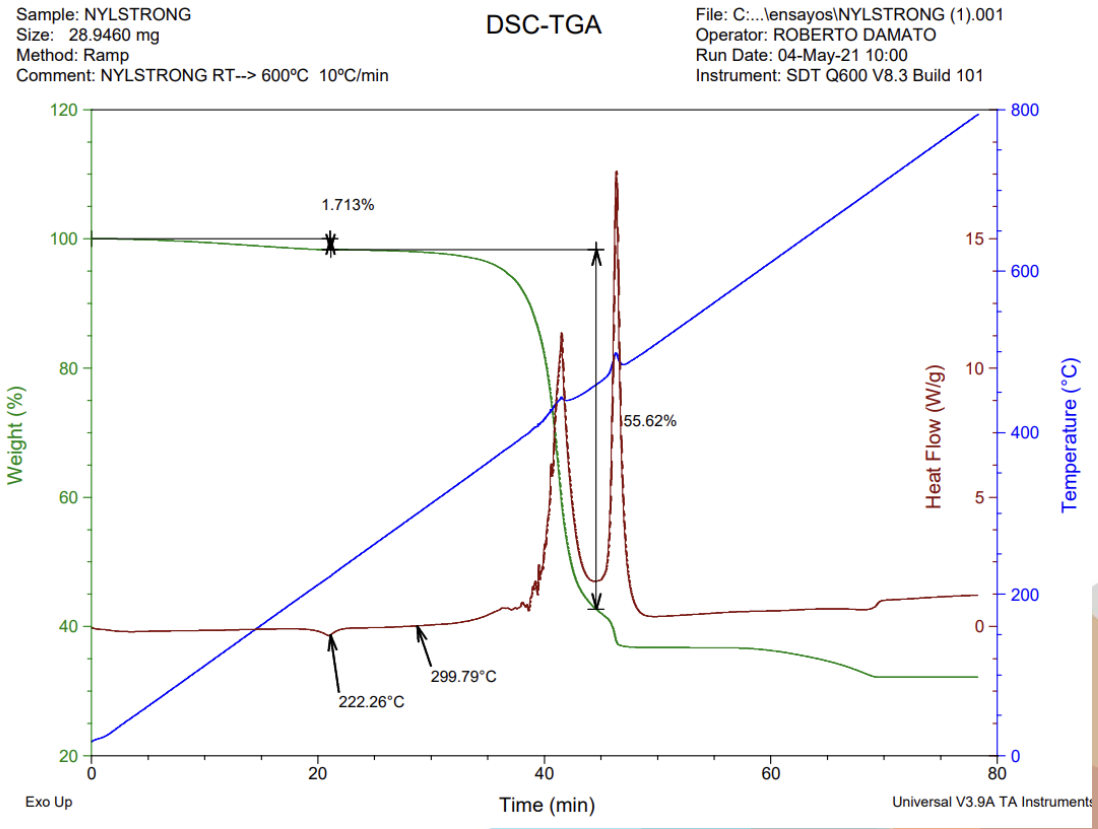

Figura 31. Resultados ensayo calorimetría de los materiales PETG esterilizable y Nylstrong

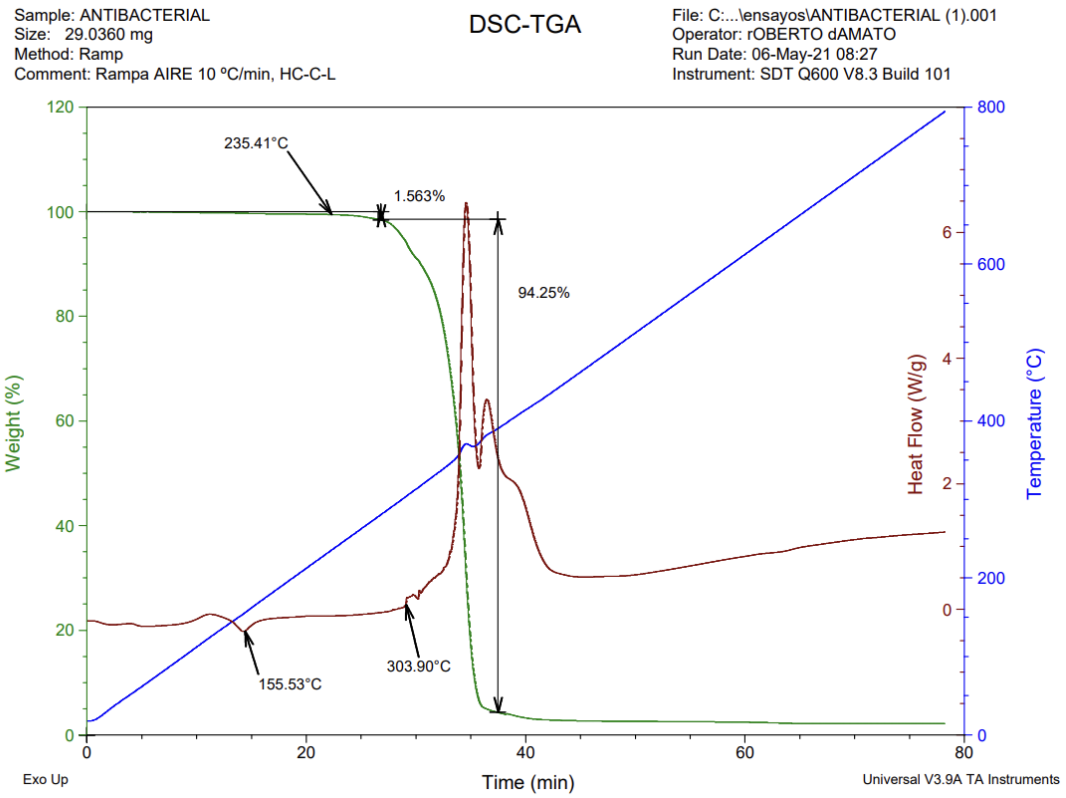

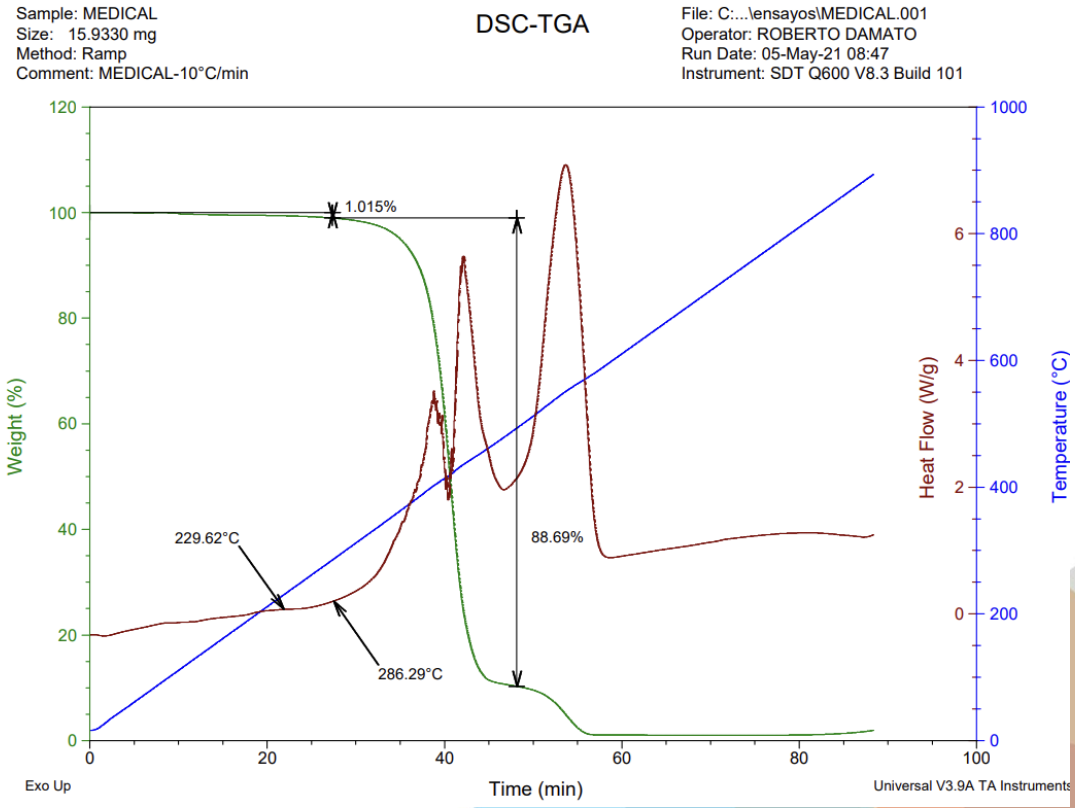

Figura 32. Resultados ensayo calorimetría de los materiales Antibacterial y Medical

Como se puede apreciar en las figuras, y como era de esperar, los materiales se comportan de formas muy diferentes dependiendo de su composición. Se puede apreciar que en las muestras de PLA (3D870 y 3D850) comienza a haber diferentes reacciones desde temperaturas inferiores a los 90ºC. Incluso, a partir de 50ºC se empiezan a ver cambios del estado. Esto supone que no sea el material más adecuado para el uso en férulas, ya que podría perder características mecánicas durante el uso a sol o en contacto a fuentes de calor. Además, interesante ver que hasta que alcanza la temperatura estable de fusión (que es superior a la recomendada por el fabricante), se producen diferentes cambios que podrían emitir componentes al aire. Estos componentes suponen entorno al 1.5% de la masa del material, antes de alcanzar la temperatura de fusión. A partir de los 260ºC, la pérdida de material es casi total en poco tiempo.

En el caso del PETG, el comportamiento es muy estable. Al alcanzar la temperatura de fusión recomendada por el fabricante, el material únicamente ha perdido un 0.07% de su masa. Es a partir de los 330ºC cuando comienza a deteriorarse. Hay que remarcar, que no se aprecia el punto de fusión de material, probablemente debido a que la muestra no era suficiente como para detectar la variación de temperatura.

El material Nylstrong, de forma similar al PETG, se comporta de una forma muy estable con el incremento de temperatura, hasta alcanzar los 222ºC, donde se aprecia un cambio en el que se evapora alguno de los componentes, produciendo una pérdida de masa superior al 1.7%. Sin embargo, la temperatura de trabajo recomendada por el fabricante es de 260ºC. Por tanto, la evaporación de sustancias que se produce hasta alcanzar la temperatura, libera al entorno diferentes componentes, que lo pueden inutilizar para el trabajo en determinados entornos.

Al analizar el material Antibacterial, se aprecia que en el punto de trabajo recomendado por el fabricante (220ºC), prácticamente no ha perdido masa, siendo a partir de los 235ºC cuando se aprecia que esto empieza a suceder. A partir de los 300ºC, el material se evapora rápidamente. Además, es curioso ver cómo en el entorno de los 120 a 160ºC se producen diferentes reacciones, que del mismo modo que en casos anteriores, pueden limitar su uso en determinados entornos.

Por último, en el caso del material Medical, su comportamiento es bastante estable, y entorno al punto de fusión, ha perdido menos del 1% de su masa, siendo a partir de los 286ºC cuando se empiezan a evaporar el resto de los componentes. Al igual que en el caso del PETG no se aprecia el punto de fusión de material, probablemente debido a que la muestra no era suficiente como para detectar la variación de temperatura.

Tras realizar este análisis por calorimetría, así como el dimensional, podemos decir que los componentes más adecuados para la fabricación por FDM de férulas, serían el PETG o el Medical. No obstante, hay que recordar tal y como se vio en el apartado 3 de este estudio, que el uso de material Medical requiere el uso de base calefactada, que no es necesario para poder emplear el PETG Esterilizable.

Los ensayos de tracción e Izod se encuentran actualmente en proceso de ser realizados y se publicarán en un futuro estudio.

Montaje de las férulas para la recogida de datos

En el primer desarrollo se realiza un prototipo de férula para brazo, en el que se estudia la posibilidad de recoger diferentes datos y se prepara una electrónica que monitorice dichos datos. Este trabajo se muestra en los artículos ***"Development of an individual smart splint to monitor different parameters during the treatment process" (Sensors, 2020)*** *y* ***"Smart Splint for diagnosis during initial stage of treatment" (TEEM 2020).***

Tras esto, se lleva a cabo el segundo desarrollo con una férula para pierna. Además, se incorpora una la electrónica autónoma, accesible a través de internet, de modo que los datos puedan ser consultados por un especialista de manera remota. Por último, se incorporan datos sobre terapias a aplicar para mejorar la evolución y recuperación de las posibles lesiones. Esta segunda fase se muestra en el artículo ***"Development of a smart leg splint by using new sensors technologies and new therapies possibilities" (Sensors, 2021)***

La posición vertical para la impresión se eligió como se muestra en la Figura 33, teniendo en cuenta el volumen de la cámara de esta máquina (200 mm x 200 mm x 400 mm). En la Tabla 10, es posible ver los parámetros de impresión establecidos en el proceso de fabricación, siguiendo las recomendaciones del fabricante del material para obtener una calidad y estructura lo suficientemente rígida.

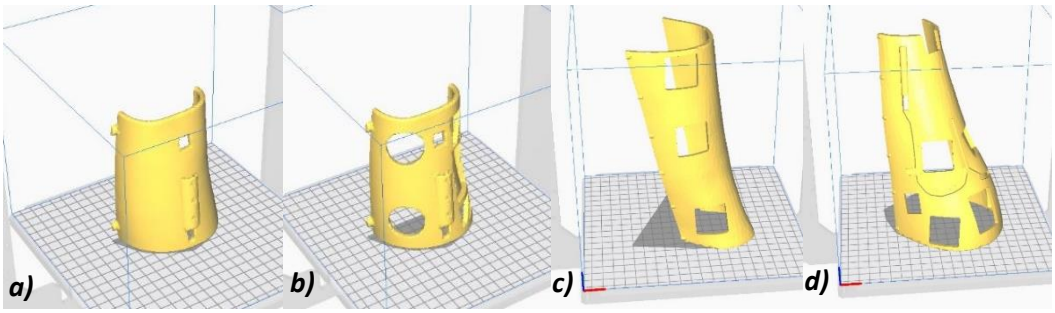

Figura 33. Colocación de las diferentes partes de las férulas para fabricación. Brazo superior (a), brazo inferior (b), pierna anterior (c) y pierna posterior (d)

Tabla 10. Parámetros de impresión

Altura de capa [mm]	**0.2**
Diámetro de extrusor [mm]	0.4
Densidad interior [%]	40
Espesor de perímetro [mm]	1
Velocidad de impresión [mm/s]	60
Temperatura [°C]	210

Unavez obtenido el modelo real, se procede al montaje de los sensores y el cableado. La figura 34a muestra las dos partes del prototipo de férula para brazo. Las figuras 34b y 34c muestran una parte de la férula del brazo con los sensores y cables, para la conexión al Arduino, totalmente integrados.

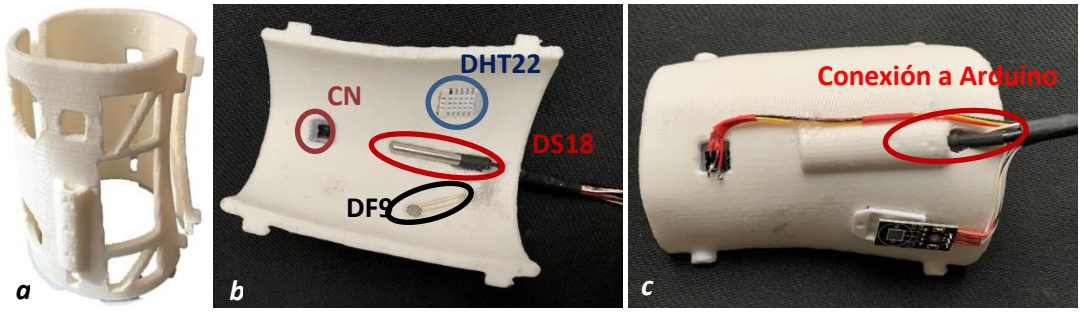

Figura 34. Modelo real de la férula de brazo obtenido de la impresora 3D (a). Férula ensamblada con los diferentes sensores (b) y cables para la conexión a la placa Arduino (c)

Una vez preparado el modelo, es necesario programar la placa Arduino para obtener los datos de estos sensores. Para este estudio, los datos se obtienen directamente de la comunicación serial entre la placa Arduino y el PC. Es importante detallar que los dos sensores de temperatura de

contacto y los dos sensores de presión se tratan digitalmente para obtener solo una temperatura y presión de contacto resultantes.

Para probar la férula del brazo ensamblada con los sensores conectados a la placa Arduino, la férula se fijó al brazo originalmente escaneado durante 1.5 h. Los datos de los sensores se recopilaron utilizando el monitor serie de Arduino cada 3 segundos y se enviaron a una tabla Excel para trazar algunas gráficas. La Figura 35 muestra el monitor en serie de los datos adquiridos mientras la férula estaba fijada al brazo del voluntario. Los datos obtenidos se muestran y explican en las siguientes secciones.

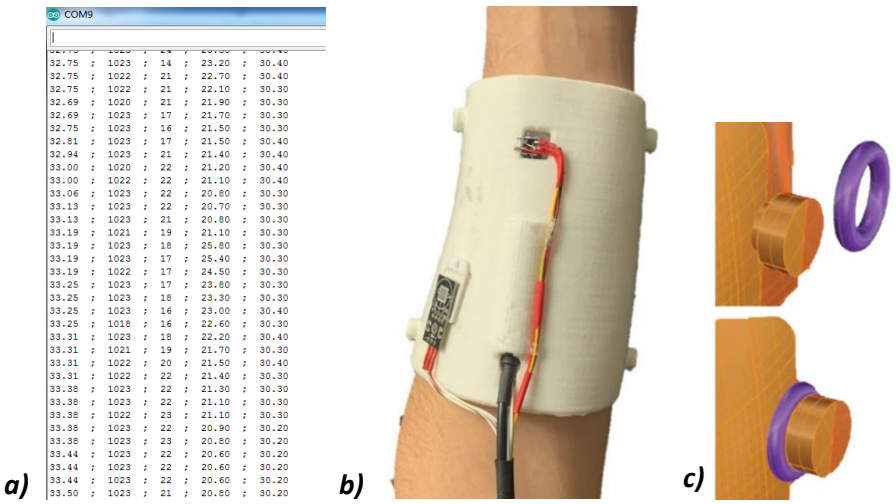

Figura 35.Ejemplo de recopilación de datos en serie utilizando la placa Arduino (a), prototipo de férula real con cableado eléctrico montado sobre el brazo (b) y vista detallada de los botones de cierre

En el caso de la férula para la pierna, los dispositivos electrónicos se ensamblan y los sensores se colocan en sus carcasas y se conectan a la placa electrónica. La Figura 36a muestra el prototipo de férula obtenido con el cableado y los sensores completamente ensamblados. En la Figura 36b es posible ver el interior de la férula con el alojamiento para los sensores.

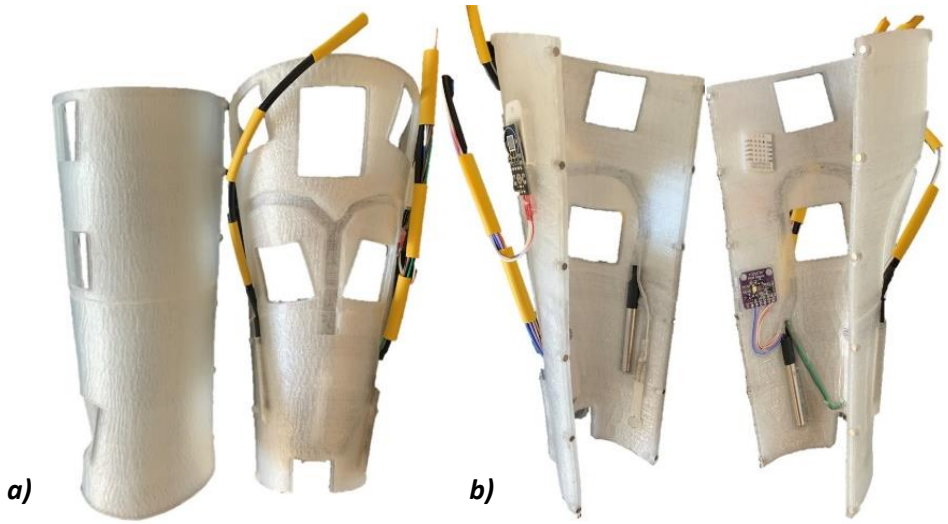

Figura 36. Férula real ensamblada con los sensores (a) y vista interior (b)

Para probar la férula de pierna completamente ensamblada en una pierna real, la férula se fijó a un voluntario sano durante 1.5 h (Figura 37). Se colocó al voluntario en posición sentada para las pruebas. Sin embargo, esta nueva "férula inteligente" es capaz de obtener datos de forma continua, por lo que el paciente no necesita adoptar posiciones particulares durante la adquisición de datos. El objetivo principal de esta prueba era recopilar datos para poder analizar si los sensores eran capaces de adquirir información correctamente. Los datos recolectados por los sensores fueron tratados con ESP32 micro y consultados a través del servidor web cada 3 segundos. En las siguientes secciones se explicarán los datos adquiridos.

Figura 37. Modelo real sobre la pierna del voluntario

Exposición de los datos recogidos por los sensores

En este apartado, se muestran y comentan los diferentes datos recogidos a través de los sensores (Temperaturas, Humedad, Presión, Presencia y Color de la piel).

Temperaturas

En la Figura 38 se muestra en rojo la temperatura media de los dos sensores en contacto con la piel. La temperatura dentro de la férula se muestra en azul. Se puede observar que los sensores en contacto con la piel registraron una temperatura ligeramente inferior a la temperatura normal de una persona (36ºC). Este hecho, se produce porque parte de la superficie de los sensores, no está en contacto real con la piel. Debido a esto, aparece un gradiente de temperatura entre el cuerpo y el medio ambiente. La distancia entre la piel y la superficie del sensor que no está en contacto con la piel es de unos 4mm. Esta distancia no es suficiente para interferir con el correcto funcionamiento del sensor. Lo que se busca en este estudio con estos sensores, es detectar un incremento o decremento de la temperatura, en comparación con el histórico. Por este motivo, la superficie del sensor que no esté en contacto no interferirá para detectar correctamente las variaciones.

Como se puede ver en el gráfico, el segundo sensor (en azul), que está completamente separado de la piel, registró alrededor de dos grados menos que los sensores en contacto. Con tan solo estas lecturas se detecta perfectamente una variación de la temperatura, que podría ser síntoma de inflamación o infección de la zona. Esta información se puede utilizar con los niveles de humedad para descubrir anomalías o diferentes situaciones durante los tratamientos.

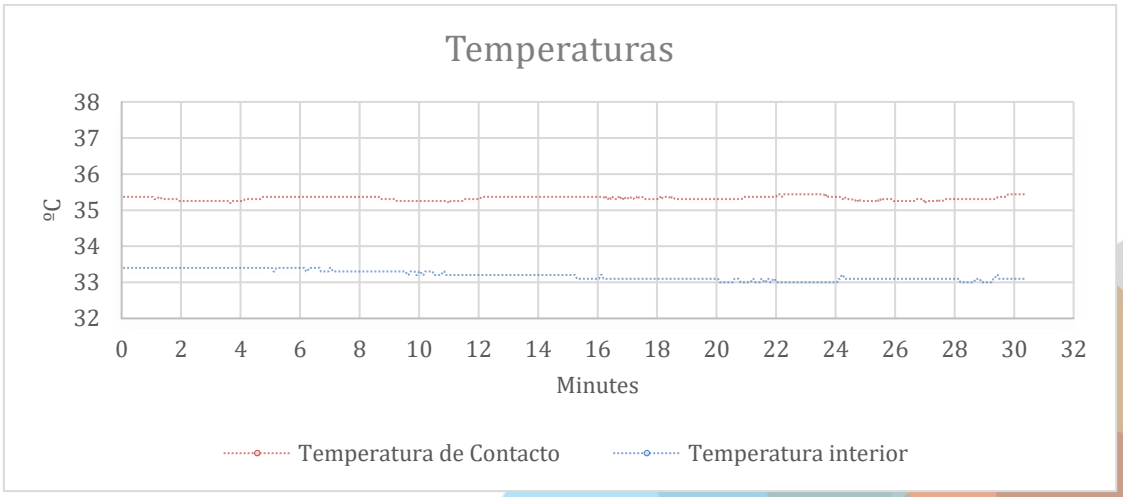

Figura 38. Gráfica de temperaturas

Humedad

El seguimiento de la humedad dentro de la férula y sus fluctuaciones nos permite saber si la zona lesionada se encuentra en un ambiente sano que evite la proliferación de bacterias, especialmente importante en casos de cirugía o lesión. Además, se ha demostrado que algunos eventos fisiológicos que pueden ocurrir después de un trauma incluyen cambios en el color de la piel debido al edema, cambios de temperatura y un aumento de la sudoración en el área afectada por la lesión [97]. La piel fría junto al aumento de la sudoración también son síntomas de algunos problemas [60]. De hecho, un cambio en la sudoración de la parte lesionada implica alteraciones centrales de la termorregulación [98]. La Figura 39 muestra el porcentaje de humedad que se registró durante la prueba dentro de la férula (en color rojo) y fuera de la férula (en color azul).

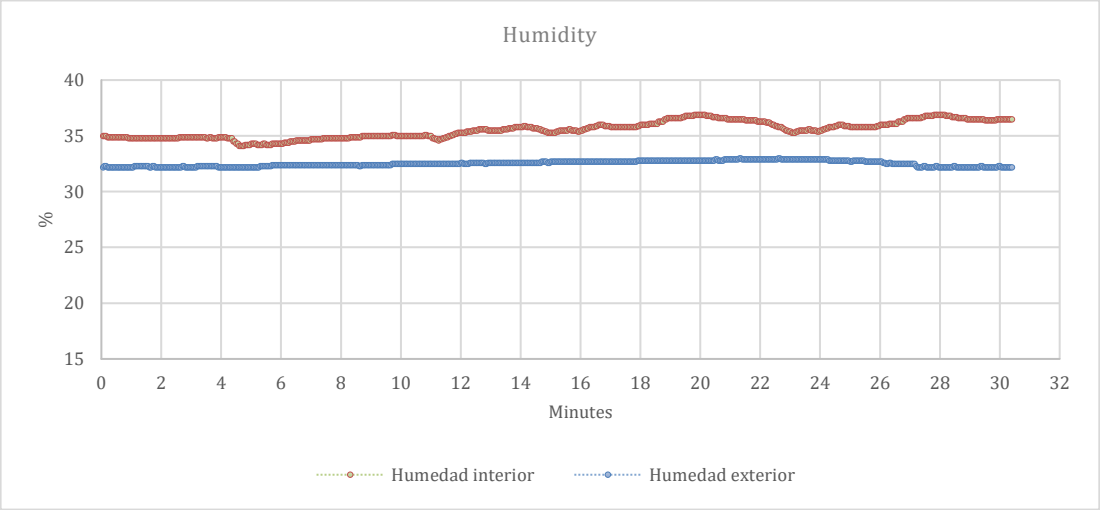

Figura 39. Gráfico de Humedad

Presión

Se colocan dos sensores para leer la presión, desfasados 90º. Uno se coloca en el eje "X" y el segundo en el eje "Y" (Figura 40). Los sensores se han colocado en estas posiciones para las pruebas, y los datos se recogen con la pierna en posición vertical y sin peso. Sin embargo, el potencial de este tipo de técnicas 3D hace posible que otros requisitos médicos también se consideren e incluyan durante el proceso de diseño, de acuerdo con los requisitos dictados por los especialistas.

Figura 40.Sensores de presión colocados con un desfase de 90º

La superficie del sensor de presión durante la fase de inmovilización de la extremidad es de 1 cm2. Teniendo en cuenta la relación 1N=1Kg/s^2 los valores de presión leídos por el sensor tendrán las unidades de gf/cm^2. La Figura 41 muestra la media de la presión detectada. Como se ilustra, durante el estado normal, el valor de la presión es constante y es igual a 60gf/cm^2. Sin embargo, cuando se produce una ligera presión debido a un proceso inflamatorio, los sensores son capaces de detectar perfectamente un incremento de esta presión. Para simular lo que ocurre en un proceso inflamatorio, se aplicó una fuerza sobre la férula entre los minutos 7 y 10. Esta variación fue detectada por los sensores, leyendo una presión que pasó de 60gf/cm2 a 100gf/cm^2. Por tanto, cuando la presión se incrementa debido a la inflamación de la zona, los sensores detectan perfectamente el incremento de la masa dentro de la férula. El gráfico muestra la presión actual y el histórico. La monitorización en tiempo real y la recopilación de datos históricos sobre la variación de presión de la zona lesionada durante el período de inmovilización, permiten al especialista controlar los fenómenos inflamatorios. Con esta información, un especialista podrá comprobar si la presión es mayor o menor que los días anteriores, para saber si la zona está sufriendo un proceso inflamatorio.

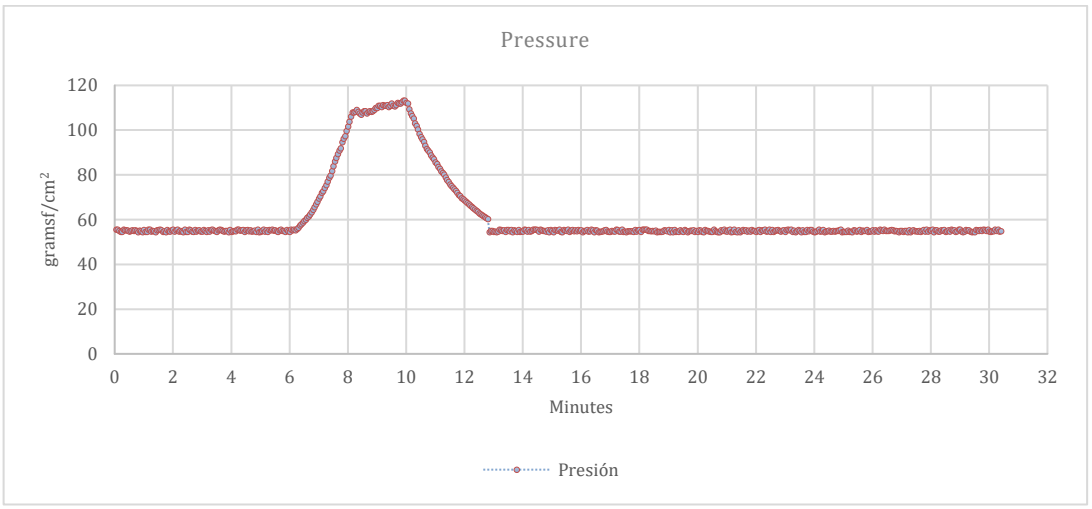

Figura 41. Gráfico de presión

Presencia

La idea principal del sensor de presencia es detectar mientras la férula está fijada correctamente. Además, es un sensor que detecta el reflejo de la luz, por lo que inicialmente se pretendía utilizar para detectar el cambio de color de la piel. Sin embargo, no fue posible utilizar el sensor para esta propuesta durante el estudio. Los colores no se detectaron correctamente con suficiente sensibilidad para detectar un enrojecimiento de la piel por inflamación u otros problemas. La figura 42 muestra el porcentaje de luz reflejada sobre la piel. Como se puede ver en la gráfica, se detecta perfectamente cuándo la férula está correctamente colocada, y cuándo no se encuentra en su lugar entre los minutos 24 y 29, espacio temporal que simula un ensamblaje y adherencia no perfectos de la férula sobre el miembro del paciente.

Figura 42. Gráfico de la reflexión

Color de piel

Es posible ver en la Figura 43 que el sensor de color es capaz de detectar un cambio de color en la piel. En la Figura 43a, la piel tiene un color normal sin signos de hematoma, mientras que en la Figura 43b el sensor detecta un incremento en los valores RGB debido a los signos de hematoma. Por ello, será posible comprobar la evolución del color durante las etapas iniciales del tratamiento, pero también en etapas posteriores. Es posible ver que los tres valores se incrementan, pero es específicamente el incremento del 38% del valor rojo lo que permite detectar el hematoma.

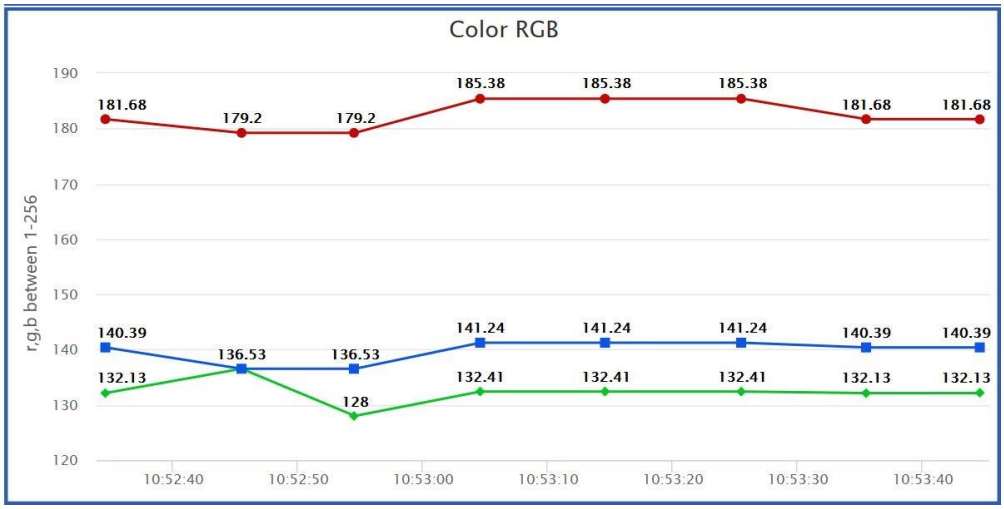

(a)

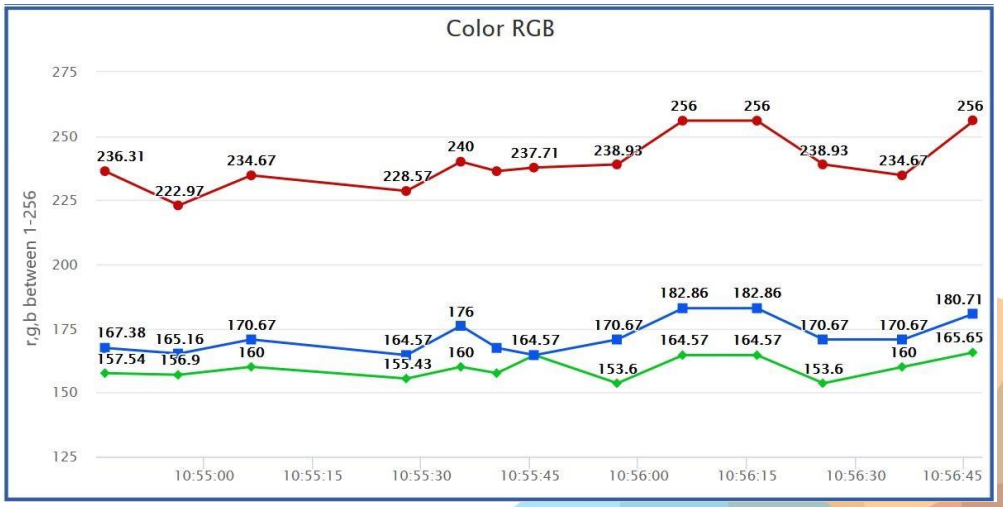

(b)

Figura 43. Gráficos del sensor de color sobre la piel sin hematoma (a) y con hematoma (b)

Diagnóstico

El conocimiento de los datos presentados en el apartado anterior permite identificar cambios de temperatura, humedad, presión o color de la piel. Combinarlos permite identificar signos de inflamación y detectar posibles problemas durante el tratamiento.

Para lograr esto, se programó un algoritmo que se puede configurar para considerar cuándo los cambios de temperatura y presión durante un período de tiempo, pueden determinar que las variaciones son producidas por un proceso de inflamación y no por una posición de la extremidad sobre un objeto específico. Los parámetros considerados se muestran en la Tabla 11. Sin embargo, estos parámetros se muestran como un ejemplo de las posibilidades del sistema, sin consideraciones médicas reales en este caso. El intervalo de tiempo sería el necesario para distinguir un valor debido a la inflamación, de una colisión, o una posición en estado de reposo. Además, para evitar una medición incorrecta de los sensores de presión, se puede considerar agregar un tercer sensor en posición opuesta. Un proceso inflamatorio producirá un incremento de volumen dentro de la férula, y un incremento de la presión en todos los sensores, de forma simultánea y coincidente en el tiempo. Sobre el rango, se propone un cambio de 5-10% del valor debido a los datos adquiridos durante las pruebas. Además, la combinación de esta información con el color de la piel y la humedad interior, que también puede ser consultada de forma remota por un especialista, dará como resultado un diagnóstico completo.

Tabla 11. Parámetros ejemplo para detectar inflamación mediante el algoritmo

Incremento de temperatura	**1.5 ^{o}C**
Incremento de presión	60 gf/cm^2
Intervalo de tiempo del incremento de temperatura	60 m
Intervalo de tiempo del incremento de presión	60 m

5. DISCUSIÓN

Este estudio muestra la combinación de técnicas tradicionales de inmovilización con nuevas técnicas de modelado y creación de prototipos en 3D. Este nuevo sistema nos permite seguir la evolución de la parte lesionada de forma muy detallada. Además, es posible aplicar tratamientos que mejoran no solo el tiempo sino también la calidad de la rehabilitación. Como se explicó anteriormente, en este estudio se han considerado como tratamientos la electroestimulación, el drenaje, la iontoforesis, el láser y el tratamiento por ultrasonidos. Sin embargo, el potencial de este tipo de técnicas 3D hace posible que otras terapias médicas también se consideren e incluyan durante el proceso de diseño, de acuerdo con los requisitos dictados por los especialistas. Estas posibilidades de tratamiento se combinan con los datos adquiridos para incluso mejorar el tratamiento. Además, crea unas zonas para la aplicación de diferentes tratamientos que produce al menos un 30% de disminución en el período de tratamiento en comparación con las férulas de yeso [25]. Agregar sensores a estas férulas permite analizar en tiempo real cómo está funcionando la terapia, así como dictar nuevos pasos para obtener el mayor progreso. Asimismo, la capacidad que permite la monitorización remota simplificaría las revisiones que debe realizar un especialista. Esto permite a los médicos seguir el progreso de más pacientes mediante el uso de datos objetivos, pudiendo mostrar alertas en una pantalla, un dispositivo móvil o también se pueden consultar de forma remota. Por otro lado, utilizando el nuevo concepto Big Data y Data Science, el dispositivo podría aprender de los diferentes síntomas para evitar problemas antes de que ocurran y también diseñar tratamientos específicos para cada lesión y paciente. Esto permitiría comparar diferentes evoluciones de diferentes tratamientos en lesiones similares. La duración del tratamiento no interfiere con la recopilación e interpretación de datos. De hecho, la recogida puede realizarse periódicamente, en función de las necesidades del médico especializado y de la evolución de la lesión. Por este motivo, la recogida de datos se realiza como señal de que el sistema funciona.

El diseño de las diferentes ventanas para los tratamientos, incluyen aristas redondeadas para evitar cualquier tipo de rozaduras o similar. En ningún caso el diseño de estas ventanas puede provocar lesiones en la extremidad afectada o por efecto de borde ya que el diseño de fabricación aditiva es posible redondear todos los bordes en contacto con la piel, ni por efecto de succión en la piel [99] ya que la férula no está indicada para soporte en carga ni produce su propio vacío por ser un diseño abierto. El diseño y la posición de las ventanas deben ser supervisados por un médico especialista, según la lesión. Estas ventanas permiten un control visual del tratamiento, lo que es especialmente crítico en las etapas iniciales. Sin embargo, las ventanas no intervienen en

el tratamiento. Además, es necesario utilizar materiales biocompatibles [100], [101] para evitar cualquier tipo de irritación, escara o úlcera.

El diseño de la férula se realiza según la zona anatómica afectada de cada paciente. Este diseño incluye un offset para adaptarse perfectamente a la zona. En los casos en los que se requiera el uso de férulas indicadas para el apoyo y la marcha de la extremidad inferior, se realizaría el correspondiente estudio estructural, y se deberían generar ventanas accesibles solo en el momento del uso mediante el diseño de un cierre. Además, este tipo de módulos permitirían despegar la férula para limpiar la piel si fuera necesario, algo que no es posible con las férulas tradicionales.

Durante casi medio siglo se han realizado investigaciones en humanos [102] y animales [103], [104] mostrando la correlación entre los patrones de temperatura y las condiciones médicas. La variación de temperatura de un área del cuerpo es producida por el metabolismo celular y el flujo sanguíneo local. Los incrementos de temperatura son normalmente el resultado de un aumento de estos factores, aunque es cierto que el flujo sanguíneo juega el papel más importante. Además, con algunos procesos patológicos o durante las diferentes etapas de formación ósea y reparación de fracturas, puede producirse una reducción del flujo sanguíneo a las zonas afectadas [105]. Esto también producirá algunas alteraciones en la temperatura superficial.

En comparación con una férula convencional, el peso del material puede producir dolores y problemas musculares. Asimismo, la falta de ventilación y la dificultad para bañarse podrían producir alergias y picor por la mala higiene de la piel y del dispositivo. Otro punto negativo de las férulas de yeso tradicionales es la dificultad para manipularlos en algunas actividades diarias por parte de los pacientes [106].

Como se puede ver en los gráficos obtenidos de los sensores, es perfectamente posible detectar variaciones de temperatura, incremento de presión, cambio del tono de la piel, y humedad dentro de la férula. Además, si se colocan más sensores de temperatura en la férula, sería posible crear un mapa digital de las diferentes áreas debajo de la férula. Esta información es especialmente útil para cuantificar los cambios de temperatura en la superficie de la piel, ya que un descenso o incremento de temperatura puede deberse a un foco inflamatorio debido al aumento en la actividad del sistema nervioso simpático [60]. La monitorización continua de estos parámetros permite conocer la progresión de la zona en cualquier momento del tratamiento, lo que permite la detección temprana de posibles complicaciones vasculares, musculares o

articulares que son difíciles de observar en caso de la férula de inmovilización tradicional, pudiendo detectar síntomas severos causados por daños a menudo irreparables.

El rendimiento y resolución de los sensores implementados fueron correctos para las pruebas, como se puede ver en las diferentes figuras. El sensor de humedad DHT22 tiene un error de histéresis de + -0,3%. No obstante, esto no es un problema ya que el sensor busca un incremento de la humedad interna en comparación con la humedad externa. El valor será alrededor de un 3-5% más alto cuando se produzca un proceso de sudoración, siendo completamente funcional. Desde el punto de vista médico, no es necesario conocer el valor absoluto, ni intentar obtener un valor óptimo, ya que esto dependerá del paciente y de la lesión. Debido a esto, el enfoque principal del estudio es analizar las nuevas capacidades detectando las variaciones en los datos adquiridos.

La temperatura registrada por el sensor en contacto con la piel es ligeramente inferior a la temperatura normal. esto se debe al gradiente de temperatura que se produce en la superficie del sensor. La superficie del sensor en contacto con la piel es de aproximadamente un 40%. El resto de la superficie está cubierta por la férula, pero no entra en contacto con la piel. Este hecho produce una diferencia de temperatura entre diferentes puntos del sensor. La superficie metálica tiende a equilibrarse debido a la conductividad térmica [107]. El sensor obtiene una temperatura final que no es la temperatura real de la piel. Sin embargo, este hecho no interfiere con el objetivo principal de este sensor, que no busca un valor absoluto, si no detectar cambios de temperatura relativos.

El sensor RGB detecta sin problema las diferentes longitudes de onda que le llegan reflejadas desde la piel. De este modo, las componentes roja, azul y verde, pueden ser analizadas para detectar un cambio de coloración que puede ser el origen de un hematoma. Del mismo modo, también se puede utilizar para monitorizar la evolución de moretones en la zona afectada. Por último, el sensor de presencia detecta perfectamente cuándo la férula está correctamente fijada.

En la etapa de fabricación, ha sido necesario contar con una máquina que permita registrar las condiciones de fabricación de las férulas, así como realizar un análisis exhaustivo de diferentes materiales, o incluso diferentes marcas del mismo material, para ver que el fabricante muestra las condiciones óptimas para una correcta impresión. Para ello, se dotó a la máquina de FDM de algunos sensores que permitan el control de las condiciones ambientales, algo que es de fundamental importancia en las aplicaciones biomédicas. Se ha desarrollado un sistema de bajo costo que permite analizar cuánto pueden cambiar los parámetros óptimos para una buena pieza

de producción FDM durante el proceso, asegurando que las condiciones mecánicas del material no disminuyan [108], a causa de perturbaciones externas a la máquina y al proceso, pero también intrínsecas a la propia máquina o al proceso. El sistema implementado no afectó al funcionamiento normal de la máquina. En muchos casos es necesita un control estricto de la temperatura o la humedad en la cámara de impresión, por ejemplo, en el caso de la fabricación mediante impresión 3D los implantes articulares cerámicos deben realizarse a baja temperatura [79]. La fluctuación de la temperatura dañaría la estructura interna del material e incluso, en otros casos, la temperatura podría producir partículas nocivas. Esto afectaría a la seguridad del operador y haría imposible el uso de la máquina en algunas salas de limpieza que se utilizan normalmente en entornos médicos [109].

Después de estudiar los diferentes parámetros que pueden interferir en la estructura final, se procedió a la recogida de datos en un proceso real. Se tomaron muestras de la temperatura del extrusor y la cámara, humedad y diámetro y velocidad de avance del filamento. Aparte de estos datos, se almacenaron las coordenadas X, Y de todas las muestras. Esto nos permitirá comprobar las condiciones del filamento depositado en todas las zonas de la estructura. Las mediciones se recopilan durante un proceso de producción real y se obtienen los datos, mostrados en la sección de resultados.

6. CONCLUSIONES

Una vez realizado el trabajo de Tesis Doctoral en el que se han desarrollado diferentes sistemas tecnológicos para la recopilación de información médica, y según los resultados obtenidos tras el análisis de los datos recogidos durante los diferentes ensayos, concluimos que:

- **Primera.** Se ha logrado dar una solución a los problemas de impresión y dotar de control de calidad a nivel industrial a la fabricación aditiva. A pesar de no ser una solución definitiva, los resultados aquí presentados ofrecen un punto de partida muy optimista para seguir desarrollando sistemas que ayuden a que la fabricación por deposición fundida sea más fiable. Esto permite también producir las piezas usando material en las condiciones correctas de temperatura, humedad o velocidad de deposición, de modo que las características mecánicas no disminuyan.

- **Segunda.** Se ha implementado con éxito un sistema de sensores en una máquina de FDM, que permite la validación de filamentos, generando un informe en el que se puede ver si el filamento tiene defectos de fabricación o si se cumplen las tolerancias dimensionales admitidas por el proceso de fabricación.

- **Tercera.** Se han analizado muestras de materiales biocompatibles para comprobar los diferentes cambios de estado que sufren los componentes con el aumento de temperatura, así como los errores dimensionales que aparecen en las piezas fabricadas, habiendo encontrado las temperaturas óptimas de trabajo de estos. Se ha podido observar, que la temperatura indicada por el fabricante de cada material no es siempre la temperatura óptima de fusión. Además, en la mayoría de los materiales se produce una evaporación de componentes, con su consecuente pérdida de masa, antes de alcanzar la temperatura indicada.

- **Cuarta.** Se han conseguido fabricar dos férulas, una para extremidad superior y una para extremidad inferior, de acuerdo con la lesión y morfología del paciente. Esto ha sido posible gracias a las nuevas tecnologías de escaneado 3D y los avances en materiales y procesos de FDM. Se han incorporado con éxito alojamientos para sensores y ventanas para posibles tratamientos sin perder la rigidez necesaria para cumplir con el propósito principal de una férula de inmovilización.

- **Quinta.** Tras fabricar las férulas diseñadas, se han implementado diferentes sensores, que permiten registrar en tiempo real diferentes datos sobre la evolución de la lesión. En concreto, los datos recogidos fueron la temperatura en varios puntos, presión en varios puntos, humedad, color de la piel, y detección de colocación de la férula, pudiendo de este modo caracterizarlas de "férulas inteligentes".

- **Sexta**. Se ha conseguido integrar toda la electrónica en un sistema autónomo, portátil, y ligero, permitiendo recoger los datos de los diferentes sensores en tiempo real. El sistema, englobado en la tecnología IoT, envía con éxito los datos por conexión bluetooth a un dispositivo móvil, y puede ser consultado a través de un servidor web desde cualquier parte del mundo, permitiendo realizar un diagnóstico remoto. Además, se ha implementado un algoritmo que permite identificar procesos de inflamación en la zona.

- **Séptima y última.** Se ha logrado realizar todo el desarrollo manteniendo la premisa de conseguirlo con un sistema de bajo coste que pueda ser implementado con diferentes tratamientos, y aplicado a diferentes lesiones.

7. BIBLIOGRAFIA

[1] A. Gebhardt, F. Schmidt, J. Hötter, W. S.-P. Procedia, and undefined 2010, "Additive manufacturing by selective laser melting the realizer desktop machine and its application for the dental industry," *Elsevier*, Accessed: Apr. 27, 2020. [Online]. Available: https://www.sciencedirect.com/science/article/pii/S1875389210005080.

[2] M. Scholz, J. Blanchfield, L. B.-… S. and Technology, and undefined 2011, "The use of composite materials in modern orthopaedic medicine and prosthetic devices: A review," *Elsevier*, Accessed: Apr. 27, 2020. [Online]. Available: https://www.sciencedirect.com/science/article/pii/S0266353811003071.

[3] W. Saringer, I. Nöbauer-Huhmann, and E. Knosp, "Cranioplasty with individual Carbon Fibre Reinforced Polymere (CFRP) medical grade implants based on CAD/CAM technique," *Acta Neurochir. (Wien).*, vol. 144, no. 11, pp. 1193–1203, 2002, doi: 10.1007/s00701-002-0995-5.

[4] F. Blaya, P. S. Pedro, J. L. Silva, R. D'Amato, E. S. Heras, and J. A. Juanes, "Design of an Orthopedic Product by Using Additive Manufacturing Technology: The Arm Splint," *J. Med. Syst.*, 2018, doi: 10.1007/s10916-018-0909-6.

[5] M. T. U. Lozano, F. B. Haro, A. Ruggiero, and J. A. J. Mendez, "Systems of digitalization and processing of anatomical pieces for their three-dimensional reconstruction," in *Proceedings of the 5th International Conference on Technological Ecosystems for Enhancing Multiculturality - TEEM 2017*, 2017, pp. 1–5, doi: 10.1145/3144826.3145402.

[6] P. Mcauliffe, J. H. Kim, D. Diamond, K. T. Lau, and B. C. O'Connell, "A sleep bruxism detection system based on sensors in a splint - pilot clinical data," *J. Oral Rehabil.*, 2015, doi: 10.1111/joor.12223.

[7] D. V. Dimitrov, "Medical internet of things and big data in healthcare," *Healthcare Informatics Research*, vol. 22, no. 3. Korean Society of Medical Informatics, pp. 156–163, Jul. 01, 2016, doi: 10.4258/hir.2016.22.3.156.

[8] Y. YIN, Y. Zeng, X. Chen, and Y. Fan, "The internet of things in healthcare: An overview," *Journal of Industrial Information Integration*, vol. 1. Elsevier B.V., pp. 3–13, Mar. 01, 2016, doi: 10.1016/j.jii.2016.03.004.

[9] Y. J. Fan, Y. H. Yin, L. Da Xu, Y. Zeng, and F. Wu, "IoT-based smart rehabilitation system," *IEEE Trans. Ind. Informatics*, vol. 10, no. 2, pp. 1568–1577, 2014, doi:

10.1109/TII.2014.2302583.

[10] Melchels, Marco, Klein, P. Travis, and & Hutmacher, "Additive manufacturing of tissues and organs," *Elsevier*, 2012, doi: 10.1016/j.progpolymsci.2011.11.007.

[11] H. N. Chia and B. M. Wu, "Recent advances in 3D printing of biomaterials," *J. Biol. Eng.*, vol. 9, no. 1, Mar. 2015, doi: 10.1186/s13036-015-0001-4.

[12] R. R. Jose, M. J. Rodriguez, T. A. Dixon, F. Omenetto, and D. L. Kaplan, "Evolution of Bioinks and Additive Manufacturing Technologies for 3D Bioprinting," *ACS Publ.*, vol. 2, no. 10, pp. 1662–1678, Oct. 2004, doi: 10.1021/acsbiomaterials.6b00088.

[13] A. Calderon, J. Griffin, and J. C. Zagal, "BeamMaker: An open hardware high-resolution digital fabricator for the masses," *Rapid Prototyp. J.*, vol. 20, no. 3, pp. 245–255, 2014, doi: 10.1108/RPJ-01-2013-0006.

[14] C. Mota, "The rise of personal fabrication," in *C and C 2011 - Proceedings of the 8th ACM Conference on Creativity and Cognition*, Nov. 2011, pp. 279–287, doi: 10.1145/2069618.2069665.

[15] G. Stemp-Morlock, "Personal Fabrication," *Commun. ACM*, vol. 53, no. 10, pp. 14–15, Jan. 2010, doi: 10.1145/1831407.1831414.

[16] J. M. D. A. Del Burgo, R. D'Amato, J. A. J. Méndez, A. S. Ramírez, F. B. Haro, and E. S. Heras, "Real time analysis of the filament for FDM 3D printers," 2019, doi: 10.1145/3362789.3362818.

[17] A. Vladescu, M. Braic, F. Azem, I. Titorencu, … V. B.-A. S., and undefined 2015, "Effect of the deposition temperature on corrosion resistance and biocompatibility of the hydroxyapatite coatings," *Elsevier*, Accessed: Apr. 27, 2020. [Online]. Available: https://www.sciencedirect.com/science/article/pii/S0169433215011770.

[18] G. I. J. Salentijn, P. E. Oomen, M. Grajewski, and E. Verpoorte, "Fused Deposition Modeling 3D Printing for (Bio)analytical Device Fabrication: Procedures, Materials, and Applications," *Anal. Chem.*, vol. 89, no. 13, pp. 7053–7061, Jul. 2017, doi: 10.1021/acs.analchem.7b00828.

[19] S. Stopp, T. Wolff, F. Irlinger, and T. Lueth, "A new method for printer calibration and contour accuracy manufacturing with 3D-print technology," *Rapid Prototyp. J.*, vol. 14, no. 3, pp. 167–172, 2008, doi: 10.1108/13552540810878030.

[20] E. W. Reutzel and A. R. Nassar, "A survey of sensing and control systems for machine and process monitoring of directedenergy, metal-based additive manufacturing," *Rapid Prototyping Journal*, vol. 21, no. 2. Emerald Group Publishing Ltd., pp. 159–167, Mar. 16, 2015, doi: 10.1108/RPJ-12-2014-0177.

[21] N. Volpato, D. Kretschek, J. A. Foggiatto, and C. M. Gomez da Silva Cruz, "Experimental analysis of an extrusion system for additive manufacturing based on polymer pellets," *Int. J. Adv. Manuf. Technol.*, vol. 81, no. 9–12, pp. 1519–1531, Dec. 2015, doi: 10.1007/s00170-015-7300-2.

[22] B. N. Turner, R. Strong, and S. A. Gold, "A review of melt extrusion additive manufacturing processes: I. Process design and modeling," *Rapid Prototyping Journal*, vol. 20, no. 3. Emerald Group Publishing Ltd., pp. 192–204, 2014, doi: 10.1108/RPJ-01-2013-0012.

[23] B. N. Turner and S. A. Gold, "A review of melt extrusion additive manufacturing processes: II. Materials, dimensional accuracy, and surface roughness," *Rapid Prototyping Journal*, vol. 21, no. 3. Emerald Group Publishing Ltd., pp. 250–261, Apr. 20, 2015, doi: 10.1108/RPJ-02-2013-0017.

[24] K.-F. Ratzsch, R. Kádár, I. F. C. Naue, and M. Wilhelm, "A Combined NMR Relaxometry and Surface Instability Detection System for Polymer Melt Extrusion," *Macromol. Mater. Eng.*, vol. 298, no. 10, pp. 1124–1132, Oct. 2013, doi: 10.1002/mame.201300243.

[25] F. Blaya, P. S. Pedro, A. B. S. Pedro, J. Lopez-Silva, J. A. Juanes, and R. D'Amato, "Design of a Functional Splint for Rehabilitation of Achilles Tendon Injury Using Advanced Manufacturing (AM) Techniques. Implementation Study," *J. Med. Syst.*, vol. 43, no. 5, 2019, doi: 10.1007/s10916-019-1247-z.

[26] T. I. Society *et al.*, "The diagnosis and treatment of peripheral lymphedema: 2016 consensus document of the International Society of Lymphology," *Acta Angiol.*, vol. 23, no. 4, pp. 171–182, 2017.

[27] B. Chikly, J. Quaghebeur, and W. Witryol, "A Controlled Comparison between Manual Lymphatic Mapping (MLM) of Plantar Lymph Flow and Standard Physiologic Maps Using Lymph Drainage Therapy (LDT)/Osteopathic Lymphatic Technique (OLT)," *J Yoga Phys Ther*, vol. 4, p. 173, 2014, doi: 10.4172/2157-7595.1000173.

[28] Y. Wei, K. Yang, M. Browne, L. Bostan, and P. Worsley, "Wearable Electrical Stimulation to

Improve Lymphatic Function," *IEEE Sensors Lett.*, vol. 3, no. 2, Feb. 2019, doi: 10.1109/LSENS.2019.2893478.

[29] C. T. Costello and A. H. Jeske, "Iontophoresis: Applications in transdermal medication delivery," *Physical Therapy*, vol. 75, no. 6. American Physical Therapy Association, pp. 554–563, Jun. 01, 1995, doi: 10.1093/ptj/75.6.554.

[30] H. Hamann, M. Hodges, and B. Evans, "Effectiveness of iontophoresis of anti-inflammatory medications in the treatment of common musculoskeletal inflammatory conditions: a systematic review," *Phys. Ther. Rev.*, vol. 11, no. 3, pp. 190–194, Sep. 2006, doi: 10.1179/108331906X144082.

[31] J. H. Rigby, B. B. Mortensen, and D. O. Draper, "Wireless versus wired iontophoresis for treating patellar tendinopathy: A randomized clinical trial," *J. Athl. Train.*, vol. 50, no. 11, pp. 1165–1173, Nov. 2015, doi: 10.4085/1062-6050-50.11.04.

[32] J. Hao, "Topical iontophoresis for local therapeutic effects," *Journal of Drug Delivery Science and Technology*, vol. 24, no. 3. Editions de Sante, pp. 255–258, Jan. 01, 2014, doi: 10.1016/S1773-2247(14)50043-3.

[33] C. Neeter, R. Thomee, K. G. Silbernagel, P. Thomee, and J. Karlsson, "Iontophoresis with or without dexamethazone in the treatment of acute Achilles tendon pain," *Scand. J. Med. Sci. Sport.*, vol. 13, no. 6, pp. 376–382, Dec. 2003, doi: 10.1046/j.1600-0838.2003.00305.x.

[34] M. A. Taskaynatan, A. Ozgul, A. Ozdemir, A. K. Tan, and T. A. Kalyon, "Effects of steroid iontophoresis and electrotherapy on bicipital tendonitis," *J. Musculoskelet. Pain*, vol. 15, no. 4, pp. 47–54, Aug. 2007, doi: 10.1300/J094v15n04_06.

[35] K. G. Baker, V. J. Robertson, and F. A. Duck, "A Review of Therapeutic Ultrasound: Biophysical Effects," *Phys. Ther.*, 2001, doi: 10.1093/ptj/81.7.1351.

[36] V. J. Robertson and K. G. Baker, "A Review of Therapeutic Ultrasound: Effectiveness Studies," *Phys. Ther.*, 2001, doi: 10.1093/ptj/81.7.1339.

[37] F. Aimbire *et al.*, "Low-level laser therapy induces dose-dependent reduction of TNFα levels in acute inflammation," *Photomed. Laser Surg.*, 2006, doi: 10.1089/pho.2006.24.33.

[38] J. M. ; Bjordal *et al.*, "Low level laser therapy reduces inflammation in activated Achilles tendinitis NASA Astrophysics Data System (ADS)," *NASA Astrophys. Data Syst.*, 2006.

[39] G. R. Ebenbichler *et al.*, "Ultrasound therapy for calcific tendinitis of the shoulder," *N. Engl. J. Med.*, 1999, doi: 10.1056/NEJM199905203402002.

[40] S. Mitragotri, "Healing sound: The use of ultrasound in drug delivery and other therapeutic applications," *Nat. Rev. Drug Discov.*, 2005, doi: 10.1038/nrd1662.

[41] J. H. Rigby, R. M. Taggart, K. L. Stratton, G. K. Lewis, and D. O. Draper, "Intramuscular heating characteristics of multihour low-intensity therapeutic ultrasound," *J. Athl. Train.*, vol. 50, no. 11, pp. 1158–1164, Nov. 2015, doi: 10.4085/1062-6050-50.11.03.

[42] J. M. Bjordal, R. A. B. Lopes-Martins, J. Joensen, and V. V. Iversen, "The anti-inflammatory mechanism of low level laser therapy and its relevance for clinical use in physiotherapy," *Phys. Ther. Rev.*, vol. 15, no. 4, pp. 286–293, Aug. 2010, doi: 10.1179/1743288X10Y.0000000001.

[43] W. Kneebone, "The Treatment of Achilles Tendonitis Using Therapeutic Laser," 2010. Accessed: Apr. 27, 2020. [Online]. Available: http://orthopedics.about.com/cs/ankleproblems/a/.

[44] X. Gao and D. Xing, "Molecular mechanisms of cell proliferation induced by low power laser irradiation," *J. Biomed. Sci.*, 2009, doi: 10.1186/1423-0127-16-4.

[45] T. I. Karu, "Mitochondrial signaling in mammalian cells activated by red and near-IR radiation," *Photochemistry and Photobiology*. 2008, doi: 10.1111/j.1751-1097.2008.00394.x.

[46] Y. Moriyama, J. Nguyen, M. Akens, E. H. Moriyama, and L. Lilge, "In vivo effects of low level laser therapy on inducible nitric oxide synthase," *Lasers Surg. Med.*, 2009, doi: 10.1002/lsm.20745.

[47] L. I. Fillipin *et al.*, "Low-level laser therapy (LLLT) prevents oxidative stress and reduces fibrosis in rat traumatized Achilles tendon," *Lasers Surg. Med.*, 2005, doi: 10.1002/lsm.20225.

[48] G. Y. F. Ng and D. T. C. Fung, "The combined treatment effects of therapeutic laser and exercise on tendon repair," *Photomed. Laser Surg.*, 2008, doi: 10.1089/pho.2007.2145.

[49] G. K. Reddy, L. Stehno-Bittel, and C. S. Enwemeka, "Laser photostimulation of collagen production in healing rabbit Achilles tendons," *Lasers Surg. Med.*, 1998, doi: 10.1002/(SICI)1096-9101(1998)22:5<281::AID-LSM4>3.0.CO;2-L.

[50] J. Joensen, N. R. Gjerdet, S. Hummelsund, V. Iversen, R. A. B. Lopes-Martins, and J. M. Bjordal, "An experimental study of low-level laser therapy in rat Achilles tendon injury," *Lasers Med. Sci.*, vol. 27, no. 1, pp. 103–111, Jan. 2012, doi: 10.1007/s10103-011-0925-y.

[51] U. R.-P. research and clinical management and undefined 2003, "The history of electrical stimulation of the nervous system for the control of pain."

[52] A. Heidland *et al.*, "Neuromuscular electrostimulation techniques: historical aspects and current possibilities in treatment of pain and muscle waisting," doi: 10.5414/CNX77S106.

[53] M. G. Rosemffet *et al.*, "Effects of Functional Electrostimulation on Pain, Muscular Strength, and Functional Capacity in Patients With Osteoarthritis of the Knee," *JCR J. Clin. Rheumatol.*, vol. 10, no. 5, pp. 246–249, Oct. 2004, doi: 10.1097/01.rhu.0000141831.40350.91.

[54] J. M. R. Martín, *Electroterapia en fisioterapia*. Médica Panamericana, 2014.

[55] K. Johansson, M. Albertsson, C. Ingvar, and C. Ekdahl, "EFFECTS OF COMPRESSION BANDAGING WITH OR WITHOUT MANUAL LYMPH DRAINAGE TREATMENT IN PATIENTS WITH POSTOPERATIVE ARM LYMPHEDEMA," Aug. 1999. Accessed: May 22, 2021. [Online]. Available: https://journals.uair.arizona.edu/index.php/lymph/article/view/17363.

[56] C. B. Aiyejusunle, T. A. Kola-Korolo, and O. A. Ajiboye, "Comparison of the effects of tens and sodium salicylate iontophoresis in the management of osteoarthritis of the knee.," *Nig. Q. J. Hosp. Med.*, vol. 17, no. 1, pp. 30–34, Jan. 2007, doi: 10.4314/nqjhm.v17i1.12539.

[57] D. I. Stasinopoulos and M. I. Johnson, "Effectiveness of low-level laser therapy for lateral elbow tendinopathy," *Photomedicine and Laser Surgery*, vol. 23, no. 4. Mary Ann Liebert, Inc. 2 Madison Avenue Larchmont, NY 10538 USA , pp. 425–430, Aug. 06, 2005, doi: 10.1089/pho.2005.23.425.

[58] K. Kaplan, O. Olivencia, M. Dreger, W. J. Hanney, and M. J. Kolber, "Achilles Tendinopathy: An Evidence-Based Overview for the Sports Medicine Professional," *Strength Cond. J.*, vol. 41, no. 5, pp. 24–40, Oct. 2019, doi: 10.1519/ssc.0000000000000485.

[59] H. Moein, R. Jhalli, A. P. Blaber, V. E. Claydon, and C. Menon, "Evaluating the efficacy of an active compression brace on orthostatic cardiovascular responses," *PLoS One*, vol. 12, no. 11, p. e0187885, Nov. 2017, doi: 10.1371/JOURNAL.PONE.0187885.

[60] X. Ju, J.-C. Nebel, and J. P. Siebert, "3D thermography imaging standardization technique

for inflammation diagnosis," in *Infrared Components and Their Applications*, Jan. 2005, vol. 5640, p. 266, doi: 10.1117/12.577055.

[61] T. Schlereth, P. D. Drummond, and F. Birklein, "Inflammation in CRPS: Role of the sympathetic supply," *Auton. Neurosci. Basic Clin.*, vol. 182, pp. 102–107, May 2014, doi: 10.1016/j.autneu.2013.12.011.

[62] DallaDS18B20 Temperature Sensors Semiconductor, "DS18B20 Temperature Sensor," *Dallas Semicond. datasheets*, 2002.

[63] L. Aosong Electronics Co., "Digital-output relative humidity & temperature sensor/module DHT22 (DHT22 also named as AM2302)," 2015.

[64] "Film Pressure Sensor DF9-40@10kg V2.0."

[65] "TCS3472 COLOR LIGHT-TO-DIGITAL CONVERTER with IR FILTER." https://cdn-shop.adafruit.com/datasheets/TCS34725.pdf (accessed Apr. 30, 2020).

[66] "Vishay Telefunken Reflective Optical Sensor with Transistor Output Description Order Instruction Ordering Code Sensing Distance Remarks CNY70 0.3 mm."

[67] "Bruise colors: Causes, timescale, and when to see a doctor." https://www.medicalnewstoday.com/articles/322742#bruise-colors-over-time-and-their-causes (accessed Jul. 13, 2021).

[68] "Tell-Tale Color Changes: Camera Can Find Age of a Bruise | Features | Oct 2012 | BioPhotonics." https://www.photonics.com/Articles/TellTale_Color_Changes_Camera_Can_Find_Age_of_a/a52130 (accessed Jul. 13, 2021).

[69] M. Patašius, V. Marozas, D. Jegelevičius, and A. Lukoševičius, "Data Exploration for Hematoma Image Analysis," Feb. 2016. Accessed: May 13, 2021. [Online]. Available: http://biomed.ktu.lt/index.php/BME/article/view/2481.

[70] H. K. Al Ghozali, Setiawardhana, and R. Sigit, "Vein detection system using infrared camera," in *Proceedings - 2016 International Electronics Symposium, IES 2016*, Feb. 2017, pp. 122–127, doi: 10.1109/ELECSYM.2016.7860987.

[71] "Automatización de la Datación de Equimosis en el Peritaje Médico Legal Peruano mediante Redes Neuronales Artificiales y Procesamiento de Imágenes."

http://cybertesis.unmsm.edu.pe/handle/20.500.12672/1071 (accessed May 26, 2021).

[72] M. A. Ghavimi *et al.*, "Comparison of edema and ecchymosis in rhinoplasty candidates after lateral nasal osteotomy using piezosurgery and external osteotomy," *J. Adv. Pharm. Technol. Res.*, vol. 9, no. 3, pp. 87–93, Jul. 2018, doi: 10.4103/japtr.JAPTR_294_18.

[73] A. Gurlek, A. Fariz, H. Aydogan, A. Ersoz-Ozturk, and A. T. Eren, "Effects of different corticosteroids on edema and ecchymosis in open rhinoplasty," *Aesthetic Plast. Surg.*, vol. 30, no. 2, pp. 150–154, Apr. 2006, doi: 10.1007/s00266-005-0158-1.

[74] J. M. De Agustín Del Burgo, F. Blaya Haro, R. D'Amato, and J. A. Juanes Méndez, "Development of a Smart Splint to Monitor Different Parameters during the Treatment Process," *Sensors*, vol. 20, no. 15, p. 4207, Jul. 2020, doi: 10.3390/s20154207.

[75] "Hire Freelance Point Cloud Modeling Services for Your Company | Cad Crowd." https://www.cadcrowd.com/architectural-design/point-cloud-modeling-services (accessed Apr. 27, 2020).

[76] A. Nurunnabi, G. West, and D. Belton, "Outlier detection and robust normal-curvature estimation in mobile laser scanning 3D point cloud data," *Pattern Recognit.*, vol. 48, no. 4, pp. 1404–1419, Apr. 2015, doi: 10.1016/j.patcog.2014.10.014.

[77] M. J. Rakotosaona, V. La Barbera, P. Guerrero, N. J. Mitra, and M. Ovsjanikov, "PointCleanNet: Learning to Denoise and Remove Outliers from Dense Point Clouds," *Comput. Graph. Forum*, vol. 39, no. 1, pp. 185–203, Feb. 2020, doi: 10.1111/cgf.13753.

[78] S. Farah, D. G. Anderson, and R. Langer, "Physical and mechanical properties of PLA, and their functions in widespread applications — A comprehensive review," *Advanced Drug Delivery Reviews*, vol. 107. Elsevier B.V., pp. 367–392, Dec. 15, 2016, doi: 10.1016/j.addr.2016.06.012.

[79] E. Soriano Heras, F. Blaya Haro, J. M. de Agustín del Burgo, M. Islán Marcos, and R. D'Amato, "Filament advance detection sensor for fused deposition modelling 3D printers," *Sensors (Switzerland)*, vol. 18, no. 5, p. 1495, May 2018, doi: 10.3390/s18051495.

[80] F. B. Haro, J. M. de Agustín del Burgo, R. D'Amato, M. I. Marcos, E. S. Heras, and J. M. G. Alonso, "Monitoring of the additive manufacturing process for the use of biomaterials in medical field," in *Proceedings of the Sixth International Conference on Technological Ecosystems for Enhancing Multiculturality - TEEM'18*, 2018, pp. 428–432, doi:

10.1145/3284179.3284252.

[81] "Print Quality Guide." https://www.simplify3d.com/support/print-quality-troubleshooting/ (accessed May 23, 2020).

[82] L. Texas Instruments incorporate, "LM35 Precision Centigrade Temperature Sensors Precision Centigrade Temperature Sensors," *Lm 35*, 2016, doi: 10.1016/j.ejps.2009.01.006.

[83] FiedlerMatthew, "Evaluating Tension and Tooth Geometry to Optimize Grip on 3D Printer Filament," *https://home.liebertpub.com/3dp*, vol. 2, no. 2, pp. 85–88, Jun. 2015, doi: 10.1089/3DP.2015.0011.

[84] "FWS_V3.2/fws_v3.2.pdf at master · jasonmarkham/FWS_V3.2 · GitHub." https://github.com/jasonmarkham/FWS_V3.2/blob/master/fws_v3.2.pdf (accessed Sep. 09, 2021).

[85] F. Decuir, K. Phelan, and B. C. Hollins, "Mechanical strength of 3-D printed filaments," 2016, doi: 10.1109/SBEC.2016.101.

[86] K. A. El-Farahaty, A. M. Sadik, and A. M. Hezma, "Study of optical and structure properties of polyester (PET) and copolyester (PETG) fibers by interferometry," *Int. J. Polym. Mater. Polym. Biomater.*, 2007, doi: 10.1080/00914030601100722.

[87] P. Maróti, B. Kocsis, A. Ferencz, M. Nyitrai, and D. Lőrinczy, "Differential thermal analysis of the antibacterial effect of PLA-based materials planned for 3D printing," *J. Therm. Anal. Calorim.*, 2020, doi: 10.1007/s10973-019-08377-4.

[88] P. Maróti, P. Varga, A. Ferencz, Z. Ujfalusi, M. Nyitrai, and D. Lőrinczy, "Testing of innovative materials for medical additive manufacturing by DTA," *J. Therm. Anal. Calorim.*, 2019, doi: 10.1007/s10973-018-7839-x.

[89] C. O'mahony *et al.*, "Determination of thermal and thermomechanical properties of biodegradable PLA blends: for additive manufacturing process," vol. 142, pp. 715–722, 2020, doi: 10.1007/s10973-020-09859-6.

[90] K. Kozlovsky, J. Schiltz, T. Kreider, M. Kumar, and S. Schmid, "Mechanical Properties of Reused Nylon Feedstock for Powder-bed Additive Manufacturing in Orthopedics," 2018, doi: 10.1016/j.promfg.2018.07.103.

[91] N. Schiavone, V. Verney, and H. Askanian, "Effect of 3D Printing Temperature Profile on

Polymer Materials Behavior," *3D Print. Addit. Manuf.*, 2020, doi: 10.1089/3dp.2020.0175.

[92] "The Value of USP Class VI Testing for Medical Device Cable and Wire - Medical Design Briefs." https://www.medicaldesignbriefs.com/component/content/article/mdb/features/articles/20248 (accessed May 22, 2020).

[93] "ISO - ISO 10993-1:2018 - Biological evaluation of medical devices — Part 1: Evaluation and testing within a risk management process." https://www.iso.org/standard/68936.html (accessed May 22, 2020).

[94] "filament printer 3d MEDICAL materials." https://www.smartmaterials3d.com/en/medical (accessed May 25, 2020).

[95] J. M. D. A. Del Burgo, F. B. Haro, R. D'Amato, A. Blaya, and J. A. J. Méndez, "Development of a Smart Leg Splint by Using New Sensor Technologies and New Therapy Possibilities," *Sensors 2021, Vol. 21, Page 5252*, vol. 21, no. 15, p. 5252, Aug. 2021, doi: 10.3390/S21155252.

[96] "ESP32 Series Datasheet Including," 2020. Accessed: Apr. 28, 2020. [Online]. Available: https://www.espressif.com/en/support/download/documents.

[97] F. Birklein, W. Künzel, and N. Sieweke, "Despite clinical similarities there are significant differences between acute limb trauma and complex regional pain syndrome I (CRPS I)," *Pain*, vol. 93, no. 2, pp. 165–171, Aug. 2001, doi: 10.1016/S0304-3959(01)00309-8.

[98] W. Jänig, "Functions of the sympathetic innervation of the skin ," *A.D. Loewy, K.M. Spyer (Eds.), Cent. Regul. Auton. Funct. Oxford Univ. Press. New York.*, pp. 334–348, 1990.

[99] D. T. Lowe, "Cupping therapy: An analysis of the effects of suction on skin and the possible influence on human health," *Complement. Ther. Clin. Pract.*, vol. 29, pp. 162–168, Nov. 2017, doi: 10.1016/J.CTCP.2017.09.008.

[100] Y. Kim *et al.*, "Effect of PEG addition on pore morphology and biocompatibility of PLLA scaffolds prepared by freeze drying," *Biomed. Eng. Lett. 2016 64*, vol. 6, no. 4, pp. 287–295, Dec. 2016, doi: 10.1007/S13534-016-0241-3.

[101] J. A. J. Hernández, E. J. G. Vicente, F. R. Sánchez, F. M. Sanchez, M. P. C. Rodríguez, and J. P. Morote, "Prevention of iatrogenic ulcers produced by therapeutic immobilization with a lower limb splint in children. Clinical trial," *Enferm. Glob.*, vol. 19, no. 3, pp. 135–154,

2020, doi: 10.6018/eglobal.393911.

[102] R. LAWSON, “Implications of surface temperatures in the diagnosis of breast cancer.,” *Can. Med. Assoc. J.*, vol. 75, no. 4, pp. 309–311, 1956.

[103] B. Ströberg, “The Use of Thermography in Equine Orthopedics,” *Vet. Radiol.*, vol. 15, no. 1, pp. 94–97, Jan. 1974, doi: 10.1111/j.1740-8261.1974.tb00676.x.

[104] L. Wang *et al.*, “Bisphosphonates Inhibit Pain, Bone Loss, and Inflammation in a Rat Tibia Fracture Model of Complex Regional Pain Syndrome,” *Anesth. Analg.*, vol. 123, no. 4, pp. 1033–1045, Oct. 2016, doi: 10.1213/ANE.0000000000001518.

[105] C. H. Rundle *et al.*, “Microarray analysis of gene expression during the inflammation and endochondral bone formation stages of rat femur fracture repair,” *Bone*, vol. 38, no. 4, pp. 521–529, Apr. 2006, doi: 10.1016/j.bone.2005.09.015.

[106] F. Blaya, P. S. Pedro, J. L. Silva, R. D’Amato, E. S. Heras, and J. A. Juanes, “Design of an Orthopedic Product by Using Additive Manufacturing Technology: The Arm Splint,” *J. Med. Syst.*, vol. 42, no. 3, 2018, doi: 10.1007/s10916-018-0909-6.

[107] K. Horai and T. Shankland, “Thermal conductivity of rocks and minerals,” *Methods Exp. Phys.*, 1987, doi: 10.1016/S0076-695X(08)60589-X.

[108] N. F. M. and E. J. Roozenburg, “Product Design: Fundamentals and Methods,” *John Wiley Son Ltd., Chichester*, 1995.

[109] P. Habibovic, U. Gbureck, C. J. Doillon, D. C. Bassett, C. A. van Blitterswijk, and J. E. Barralet, “Osteoconduction and osteoinduction of low-temperature 3D printed bioceramic implants,” *Biomaterials*, vol. 29, no. 7, pp. 944–953, Mar. 2008, doi: 10.1016/J.BIOMATERIALS.2007.10.023.

8. ÍNDICE DE FIGURAS

9. ÍNDICE DE TABLAS

ANEXOS

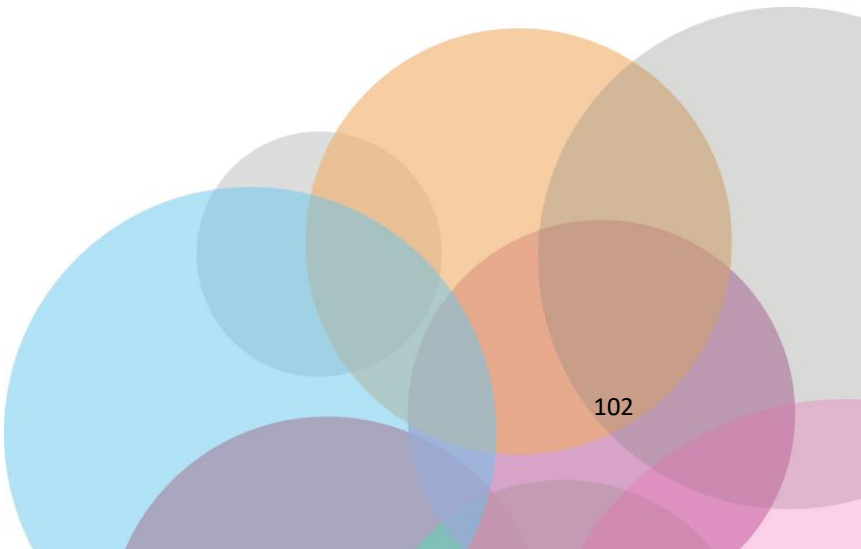

CONGRESOS INTERNACIONALES

ANEXO I:

Conferencia: Seventh International Conference on Technological Ecosystems for Enhancing Multiculturality. October 2019, León

Autores: J.M. de Agustín del Burgo; R. D'Amato; J.A. Juanes Méndez; A. Sánchez Ramírez; F. Blaya Haro; E. Soriano Heras; J.M. Garcia Alonso

Título: Real time analysis of the filament for FDM 3D printers

Publicación: TEEM'19, October 16–18, 2019, León, Spain © 2019 Association for Computing Machinery. ACM ISBN 978-1-4503-7191-9/19/10. DOI: https://doi.org/10.1145/3362789.3362818

ANEXO II:

Conferencia: TEEM'20: Eighth International Conference on Technological Ecosystems for Enhancing Multiculturality. October 2020

Autores: J.M. de Agustín del Burgo; F. Blaya Haro; R. D'Amato; J.A. Juanes Méndez;

Título: Smart splint for diagnosis during initial stage of treatment

Publicación: TEEM'20, October 21–23, 2020, Salamanca, Spain© 2020 Association for Computing Machinery. ACM ISBN 978-1-4503-8850-4/20/10. DOI: https://doi.org/10.1145/3434780.3436610

ANEXO I:

REAL TIME ANALYSIS OF THE FILAMENT FOR FDM 3D PRINTERS

Este proyecto plantea la necesidad de desarrollar un sistema de control de calidad para los procesos de fabricación por deposición fundida. El principal problema de esta tecnología es que, si los parámetros ambientales no se controlan suficientemente, se crea una inexactitud entre las propiedades mecánicas y estéticas del producto. Esto provoca que las piezas no cumplan con los requisitos del mercado ya que no pueden garantizar un rendimiento unificado.

Para ello, se llevará a cabo una prueba de concepto que implementa los sensores necesarios en una máquina de pruebas. Los sensores recogerán las medidas mediante un microcontrolador Arduino. La información obtenida será procesada con el fin de realizar los informes que indiquen si el proceso de fabricación cumple con los requisitos esperados.

Con este sistema es posible mejorar los resultados de fabricación por deposición fundida y asegurar estándares de calidad. En el futuro, el sistema podría mejorarse de acuerdo con los parámetros de calidad exigidos por las normas ISO para los filamentos de impresión y también utilizarse para certificarlos.

Considerando todo lo anterior, este es sin duda un campo de investigación que aún tiene mucho por desarrollar y se espera que este trabajo sea un aporte para futuras investigaciones.

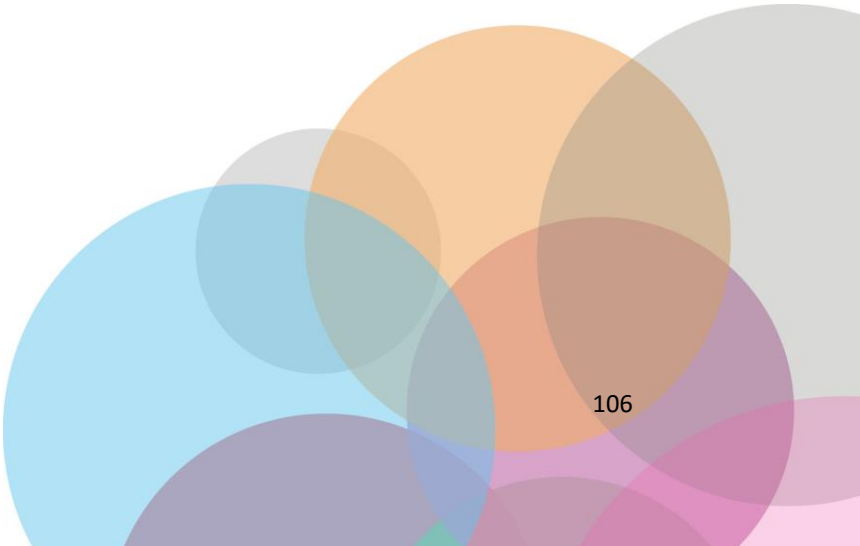

Real time analysis of the filament for FDM 3D printers [*]

José M. de Agustín del Burgo[†]
Universidad Politécnica de Madrid
28012 Madrid, Spain
jm.deagustin@alumnos.upm.es

Roberto D'Amato
Universidad Politécnica de Madrid
28012 Madrid, Spain
r.damato@upm.es

Juan Antonio Juanes Méndez
VisualMed Systems Group
Universidad de Salamanca
Salamanca, Spain
jajm@usal.es

Alberto Sánchez Ramírez
Universidad Politécnica de Madrid
28012 Madrid, Spain
alberto.sanchezr@upm.es

Fernando Blaya Haro
Universidad Politécnica de Madrid
28012 Madrid, Spain
Fernando.blaya@upm.es

Enrique Soriano Heras
Department of Mechanical Engineering, University Carlos III of Madrid 28911 Spain
esoriano@ing.uc3m.es

ABSTRACT

This project raises the need to develop a quality control system for manufacturing processes by melt deposition. The main problem with this technology is that, if the environmental parameters are not sufficiently controlled, inaccuracy is created between the mechanical and aesthetic properties of the product. This causes that the pieces do not meet the requirements for the market since they cannot guarantee a unified performance.

For this purpose, a proof of concept that implements the necessary sensors in a testing machine will be carried out. The sensors will collect the measurements by means of an Arduino microcontroller. The obtained information will be processed in order to make the reports that indicate if the manufacturing process meets the expected requirements.

With this system it is possible to improve the manufacturing results by melted deposition and to assure quality standards. In the future, the system could be improved according to the quality parameters required by the ISO standards for printing filaments and also used to certify them.

Considering all the aforementioned, this is undoubtedly a field of research that still has much to develop and it is expected that this work will be a contribution for future research.

CCS CONCEPTS

• Hardware → Bio-embedded electronics

KEYWORDS

3D printing, melt deposition, quality control, printing filaments, Marlin, sensing.

[*]Article Title Footnote needs to be captured as Title Note
[†]Author Footnote to be captured as Author Note

TEEM'19, October 16–18, 2019, León, Spain
 ACM ISBN 978-1-4503-7191-9/19/10…$15.00 https://doi.org/10.1145/3362789.3362818

ACM Reference format:
José M. de Agustín del Burgo, Roberto D'Amato, Juan Antonio Juanes Méndez, Alberto Sánchez Ramírez, Fernando Blaya Haro and Enrique Soriano Heras. 2019. Insert Your Title Here: Insert Subtitle Here. In *Proceedings of ACM TEEM conference (TEEM'18). ACM, New York, NY, USA,5 pages.*

1 Introduction

It[1] is a fact that 3D printing is positioning itself as the process of manufacture of the 21st century. In particular, the manufacture by deposit of filament (FDM) has spread more than any other thanks to the large community of developers who have been interested in this. This has led to an increase in the supply available in the market, which once has brought as a drastic price and has expanded the variety of materials with which they can be manufactured; for example, conductors of electricity, biodegradable, resistant or biocompatible.

The increase in manufacturing at a particular and professional level requires an increase in print quality, a reduction in machine costs and an increase in the knowledge of the scientific community [1] [2] [3].

When making three-dimensional impressions by addition it is necessary to control several parameters to achieve an optimal final product. In many cases it is necessary to monitor the process in person when it is the first time you want to manufacture an object, since the failure rate is relatively high in FDM.

During the deposition process, many of the variables that contribute to improving or worsening the final result are subject to disturbances that come from the system itself as well as from others outside the machine. This type of deviations is difficult to control, as happens with the variability of the material, variations in the outside and inside temperature of the machine, humidity or

[1] The existing Bibstrip data, copyright text and permission block in the sample file are dummy values, so the user needs to provide the correct values required for the submission in the metadata dialog box.

deviations in the printing area [4]. Currently, the sensorized and the control of additive manufacturing processes, is presented as an evolution of the methods, categorized as sensorized and control of the variables and sensorized and control of manufacturing attributes [5]. The control and optimization of the filament production operations, contribute to get better quality of the filament, but it still reaches large tolerances [6]; [7]; [8]; [9].

2 Materials and Methods

The initial purpose is to perform a real-time analysis of the printing parameters related to the filament that can affect the final quality of the product. The object of investigation will focus on the parameters for biocompatible materials due to its great complexity.

The procedure will be based on sensors installed in the electronics of a testing machine that will be responsible for collecting the relevant parameters, in this case humidity, ambient temperature at several points, actual filament diameter and filament entry speed [10]. Additionally, the printer will communicate with the system through SPI to supply in a complementary way the height data of the Z axis and the temperature of the extruder.

Then it will be necessary to program a communication algorithm between the controller board of the sensors and the printer to coordinate the printing with the data collection in addition to extracting data directly from the parameters of the machine.

The final stage will be to collect via serial port all this information of each printing process and prepare reports in which you can see in detail if quality standards have been maintained throughout the process. If it has not been maintained, it will also be possible to locate the exact point of the piece where it was not met and even predict future structural failures.

With all this, it is intended to demonstrate that objects can be manufactured by melting deposition with quality standards. Table 1 shows the sensors specifications.

Sensor	Measure	Precision	Range	Frequency
DHT11	Humidity	±5% RH	20% / 90%	500Hz-2kHz
LM35	Temperature	±0.5°C	−55°C / 150°C	-
NTC Thermistor	Temperature	±0.5°C	-55°C / +125°C	-
DS18B20 digital thermometer	Temperature	±2°C	-55°C / +125°C	-
TSL1401CL Linear sensor	Diodes	1%	0.2V / 2,4V	8MHz
Optical encoder HC-020K	Encoder	0,01 mm	-	100KHz

Table 1. Sensors specifications

Humidity sensor: The humidity sensor chosen is the DHT11 is a pre-calibrated sensor with a digital output signal.

Temperature sensor: In terms of temperature, two LM35 sensors have been used, since it is the one with the most precision and temperature range among the analyzed ones. This device is a linear temperature sensor that consists of an integrated circuit and an encapsulation. It generates an output voltage proportional to the temperature of 10mV / ° C [11]. The functions that relate the temperature and output voltage are:

$$T = 100 \cdot Vout \quad (1)$$

And as the analog / digital converter of the microcontroller has a 10-bit resolution with a reference voltage of 5V:

$$T = 100 \cdot Ain \frac{Vref}{2^{10}} \quad (2)$$

Where T = measured temperature, Vref = 5V and Ain = signal read by the plate.

Feed sensor: The encoder will be used to measure the feed rate filament at the entrance of the extruder. An optical encoder consists of a photo-switch and a wheel with notches that activate and deactivate it. In figure 1 it is possible to see an example of how an encoder works.

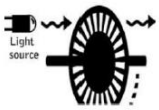

Figure 1. Light encoder

The linear movement of the filament is transformed by a toothed shaft [12] into a rotational movement that is measured by the encoder counting the pulses of light. It is intended to obtain the speed and distance traveled of the material at the entrance of the extruder, not after being extruded. To get the distance:

$$X = X_0 + \frac{n \cdot \pi \cdot D}{N} \quad (3)$$

Where x = total distance, x0 = previous measured distance, n = detected pulses, D = diameter of the dentate axis, N = 20 (notches of the wheel). To measure the velocity, it would simply be necessary to divide the distance measured from the last sample between the sampling time.

$$v = \frac{n \cdot \pi \cdot D}{N \cdot t} \quad (4)$$

Diameter sensor: The diameter sensor is the "3D Printer Filament Width Sensor V3.2" designed by JasonKits [13]. Its main component is the TSL1401CL, a 128-bit photodiode array sensor arranged in line. By means of a control PCB, the shadow projected by the filament on the photodiode sensor is passed to an output voltage corresponding to the diameter in millimeters. In this way a projection of 1.75mm thick generates the plate an output of 1.75V. This signal is collected by the analog / digital converter of the microcontroller for its use.

Through the combination of feed sensor and diameter sensor we can obtain the real-time measurement of the material flow that enters the extruder:

$$\bar{Q} = \bar{v} \cdot A = \bar{v} \cdot \pi \cdot \frac{D^2}{4} \quad (5)$$

Where Q = flow, v = speed of the filament, A = area of the section and D = diameter of the filament.
With all these data, it will be possible to make a report for each manufacturing process, according to the conditions in which the process has been carried out.

3 Results

In order to evaluate the real usefulness of this system of measurement and analysis of data has been subjected to trials. It is tried to demonstrate that a meticulous control of the temperature and a traceability of the printing process are determining to ensure an optimum result. To do so, benchmarking models have been designed to be printed on the test machine and be tested with different procedures.
During the printing of each one of the pieces individually, the information coming from the sensing system designed throughout this project has been collected.
The printing material has been the filament of PLA 1,75mm transparent color of the BQ brand, since it offers deviations of ± 0,03mm and an optimum printing temperature of 210 ± 10oC. The program chosen for the generation of G-code has been Cura, since in addition to being the most used it is open source and free.
The printing parameters common to all models are:

- Layer height: 0.15mm
- First layer height: 0.3mm
- Wall Thickness: 0.8mm
- Thickness up / down: 0.8mm
- Fill density: 50%
- Print speed: 70mm / s
- Ventilation: Yes
- Support: No
- Retraction: Yes

Two types of specimens have been modeled. The first one corresponds to 50x25x5mm dimensions so that they can be printed with vertical orientation. The temperature has been pre-established at 210ºC; however, 5 models have been generated with constant temperature and another 5 with a temperature drop programmed at 195ºC during 5 layers at a height of 15mm to cause a supposed breaking point. With these specimens we try to see how a lack of temperature affects the mechanical resistance of the layers. In the models with the programmed temperature defect, a transverse region with a slightly different finish than the rest of the piece is observed, agreeing with the zone of rupture.
The second type corresponds to standardized samples of 170x20x4mm and have been manufactured horizontally in two batches of 5 units at different temperatures each batch. A lot with a temperature of 210ºC, since it is the temperature recommended by the manufacturer and another one at 225ºC. With this test we want to see how the overheating affects the mechanical and physical properties of the material. No apparent visual difference was observed between any of the two batches; however, in the batch at 225ºC some failed processes were obtained, since the adherence of the material to the bed was so high that it caused them to break when trying to detach them. Figure 2 shows the benchmarking printed models.

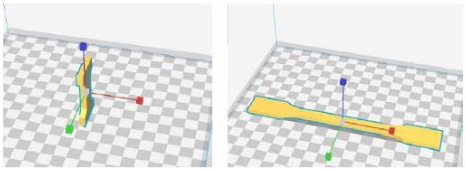

Figure 2. Benchmarking models

Once the specimens of both types have been printed and labeled, a dimensional analysis has been carried out without knowing the type of each specimen to ensure a non-arbitrary process. The most relevant dimensions of the pieces have been measured with a precision gauge. Figure 3 shows the measures of verrtical models.

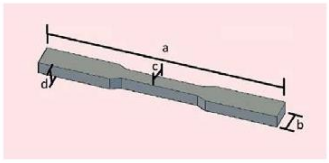

Figure 3. Measures of the vertical benchmarking models

Vertical 1	A	B	C	D
1.1	49.50	25.30	12.75	5.25
1.2	49.55	25.35	12.65	5.20
1.3	49.40	25.35	12.65	5.35
1.4	49.35	25.30	12.70	5.15
1.5	49.45	25.35	12.65	5.25
Mean:	49.45	25.33	12.68	5.24

Table 2. Vertical models with established temperature in mm

Vertical 2	A	B	C	D
2.1	49.50	25.30	12.65	5.25
2.2	49.70	25.25	12.60	5.30
2.3	49.60	25.30	12.60	5.30
2.4	49.70	25.35	12.65	5.35
2.5	49.70	25.25	12.60	5.25
Mean:	49.64	25.29	12.62	5.29

Table 3. Vertical models with temperature variation in mm

Tables 2 and 3 shows the results in vertical orientation at 210 and 225 degrees. There is no significant difference between the dimensions of the vertical lots. This is because most of the process has been brought to the same temperature (210ºC) in both cases. It is remarkable the particularity that in the Z axis (dimension A) the

measurements are up to 0.65 mm below the expected, this can be a correct correction of a rush of the Z axis deducing that there has been a dilation of the material between 0.12 mm and 0.33 mm on average. For the measurement of the horizontal models, following configuration has been chosen (Figure 4):

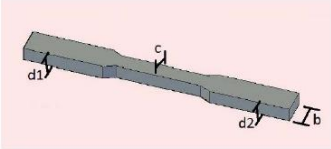

Figure 4. Measures of the horizontal benchmarking models

Horizontal 1	B	C	D1	D2
1.1	20.25	10.25	3.65	3.80
1.2	20.40	10.35	3.70	4.00
1.3	20.35	10.30	3.45	3.65
1.4	20.30	10.30	3.70	3.95
1.5	20.25	10.25	3.70	3.95
Mean:	20.31	10.29	3.64	3.87

Table 4. Horizontal models at 210°C in mm

Horizontal 2	B	C	D1	D2
2.1	20.50	10.20	3.55	3.90
2.2	20.45	10.20	3.35	3.70
Failed				
Failed				
2.3	20.50	10.25	3.60	3.95
2.4	20.40	10.20	3.45	3.70
Failed				
2.5	20.40	10.20	3.55	3.75
Mean:	20.45	10.21	3.49	3.79

Table 5. Horizontal models at 225°C in mm

Tables 4 and 5 shows the results in horizontal orientation at 210 and 225 degrees. The first noticeable difference between the two lots is the failure rate, since in the 225ºC lot it is much higher due to an excess fragility of the pieces that makes that when they are extracted from the base some of them have resulted damaged.

3.1 Traction Test

The test consists of subjecting the model to an axial stress of increasing tension until it causes the rupture. In this way, a tension/deformation graph is obtained, from which certain measurements can be extracted, such as the Young's modulus (E), maximum strength (Fmax), tensile strength (σmax) and the elastic limit (σe) among others.

With this test, we intend to observe how superheating influences the mechanical properties of horizontal specimens or an insufficient temperature at the point of rupture of vertical specimens. The results for the vertical models are showed in table 6 and 7:

Vertical 1	E (Mpa)	σe (%)	Fmax (N)	σmax (MPa)	E·Fmax (mm)
1.1	Failed				
1.2	598.32	4.416	1072.333	0.48	1.264
1.3	561.718	8.495	1435.333	0.68	2.488
1.4	720.698	6.34	1470.667	22.057	1.898
1.5	819.079	4.84	1515.667	22.732	1.453
Mean:	674.954	6.023	1373.500	11.487	1.776

Table 6. Stress tests in vertical models with established temperature

Vertical 2	E (Mpa)	Σe (%)	Fmax (N)	σmax (MPa)	E·Fmax (mm)
2.2	740.12	5.01	1135.33	0.66	1.45
2.2	690.18	5.16	1180.33	0.66	1.45
2.3	781.73	7.63	1572.00	0.65	1.67
2.4	775.77	4.74	1377.33	0.70	1.37
2.5	802.15	4.56	1308.33	19.62	1.37
Mean:	757.99	5.42	1314.66	4.46	1.46

Table 7. Stress tests in vertical models with temperature variation

It is observed that in the models without programmed failure the breaking point is centered in the part, while in those with the programmed temperature decrease, the breaking point is displaced towards where this defect was located. Table 8 and 9 show the stress tests for the horizontal models:

Horiz 1	E (Mpa)	σe (%)	Fmax (N)	σmax (MPa)	E·Fmax (mm)
1.1	1369.40	5.05	1423.33	38.20	3.82
1.2	1557.34	4.12	1583.67	43.09	3.57
1.3	1299.08	4.88	1270.33	34.12	3.70
1.4	1508.72	4.28	1491.67	40.12	3.47
1.5	1474.37	4.66	1427.00	38.10	3.44
Mean:	1441.78	4.59	1439.20	38.72	3.60

Table 8. Stress tests in horizontal models printed at 210°C

Horiz 2	E (Mpa)	σe (%)	Fmax (N)	σmax (MPa)	E·Fmax (mm)
2.1	1347.40	4.73	1447.67	38.93	3.84
2.2	1313.01	3.79	1220.00	33.13	3.31
2.3	1243.73	4.11	1265.67	34.43	3.65
2.4	1349.47	4.24	1408.67	38.29	3.76
2.5	1441.79	4.58	1386.00	37.10	3.52
Mean:	1339.08	4.29	1345.60	36.37	3.61

Table 9. Stress tests in horizontal models printed at 225°C

The horizontal specimens have similar properties with a maximum axial force between 1300N and 1500N. They show plastic deformation.

4 Discussions

The first test piece maintains a constant temperature within a predetermined range while the second has a temperature drop that is recorded by the system. Later in the tensile tests these models that had the temperature drop had a 61.16% lower mechanical resistance than the rest. As for the horizontal models, a much greater resistance is detected, as expected, since the axial force is parallel to the threads forming the part and there is no weakening per layer. It is also observed that the specimens that have been overheated bear 6.5% less tension because the material has partially degraded when exceeding the recommended printing temperature. In the following charts (Figures 5,6,7, 8 and 9), it is showed the variation of temperature in vertical models and the stress test results.

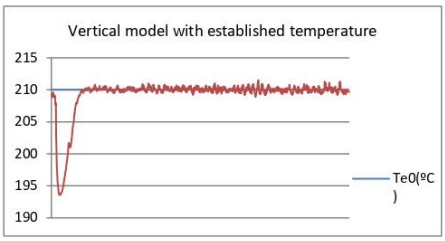

Figure 5. Vertical model with established temperature

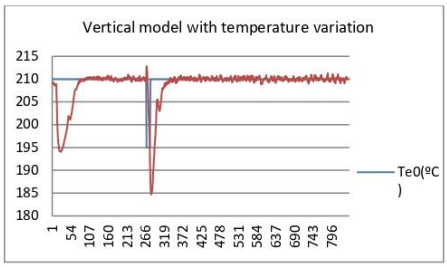

Figure 6. Vertical model with temperature variation

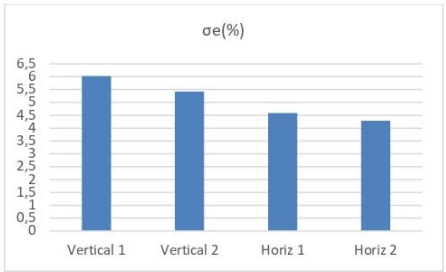

Figure 7. σ_ε(%) result for the different tests

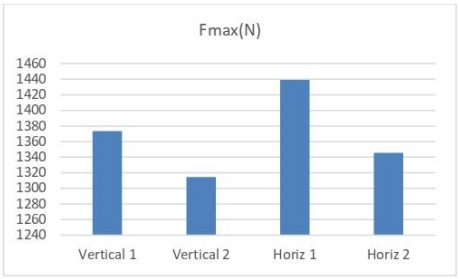

Figure 8. F_{max} (N) result for the different tests

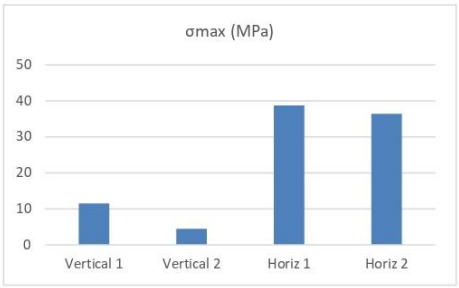

Figure 9. σ_{max} (MPa) result for the different tests

With this it is demonstrated that this system is capable of detecting faults during the manufacturing process and discarding those products, however, possible improvements of the prototype have been detected as being a proof of concept.

The control of environmental conditions for 3d printing is of fundamental importance in biomedical applications. In fact, in many cases strict control of the temperature or humidity in the printing chamber is needed. In the case of manufacturing by 3D printing bio-ceramic joint implants has to be performed at low temperature [14]. The fluctuation of the temperature would damage the internal structure of the material. In other cases, the temperature could produce novice particles. This would affect to the operator safety and would make impossible to use the machine in some cleaning rooms that are normally used in medical ambient [15].

5 CONCLUSIONS

With this innovation project, it is intended to provide a solution for the printing problems and provide quality control at an industrial level to additive manufacturing. Despite being far from offering a definitive solution, the results presented here offer a very optimistic starting point to continue developing systems that help manufacturing by molten deposition to be more reliable.

It is also showed some stress results that should be taken into account when positioning a new model to be produced using a FDM process.
This also should be used to produce the parts using material in tis correct conditions of temperature, humidity or deposition speed, so that the mechanical characteristics are not decreased [16].
Possible improvements include the use of more precise sensors such as an encoder with sense detection, reverse information to the printer to control printing actively in real time, create alerts that notify when a parameter exceeds the limits and stop the process if necessary.
Another application for which this technology could be worth, is the validation of filaments by precision laser sensors, generating a report in which it can be seen if the filament has manufacturing defects or if the dimensional tolerances are met.

REFERENCES

[1] Ariel Calderon James Griffin Juan Cristóbal Zagal, (2014),"BeamMaker: an open hardware high-resolution digital fabricator for the masses", Rapid Prototyping Journal, Vol. 20 Iss 3 pp. 245 – 255

[2] Mota, C. (2011), "The rise of personal fabrication", Proceedings of the 8th ACM Conference on Creativity and Cognition, ACM Press, Atlanta, GA, p. 279.

[3] Stemp-Morlock, G. (2009). "Personal fabrication", Technology, 53 (1). 2-3.

[4] Sebastian Stopp Thomas Wolff Franz Irlinger Tim Lueth, (2008),"A new method for printer calibration and contour accuracy manufacturing with 3D-print technology", Rapid Prototyping Journal, Vol. 14 Iss 3 pp. 167 – 172

[5] Edward W. Reutzel and Abdalla R. Nassar Rapid Prototyping Journal Volume 21 · Number 2 · 2015 · 159–167

[6] Volpato, N., Kretschek, D., Foggiatto, J. A., & da Silva Cruz, C. G. (2015). Experimental analysis of an extrusion system for additive manufacturing based on polymer pellets. The International Journal of Advanced Manufacturing Technology, 1-13.

[7] Turner, B. N., and Gold, S. A. (2015). A review of melt extrusion additive manufacturing processes: II. Materials, dimensional accuracy, and surface roughness. Rapid Prototyping Journal, 21(3), 250-261

[8] Turner, B. N., Strong, R., and Gold, S. A. (2014). A review of melt extrusion additive manufacturing processes: I. Process design and modeling. Rapid Prototyping Journal, 20(3), 192-204.

[9] Ratzsch, K. F., Kádár, R., Naue, I. F., & Wilhelm, M. (2013). A Combined NMR Relaxometry and Surface Instability Detection System for Polymer Melt Extrusion. Macromolecular Materials and Engineering, 298(10), 1124-1132

[10] Simplify3D, «Print Quality Troubleshooting Guide», 2016. [On Line]. Available in: https://www.simplify3d.com/support/print-quality-troubleshooting/. [Accessed: 27-jul-2018].

[11] L. Datasheet, «LM35 Precision centigrade temperature sensors», Retrieved Sept.13th, n.o November, 2017.

[12] M. Fiedler, «Evaluating Tension and Tooth Geometry to Optimize Grip on 3D Printer Filament», 3D Print. Addit. Manuf., vol. 2, n.o 2, pp. 85-88, jun. 2015.

[13] JasonKits, «Filament Width Sensor», 2018. [On Line]. Available in: https://github.com/jasonmarkham/FWS_V3.2/blob/master/fws_v3.2.pdf [Accessed: 27-jul-2018]

[14] Soriano Heras, Enrique; Blaya Haro, Fernando; de Agustín del Burgo, José M.; Islán Marcos, Manuel; D'Amato, Roberto. 2018. Filament Advance Detection Sensor for Fused Deposition Modelling 3D Printers. Sensors 18, no. 5: 1495

[15] P. Habibovic, U. Gbureck, C. J. Doillon, D. C. Bassett, C. A. van Blitterswijk, and J. E. Barralet, "Osteoconduction and osteoinduction of low-temperature 3D printed bioceramic implants," Biomaterials, vol. 29, no. 7, pp. 944–953, Mar. 2008.

[16] Roozenburg, N. F., and Eekels, J. (1995). Product design: fundamentals and methods (Vol. 2). Chichester: Wiley.

universidad de león

José María De Agustin Del Burgo

con DNI núm. 51118583W

ha asistido con asiduidad y aprovechamiento al

Congreso, Jornada, Seminario o Taller

7th edition of the Technological Ecosystems for Enhancing Multiculturality (TEEM 2019)

celebrado en León

del 16/10/2019 al 18/10/2019

con una duración de 24 horas / 1 crédito/s ECTS organizado por el Vicerrectorado de Relaciones Institucionales y con la Sociedad de la Universidad de León.

Y para que así conste, se expide la presente certificación.

En León, a 18 de octubre de 2019

V.º B.º La Vicerrectora — El Director — Los Directores

María Dolores Alonso-Cortés Fradejas

Miguel Ángel Conde González

Camino Fernández Llamas

Francisco J. García Peñalvo

Libro de registro: A30113

Nota: La presente certificación no tiene el carácter oficial establecido en el artículo 28.1 de la Ley Orgánica de Reforma Universitaria.

TEEM'19
TECHNOLOGICAL ECOSYSTEMS FOR ENHANCING MULTICULTURALITY
LEÓN 16-18 OCTOBER 2019

We, hereby, certify that:

José María De Agustín Del Burgo

has attended the 7th International Conference in Technological Ecosystems for Enhancing Multiculturality (TEEM 2019).

The conference has been held in León, Spain, on October 16-18, 2019 and organized jointly by the Robotics Group and GRIAL Research Group with the support of the University of León.

Signed by:

TEEM'19

Miguel Ángel Conde
TEEM2019 Conference Chair

universidad de león
GRUPO DE ROBÓTICA
GRIAL

TEEM'19
TECHNOLOGICAL ECOSYSTEMS FOR ENHANCING MULTICULTURALITY
LEÓN 16-18 OCTOBER 2019

We, hereby, certify that:

José María de Agustín del Burgo

has presented the paper entitled:

Real time analysis of the filament for FDM 3D printers

at the 7th International Conference in Technological Ecosystems for Enhancing Multiculturality (TEEM 2019).

The conference has been held in León, Spain, on October 16-18, 2019 and organized jointly by the Robotics Group and GRIAL Research Group with the support of the University of León.

Signed by:

TEEM'19

Miguel Ángel Conde
TEEM2019 Conference Chair

universidad de león

GRUPO DE ROBÓTICA

GRIAL

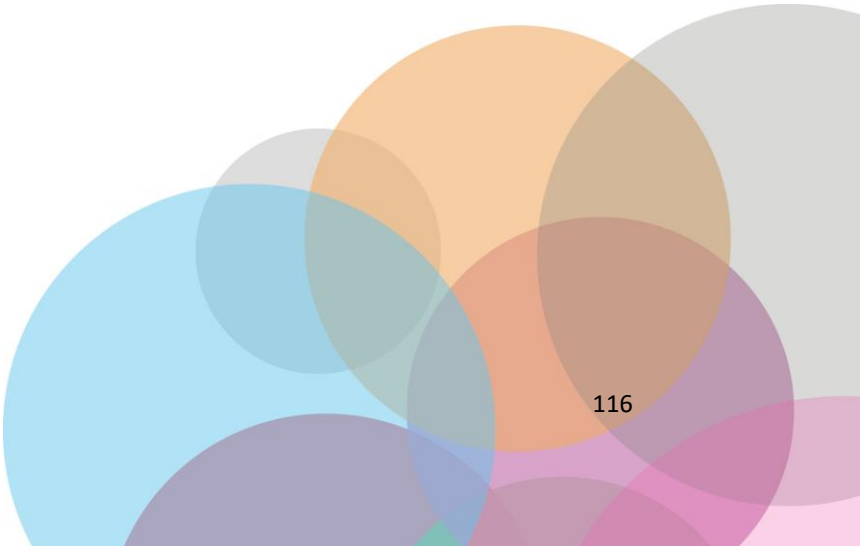

ANEXO II:

SMART SPLINT FOR DIAGNOSIS DURING INITIAL STAGE OF TREATMENT

Hoy en día, tras sufrir determinadas lesiones por rotura musculoesquelética, el único tratamiento disponible es el uso de yeso. Sin embargo, este tipo de tratamiento, que es similar al utilizado originalmente por los persas en el siglo X, tiene algunas desventajas, que todavía están presentes en la actualidad. Suele causar malestar debido a el peso (alrededor de 1,5 kg) y las restricciones para refrescar la piel. Además, no es sumergible y no es posible aplicar ciertos tipos de tratamientos, como ultrasonidos o infrarrojos. También puede aparecer complicaciones a nivel vascular, muscular o incluso articular debidas a estos problemas.

Este proyecto tiene como objetivo mostrar que existe una opción que solucionaría estos inconvenientes. Además, sería permiten una recuperación más rápida y mejor, combinando prototipos 3D, 3D escaneo, medicina, ingeniería y evolución de materiales. Este estudio propone el uso de la integración de sensores dentro de las férulas para detectar cualquier tipo de problema durante el proceso de tratamiento. Estos sensores se diferentes datos como presión, color, humedad y temperatura de la férula. Después de eso, estos parámetros se analizan para determinar cualquier evolución inesperada y enviada por canales telemáticos para ser consultado a distancia por un especialista.

Smart splint for diagnosis during initial stage of treatment

José M. de Agustín del Burgo
Universidad de Salamanca, Salamanca, Spain
id00792219@usal.es

Fernando Blaya Haro
Universidad Politécnica de Madrid, 28012 Madrid, Spain
Fernando.blaya@upm.es

Roberto D'Amato†
Universidad Politécnica de Madrid, 28012 Madrid, Spain
r.damato@upm.es

Juan Antonio Juanes Méndez
VisualMed Systems Group, Universidad de Salamanca, Salamanca, Spain
jajm@usal.es

ABSTRACT

Nowadays, after suffering certain musculoskeletal rupture injuries, the only treatment available is the use of plaster cast. However, this type of treatment, that is similar to the used originally by the Persians in the 10th century, has some disadvantages, that are still present nowadays. It usually causes discomfort due to the weight (around 1,5kg) and the restrictions to refresh the skin. Moreover, it is not submersible and it is not possible to apply certain kind of treatments, like ultrasounds or infrared. It also may appear complications at the vascular, muscular or even articular level due to these problems.This project aims to show there is a really possible option that would solve these inconvenient. Moreover, it would allow a faster and better recovery, combining 3D prototyping, 3D scanning, medicine, engineering and materials evolution. This study proposes the use of sensor integration inside the splints to detect any kind of problem during the treatment process. These sensors get different data like pressure, color, humidity and temperature from the splint. After that, these parameters are analyzed to determine any unexpected evolution and sent by telematic channels to be consulted remotely by a specialist.

CCS CONCEPTS

• **Applied computing** → Life and medical sciences; Health informatics.

KEYWORDS

Smart Splint, 3D printing, Sensors, Treatment evolution

ACM Reference Format:
José M. de Agustín del Burgo, Fernando Blaya Haro, Roberto D'Amato†, and Juan Antonio Juanes Méndez. 2020. Smart splint for diagnosis during initial stage of treatment. In *Eighth International Conference on Technological Ecosystems for Enhancing Multiculturality (TEEM'20), October 21–23, 2020, Salamanca, Spain.* ACM, New York, NY, USA, 9 pages. https://doi.org/10.1145/3434780.3436610

TEEM'20, October 21–23, 2020, Salamanca, Spain

ACM ISBN 978-1-4503-8850-4/20/10…$15.00
https://doi.org/10.1145/3434780.3436610

1 INTRODUCTION

Industrial Design and Advanced Manufacturing has made it possible an enormous growing of New Industry. Moreover, the optimization of the process [1], [2], the new concept of materials [3] and the decrease of costs [4] are some achievements that has produced an expansion of these technics further than the industrial area to applications known as Bioengineering [5].

The implementation of fused deposition modelling (FDM) or selective laser fusion (SLM) in the healthcare industry, allows benefits in terms of design and customization of medical devices and implants. Clear examples of these advances are craniomaxillofacial surgery prothesis [6], different therapies for obstructive sleep apnea (OSA) [7], [8], orthopedics surgery [9] or rehabilitation [10], Moreover, it simultaneously improves wearing comfort and hygiene. Many developments have been carried out, like exoskeletons [11], assistive devices or prosthesis. Although these specialties are very demanded [12] specially in developed countries, it is necessary a level of maturity and development technologically speaking, to get a real change in the actual model.

Also, the incursion of this new 3D techniques in medical processes, makes it possible to include smart systems that will allow to analyze different medical states of the evolution process. These kinds of systems that includes small electronic devices, microprocessors, programming systems and data communication, are responsible of monitoring and treatment of different data, that could also be sent to an application or a mobile device [13]. Moreover, these data can be compared and treated using Artificial Intelligence in medicine [14] to detect any kind of problems, so it opens a big new world of treatment and diagnostic possibilities.

This study focuses on the implementation of all of these concepts. It will be showed the development and prototyping of a smart immobilization splint using a 3D scanner using biocompatible material. This splint will incorporate different windows for possible treatments like lymph drainage, iontophoresis, ultrasound, laser or electrostimulation. It will also include sensors that will be placed to get pressure, temperature, color skin and humidity of the immobilized area.

2 MATERIALS AND METHODS

In this section it is explained and presented the different steps that are followed to design a 3D virtual model of the splint that will be produced later. In this case, it was used as model the right leg of a 29 years old volunteer, that will be the basis to create digitally the splint where the tests will be carried out. In this case, there was

Table 1: Sensors technical specifications

Sensor Model	DS18B20	DHT22	DF9-40	TCS34725
Dimensions (*mm*)	6 x 6 x 50	15 x 7,7 x 20	40 x 20 x 0,25	25 x 20 x 1,5
Power voltage (*V*)	3,0 - 5,5	3,3 – 6	5	5
Working range	-55*{°}C* to 125*{°}C*	-40*{°}C* to 80*{°}C* 0 to 100% *RH*	0-500 *g*	-
Resolution	± 0,0625*{°}C*	0,1*{°}C*, 0,1% *RH*	14,5 *g*	-

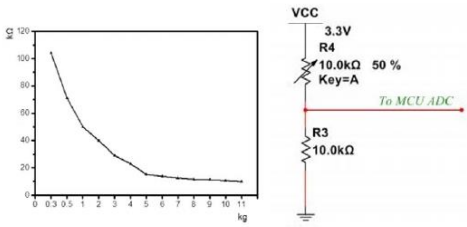

Figure 1: DF9-40 behavior (a) and pull-down resistor configuration (b)

Figure 2: ESP TTGO board

no injury. Also, this process could be applied on other anatomical regions [13] [15].

2.1 Sensing technologies

When an injury occurs, it may appear normal inflammatory signs like increased skin temperature, changes in skin color, cool skin, increased sweating or edema. These symptoms may appear due to different problems that may be suffering the patient [16], [17].

The sensors implemented will be the responsible of monitor some parameters to carry out a diagnostic. The parameters considered are pressure, temperature, humidity and skin color. The data obtained are combined to determine if there are any signal of unexpected evolution during the treatment. The sensors proposed to be used are: two temperature sensors (DS18B20) [18] in direct contact with the skin, one temperature and humidity sensor (DHT22) [19] to get the temperature and humidity between the skin and the splint, two pressure sensors (DF9-40) [20] and one color sensor TCS34725 [21]. Table 1 summarizes the technical specifications of these sensors.

- DS18B20 sensors (Dallas Semiconductor™ Maxim Integrated Products, Inc., Dallas, USA) are 1-Wire digital temperature sensor. It reports degrees in Celsius, with a precision of 9 to 12-bit.
- DHT22 sensor (Aosong Electronics Co., Ltd., Guangzhou, China) utilizes exclusive digital-signal-collecting-technique and humidity sensing technology, its sensing elements is connected with 8-bit single-chip computer
- DF9-40 sensor (Zhengzhou Winsen Electronics Technology Co., Ltd, Zhengzhou, China) is a film pressure based on flexible pressure sensing technology (Figure 1).

In order to measure the applied force, it will be necessary to build a voltage divider circuit with a pull-down resistor (Figure 1b). This circuit creates a variable voltage output that can be read by the ADC (analog to digital converter) input of the microcontroller. It means that for a simple force-to-voltage conversion the Force Sensing Resistor (R_4) device is tied to a measuring resistor (R_3) in a voltage divider. In this case, a 10kΩ resistor will be used. The output voltage (V_{out}) that is possible to measure with the Arduino is described by the following equation:

$$V_{out} = \frac{V_{cc} \cdot R3}{R3 + R4} \quad (1)$$

TCS3472 sensor provides a digital return RGB values (Red Green Blue), and it also clears the light sensing values. It includes an IR blocking filter, which minimizes the IR spectral component of the light, making it possible to get accurate color measurements.

These sensors will be controlled by a ESP32 micro [22], mounted on TTGO OLED Display and Battery Board, that also includes Wi-Fi and Bluetooth. This micro will read the data from the different sensors and will show the information on the display. This info can be consulted using a mobile device connected by Bluetooth, and also, a Webserver can be implemented in ESP32, to be consulted by accessing from anywhere. Moreover, it includes a battery (in this case Li-ion 12.21AH) so it is not necessary to have it connected to a power source (Figure 2).

Table 2: Technical specifications of Sense®3D scanner

Max Scanning Volume	2 x 2 x 2 (m)
Min Scanning Volume	0,2 x 0,2 x 0,2 (m)
Working Distance	0,2 – 1,6 (m)
Number of cameras	2
Class Certified Laser Product	1
Resolution at 0.5 m	1 (mm)

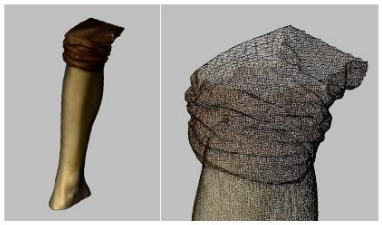

Figure 3: Mesh surface (a) and detailed view (b)

2.2 3D Model and Design

As explained in previous studies, first step is to get the 3D model of the part that is going to be immobilized [4]. In this case it is used a 3D Systems Sense®scanner, that offers enough technical specifications to get a good quality model. Table 2 shows the technical specifications.

When the scanning process is finished, a 3D points cloud is obtained, that must be cleaned and treated posteriorly to get the 3D model to begin the designing process. In this point, it starts a process to convert the points cloud to a solid model that can be handled using a parametric design program. First, it obtained a mesh surface by using the 3D CAD software Geomagic FreeForm (3D Systems, Inc., United States). Figure 3 shows the resultant mesh surface.

This mesh has to be cut to select the desired area, and an offset of 0.5mm is included, that will allow greater comfort due to the member will not be pressed. Also, in this step, it is generated the thickness of the model (3,7mm), considering the posterior fixing of sensors and to get a ruggedized splint (Figure 4).

At this point, it is a clean mesh surface. Now, it is necessary to reduce the triangles but keeping the quality and details of the model. The mesh is sent to 3D CAD Geomagic Design X™ Software (3D Systems, Inc., United States). To complete the mesh and to reduce it. At first, the mesh was formed by 67376 triangles, and after the treatment, these triangles are reduced to 10820, which means a reduction of an 84% that will be sent to another software to convert it to a solid.

This software is CATIA™ 3DEXPERIENCE®3D Software (Dassault Systèmes®, France) that allows after different steps to get a solid and parametric model (Figure 5).

After this process, it is possible to handle the file with a parametric design program. In this case, it is used Inventor Professional 2020

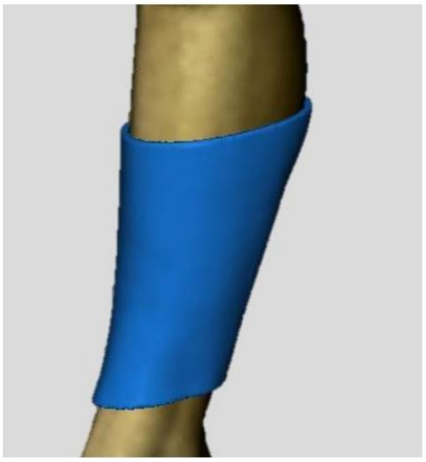

Figure 4: Mesh over the original 3D model

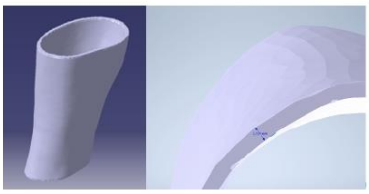

Figure 5: Solid 3D model and view of the thickness

(Autodesk, United States). Using this program, it will be designed the final splint, including the housings for the sensors and the windows for the treatments (Figure 6). In this study, are considered lymph drainage, iontophoresis, ultrasound, laser and electrostimulation treatment. Also, the splint is divided in two different parts, to make it possible to mount it on the limb. The final 3D design is showed in Figure 7

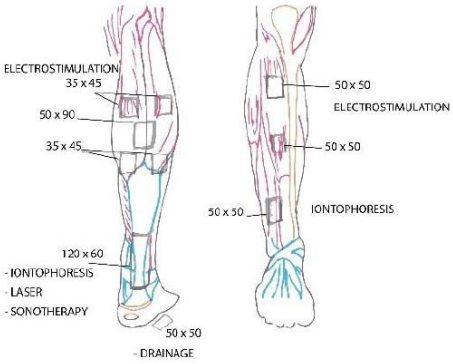

Figure 6: Therapeutic windows to be designed [23]

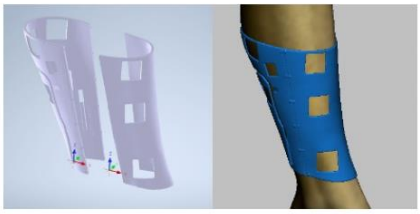

Figure 7: Final 3D splint with housings and windows

2.3 Additive manufacturing

Once the final model is designed, it is sent to a software that prepares the file to be manufactured using a Fusion Deposition Modelling (FDM) 3D printer (Figure 8). In this case, it was used the 3D "TotalPrinter" machine. This 3D printer was designed, developed, and manufactured in the Aditive Manufacturing and Rapid Prototype Laboratory of the Escuela Tecnica Superior de Ingenieria y Diseño Industrial at Universidad Politecnica de Madrid. This machine allows continuous temperature and humidity control of the printing chamber and of extruder temperature with the aim of optimizing the process [24] and obtaining an homogeneous splint in terms of adhesion of the various printing layers, density of the material and mechanical characteristics [25]. In addition, this 3D printing machine allows continuous monitoring of the thickness of the PLA filament used as reported in the study of J. M. D. A. Del Burgo et al. (2018) [26].

To build the real model, it was used PLA biocompatible material with a diameter of 1.75mm. The printing parameters for the manufacturing of the leg splint are shown in the table 3, according to the material manufacturer's recommendations to get a sufficiently rigid and quality structure.

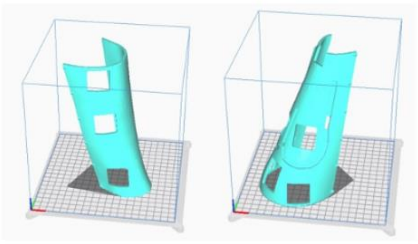

Figure 8: Parts of the splint being processed for printing

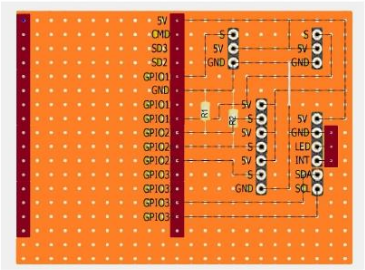

Figure 9: Electronic board for the data acquisition

Figure 10: Real model of the splint assembled with the sensors electronic board

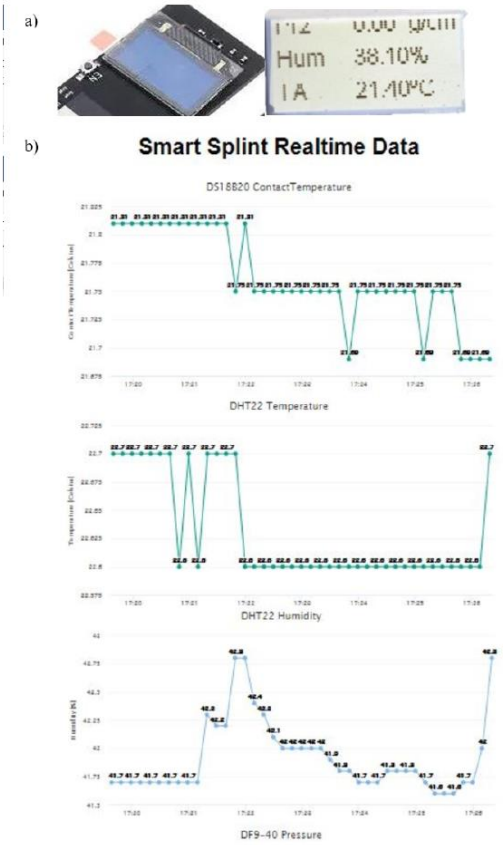

Figure 11: OLED display showing the collected data (a) and web server image (b)

Table 3: Printing parameters

Layer height (mm)	0,2
Extruder (mm)	0,4
Print density (%)	40
Thickness perimeter (mm)	1
Print speed (mm/s)	60
Temperature (°C)	210

3 RESULTS

In this section is showed the splint completely assembled with the sensors and electronic board placed in their housings. After that, it is presented the monitored parameters and the graphs obtained during the sampling.

3.1 3D Model and Design

In order to get the data from the sensors, using the ESP32 microcontroller, it is necessary to develop a small electronic PCB to connect everything needed. This board includes the connections for the controller, resistors and connectors for the sensors. It will supply 5v

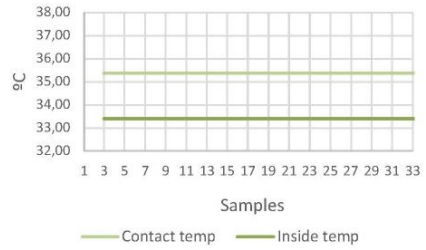

Figure 12: Temperatures graph

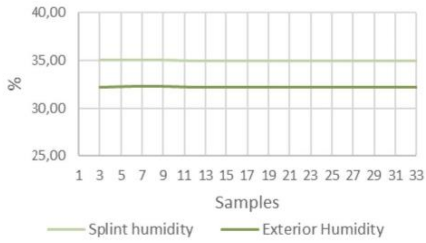

Figure 13: Humidity graph

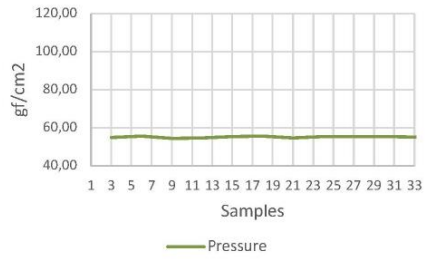

Figure 14: Sensed pressure inside the splint

and ground from the micro controller battery board to each sensor (Figure 9).

This electronic board is assemblied with the sensors and ESP32 microcontroller in the manufactured splint. Figure 10 shows the fully assembled real product. As it is possible to see, the sensors of temperature are placed in two different areas. Also, the sensors of pressure are placed in two different axis (X, Y) in order to get the force in two different directions.

3.2 Sensing technologies

To carry out the tests, the two contact temperatures are combined in one, and same for the two sensors of pressure. Also, to compare the humidity inside the splint with the environmental humidity, it is used a second humidity sensor outside the splint.

The splint is placed over the leg of the volunteer for 1.5hours, that makes a total of 5400s. The data are sampled every 3 seconds, making a total of 1800 samples for each parameter read. These data are collected using a serial monitor from the microcontroller and sent to excel to plot some graphs.

The data are showed on a web server to be consulted from anywhere using a device connected to the Internet. Also, they are showed in a small scrolling OLED display included in the electronic board so that it can be consulted directly without using any other device (Figure 11a).

3.2.1 Temperatures. As explained before, the two contact temperatures are combined to get the average and this is sampled. Also, it is sampled the interior temperature but not in contact with the skin. This is showed in Figure 12

As it is possible to see, the sampled contact temperature is slightly lower than the temperature of a person (36ºC). This fact is completely normal, due to there is only one face of the sensor in real contact with the skin, and the sensor detects also the surface not in contact, which is at lower temperature. However, this info is enough to detect any change of the temperature of the zone.

Moreover, it is possible to see in the graph that the temperature registered by the sensor placed not in contact to the skin is around two degrees inferior. This information may be used with in combination with the contact temperatures and the humidity level to diagnostic anomalies during the treatments.

3.2.2 Humidity. To compare the humidity inside the splint with the environmental humidity, it is used a second humidity sensor thar monitors this second parameter. The acquired data are showed in Figure 13

The knowledge of this parameter allows to anticipate to the appearance of bacteria due to humidity, which is especially critical in case of surgery injuries. Also, an increment of sweating is symptom of problems that may happen after an injury [16].

3.2.3 Pressure. For the measurement of the pressure, there are combined two pressure sensors. One of them is placed in one axis, and later are combined electronically to show only one data. The used sensors detect the force applied. According to this, it is possible to get the pressure by the following equations:

$$p = \frac{F}{A} \tag{2}$$

Where p is the pressure, F is the magnitude of the normal force, A is the area of the surface on contact.

The sensor used has a surface of $1cm^2$, and according to $1N=1Kg/s^2$:

$$p = \frac{N}{m^2} = \frac{kg}{m * s^2} = \frac{gf}{cm^2} \tag{3}$$

As it is possible to see in Figure 14, between samples 400 and 700 it was perfectly detected a pressure of 110 gf/cm^2. During the rest of the time, it was measured around 55 gf/cm^2 in idle state.

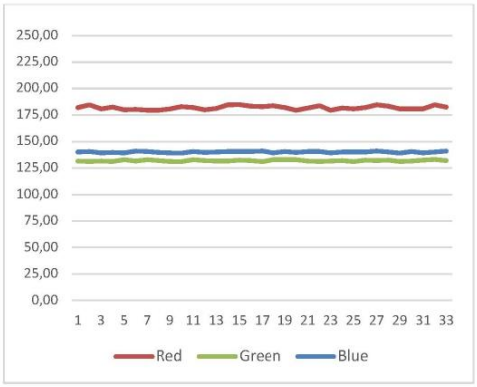

Figure 15: RGB Data with no hematoma signs

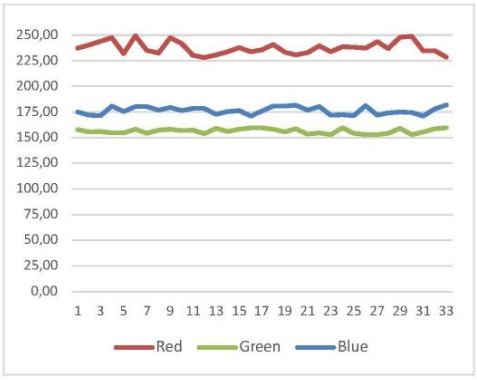

Figure 16: RGB Data with hematoma signs

Thereby, if the pressure of the area is increased due to the inflammatory signs, these sensors will perfectly detect the increment of the pressure inside the splint.

3.2.4 Color. Color categories and physical specifications of color are associated with objects through the wavelengths of the light that is reflected from them and their intensities. This reflection is read by the sensor to get the information from the skin. The sensor uses the RGB color model. This model is is an additive color model in which red, green, and blue light are added together in various ways to reproduce a broad array of colors.

The data may oscilate between the values 0 (no color component detected) and 255 (max value of the color component detected). Figure 15 shows the data adquired when the sensor is placed over a region of skin with no hematomas, whereas Figure 16 shows the data when the sensor is placed over a hematoma.

As it is possible to see, the values of red and blue components are increased when the sensor is placed over an hematoma. This way, it is possible to detect when an hematoma shows up in the region of the skin. The increment is about a 33% of the red value, a 23% of the green value, and a 28% of the blue. This variation may determine the aparition of an hematoma.

4 DISCUSSIONS

It is possible to find a relation between temperature patterns and medical conditions [27-29]. This is due to metabolism and local blood flow, that generates located temperature variations. Also, bone formation other disease processes are also be responsible of a reduction in blood flow. This fact, will produce alterations in surface temperature [30]. It is possible to see in the different charts, that the temperature, pressure and humidity variations, are perfectly detected by the sensors mounted on the splint.

It would also be possible to create a digital mapping of the temperatures under the splint by adding more sensors. All these collected data quantify temperature changes in skin surface that may be both cold and hot responses, which may co-exist with pain during inflammatory processes [15]. The possibility of getting a continuous monitoring of these parameters, allows to know the progression at any time of the treatment. This makes it possible an early detection of joint, vascular or muscular complications that are difficult to observe if the immobilization splint is not removed previously.

It is possible to see that the sensor in contact with the skin detects a temperature slightly lower than the normal body temperature. This fact is due to the gradient of temperature that occurs on the metallic sensor surface. The sensor has about a 40% of the surface in contact with the skin. The 60% of the surface is not in contact by the skin due to its cylindrical form. Due to this, it comes up a difference of temperature on the sensor surface, between different areas. Due to the thermal conductivity, the metallic surface tends to get an equilibrium between the different areas [30]. Finally, the sensor gets a temperature that is not the real skin temperature whereas it is the mean temperature obtained from the whole surface. However, this is not a problem, as it is enough information to detect both decremental and incremental temperature changes.

The humidity and pressure values are also correctly acquired. As with the temperature, it is possible to detect variations due to internal sweating, and pressure produced by an inflammatory process.

Finally, by using the RGB sensor, it is possible to detect variations in the three components of the light (red, green and blue). When a hematoma shows up, the concentration of blood on a determinate area, produces a change on the color of the skin. The sensor is able to detect a variation of the three studied components of the light, so it avoids the necessity of removing the splint to detect the creation of a hematoma.

5 CONCLUSIONS

With this innovative project, it is intended to provide an evolution for the traditional splints, that have remained practically intact since their invention in the tenth century.

The 3D FDM splint fabrication makes it possible to create different housings for the implementation of different sensors on the splints. These sensors may be used to get different information during the treatment process, to be monitored by a specialist remotely. Moreover, the use of 3D printing allows to create different holes to apply different treatments that might make it shorter de length of the treatment.

As it is showed in this study, this autonomous system, powered by a battery, is able to get the information from the sensors. This information and different parameters considered at the beginning of this study, may be consulted remotely.

It is proposed as an evolution of this study, the incorporation of an algorithm that may notify of an unexpected evolution by using the different collected data.

REFERENCES

[1] U. Jammalamadaka and K. Tappa, "Recent advances in biomaterials for 3D printing and tissue engineering," Journal of Functional Biomaterials. 2018.
[2] A. Bandyopadhyay, S. Bose, and S. Das, "3D printing of biomaterials," MRS Bull., 2015.
[3] H. N. Chia and B. M. Wu, "Recent advances in 3D printing of biomaterials," J. Biol. Eng., 2015.
[4] F. Blaya, P. S. Pedro, J. L. Silva, R. D'Amato, E. S. Heras, and J. A. Juanes, "Design of an Orthopedic Product by Using Additive Manufacturing Technology: The Arm Splint," J. Med. Syst., vol. 42, no. 3, 2018.
[5] S. Affatato, A. Ruggiero, J. S. De Mattia, and P. Taddei, "Does metal transfer affect the tribological behaviour of femoral heads? Roughness and phase transformation analyses on retrieved zirconia and Biolox®Delta composites," Compos. Part B Eng., vol. 92, pp. 290–298, May 2016.
[6] S. Ghai, Y. Sharma, N. Jain, M. Satpathy, and A. K. Pillai, "Use of 3-D printing technologies in craniomaxillofacial surgery: a review," Oral and Maxillofacial Surgery, vol. 22, no. 3. Springer Verlag, pp. 249–259, Sep-2018.
[7] N. M. García, F. Blaya, E. L. Urquijo, E. S. Heras, and R. D'Amato, "Oral appliance for Obstructive Sleep Apnea: Prototyping and Optimization of the Mandibular Protrusion Device," J. Med. Syst., vol. 43, no. 5, p. 107, May 2019.
[8] N. Montesdeoca, E. Lechosa, F. B. Haro, R. D'Amato, and J. A. Juanes, "Design of thermoplastic oral appliance with mouth opening control to treat obstructive sleep apnea," in ACM International Conference Proceeding Series, 2019, pp. 404–410.
[9] J. S. Mulford, S. Babazadeh, and N. Mackay, "Three-dimensional printing in orthopaedic surgery: review of current and future applications," ANZ journal of surgery, vol. 86, no. 9. Blackwell Publishing, pp. 648–653, Sep-2016.
[10] C. Lunsford, G. Grindle, B. Salatin, and B. E. Dicianno, "Innovations With 3-Dimensional Printing in Physical Medicine and Rehabilitation: A Review of the Literature," PM and R, vol. 8, no. 12. Elsevier Inc., pp. 1201–1212, Dec-2016.
[11] J. Cernohorsky and M. Cadek, "Smart rehabilitation splint," in Mechanisms and Machine Science, 2017.
[12] J. Evill and O. Evill, "Cortex Evill," 2013. .
[13] J. M. De Agustin Del Burgo, F. Blaya Haro, R. D'Amato, and J. A. Juanes Méndez, "Development of a Smart Splint to Monitor Different Parameters during the Treatment Process," Sensors, vol. 20, no. 15, p. 4207, Jul. 2020.
[14] P. Hamet and J. Tremblay, "Artificial intelligence in medicine," Metabolism., 2017.
[15] F. Blaya, P. S. Pedro, A. B. S. Pedro, J. Lopez-Silva, J. A. Juanes, and R. D'Amato, "Design of a Functional Splint for Rehabilitation of Achilles Tendon Injury Using Advanced Manufacturing (AM) Techniques. Implementation Study," J. Med. Syst., vol. 43, no. 5, 2019.
[16] X. Ju, J.-C. Nebel, and J. P. Siebert, "3D thermography imaging standardization technique for inflammation diagnosis," in Infrared Components and Their Applications, 2005, vol. 5640, p. 266.
[17] T. Schlereth, P. D. Drummond, and F. Birklein, "Inflammation in CRPS: Role of the sympathetic supply," Auton. Neurosci. Basic Clin., vol. 182, pp. 102–107, May 2014.
[18] Dallas Semiconductor, "Programmable Resolution 1-Wire®Digital Thermometer," 2002.
[19] L. Aosong Electronics Co., "Digital-output relative humidity & temperature sensor/module DHT22 (DHT22 also named as AM2302)," 2015.
[20] "Film Pressure Sensor DF9-40@10kg V2.0."
[21] "TCS3472 COLOR LIGHT-TO-DIGITAL CONVERTER with IR FILTER." [Online]. Available: https://cdn-shop.adafruit.com/datasheets/TCS34725.pdf. [Accessed: 30-Apr-2020].
[22] "ESP32 Series Datasheet Including," 2020.
[23] F. B. Haro, J. Lopez-Silva, P. S. Pedro, J. A. Juanes, A. B. S. Pedro, and R. D'Amato, "Design and prototyping by additive manufacturing of a functional splint for rehabilitation of Achilles tendon intrasubstance rupture," in ACM International Conference Proceeding Series, 2018.
[24] F. B. Haro *et al.*, "Monitoring an Analysis of Perturbations in Fusion Deposition Modelling (FDM) Processes for the Use of Biomaterials," J. Med. Syst., vol. 43, no. 5, p. 109, May 2019.
[25] F. B. Haro, J. M. de Agustín del Burgo, R. D'Amato, M. I. Marcos, E. S. Heras, and J. M. G. Alonso, "Monitoring of the additive manufacturing process for the use of biomaterials in medical field," in Proceedings of the Sixth International Conference on Technological Ecosystems for Enhancing Multiculturality - TEEM'18, 2018, pp. 428–432.

[26] J. M. D. A. Del Burgo, R. D'Amato, J. A. J. Méndez, A. S. Ramírez, F. B. Haro, and E. S. Heras, "Real time analysis of the filament for FDM 3D printers," in ACM International Conference Proceeding Series, 2019.
[27] R. LAWSON, "Implications of surface temperatures in the diagnosis of breast cancer.," Can. Med. Assoc. J., vol. 75, no. 4, pp. 309–311, 1956.
[28] B. Ströberg, "The Use of Thermography in Equine Orthopedics," Vet. Radiol., vol. 15, no. 1, pp. 94–97, Jan. 1974.
[29] L. Wang *et al.*, "Bisphosphonates Inhibit Pain, Bone Loss, and Inflammation in a Rat Tibia Fracture Model of Complex Regional Pain Syndrome," Anesth. Analg., vol. 123, no. 4, pp. 1033–1045, Oct. 2016.
[30] C. H. Rundle *et al.*, "Microarray analysis of gene expression during the inflammation and endochondral bone formation stages of rat femur fracture repair," Bone, vol. 38, no. 4, pp. 521–529, Apr. 2006.

TEEM'20 ONLINE CONFERENCE
Technological Ecosystems for Enhancing Multiculturality, 21-23 October 2020

We, hereby, certify that the paper entitled

José Maria de Agustín del Burgo, Fernando Blaya Haro, Roberto D'Amato and Juan Antonio Juanes Méndez. Smart splint for diagnosis during initial stage of treatment

has been presented at the 8th International Conference in Technological Ecosystems for Enhancing Multiculturality (TEEM 2020).

The conference was held in Salamanca, Spain, on October 21-23, 2020 and organized by the Research GRoup in InterAction and eLearning (GRIAL) and Research Institute for Educational Science (IUCE) at the University of Salamanca.

Signed by

Francisco J. García Peñalvo
TEEM2020 Conference Chair

FIRMADO POR	FECHA FIRMA
GARCIA PEÑALVO FRANCISCO JOSE	26-10-2020 21:09:15

Documento firmado electrónicamente - Patio de Escuelas, núm 1, 2.ª planta (Edificio de Rectorado) - 37071 Salamanca
Universidad de Salamanca

TEEM'20
ONLINE CONFERENCE
Technological Ecosystems for Enhancing Multiculturality, 21-23 October 2020

The 8th International Conference on Technological Ecosystems for Enhancing Multiculturality (TEEM 2020) awards the contribution

José Maria de Agustín del Burgo, Fernando Blaya Haro, Roberto D'Amato and Juan Antonio Juanes Méndez. Smart splint for diagnosis during initial stage of treatment

as the conference best paper in the category of

Track 8. State-of-the-art technologies at the service of medical training and practice to foster Digital Health Ecosystems

The conference was held in Salamanca, Spain, on October 21-23, 2020 and organized by the Research GRoup in InterAction and eLearning (GRIAL) and Research Institute for Educational Science (IUCE) at the University of Salamanca.

Signed by

Francisco J. García Peñalvo
TEEM2020 Conference Chair

FIRMADO POR	FECHA FIRMA
GARCIA PEÑALVO FRANCISCO JOSE	20-11-2020 10:59:21

Documento firmado electrónicamente - Patio de Escuelas, núm 1, 2.ª planta (Edificio de Rectorado) - 37071 Salamanca
Universidad de Salamanca

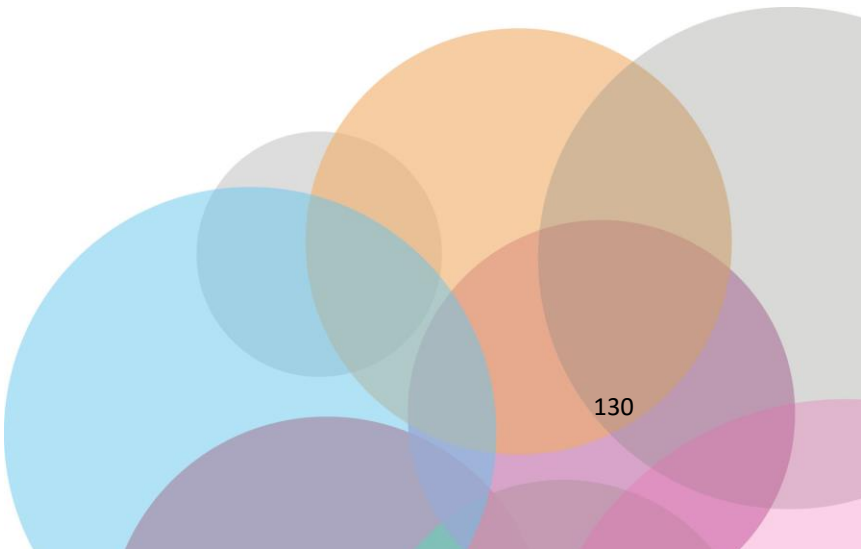

ARTÍCULOS EN REVISTAS

ANEXO III:

Soriano Heras, E., Blaya Haro, F., De Agustín del Burgo, J. M., Islán Marcos, M., & D'Amato, R. (2018). Filament advance detection sensor for fused deposition modelling 3D printers. Sensors, 18(5), 1495. DOI: 10.3390/s18051495

ANEXO IV:

Haro, F. B., Del Burgo, J. M. D. A., D'Amato, R., Islán, M., Heras, E. S., Alonso, J. M. G., & Mendez, J. A. J. (2019). Monitoring an Analysis of Perturbations in Fusion Deposition Modelling (FDM) Processes for the Use of Biomaterials. Journal of Medical Systems, 43(5), 1-8. DOI: 10.1007/s10916-019-1236-2

ANEXO V:

De Agustín Del Burgo, J. M., Blaya Haro, F., D'Amato, R., & Juanes Méndez, J. A. (2020). Development of a Smart Splint to Monitor Different Parameters during the Treatment Process. Sensors, 20(15), 4207. DOI: 10.3390/s20154207

ANEXO VI:

De Agustín Del Burgo, J. M., Blaya Haro, F., D'Amato, R., Blaya, A., & Juanes Méndez, J. A. (2021). Development of a Smart Leg Splint by Using New Sensor Technologies and New Therapy Possibilities. Sensors, 21(15), 5252.

ANEXO III:

FILAMENT ADVANCE DETECTION SENSOR FOR FUSED DEPOSITION MODELLING 3D PRINTERS

El propósito principal de este artículo es presentar un sistema para detectar problemas de extrusión en impresoras 3D de fabricación por deposición fundida (FDM) comprobando que el filamento avanza correctamente.

Después de varios años utilizando este tipo de máquinas, los autores detectaron que no existe ningún sistema para detectar el problema principal en las máquinas FDM. Los autores pensaron en diferentes sensores y utilizaron el método de objetivos ponderados, uno de los métodos de evaluación más comunes, para comparar conceptos de diseño basados en un valor general por concepto de diseño. Teniendo en cuenta las puntuaciones obtenidas de cada especificación, la mejor opción para este trabajo es el codificador óptico. Una vez elegido el sensor, es necesario diseñar la parte donde se instalará sin interferir con el funcionamiento normal de la máquina. Para ello se empleó la metodología de escaneo de fotogrametría.

El dispositivo desarrollado detecta perfectamente el avance del filamento sin afectar el funcionamiento normal de la máquina. Asimismo, se logra el objetivo primordial del sistema, evitar pérdidas de material, energía y desgaste mecánico, manteniendo la premisa de fabricar un producto de bajo costo que no aumente significativamente el costo de la máquina. Este desarrollo ha permitido utilizar la impresora con restos de filamentos de bobina, que no se gastaron porque no eran suficientes para completar una impresión. Además, este desarrollo ha permitido imprimir modelos en dos colores con un solo extrusor.

sensors

MDPI

Article

Filament Advance Detection Sensor for Fused Deposition Modelling 3D Printers

Enrique Soriano Heras [1,*], Fernando Blaya Haro [2], José M. de Agustín del Burgo [2], Manuel Islán Marcos [2] and Roberto D'Amato [2]

[1] Departamento de Ingeniería Mecánica, Universidad Carlos III de Madrid, Avda. de la Universidad, 30, 28911 Leganés, 28012 Madrid, Spain
[2] Escuela Técnica Superior de Ingeniería y Diseño Industrial, Universidad Politécnica de Madrid, Ronda de Valencia, 3, 28012 Madrid, Spain; fernando.blaya@upm.es (F.B.H.); jm.deagustin@alumnos.upm.es (J.M.d.A.d.B.); manuel.islan.marcos@upm.es (M.I.M.); r.damato@upm.es (R.D.A)
* Correspondence: esoriano@ing.uc3m.es; Tel.: +34-636-835501

Received: 21 April 2018; Accepted: 7 May 2018; Published: 9 May 2018

check for updates

Abstract: The main purpose of this paper is to present a system to detect extrusion failures in fused deposition modelling (FDM) 3D printers by sensing that the filament is moving forward properly. After several years using these kind of machines, authors detected that there is not any system to detect the main problem in FDM machines. Authors thought in different sensors and used the weighted objectives method, one of the most common evaluation methods, for comparing design concepts based on an overall value per design concept. Taking into account the obtained scores of each specification, the best choice for this work is the optical encoder. Once the sensor is chosen, it is necessary to design de part where it will be installed without interfering with the normal function of the machine. To do it, photogrammetry scanning methodology was employed. The developed device perfectly detects the advance of the filament without affecting the normal operation of the machine. Also, it is achieved the primary objective of the system, avoiding loss of material, energy, and mechanical wear, keeping the premise of making a low-cost product that does not significantly increase the cost of the machine. This development has made it possible to use the printer with remains of coil filaments, which were not spent because they were not sufficient to complete an impression. Also, printing models in two colours with only one extruder has been enabled by this development.

Keywords: rapid prototyping; fused deposition; filament jams; extrusion failures; photogrammetry; manufacturing system

1. Introduction

The application of 3D printing technologies is ideal not only for the home-user or for tooling production, but the improvements of the quality and of the mechanical property mean that they are increasingly being used for direct manufacturing [1]. In fact, for aerospace industry—which needs to produce a small number of highly complex aircraft components—the application of 3D printing technologies is ideal [2,3]. In the medical sector, in the same manners, due to the need for personalized one-off products, the AM is the ideal technique to address this need. This is can bee seen in several applications like orthodontics, prosthetics, orthotics, implants, and organ replacement [4,5].

Nowadays, the use of 3D printers has extended beyond the research laboratories. It is possible to find them, more and more frequently, in houses, where they are used by non-technical users; or in factories, where an error in the operation can suppose great losses [6]. Therefore, these machines must remain 100% reliable with near-zero failed prints due to mechanical and electro-mechanical malfunctions.

After several years of development and improvement, the most important failure has not been corrected, jams in the extruder. Some researches and engineers have optimized the grip force on the 3D printer filament and even have developed novel feeding mechanisms [7,8]. This extrusion problem occurs to FDM 3D printers when the filament does not move as it is desired, and may be due to damage, stress, dust, and small debris in filament. Nevertheless, the most common problems arise from a wrong filament diameter, a breaking of the filament, or simply that the filament coil is over. In these cases, the printer keeps on moving, but it does not deposit any material [9].

Although manufacturers and researches are constantly improving polymer manufacturing processes, including fiber spinning and injection molding, the product quality and production efficiency is influenced by multiple processing and material parameters—such as the nominal shear and shear history, process temperature, or long chain branching—mechanisms that currently are not completely understood. The control and optimization of such operations contribute to get closer and closer to the nominal filament size but it still moves in fairly large tolerances [8,10–12]. In Figure 1, it is possible to see the imperfections that can be found in a new filament.

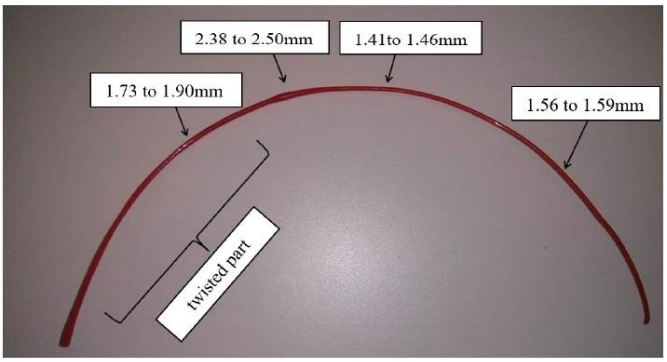

Figure 1. Defects in a filament sample.

The aim of this study is to present a new method in order to detect all these extrusion failures that can may be produced by: a coil knot, an extruder jamming or, simply, that the filament coil is over. This can detect the correct filament advancement in the extruder. To reach this goal, it is initially thought of a mechanical switch that detects when the filament fails to move, but although it seems trivial to cases in which the filament breaks or runs out, it is more difficult to detect the correct advance. For this reason, we propose to use a rotation encoder driven by the movement of the filament. The printer should consult repeatedly, while printing, that the encoder is rotating and therefore the filament goes forward. In the event that no progress is detected, the machine will stop and offer the option to change the filament, reload it, and continue printing without having to discard the part.

2. Review of Extruder-Filament Sensors Used for Current 3D Printers

2.1. Mechanical Sensor

Mechanical sensors have been widely implemented in 3D printers, majority of them use a mechanical button to stay on while filament is detected could easily detect filament end or breakage to stop the printing. It is possible to find some detection systems using mechanical filament breakage sensors, but this kind of system does not solve the main problem, which is a filament jam, due to the state of the switch being unable to change [13].

2.2. Load Cell Sensor

As the extruder feeds the filament to the hot end, the extruder is effectively pushing against the filament, causing the extruder to apply extra load on the load cell. Load cells have strain gauges attached that change in electrical resistance when under different loads. This resistance change provides small voltage levels that can be amplified and then read by an analogue to digital converter. Unfortunately, a load cell sensor could make it difficult to calibrate without a suitable weighing platform and stand [14].

2.3. Rotary Encoder

A rotary encoder, is an electro-mechanical device that converts the angular position or motion of a shaft or axle to an analog or digital code [15]. There are two main types: absolute and incremental. The output of absolute encoders indicates the current position of the shaft, making them angle transducers. The output of incremental encoders provides information about the motion of the shaft, which is typically further processed elsewhere into information such as speed, distance, and position. The encoder may have mechanical problems due to the high accuracy needed in fabrication. Environmental pollution can be a source of interference in optical transmission as well, which is particularly sensitive to shock and vibration. The rotary encoders' operating temperature is limited by the presence of electronic components.

2.3.1. Mechanical Encoder

Mechanical encoders have an axis that spins internally, thus activating different pins depending on the direction of rotation and speed. Although this type of encoder seems easy to use as first, the resistance of the rotation axis is not desired. It could increase the resistance of the filament feed and it could affect the proper operation of the extruder.

2.3.2. Optical Encoder

The principle of operation of an optical encoder is based on the so-called photo couplers. These are small chips consisting of a diode as a photo emitter and a transistor which act as photoreceptors. This element is responsible for detecting the presence/absence of light through a concentric axis, it is manufactured with slots that allow the light to go through the disc to obtain the final measure [16].

3. Filament Auto-Detection System Development

3.1. Election of the Sensor

The weighted objectives method is one of the most common evaluation methods for comparing design concepts based on an overall value per design concept [17]. This method makes a direct comparison of the design. To do this, the weighted objective method assigns scores to the degree to which a design alternative satisfies a criterion. However, the criteria that are used to evaluate the design alternatives might differ in their importance. For example, the cost can be of less importance than appealing aesthetics. To deal with it, the method allows the assigning of weights to different criteria. This allows the decision-maker to take into account the difference in importance between criteria. At the end of the method, the alternative that best suits the criteria can be seen.

The biggest disadvantage of using other methods like the Datum method or the Harris profile is that the scores per criterion cannot be aggregated into an overall score of the design alternative.

The selected criteria, compared in Table 1, are the following:

E1. Filament detection (yes-no)
E2. Detecting the advance of the filament
E3. Not interference with normal movement of the filament
E4. Adaptability of the output signal
E5. Price

E6. Durability

Table 1. Filament detection sensor evaluation.

Sensor	E1	E2	E3	E4	E5	E6	Amount	Compensation	Weight	%
E1	X	0.0	0,0	1.0	0.5	0.5	1.5	2.5	0.167	16.67
E2	1.0	X	0.5	0.5	0.5	0.5	2.5	3.5	0.233	23.33
E3	1.0	0.5	X	1.0	0.5	1.0	3.0	4.0	0.267	26.67
E4	0.0	0.5	0.0	X	0.5	0.0	1.0	2.0	0.133	13.33
E5	0.5	0.5	0.5	0.0	X	0.5	1.5	2.5	0.167	16.67
E6	0.5	0.5	0.0	1.0	0.5	X	2.5	3.5	0.233	23.33
Total							9.5	14.5	0.967	96.67

Taking into account the scores (see Table 2), and as expected, the sensor that best meets the specifications is the optical encoder. In this work, an inexpensive bi-directional optical incremental encoder is used.

Table 2. Sensor marks.

Sensor 1	Mark	Satisfaction	Final Mark	Sensor 2	Mark	Satisfaction	Final Mark	Sensor 3	Mark	Satisfaction	Final Mark
E1	16.67	100%	16.67	E1	16.67	100%	16.67	E1	16.67	100%	16.67
E2	23.33	0%	0.00	E2	23.33	100%	23.33	E2	23.33	100%	23.33
E3	26.67	100%	26.67	E3	26.67	25%	6.67	E3	26.67	100%	26.67
E4	13.33	100%	13.33	E4	13.33	75%	10.00	E4	13.33	75%	10.00
E5	16.67	100%	16.67	E5	13.33	75%	10.00	E5	13.33	75%	10.00
E6	23.33	75%	17.50	E6	16.67	75%	12.50	E6	16.67	50%	8.33
		Total	73.33			Total	79.17			Total	95.00

3.2. Hardware Assembly

3.2.1. Assembly Part Design

Once the sensor is chosen, it is necessary to design the part where it will be installed. It must be taken into account that it cannot interfere with the normal function of the machine. For the 3D printing of the prototype, a Prusa i3 BQ Hephestos printer has been used. In order to do it, we will employ photogrammetry scanning methodology since it will be possible to do it in a precise way [18].

This method uses reverse engineering, thus allowing us to reduce the costs of the development.

After taking numerous pictures of the object, they are processed using a computer software so that common points are identified on each image. A line of sight (or ray) can be constructed from the camera location to the point on the object. It is the intersection of these rays (triangulation) which determine the three-dimensional location of the point.

The result of the process is a digital tridimensional object which can be used as a model to design the rest of the parts. It is interesting to include graphic scales to get the correct dimensions of the digital model. Figure 2a shows a sample of a total of 74 images involved in the process.

After taking numerous pictures of the object, they are processed using computer software so that common points are identified on each image.

A line of sight (or ray) can be constructed from the camera location to the point on the object. It is the intersection of these rays (triangulation) that/which determines the three-dimensional location of the point.

The result of the process is a digital tridimensional object which can be used as a model to design the rest of the parts. It is interesting to include graphic scales to get the correct dimensions of the digital model.

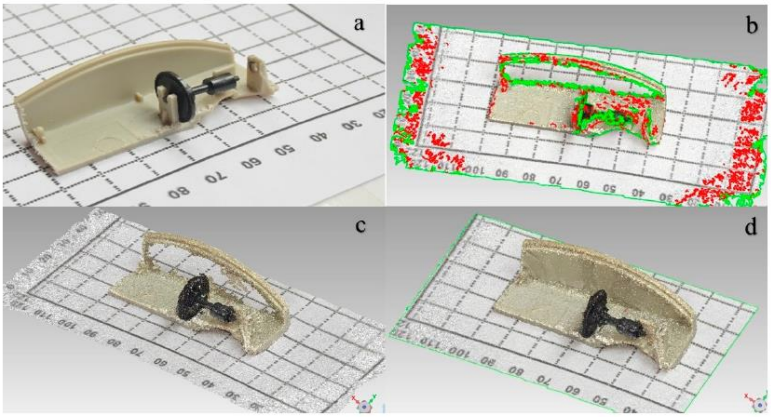

Figure 2. Images for photogrammetry process: (**a**) Real figure; (**b**) point cloud; (**c**) and (**d**) digital model.

The software locates the pictures and shapes a point cloud of the scanned object. The process is shown in Figure 2a (real figure), b (point cloud), c,d (digital model) where it is possible to see the pictures completely orientated and the formatted points cloud.

As it is possible to notice in Figure 2c, there are some defective parts. This is due to the brightness of the object, so it is necessary to perform a repair of the digital model, so a model as similar as possible to the original can be reached.

In order to achieve this, first of all a filter of the points is performed to remove the noise by eliminating points spaced of the set a specified size. After this, different holes are detected. In this case, a total of 698 of holes which 670 are closed automatically since have a small size. The remaining 28 holes are manually closed to keep the original form. An automatic reparation of errors is carried out, and finally, it is possible to get the solid digital model. Figure 2d shows an image of the final virtual model.

Once the three-dimensional solid model is obtained, it is exported to a 3D design program for modeling the part where it will be assembled.

In this way, it is possible avoid design errors that have to make too many iterations to find the optimal model. In Figure 3b,c, the real product made with a 3D printer is showed disassembled and assembled. As it is possible to see, the filament will make that the encoder moves when it is advancing.

3.2.2. System Assembly

The whole system is installed on the top of the printer, so that the filament goes through the sensor. After the sensor, the filament is leaded through a Teflon tube to the hot-end, analogously to the Bowden system.

After checking that the system does not interfere in the normal function of the machine, it is connected to the main electronic board of the printer (an Arduino Mega board).

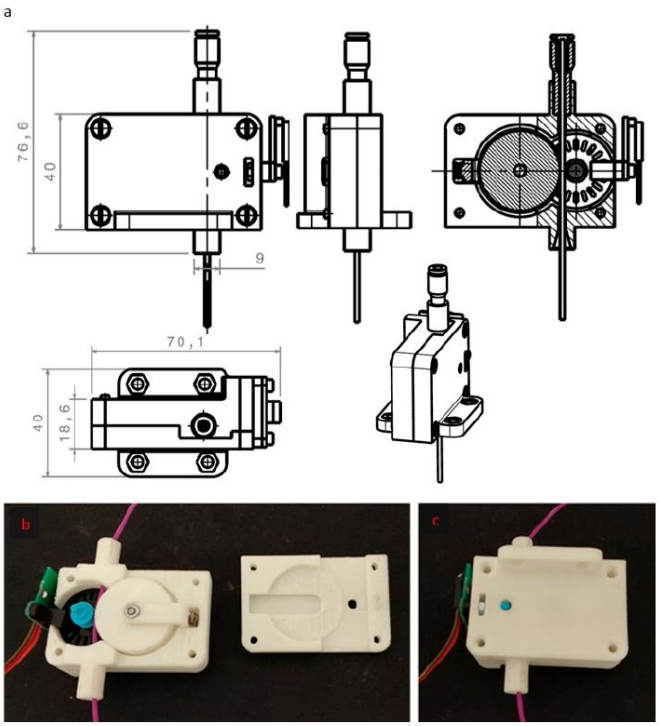

Figure 3. Real product: (**a**) Optimal design model; (**b**) and (**c**) Real product made with a 3D printer.

3.2.3. Firmware Modifications

Once the system is installed, it is necessary to modify the firmware of the machine, so it is possible to get the sensor signal and act accordingly. Since the encoder works asynchronously, it is necessary to use program interruptions to get the signal correctly. These interruptions will detect whether the filament is moving or is blocked. Moreover, it will be possible to calculate the speed at which the filament is advancing in order to be sure about the quantity of material deposited.

However, after repeated tests, it is observed that the interruptions take place very frequently, which interferes with the operation of the printer. To avoid this problem, a new electronic configuration is proposed. A slave board will be programmed to control the encoder signal and to communicate with the master board to indicate if there is an error in the filament advance. This way, we can dedicate this new board to also calculate the speed of the filament, as with only one board it was very difficult due to the main boar must work in a fluent way to control the motors correctly. A new pause menu is also implemented in the master board, since error filament was not previously available.

Once an error in advancing filament is detected, the printer activates the implemented pause mode due to filament error, at which point it is possible to load and unload the actual filament to continue printing to avoid losing the piece.

4. Performance Evaluations

4.1. Filament Defects

Although most of filament producers for 3D machines are constantly developing and improving their products, the manufacturing method has so far prevented achieving a filament with a constant diameter. This excess in diameter is sometimes too much for the machine, causing bad finishing models, jamming of the extruder, or even damaging the extruder. In order to check the filament diameter of different producers in this study, a sample with a length of 300 cm, for each providers, was taken. The filament diameters was investigate by using a sensor with a resolution of 0.01 mm.

Figure 4 shows the diameter variation (whose nominal value is 1.75 mm) in X and Y axis, from different filament providers (A, B, C, D).

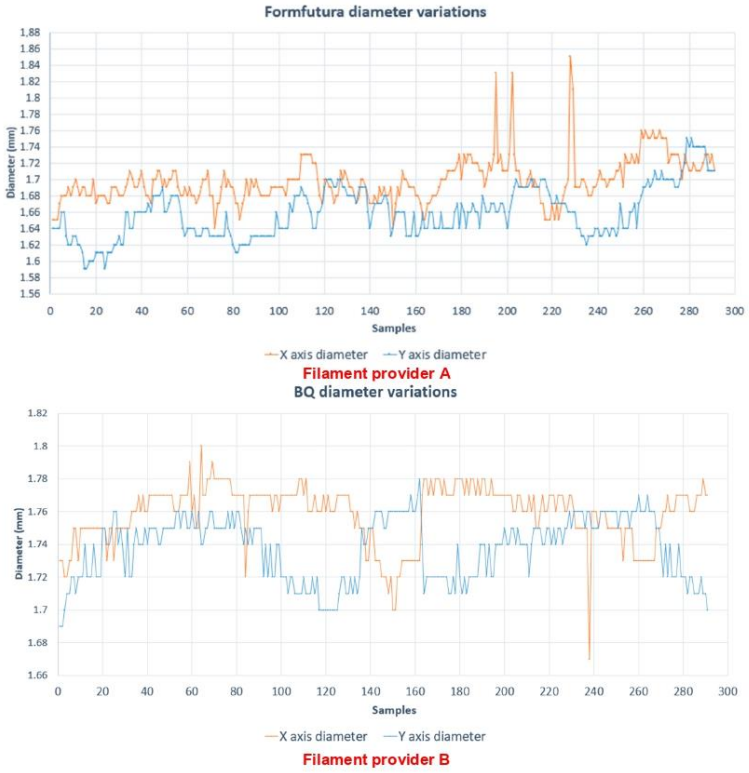

Figure 4. *Cont.*

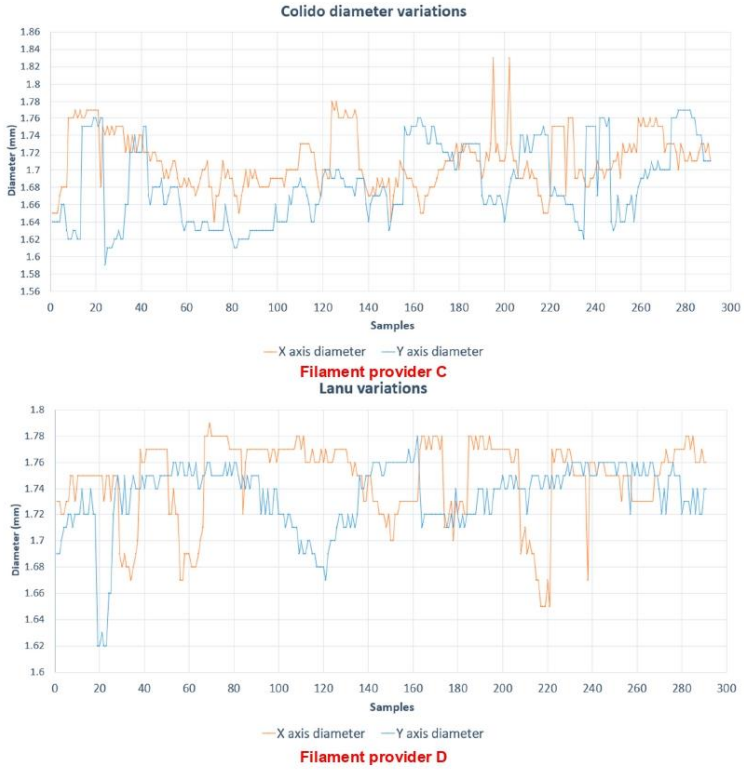

Figure 4. Diameter variation for four different filament providers (A, B, C, D).

By analyzing these samples (see Table 3), it is possible to see that the diameter varies from 1.56 mm to 1.85 mm. This is the principal reason for extruder obstructions.

Table 3. Maximum, minimum, and mean of filaments.

Provider	Maximum (mm)	Minimum (mm)	Mean (mm)
A	1.85	1.59	1.68
B	1.8	1.67	1.75
C	1.84	1.56	1.75
D	1.83	1.59	1.78

Any of these failures means that leaving the printer in operation will mean losing the piece that was being created, requiring the manufacturer to start again. In addition, by continuing printing without really extruded plastic, the machine consumes energy and produces an unnecessary wastage. Due to this reason, the operator must be aware of the machine as long as it is operating, ensuring that the plastic flows without problem, which is especially difficult when the piece takes several hours to be produced.

4.2. Evaluation of the Implemented System

The installed system does not affect the print quality of the machine. It has been found that the time set for detecting advancing filament problems detects an error in time without producing false positives. In Table 4, the error is displayed on the printer.

Table 4. Error menu.

Filament error. Push the button to change the filament.
Extract the filament when the motor stopes.
Insert the new filament and push the button.
When you see come out the filament, press the button to continue printing.

Figure 5 shows an object produced by a 3D printer where two filament feed errors were forced.

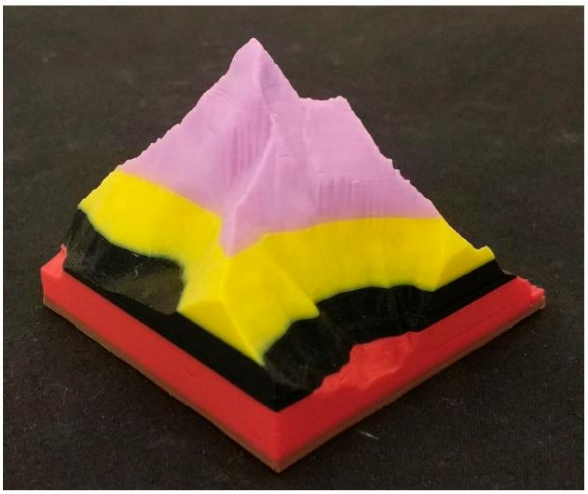

Figure 5. Model produced after five filament advance problems.

5. Conclusions

The aim of the paper is to present a system to detect extrusion failures in fused deposition modelling (FDM) 3D printers by sensing that the filament is moving forward properly. In this study, different sensors and the weighted objectives method, one of the most common evaluation methods for comparing design concepts based on an overall value per design concept were used.

The installed system achieves perfectly detect the advance of the filament without affecting the normal operation of the machine. The implementation of a slave board that gets the encoder signal, can calculate the filament speed so that it is possible not only to know when there is a filament advance problem, but also to adjust the extrusion speed if the adjusted speed does not match with the real speed.

This has enabled the use of the printer with remaining coil filament which had not been used before because it was insufficient to complete an impression. With this system, when the filament finishes, the printer enters into a standby state waiting for the user to introduce a new filament.

Therefore, the primary objective of the system is achieved, avoiding loss of material, energy, and mechanical wear, keeping the premise of making a low-cost product that does not significantly

increase the cost of the machine. The electronic encoder has a price of 2–5 €, the box for it has be produced with a 3D printer and the new electronic slave board has a price between 1–3 €.

This low cost system could be implemented in any printer, as it does not interfere with the normal functions of the machine, as it is mounted at the entrance of the filament.

Author Contributions: Formal analysis, R.D.A.; Investigation, E.S.H. and J.M.d.A.d.B.; Methodology, E.S.H. and J.M.d.A.d.B.; Project administration, F.B.H. and M.I.M.; Resources, F.B.H., M.I.M. and R.D.A.; Software, E.S.H. and José María de Agustín del Burgo; Supervision, F.B.H. and M.I.M.; Writing original draft, E.S.H. and José María de Agustín del Burgo; Writing review & editing, E.S.H. and R.D.A.

Funding: This research received no external funding.

Conflicts of Interest: The authors declare no conflict of interest.

References

1. Krolczyk, G.; Raos, P.; Legutko, S. Experimental analysis of surface roughness and surface texture of machined and fused deposition modelled parts/Eksperimentalna analiza povrsinske hrapavosti i teksture tokarenih i talozno ocvrsnutih proizvoda. *Teh. Vjesn. Tech. Gaz.* **2014**, *21*, 217–222.
2. Guo, N.; Leu, M.C. Additive manufacturing: Technology, applications and research needs. *Front. Mech. Eng.* **2013**, *8*, 215–243. [CrossRef]
3. Lyons, B. Additive Manufacturing in Aerospace: Examples and Research Outlook. *Bridge* **2012**, *42*, 13–19.
4. Lozano, M.T.U.; Haro, F.B.; Juanes, J.A. Fast Scanning Technology and 3D Prototype of Bones for Teaching Purpose. In Proceedings of the INTED2017, Valencia, Spain, 6–8 March 2017; pp. 1610–1616.
5. Blaya, F.; Pedro, P.S.; Silva, J.L.; D'Amato, R.; Heras, E.S.; Juanes, J.A. Design of an Orthopedic Product by Using Additive Manufacturing Technology: The Arm Splint. *J. Med. Syst.* **2018**, *42*, 54. [CrossRef] [PubMed]
6. Pearce, J.M.; Blair, C.M.; Laciak, K.J.; Andrews, R.; Nosrat, A.; Zelenika-Zovko, I. 3-D Printing of Open Source Appropriate Technologies for Self-Directed Sustainable Development. *J. Sustain. Dev.* **2010**, *3*, 17–29. [CrossRef]
7. Fiedler, M. Evaluating Tension and Tooth Geometry to Optimize Grip on 3D Printer Filament. *3D Print. Addit. Manuf.* **2015**, *2*, 85–88. [CrossRef]
8. Volpato, N.; Kretschek, D.; Foggiatto, J.A.; Gomez da Silva Cruz, C.M. Experimental analysis of an extrusion system for additive manufacturing based on polymer pellets. *Int. J. Adv. Manuf. Technol.* **2015**, *81*, 1519–1531. [CrossRef]
9. Bell, C. *3D Printing with Delta Printers*; Apress: Berkely, CA, USA, 2015.
10. Turner, B.N.; Gold, S.A. A review of melt extrusion additive manufacturing processes: II. Materials, dimensional accuracy, and surface roughness. *Rapid Prototyp. J.* **2015**, *21*, 250–261. [CrossRef]
11. Turner, B.N.; Strong, R.; Gold, S.A. A review of melt extrusion additive manufacturing processes: I. Process design and modeling. *Rapid Prototyp. J.* **2014**, *20*, 192–204. [CrossRef]
12. Ratzsch, K.F.; Kádár, R.; Naue, I.F.C.; Wilhelm, M. A combined NMR relaxometry and surface instability detection system for polymer melt extrusion. *Macromol. Mater. Eng.* **2013**, *298*, 1124–1132. [CrossRef]
13. Heywood, M. Airtripper Extruder Filament Force Sensor—Design & 3D Print. 2013. Available online: http://airtripper.com/1473/airtripper-extruder-filament-force-%09sensor-design-3d-print/ (accessed on 5 May 2018).
14. Heywood, M. Electronic Kitchen Scales Teardown versus Load Cells. 2013. Available online: http://airtripper.com/1397/electronic-kitchen-scales-teardown-versus-load-cells/ (accessed on 5 May 2018).
15. Zinniel, R.L.; Batchelder, J.S. Volumetric Feed Control for Flexible Filament. U.S. Patent 6058957A, 11 June 2000.
16. Nihommori, S.; Sakagami, S.; Yaku, T. Optical Encoder. U.S. Patent 6,635,863, 21 October 2003.
17. Stoop, J.A. Product design: Fundamentals and methods. *Saf. Sci.* **1996**, *24*, 233–236. [CrossRef]
18. Egels, Y.; Kasser, M. *Digital Photogrammetry*; CRC Press: Boca Raton, FL, USA, 2003.

ANEXO IV:

MONITORING AN ANALYSIS OF PERTURBATIONS IN FUSION DEPOSITION MODELLING (FDM) PROCESSES FOR THE USE OF BIOMATERIALS

Durante un proceso de producción FDM, existen diferentes perturbaciones externas a las características de la máquina que pueden afectar al proceso de producción. Estas alteraciones harán que el resultado final difiera del deseado. Además, estas alteraciones, como la temperatura o la humedad de la cámara, son extremadamente importantes en caso de utilizar materiales biocompatibles. El uso de este tipo de materiales en ambiente no controlado, puede ocasionar que se modifiquen o pierdan sus propiedades, lo que inutilizará el producto. Aparte de estas perturbaciones externas, también deben tenerse en cuenta las condiciones de la máquina a la que se somete el material, como la temperatura, las vibraciones o la velocidad de extrusión. El seguimiento de todos estos datos permitirá conocer las condiciones a las que estuvo expuesto el producto durante el proceso. De esta forma podrá verificar la validez del producto final.

Por estas razones, el propósito de este trabajo es monitorizar las condiciones de producción de estructuras con materiales biocompatibles mediante la técnica de modelado por deposición fundida (FDM). Este seguimiento nos permitirá obtener un informe que garantice las características técnicas y geométricas del modelo y las propiedades del biomaterial. Los parámetros elegidos para monitorizar son: Diámetro del filamento, temperatura en la boquilla de extrusión, temperatura ambiente en cámara cerrada, humedad ambiental en cámara cerrada.

Los resultados obtenidos, presentan variaciones de hasta un 3% en la temperatura de la boquilla de la extrusora con respecto a la temperatura establecida. En el caso del diámetro del filamento la diferencia con respecto al valor proporcionado por el proveedor del filamento es del 13,7%. Además, los resultados muestran cómo la humedad ambiente en cámara cerrada ha cambiado en 2 puntos porcentuales y la temperatura ambiente en cámara cerrada se ha incrementado 6,52 ° con respecto a los valores establecidos.

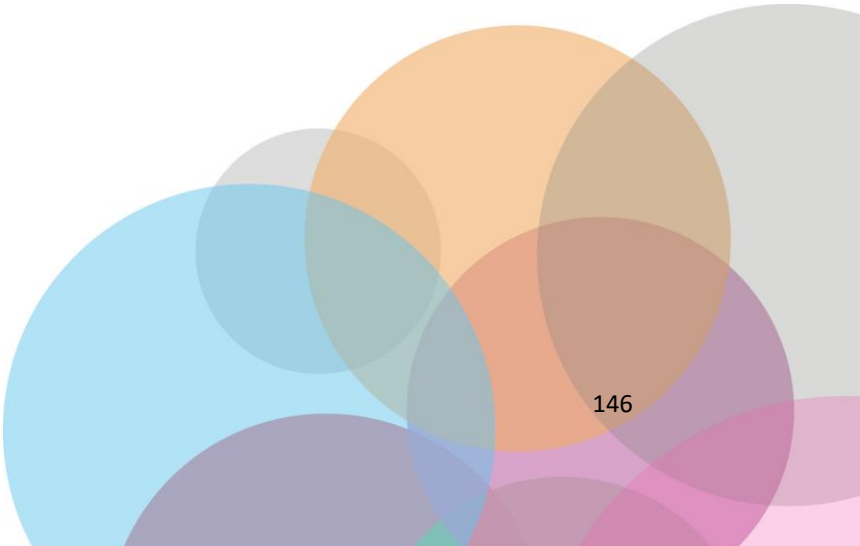

Journal of Medical Systems (2019) 43: 109
https://doi.org/10.1007/s10916-019-1236-2

EDUCATION & TRAINING

Monitoring an Analysis of Perturbations in Fusion Deposition Modelling (FDM) Processes for the Use of Biomaterials

Fernando Blaya Haro[1] · José María de Agustín del Burgo[1] · Roberto D'Amato[1] · Manuel Islán[1] · Enrique Soriano Heras[2] · Jesus Manuel Garcia Alonso[3] · Juan Antonio Juanes Mendez[4]

Received: 19 December 2018 / Accepted: 6 March 2019 / Published online: 19 March 2019

Abstract
During an FDM production process, there are different external disturbances to the characteristics of the machine that can affect to the production process. These disturbances will cause the final result differs from the desired one. Moreover, these disturbances, such as temperature or chamber humidity, are extremely important in case of using biocompatible materials. The use of these kind of materials with not controlled environment, can cause them to modify or loss of their properties; what will make the product unusable. Apart from these external disturbances, the conditions of the machine to which the material is subjected must also be considered, such as temperature, vibrations or extrusion speed. The monitoring of all these data will allow to know the conditions to which the product was exposed during the process. In this way, it will be able to verify the validity of the final product. For these reasons, the purpose of this work is to monitor the conditions of production of structures with biocompatible materials by fused deposition modelling (FDM) technique. This monitoring will allow us to obtain a report that guarantee the technical and geometrical characteristics of the model and the biomaterial properties. The parameters chosen to be monitored are: Diameter of filament use, temperature in extrusion nozzle, ambient temperature in closed chamber, ambient humidity in closed chamber. The obtained results, after collected and analysing the data, present variations of up to 3% in the temperature of the nozzle of the extruder with respect to set temperature. In the case of the filament diameter the difference with respect to the value provided from the filament supplier is of 13,7%. In addition, the results show how the ambient humidity in closed chamber has changed by 2 percentage points and the ambient temperature in closed chamber has been increased 6,52 °C with respect to the set values.

Keywords Additive manufacturing process · Biomaterials · Sensor · Medical application

Introduction

The reduction of costs and production times in various industrial sectors is due to the attention of the engineering world paid to improve the quality of products and services with the optimization of industrial processes [1, 2]. In the case of medical application, this has allowed to improve the performance of materials used for prosthetic implants in the case of knee [3]

This article is part of the Topical Collection on *Education & Training*

✉ Roberto D'Amato
r.damato@upm.es

Fernando Blaya Haro
fernando.blaya@upm.es

José María de Agustín del Burgo
jm.deagustin@alumnos.upm.es

Manuel Islán
manuel.islan.marcos@upm.es

Enrique Soriano Heras
esoriano@ing.uc3m.es

Jesus Manuel Garcia Alonso
jesusmanuel.garcia@salesianosatocha.es

Juan Antonio Juanes Mendez
jajm@usal.es

[1] Technical University of Madrid, 28012 Madrid, Spain
[2] Department of Mechanical Engineering, University Carlos III of Madrid, 28911 Leganés, Spain
[3] Salesian Institute of Madrid, 28012 Madrid, Spain
[4] University of Salamanca, Campus Miguel de Unamuno, 37007 Salamanca, Spain

and hip joint [4, 5] or in the case in which the aims was to study and optimize the tribological performances of the human joint implant materials [6, 7]. In this last case, in recent years, the optimization of the performance of biomedical products has been made possible also by scientific studies on the simulation of the dynamic behaviour of human joints [8, 9]. Particular attention has been paid to the geometric parameters used in the implementation of the mathematical models developed. Among these, for example, the algorithms for the morphometric fit of the bone surfaces that form the tribological contact of the ankle human joint [10]. The same techniques and procedures, in recent years, have been adapted and improved to be applied in Finite Element Modelling (FEM) analyses of the dynamic behaviour of soft tissues, such as tendons, ligaments, fibrous tissues, synovial membranes (which are connective tissue), and muscles, nerves and blood vessels that form the human joint [11, 12]. The same happened in the case of biomedical products printed in 3D such as the splints for arms or legs for people who had suffered fractures or specific diseases, such as rupture of the Achilles tendon [13]. In fact, a perfect geometric modelling and knowledge of the morphometric parameters of the limbs to be immobilized, has allowed to optimize and improve the production and 3D printing of the customized product. This is thanks to the development of additive manufacturing processes such as 3D printing [14]. This is thanks to the development of additive manufacturing processes such as 3D printing. In fact, the new layered additive manufacturing techniques have come to be recognized as the fourth industrial revolution. The increase in manufacturing at a particular and professional level requires an increase in print quality, a reduction in machine costs and an increase in the knowledge of the scientific community [15–17]. Still in the medical field, the application of engineering applied to sectors related to human health has allowed the development and production of hospital equipment. During the deposition process, many of the variables that contribute to improving or worsening the final result are subject to disturbances that come from the system itself as well as from others outside the machine. This type of deviations is difficult to control, as happens with the variability of the material, variations in the outside and inside temperature of the machine, humidity or deviations in the printing area [18]. All these variables, like temperature, humidity, vibrations etc. will affect to increment or decrement the different forces of adhesion and cohesion between the layers of the same material, but also when working with different materials [19, 20]. Currently, the sensorized and the control of additive manufacturing processes, is presented as an evolution of the methods, categorized as sensorized and control of the variables and sensorized and control of manufacturing attributes [21]. Most of the cases, the disturbances produced during the process are assumable with a post processed so that the final product can be fully functional. However, when the material employed is a biomaterial or a biocompatible material, it is necessary to control during the whole process the conditions in which the structure is formed. It will make possible to discriminate and analyse zones that may have been affected by these variations and, consequently, it will make possible to make decisions about the validity or rejection of the final object. In this paper, it will be showed a data collection system for temperature, humidity and filament diameter, during the process in a fused deposition machine for the subsequent obtaining of reports on the conditions in which the piece has been produced. In addition, this methodology is presented as a low cost system that could be installed on any FDM machine with similar characteristics.

Materials and methods

First point in the study, was carried out by collecting measures of different parameters, maintaining the focus on two specific goals [22]:

- Study how the different production conditions affect the final structure.
- Evaluate the realization of a control over these data, in order to guarantee the optimal conditions during the realization of a structure with biocompatible characteristics.

To do this, the following parameters have chosen to be monitored:

- Diameter of filament used
- Temperature in extrusion nozzle
- Ambient temperature in closed chamber
- Ambient humidity in closed chamber

Diameter of filament used

Filament diameter is of great importance to be considered due to its variations in the manufacturing process that can cause the final result to vary notably. Although manufacturers and researches try constantly to improve the polymer manufacturing process, including spinning and injection moulding., The product quality and efficiency are influenced by multiple processing parameters and materials, such as nominal cutting and shearing, the temperature of the process or the branch, that currently are not fully understood. The control and optimization of such operations contribute to getting closer and closer to the nominal size of the filament, but it still moves in quite large tolerances [21, 23–25]. It was analysed the diameter fluctuations of different FDM plastic providers. There were taken samples of a length of 3 m of filament each centimetre, by using a sensor with a resolution of 0,01 mm. Four brands were analysed with a nominal diameter of 1,75 mm, and the results are shown in Fig. 1.

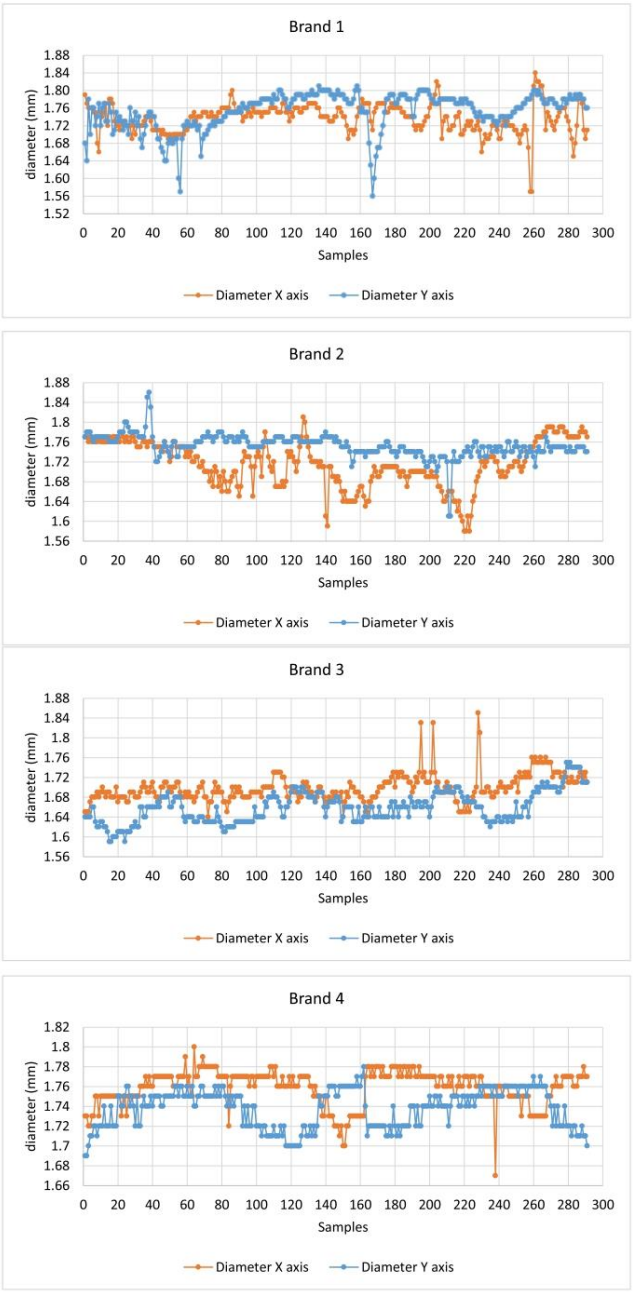

Fig. 1 Diameter fluctuations of 4 different filament providers

Analysing these samples, it comes up hat the diameter quality is very low. It varies from 1,56 to 1,86 mm, see Table 1. It is due to that the manufactures normally check the diameter with a lower frequency and get the medium value as quality test.

With these data, it is possible to calculate the variations of volume deposited during the process of extrusion:

$$volume = \pi * radio^2 * length$$

Analysing a length of 10 mm of filament, the variation of volume deposited can varies up to 33.51% of the nominal value (Table 2).

These data can explain the reason why the produced models use to have defect parts as a volume higher than the theoretical model or a lack of material in some layers. The deposited material not only affect to the dimensions and mechanical characteristics of the piece and the exterior finish, it can also result in discomfort or friction in the case of being in contact with the skin. In Fig. 2 it is possible to check the error that appears when producing a piece of thickness 1 mm with two portions of filament of average 1,73 mm and 1,82 mm in diameter [22].

Extruder temperature

For a correct extrusion process, it is necessary to get and maintain an optimal nozzle temperature. If the temperature achieves high values, the material will change its properties, even changing to a crystalized state that will ruin the model and even the nozzle. In case that the temperature was just some degrees higher than the optimal, the expansion of the material will not be constant, therefore the final dimension will be wrong.

Other way, if the temperature is lower than recommended for a specific material, the adhesion between layers will not be correct and it will appear breakpoints. These breakpoints are not visible, so it is of high importance to take care of this problem, as it could produce a higher problem during the use of the part.

Table 1 Sampled data analysis

Brand	Maximum [mm]	Minimum [mm]	Average [mm]
1	1,86	1,57	1,78
2	1,80	1,68	1,76
3	1,82	1,58	1,67
4	1,83	1,56	1,73

Table 2 Volumes deposited in 10 mm of advance

Diameter	Volume [mm^3]
1,75 mm (nominal)	24,05
1,56 mm (minimum)	19,11
1,86 mm (maximum)	27,17
1735 mm (average)	23,50

Chamber temperature and humidity

Similar case happens with the chamber temperature. A correct and controlled atmosphere of temperature and humidity, will guarantee the correct adhesion between the layers, and the properties of the final produced part.

In case of using biomaterials, the importance of controlling this temperature and humidity is even greater, as it could lose it biomaterial properties [19].

Results and discussions

After studying the different parameters that can interfere in the final structure, it is proceed to collect data in a real process. It will be taken samples of extruder and chamber temperature, humidity and filament diameter. Apart of these data, it will be stored the coordinates X, Y and layer of all the samples. This will allow us to check the conditions of the deposited filament in all the zones of the structure.

Measurements are collected during a real production process and are obtained the following data, showed in Figs. 3, 4, 5, and 6. The measurement of each one of the sensors has been collected every 30 s for 74,5 min, obtaining a total of 149 samples [22].

- Extruder Temperature

As can be seen, the extrusion temperature is not at all constant, due mainly to variations in the air flow of the fan of the nozzle, which, by influencing the surface of the piece being made, varies constantly according to the geometry of it, making it difficult to control.

- Chamber temperature

The temperature in the chamber increases during the process, due to the heat that comes from the nozzle, the deposited material and the machine itself (both electronics and mechanics).

- Chamber humidity

Fig. 2 Error due to filament diameter variations

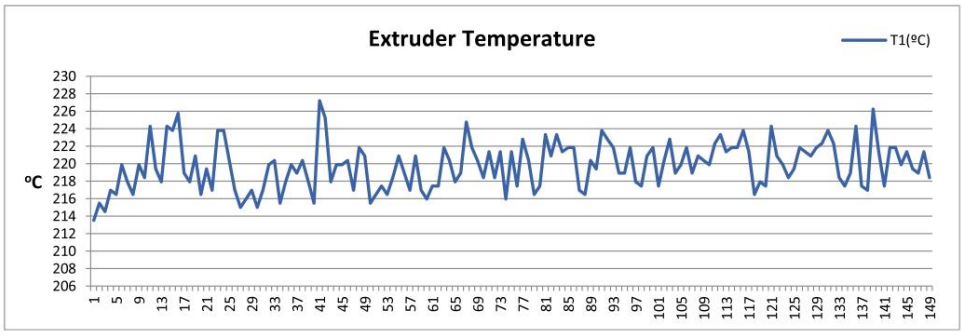

Fig. 3 Extruder Temperature

The humidity decreases slightly during the process, due to the increase in temperature of the chamber.

- Filament diameter

The filament diameter varies greatly, reaching maximums of 1,94 mm and minima of 1,64 mm.

In many cases, strict control of the temperature or humidity in the printing chamber is needed. In the case of

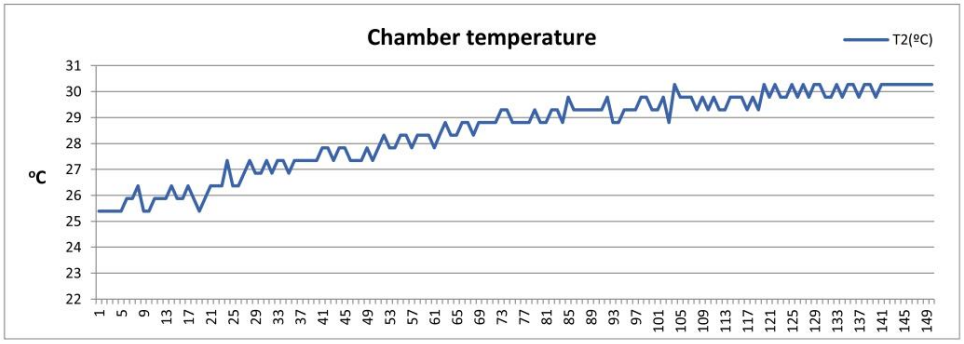

Fig. 4 Chamber temperature

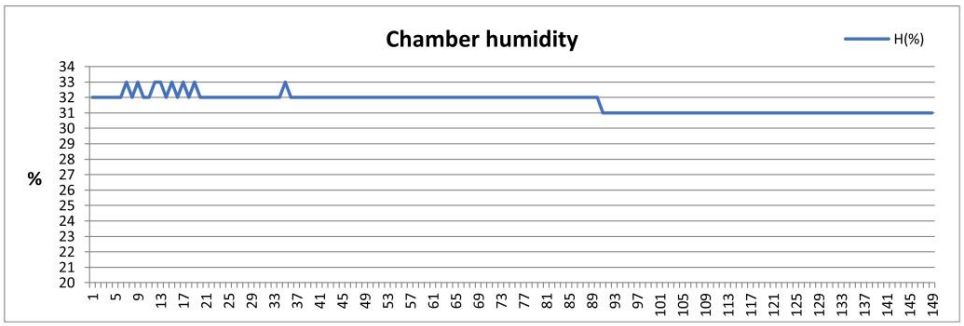

Fig. 5 Chamber humidity

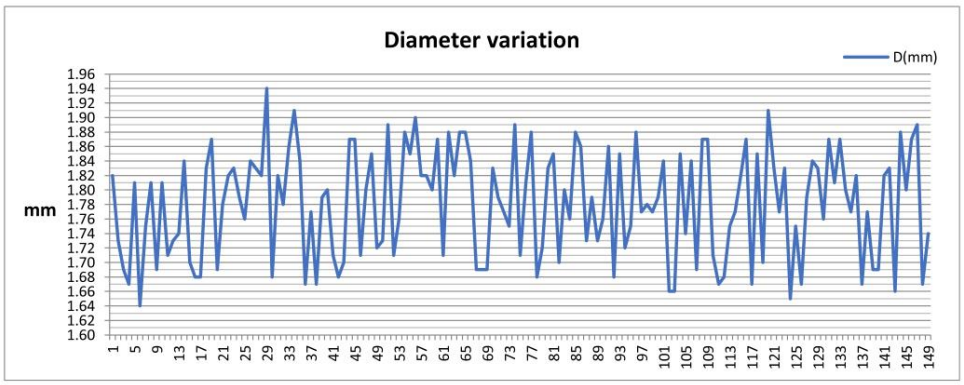

Fig. 6 Filament diameter

manufacturing by 3D printing bio-ceramic joint implants has to be performed at low temperature. The fluctuation of the temperature would damage the internal structure of the material. In other cases, the temperature could produce novice particles. This would affect to the operator safety and would make impossible to use the machine in some cleaning rooms that are normally used in medical ambient [26].

After analysing the data and obtaining the results shown in Table 3, there are variations of up to 3% in the temperature of the nozzle or 13,7% in the diameter. In addition, the humidity has changed by 2 percentage points and the ambient temperature has been increased 6,52 °C:

Conclusions

In this study a low-cost system that allows to analyse how much the optimal parameters for a good FDM production part, can change during the process, has been developed. In fact, the disturbances external to the machine and the process, but

Table 3 Analysis of collected data

	Humidity (%)	Chamber temperature [°C]	Extruder temperature [°C]	Filament diameter [mm]
Nominal	*Not controlled*	*Not controlled*	220	1,75
Average	31,64	25,56	218,28	1,78
Maximum	33,00	34,67	227,20	1,96
Minimum	31,00	19,04	213,53	1,61

also intrinsic from the machine or the process can affect the 3D manufacturing of the part.

As expected, the data obtained from these disturbances are really far to be constant; furthermore, the variation is produced during all the process, without reaching a stable value. With the present study has been possible to analyse different materials, different brands of the same material, in order to see that the manufacturer shows the optimal conditions for a correct printing. However, it is impossible to maintain these conditions with this production system implemented in these kind of machines. It would be necessary to develop an upgrade of the machines to reach this target.

From this point, there are two clear lines of investigation. First of them, implementing a system that can measure the disturbances and achieves the goal of correct them. The second one, implementing a system that gets this type of data during the process, what will make possible to compare with the optimal.

The control of environmental conditions for 3D printing is of fundamental importance in biomedical applications.

In addition, it is intended to complement the measures already obtained with others such as:

- Extra temperature sensors: In different areas of the chamber, which will allow detecting the different temperatures in the different zones to try to control the air flow.
- Vibrations: It will allow detecting errors in the deposition of the material. Also in the future it would be possible to try to correct them.
- Deposition speed: It will make possible to do the filament deposition on an accurate way speed and together with the measurement of the diameter, it will allow to calculate the volume of material deposited at each moment.

The set of all these measures will give us a full report of the conditions that occur during the process, in addition to help to correct them.

Compliance with Ethical Standards Fernando Blaya Haro declares that he has no conflict of interest. José María de Agustín del Burgo declares that he has no conflict of interest. Roberto D'Amato declares that he has no conflict of interest. Manuel Islán declares that he has no conflict of interest. Enrique Soriano Heras declares that he has no conflict of interest. Jesus Manuel Garcia Alonso declares that he has no conflict of interest. Juan Antonio Juanes Mendez declares that he has no conflict of interest.

This article does not contain any studies with human participants performed by any of the authors.

This article does not contain any studies with animals performed by any of the authors.

References

1. Wojciechowski, S., Maruda, R. W., Barrans, S., Nieslony, P., and Krolczyk, G. M., Optimisation of machining parameters during ball end milling of hardened steel with various surface inclinations. *Measurement* 111:18–28, 2017.
2. Jarosz, K., Löschner, P., Niesłony, P., and Krolczyk, G., Optimization of CNC face milling process of Al-6061-T6 aluminum alloy. *J. Mach. Eng.* 17(1):69–77, 2017.
3. Ruggiero, A., Merola, M., and Affatato, S., On the biotribology of total knee replacement: A new roughness measurements protocol on in vivo condyles considering the dynamic loading from musculoskeletal multibody model. *Measurement* 112:22–28, 2017.
4. Merola, M., Ruggiero, A., De Mattia, J. S., and Affatato, S., On the tribological behavior of retrieved hip femoral heads affected by metallic debris. A comparative investigation by stylus and optical profilometer for a new roughness measurement protocol. *Measurement* 90:365–371, 2016.
5. Ruggiero, A., Merola, M., and Affatato, S., Finite element simulations of hard-on-soft hip joint prosthesis accounting for dynamic loads calculated from a musculoskeletal model during walking. *Materials (Basel).* 11(4):574, 2018.
6. Ruggiero, A., D'Amato, R., and Gómez, E., Experimental analysis of tribological behavior of UHMWPE against AISI420C and against TiAl6V4 alloy under dry and lubricated conditions. *Tribol. Int.* 92:154–161, 2015.
7. Ruggiero, A., D'Amato, R., Gómez, E., and Merola, M., Experimental comparison on tribological pairs UHMWPE/TIAL6V4 alloy, UHMWPE/AISI316L austenitic stainless and UHMWPE/AL2O3 ceramic, under dry and lubricated conditions. *Tribol. Int.* 96:349–360, 2016.
8. Ruggiero, A., Gòmez, E., and D'Amato, R., Approximate analytical model for the squeeze-film lubrication of the human ankle joint with synovial fluid filtrated by articular cartilage. *Tribol. Lett.* 41(2): 337–343, 2011.
9. Ruggiero, A., Gómez, E., and D'Amato, R., Approximate closed-form solution of the synovial fluid film force in the human ankle joint with non-Newtonian lubricant. *Tribol. Int.* 57:156–161, 2013.
10. 'amato, R. D., Calvo, R., and Mez, E. G., Sensitivity study of the morphometric fitting on the pressure field inside ankle joints. *Case Stud. Mech. Syst. Signal Process.* 1:8–14, 2015.
11. Islan, M., Blaya, F., San Pedro, P., D'Amato, R., Lechosa Urquijo, E., and Juanes, J. A., Analysis and fem simulation methodology of dynamic behavior of human rotator cuff in repetitive routines: Musician case study. *J. Med. Syst.* 42(3), 2018.
12. Marcos, M. I., Urquijo, E. L., Haro, F. B., D'Amato, R., Juanes, J. A., and Heras, E. S., Finite element simulation and analysis of the behavior under load of a human shoulder. In Proceedings of the Sixth International Conference on Technological Ecosystems for Enhancing Multiculturality - TEEM'18, 2018, pp 454–461.
13. Haro, F. B., Pedro, P. S., Pedro, A. B. S., Lopez-Silva, J., Juanes, J. A., and D'Amato, R., Design and prototyping by additive manufacturing of a functional splint for rehabilitation of Achilles tendon intrasubstance rupture. In Proceedings of the Sixth International Conference on Technological Ecosystems for Enhancing Multiculturality - TEEM'18, 2018, pp 433–439.
14. Blaya, F., San Pedro, P., López Silva, J., D'Amato, R., Soriano Heras, E., and Antonio Juanes, J., Design of an Orthopedic Product by using additive manufacturing technology: The arm splint. *J. Med. Syst.* 42:3, 2018.
15. Calderon, A., Griffin, J., and Zagal, J. C., BeamMaker: An open hardware high-resolution digital fabricator for the masses. *Rapid Prototyp. J.* 20(3):245–255, 2014.
16. Mota, C., The rise of personal fabrication. In Proceedings of the 8th ACM conference on Creativity and cognition - C&C '11, 2011, p 279.
17. Stemp-Morlock, G., and Graeme, Personal fabrication. *Commun. ACM* 53(10):14, 2010.
18. Stopp, S., Wolff, T., Irlinger, F., and Lueth, T., A new method for printer calibration and contour accuracy manufacturing with 3D-print technology. *Rapid Prototyp. J.* 14(3):167–172, 2008.

19. Hashemi Sanatgar, R., Campagne, C., and Nierstrasz, V., Investigation of the adhesion properties of direct 3D printing of polymers and nanocomposites on textiles: Effect of FDM printing process parameters. *Appl. Surf. Sci.* 403:551–563, 2017.
20. Stabile, L., Scungio, M., Buonanno, G., Arpino, F., and Ficco, G., Airborne particle emission of a commercial 3D printer: The effect of filament material and printing temperature. *Indoor Air* 27(2): 398–408, 2017.
21. Reutzel, E. W. and Nassar, A. R., A survey of sensing and control systems for machine and process monitoring of directedenergy, metal-based additive manufacturing. *Rapid Prototyp. J.* 21(2). Emerald Group Publishing Ltd., pp. 159–167, 16-Mar-2015.
22. Soriano Heras, E., Blaya Haro, F., de Agustín del Burgo, J. M., Islán Marcos, M., and D'Amato, R., Filament advance detection sensor for fused deposition modelling 3D printers. *Sensors (Switzerland)* 18(5):1495, 2018.
23. Soriano Heras, E., Blaya Haro, F., de Agustín del Burgo, J., Islán Marcos, M., and D'Amato, R., Filament advance detection sensor for fused deposition modelling 3D printers. *Sensors* 18(5):1495, 2018.
24. Volpato, N., Kretschek, D., Foggiatto, J. A., and Gomez da Silva Cruz, C. M., Experimental analysis of an extrusion system for additive manufacturing based on polymer pellets. *Int. J. Adv. Manuf. Technol.* 81(9–12):1519–1531, 2015.
25. Turner, B. N., and Gold, S. A., A review of melt extrusion additive manufacturing processes: II. Materials, dimensional accuracy, and surface roughness. *Rapid Prototyp. J.* 21(3):250–261, 2015.
26. Habibovic, P., Gbureck, U., Doillon, C. J., Bassett, D. C., van Blitterswijk, C. A., and Barralet, J. E., Osteoconduction and osteoinduction of low-temperature 3D printed bioceramic implants. *Biomaterials* 29(7):944–953, 2008.

ANEXO V:

DEVELOPMENT OF A SMART SPLINT TO MONITOR DIFFERENT PARAMETERS DURING THE TREATMENT PROCESS

Para determinadas lesiones por rotura del sistema musculoesquelético, el único tratamiento disponible es el uso de férulas de inmovilización. Este tipo de tratamiento suele provocar molestias y ciertos contratiempos en los pacientes. Además, se suelen generar otras complicaciones a nivel vascular, muscular o articular. Actualmente, existe una alternativa realmente posible que solucionaría estos problemas e incluso permitiría una recuperación más rápida y mejor. Esto es posible gracias a la aplicación de la ingeniería sobre técnicas de fabricación aditiva y al uso de materiales biocompatibles disponibles en el mercado. Este estudio propone el uso de estos materiales y técnicas, incluida la integración de sensores dentro de las férulas.

Los principales parámetros considerados a estudiar son la presión, la humedad y la temperatura. Estos aspectos se combinan y analizan para determinar cualquier tipo de evolución inesperada del tratamiento. De esta manera, será posible monitorizar algunas señales que serían estudiadas para detectar problemas que están asociados a la etapa inicial del tratamiento. El objetivo de este estudio es generar una férula inteligente mediante el uso de biomateriales y técnicas de ingeniería basadas en el sistema avanzado de fabricación y sensores, para fines clínicos. Los resultados muestran que el prototipo de la férula inteligente permite obtener datos cuando se coloca sobre el brazo de un paciente. Se leen dos temperaturas durante el tratamiento: en contacto con la piel y entre piel y férula. Las variaciones de humedad debidas al sudor dentro de la férula también son leídas por un sensor de humedad. Un sensor de presión detecta ligeros cambios de presión dentro de la férula. Además, se ha incluido un sensor de infrarrojos como detector de presencia.

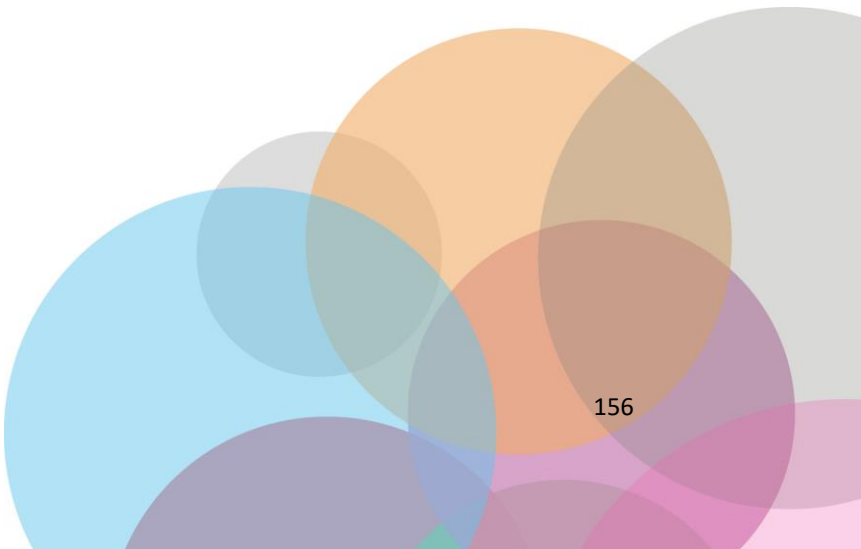

sensors

MDPI

Article

Development of a Smart Splint to Monitor Different Parameters during the Treatment Process

José María De Agustín Del Burgo [1], Fernando Blaya Haro [2], Roberto D'Amato [2,*] and Juan Antonio Juanes Méndez [1]

[1] Campus Miguel de Unamuno, Universidad de Salamanca, 37007 Salamanca, Spain; id00792219@usal.es (J.M.D.A.D.B.); jajm@usal.es (J.A.J.M.)

[2] ETSIDI-Departamento de Ingeniería Mecánica, Química y Diseño Industrial, Universidad Politécnica de Madrid (UPM), Ronda de Valencia 3, 28012 Madrid, Spain; fernando.blaya@upm.es

* Correspondence: r.damato@upm.es; Tel.: +34-91-067-7654

Received: 27 May 2020; Accepted: 27 July 2020; Published: 29 July 2020

check for updates

Abstract: For certain musculoskeletal complex rupture injuries, the only treatment available is the use of immobilization splints. This type of treatment usually causes discomfort and certain setbacks in patients. In addition, other complications are usually generated at the vascular, muscular, or articular level. Currently, there is a really possible alternative that would solve these problems and even allows a faster and better recovery. This is possible thanks to the application of engineering on additive manufacturing techniques and the use of biocompatible materials available in the market. This study proposes the use of these materials and techniques, including sensor integration inside the splints. The main parameters considered to be studied are pressure, humidity, and temperature. These aspects are combined and analyzed to determine any kind of unexpected evolution of the treatment. This way, it will be possible to monitor some signals that would be studied to detect problems that are associated to the very initial stage of the treatment. The goal of this study is to generate a smart splint by using biomaterials and engineering techniques based on the advanced manufacturing and sensor system, for clinical purposes. The results show that the prototype of the smart splint allows to get data when it is placed over the arm of a patient. Two temperatures are read during the treatment: in contact with the skin and between skin and splint. The humidity variations due to sweat inside the splint are also read by a humidity sensor. A pressure sensor detects slight changes of pressure inside the splint. In addition, an infrared sensor has been included as a presence detector.

Keywords: smart splint; biomedical sensor; iot; additive manufacturing; personalized medicine; health monitoring

1. Introduction

The new industry is experiencing an enormous growth, thanks to the use of techniques that include advanced manufacturing and industrial design. Moreover, the optimization of the process [1–3], the development of new materials by manufacturers [4–6], or the decrease of environmental costs [7] are some achievements that make it possible to expand these technics further than the industrial area. Nowadays, these techniques are being transferred to medicine areas, by applications known as bioengineering [8].

Among all emerging technologies in the area of bioengineering, the implementation of additive manufacturing (AM) in the healthcare industry has led to several benefits. The design freedom allows customization of surgical equipment, medical devices, and implants. In fact, anatomy for pedagogical objectives [9,10], craniomaxillofacial surgery [11], oral appliance therapy for snoring and obstructive

sleep apnea (OSA) [12,13], orthopedics surgery [14], and rehabilitation [15] are some examples in which the benefits of fused filament fabrication (FFF) technology could improve the clinical course of patients. These new techniques allow to improve wearing comfort and better hygiene due to the bio-compatible and sterilizable properties [16]. Over this fields, many developments have been carried out in recent years, like exoskeletons [17], prosthesis, or assistive devices. These specialties are in demand in developed countries [18], but a level of maturity and technological development is necessary to promote a change in the actual model. Moreover, both orthopedics and rehabilitation are specialties of medicine very conducive and receptive to all kinds of technological developments or applications in the field of research, development, and innovation (R&D&I).

Thanks to the use of different methods of industrial three-dimensional digitization and reverse engineering, advanced manufacturing has generated a recent emergence of solutions. Based on additive manufacturing it has allowed a great advance in products of mass use such as splints, braces, prostheses, or assistive devices [19]. Moreover, these techniques, combined with new sensors and actuators, have revolutionized the applications of exoskeletons by the hand of robotics [20]. Products such as splints made by additive manufacturing offer great advantages over classical methods of permanent and splinting (splinting) or commercial immobilization (braces, corsets, etc.). Some of these advantages are adaptation, personalization, hygiene, materials used, or environmental impact, among others. The incursion of these new 3D techniques in medical processes allows to include smart systems to analyze different states of the medical evolution process [21]. This study proposes to combine 3D techniques with electronic systems to develop a new era of splints that have not been achieved before. The use of these kind of systems, which include small electronic boards, programming systems, and data communication, would make possible to monitor parameters as temperature and pressure. These parameters would be sent to an application running on a portable device and compared in a database with other similar treatments data or sent to the doctor to see if the process is evolving correctly. This way, it is possible to include the smart splints into the use of big data in healthcare and the Internet of Things (IoT) movement [22,23]. In fact, it has been shown that the use of the IoT, allows data exchange through network connectivity and devices integrated with hardware, software, and sensors [24]. This, applied to medicine, will lead to a reduction in costs and inefficiencies and better patient satisfaction in terms of medical care. One of the factors for the use of IoT in medicine and in rehabilitation [25] are medical devices (things) integrated with a detection technology for the continuous acquisition of physiological data from patients. For these reasons, the purpose of this study is to present how to design and manufacture a smart and functional splint in order to monitor different physiological parameters of the patient and of the device (skin temperature, humidity, pressure, and color changes on the skin). In this manner, it is possible to have a continuous data acquisition that allows to improve the treatment outcomes and to reduce recovery times and healthcare costs.

2. Material and Methods

In this section, it will be explained and presented all the steps followed in this study in order to 3D model, design, prototype manufacture, and assemble a smart and functional arm splint. The arm of a 29-year-old volunteer as a model was used. In this case, there is no lesion, but it will be used as the basis to create the splint where the tests are performed. The same process could be applied to other anatomical regions [26].

2.1. 3D Model and Design

As reported in other previous studies, the first step was to get the 3D model of the injured part [7]. From that point, the splint is modeled over this part, considering the areas where the sensors are placed. A commercial scanner (Sense™ 3D scanner, 3D Systems Inc., Rock Hill, SC, USA) was used for the digitalization of the arm at a distance of 40 cm according to the manufacturer's instructions. The technical specifications of the scanner are shown in Table 1.

Table 1. Technical specifications of the Sense™ 3D scanner.

Maximum Scan Volume	2 × 2 × 2 (m)
Minimum Scan Volume	0.2 × 0.2 × 0.2 (m)
Working Distance	0.2–1.6 (m)
Number of Cameras	2
Class Certified Laser Product	1
Resolution at 0.5 m	1 (mm)

It is possible to scan the entire area, at once or in several times if necessary due to limitations produced by a possible injury. Later, the software joins the points cloud. Figure 1 shows the scan process, and the 3D point cloud obtained the total time for the scanning process is 6 min.

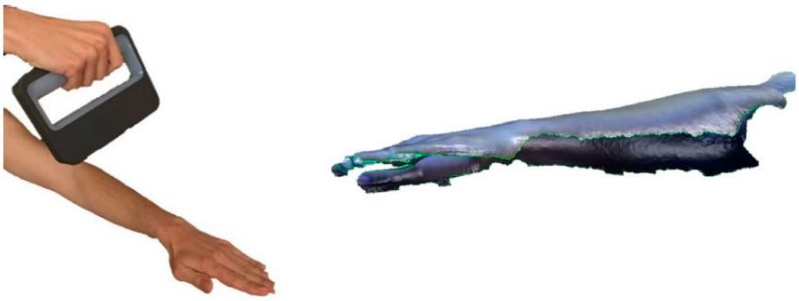

(**a**) (**b**)

Figure 1. Scanning process of the arm to get the digital model (**a**) and points cloud (**b**).

Once the 3D point cloud is obtained, post-processing is carried out by using a 3D CAD software Geomagic FreeForm (3D Systems, Inc., United States). The 3D scanned models are shown in Figure 2.

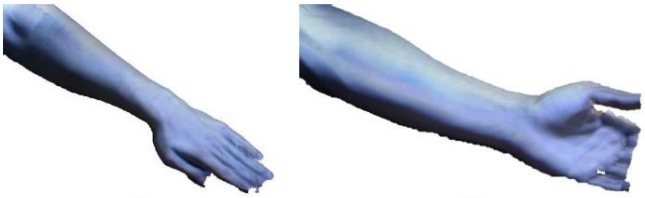

(**a**) (**b**)

Figure 2. 3D model of the arm obtained after the scanning process: top side (**a**) and bottom side (**b**).

With this software, it was possible to clean the point cloud by filling the holes due to noise appearing during the scanning process and by correcting with a smoothing algorithm any minor anomalies due to some misplaced points of the cloud or due to surfacing process. With this procedure, it was possible to obtain a simpler mesh of the arm by limiting the area of the interest started from a point cloud. Starting from this mesh and creating an offset of 0.5 mm, the solid which is the basis of the splint is created. Figure 3 shows the mesh of the scanned arm and the solid digital model obtained.

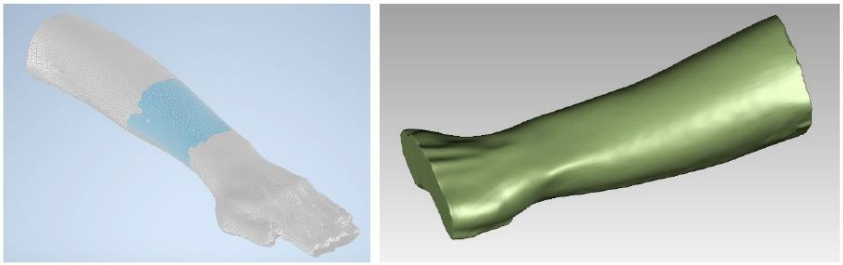

(**a**) (**b**)

Figure 3. Post processed: mesh of the scanned arm (**a**) and solid digital model obtained from the clean mesh (**b**).

The solid digital model shown in Figure 3b represents the first step of the design of the splint. In fact, the solid surface created represents the internal face of the splint in direct contact with the skin of the patient's arm. Once this reference surface of the splint has been created, a 5 mm thickness solid is generated as shown in Figure 4.

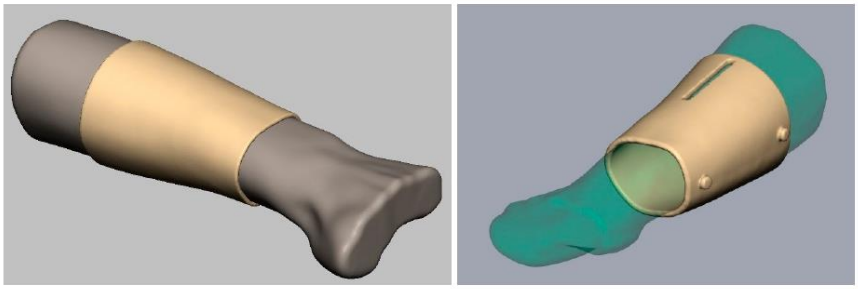

(**a**) (**b**)

Figure 4. Initial solid obtained from the points cloud (**a**) and initial stage of the design, including the hole for the temperature sensor and closing buttons (**b**).

Once the body of the splint has been created, it was necessary to divide it in two parts to make the mounting possible, which is later joined with a mechanical closure (Figure 5a). In addition, the places for the sensors are designed and some holes are introduced as shown in the Figure 5a–c. The function of these holes and windows is manifold. In fact, they allow, on the one hand, direct medical inspection of the injured part, aeration of the skin in contact with the splint and, on the other, the possibility of using electromedical devices for rehabilitation during immobilization of the limb. Figure 6 shows the final modeled splint over the initial 3D model.

2.2. *Sensing Technologies*

In this section, devices for data acquisition in the IoT-based healthcare system and used in this study are discussed. When an injury occurs, normal inflammatory signs such as increased skin temperature, edema, changes in skin color, and pain may appear. In addition, cool skin and increased sweating are symptoms of different problems that the patient may be suffering from [27,28].

After the scanning, the splint is designed according to the 3D obtained model, incorporating the sensors housings. These sensors will be used to get the information of the splint and patient. At this point in the study, the sensors are custom positioned in the exact areas of the anatomical part to be

monitored. The position adjustments and the verification of their correct behavior and setting will also be allowed.

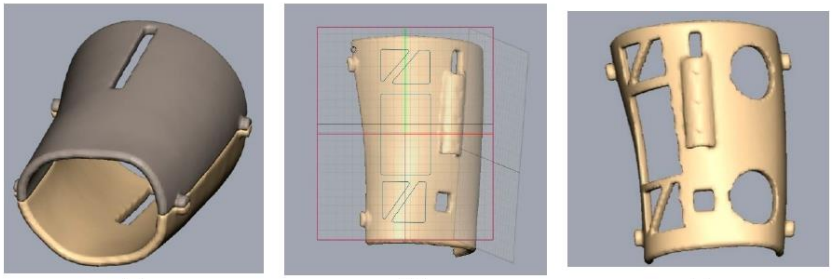

(**a**) (**b**) (**c**)

Figure 5. Different steps during the modeling of the splint: division of the splint (**a**), design of different sensor holes (**b**), and final top side splint (**c**).

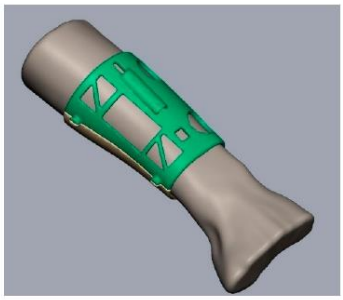

Figure 6. Final result of the modeled splint over the patient arm.

The main parameters considered to be studied are pressure, and temperature. These aspects are combined to determine any kind of unexpected evolution of the treatment as inflammatory processes, and temperature increments due to inflammation or infections in the affected area. In addition, it will be studied the possibility of detecting changing colors of the skin and humidity. The sensors incorporated to the splint are: two temperature sensors in direct contact with the skin (DS18B20) [29], one temperature and humidity sensor to get the temperature and humidity between the skin and the splint (DHT22) [30], two pressure sensors (DF9-40) [31], and one presence sensor (CNY70) [32]. The technical specifications of all sensors are summarized in Table 2.

Table 2. Technical specifications of the sensor.

Sensor Serial Number	DS18B20	DHT22	DF9-40	CNY70
Dimensions (mm)	6 × 6 × 50	15 × 7.7 × 20	40 × 20 × 0.25	7 × 7 × 6
Power voltage (*V*)	3.0–5.5	3.3–6	5	5
Working range	−55 °C to 125 °C	−40 °C to 80 °C 0 to 100% RH	0–500 g	0 to 10 mm
Resolution	± 0.0625 °C	0.1 °C 0.1% RH	14.5 g	–

The DS18B20 sensors (Dallas Semiconductor™ Maxim Integrated Products, Inc., Dallas, TX, USA) are 1-Wire digital temperature sensor. It reports degrees in Celsius, with a precision of 9 to 12-bit.

Each sensor has a unique 64-Bit serial number etched into it, which allows a huge number of sensors to be used on one data bus.

The DHT22 sensor (Aosong Electronics Co., Ltd., Guangzhou, China) utilizes exclusive digital-signal-collecting-technique and humidity sensing technology, its sensing elements is connected with 8-bit single-chip computer.

The DF9-40 sensor (Zhengzhou Winsen Electronics Technology Co., Ltd., Zhengzhou, China) is a film pressure based on flexible pressure sensing technology. In order to measure the applied force with an Arduino, it will be necessary to build a voltage divider circuit with a pull-down resistor. This circuit creates a variable voltage output that can be read by the ADC (analog to digital converter) input of the microcontroller. It means that for a simple force-to-voltage conversion, the force sensing resistor (R_{FSR}) device is tied to a measuring resistor (R_M) in a voltage divider. In this case, a 10kΩ resistor will be used. The output voltage (V_{out}) which is possible to measure with the Arduino is described by the following equation:

$$V_{out} = \frac{V_{cc} \cdot R_M}{R_M + R_{FSR}}. \quad (1)$$

Note that the output voltage measure is the voltage drop across the pull-down resistor. When no force is applied, the FSR resistance will be really high, for example, 10 MΩ. Using a 10 kΩ pull-down resistor and a V_{CC} of 5 V, results in the following output when no force is applied V_{OUT} = 0.005 V. When the FSR is pressed, the resistance goes down to roughly 200 Ω. This results in the following output voltage V_{OUT} = 4.9. Similar developments have been carried out in other studies for other medical applications [19].

The CNY70 sensor (Vishay Telefunken, Heil- bronn, Germany) is a reflective sensor that includes an infrared emitter and phototransistor in a leaded package with a daylight blocking filter. This sensor can detect the quantity of light reflected on a surface depending on the distance. However, if we set a distance, it is possible to detect different colors depending on the infra-red light absorbed by that color. It will be tested if it is possible to detect color changes on the skin. In order to use this sensor, is necessary to build a voltage divider circuit with a pull-down resistor as in case of the pressure sensor. In this case, a 39 kΩ is used.

All these sensors have been controlled by using an Arduino UNO board [33], which will get info from the four sensors and combine to achieve a full diagnostic.

2.3. Additive Manufacturing

After the digital modeling and design process, the file obtained is sent to a slicer that prepares the part to be produced by using the additive manufacturing process (Figure 7). The splint was manufactured by using a fusion deposition modeling (FDM) 3D printer "TotalPrinter" machine (Figure 7a). This 3D printer was designed, developed, and manufactured in the Additive Manufacturing and Rapid Prototype Laboratory of the Escuela Técnica Superior de Ingeniería y Diseño Industrial at Universidad Politécnica de Madrid. This 3D printer allows continuous temperature and humidity control of the printing chamber and of extruder temperature with the aim of optimizing the process [34] and obtaining an homogeneous splint in terms of adhesion of the various printing layers, density of the material, and mechanical characteristics [35]. In addition, this 3D printing machine allows continuous monitoring of the thickness of the PLA filament used as reported in the study of Soriano et al. (2018) [36] and in the study of J. M. D. A. Del Burgo et al. (2018) [37].

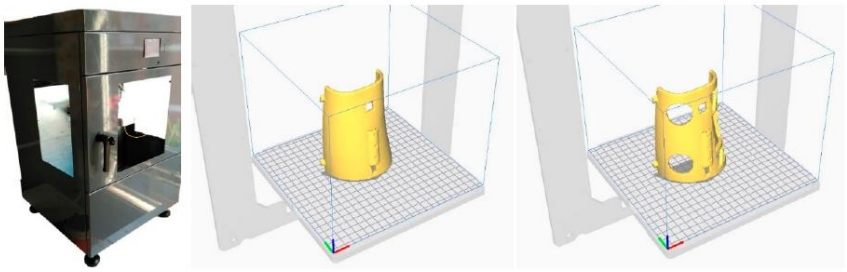

(**a**) (**b**) (**c**)

Figure 7. TotalPrinter machine developed to work with biomaterials (**a**). G-Code process generation for 3D printing for the different parts of the splint (**b**) and (**c**).

The material chosen for the prototype was biocompatible material PLA filament with a diameter of 1.75 mm. The vertical printing position was chosen for the two parts of the splint as shown in the Figure 7b,c by taking in account the volume of the printing chamber (200 mm × 200 mm × 400 mm). The printing parameters used for the manufacturing of the arm splint are shown in the Table 3. These parameters were chosen according to the material manufacturer's recommendations to obtain a sufficiently rigid and quality structure.

Table 3. Printing parameters.

Layer height [mm]	0.2
Extruder [mm]	0.4
Print density [%]	40
Thickness perimeter of closure of each layer [mm]	1
Print speed [mm/s]	60
Temperature [°C]	210

3. Results

In this section, the following is presented: the splint assembled with the sensors placed in their housings, the configuration of the micro controller for the collection of the monitored parameters, and the results obtained in the sampling.

3.1. 3D Model and Design

Figure 8a shows the two parts of the arm splint prototype. Figure 8a,b shows one part of the arm splint with the sensors and wires, for the connection to the Arduino, fully integrated.

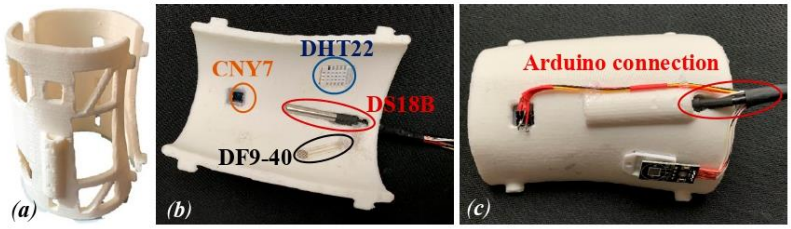

Figure 8. The real model of the arm splint obtained from the 3D printer (**a**). Splint assembled with the different sensors (**b**) and wires for the connection to the Arduino board (**c**).

Once the model is prepared, it is necessary to program the Arduino board to get the data from these sensors, and to design a small circuit that includes the necessary electronic parts to connect the sensors. For this study, the data are obtained directly from the serial communication between the Arduino board and the PC. Figure 9 shows the developed electronic adopted in this study. However, these data could be sent easily to a Bluetooth or Wi-Fi device like a smartphone or tablet. It is important to report that the two contact temperature sensors and the two pressure sensors are treated digitally to get just one resultant contact temperature and pressure.

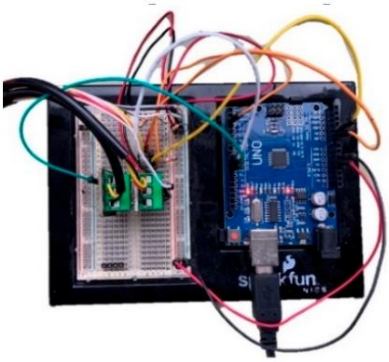

Figure 9. Electronic board wiring to get the data during the tests.

3.2. Sensing Technologies

In order to test the arm splint assembled with the sensors connected to the Arduino board, the splint was fixed to the originally scanned arm for 1.5 h. The data from the sensors were collected using the Arduino serial monitor every 3 s and sent to excel to plot some graphs. Figure 10 shows the serial monitor of the acquired data while the splint was fixed to the arm of the volunteer. The obtained data are shown and explained in the following sections.

(**a**) (**b**) (**c**)

Figure 10. Example of the serial data collection using the Arduino board (**a**), real splint prototype with electrical wiring mounted over the arm (**b**) and detailed view of the closing buttons (**c**).

3.2.1. Temperatures

In Figure 11, the mean temperature of the two sensors in contact with the skin is shown in orange. The temperature inside the splint is shown in blue.

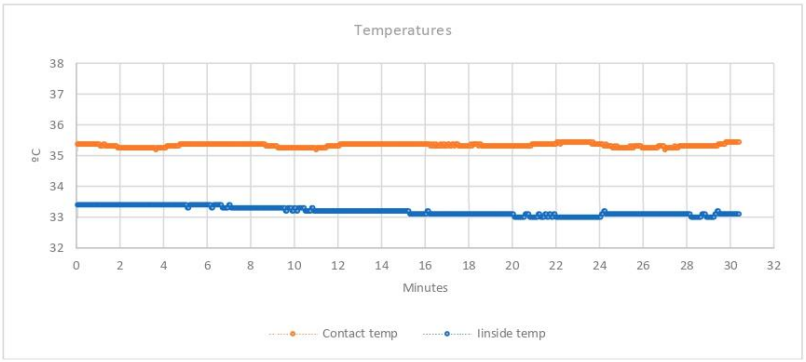

Figure 11. Temperatures graph.

It is possible to see that the sensors in contact with the skin, registered a temperature slightly lower than the normal temperature of a person (36 °C). This fact, is produced because part of the surface of the sensors, is not in real contact with the skin. Due to this, it appears a gradient of temperature between the body and the environment. However, the distance between the skin and the surface of the sensor that is not in contact with the skin, is around 4 mm. This distance is not enough to interfere with the correct sensor operation. What the authors are looking for in this study with these sensors, is to detect an increment or decrement of the temperature, compared with the historical. For this reason, the surface of the sensor not in contact will not interfere to detect correctly the variations.

As it is possible to see in the graph, the second sensor (in blue), that is completely separated from the skin, registered around two degrees less than the sensors in contact. With just these readings, a variation of the temperature is perfectly detected, which could be a symptom of inflammation or infection of the area. This info may be used with the humidity levels to discover anomalies or different situations during the treatments.

3.2.2. Humidity

The knowledge of this parameter is crucial to avoid the appearance of bacteria due to humidity, especially in the case of surgery or injuries. In addition, as explained previously, cool skin and increased sweating are symptoms of some problems that may appear after an injury [27]. Figure 12 shows the percentage of humidity registered during the test. The orange line shows the humidity between the splint and the skin. The blue line shows the environmental humidity (which was sampled with a second similar sensor). These data change due to the environmental conditions and the humidity generated by the patient through sweat.

3.2.3. Pressure

The used sensor has a surface of 1 cm^2. Figure 13 shows the mean pressure detected by the two sensors. It is possible to see in the graph that at normal state, a pressure of 60 gf/cm^2 is detected. This pressure is produced by the normal pressure of the splint over the body so that the position of the joint is maintained for the treatment. For the tests, between min 6 and min 12, a force over the splint is applied, by simulating an inflammatory process. This variation is detected by the sensors, reading a pressure change from 60 to 100 gf/cm^2. The graph shows the actual pressure and also the

historical. With this information, a specialist may check if the pressure is higher or lower than the previous days, in order to know if the area is suffering an inflammatory process. The doctor may check the data as often as necessary. Thereby, when the pressure is increased due to the inflammation of the area, the sensors perfectly detect the increment of the mass inside the splint.

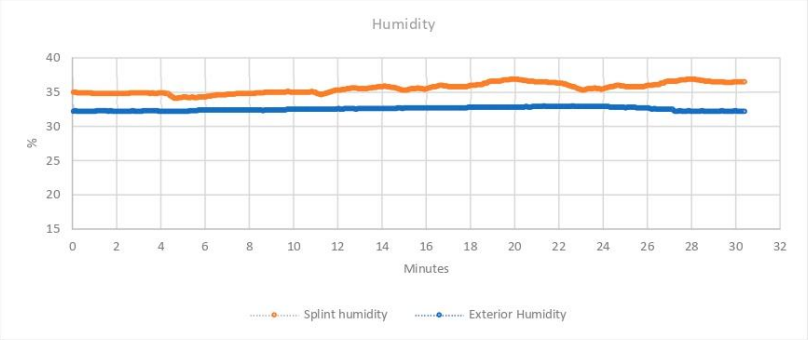

Figure 12. H Collected data of the humidity sensor.

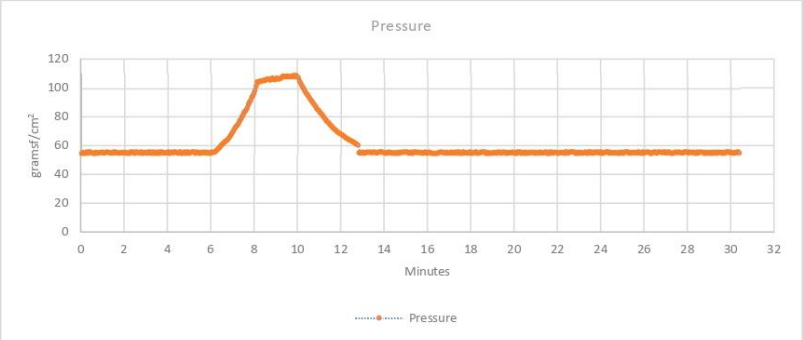

Figure 13. Collected data of the pressure sensor 3.2.4 Presence.

The main idea of the presence sensor is to detect, whereas the splint is fixed correctly. Moreover, it is a sensor that detects the light reflection, so it was pretended to be used to detect color change of the skin. However, it was not possible to use the sensor for this propose in this study. The colors were not correctly detected with enough sensibility to detect a redness of the skin due to inflammation or other problems. In fact, it should be remembered that in this study, the patient, on whom the splint has been tested, is not affected by any pathology that can cause redness or, at least, the change of skin color. Figure 14 shows the percentage of the light reflected over the skin. As it is possible to see in the graph, it is perfectly detected, whereas the splint is not fixed correctly between the min 24 and 29. In fact, in this temporal space simulated in not perfect assembly and adhesion of the splint to the patient's arm.

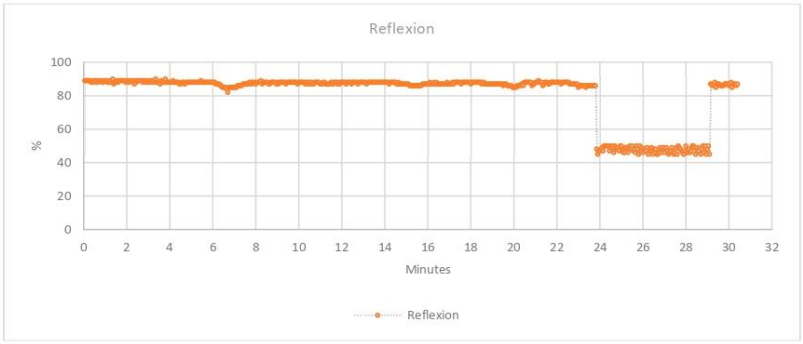

Figure 14. Collected data of the light reflection sensor over the skin.

4. Discussions

For nearly half a century, research has been conducted on humans [38] and animals [39,40], showing the correlation between temperature patterns and medical conditions. The temperature variation of an area of the body is produced by cell metabolism and local blood flow. The increments in temperature are normally the result of an increase of these factors, although it is true that blood flow plays the most important role. Moreover, with some disease processes or during the different bone formation stages and fractures repair, it may occur a reduction in blood flow to the affected areas [41]. This will also produce some alterations in surface temperature.

In the case of using a conventional arm splint, the weight of the material may produce pain in the neck. In addition, the lack of ventilation and the difficulty of bathing could produce allergies and itching due to the poor hygiene of the skin and the device. Another negative point of traditional cast implants is the difficulty of handling it in some daily activities by patients [7].

This study proposes the implementation of a series of sensors to detect possible problems during the whole time of the treatment. The duration of the treatment does not interfere with the data collection and interpretation. In fact, the collection may be carried out periodically, depending on the specialized doctor necessities and on the injury evolution. For this reason, the data collection is carried out as a sign that the system works.

As it is possible to see in the charts obtained from the sensors, it is perfectly possible to detect temperature variations, pressure increment, and humidity inside the splint. Besides, if more temperature sensors are situated in the splint, it would allow to create a digital mapping of the different areas under the splint. This information to quantify temperature changes in skin surface indicates both hot and cold responses which may co-exist if the pain associated with an inflammatory focus excites an increase in sympathetic activity [27]. Continuous monitoring of these parameters allows to know the progression of area at any time of the treatment. This allows early detection of possible vascular, muscular, or joint complications that are difficult to observe without the removal of the immobilization splint or through severe symptoms caused by often irreparable damage.

The temperature registered by the sensor in contact with the skin, is slightly lower than the normal temperature. This is due to the temperature gradient that occurs on the sensor surface. The sensor surface in contact with the skin is about a 40%. The rest of the surface is covered by the splint but not in contact with the skin. This fact produces a difference of temperature between different points of the sensor. The metallic surface tends to get an equilibrium due to thermal conductivity [38]. The sensor gets a final temperature that is not the real skin temperature. However, this fact does not interfere with the main purpose of this sensor, which is to detect incremental temperature changes.

Temperature, humidity, and pressure are correctly detected by the sensors. In addition, the presence sensor detects perfectly, whereas the splint is correctly fixed. However, the presence sensor cannot be

used for its second propose, detecting color changes by the variations of the reflection due to the skin color. This sensor has not enough sensibility to detect light variations. Moreover, it does not include an RGB sensor to detect different wavelengths, making it really difficult to use the sensor for this purpose. Therefore, the use of such a sensor for the proposed purpose is not estimated.

5. Conclusions

The main objective of this work was the study, design, and manufacture of a smart and immobilization splint to monitor different parameters about the real evolution of an injury. This makes it possible to have real-time data to diagnose any kind of problem that is not possible to detect with traditional splints. The current state of the technology allows the realization of particular and individualized immobilization splints by using advanced manufacturing, based on fused deposition modeling, 3D digitalization, and reverse engineering. Moreover, the knowledge of these parameters, might reduce the curing time as some treatments can be applied in this kind of splint but not in traditional splints.

In this study it is shown an interesting and really possible evolution of the traditional splints, to provide them with the term "intelligent". The great possibilities that it offers by this kind of splint is fully demonstrated. However, there are some improvements that are proposed to be carried out in future studies:

- Implementation of a sensor to detect color changes of the skin: This would make it possible to detect bruising and redness, which would allow to get more data for the diagnostic.
- Sending these data to a Bluetooth device that allows remote medical monitoring of the treatment applied and the application of an alarm system in the event of complications, as well as the generation of the data dump in a database for study.
- Integration into functional splints based on rehabilitation techniques in the immobilization phase. This would make it necessary to incorporate a battery to get a full autonomous system.

To finish this study, the main objective is considered to have been achieved, by the incorporation of these sensors and demonstrated that it is possible to detect complications in the treatment of injuries using immobilization splints.

Author Contributions: Conceptualization, J.M.D.A.D.B. and F.B.H.; Formal analysis, F.B.H., R.D. and J.A.J.M.; Investigation, J.M.D.A.D.B. and F.B.H.; Methodology, J.M.D.A.D.B., F.B.H., R.D. and J.A.J.M.; Project administration, J.A.J.M.; Resources, F.B.H. and R.D.; Software, F.B.H. and R.D.; Supervision, F.B.H., R.D. and J.A.J.M.; Validation, R.D.; Writing–original draft, J.M.D.A.D.B.; Writing–review & editing, F.B.H., R.D. and J.A.J.M. All authors have read and agreed to the published version of the manuscript.

Funding: This research received no external funding.

Conflicts of Interest: The authors declare no conflict of interest.

References

1. Jammalamadaka, U.; Tappa, K. Recent advances in biomaterials for 3D printing and tissue engineering. *J. Funct. Biomater.* **2018**, *9*, 22. [CrossRef]
2. Tappa, K.; Jammalamadaka, U. Novel biomaterials used in medical 3D printing techniques. *J. Funct. Biomater.* **2018**, *9*, 17. [CrossRef]
3. Bandyopadhyay, A.; Bose, S.; Das, S. 3D printing of biomaterials. *MRS Bull.* **2015**. [CrossRef]
4. Chia, H.N.; Wu, B.M. Recent advances in 3D printing of biomaterials. *J. Biol. Eng.* **2015**, *9*, 1–14. [CrossRef]
5. Guvendiren, M.; Molde, J.; Soares, R.M.D.; Kohn, J. Designing Biomaterials for 3D Printing. *ACS Biomater. Sci. Eng.* **2016**, *2*, 1679–1693. [CrossRef] [PubMed]
6. Valášek, P.; D'Amato, R.; Müller, M.; Ruggiero, A. Musa textilis Cellulose Fibres in Biocomposites—An Investigation of Mechanical Properties and Microstructure. *BioResources* **2018**, *13*, 3177–3194. [CrossRef]

7. Blaya, F.; Pedro, P.S.; Silva, J.L.; D'Amato, R.; Heras, E.S.; Juanes, J.A. Design of an Orthopedic Product by Using Additive Manufacturing Technology: The Arm Splint. *J. Med. Syst.* **2018**, *42*. [CrossRef] [PubMed]
8. Affatato, S.; Ruggiero, A.; De Mattia, J.S.; Taddei, P. Does metal transfer affect the tribological behaviour of femoral heads? Roughness and phase transformation analyses on retrieved zirconia and Biolox®Delta composites. *Compos. Part B Eng.* **2016**, *92*, 290–298. [CrossRef]
9. Lozano, M.T.U.; D'Amato, R.; Ruggiero, A.; Manzoor, S.; Haro, F.B.; Méndez, J.A.J. A study evaluating the level of satisfaction of the students of health sciences about the use of 3D printed bone models. In Proceedings of the Sixth International Conference on Technological Ecosystems for Enhancing Multiculturality-TEEM'18, Salamanca, Spain, 24–26 October 2018.
10. Ugidos Lozano, M.T.; Blaya Haro, F.; Ruggiero, A.; Manzoor, S.; Nuere Menendez-Pidal, S.; Juanes Méndez, J.A. Different Digitalization Techniques for 3D Printing of Anatomical Pieces. *J. Med. Syst.* **2018**, *42*, 46. [CrossRef] [PubMed]
11. Ghai, S.; Sharma, Y.; Jain, N.; Satpathy, M.; Pillai, A.K. Use of 3-D printing technologies in craniomaxillofacial surgery: A review. *Oral Maxillofac. Surg.* **2018**, *22*, 249–259. [CrossRef] [PubMed]
12. García, N.M.; Blaya, F.; Urquijo, E.L.; Heras, E.S.; D'Amato, R. Oral appliance for Obstructive Sleep Apnea: Prototyping and Optimization of the Mandibular Protrusion Device. *J. Med. Syst.* **2019**, *43*, 107. [CrossRef] [PubMed]
13. Montesdeoca, N.; Lechosa, E.; Haro, F.B.; D'Amato, R.; Juanes, J.A. Design of thermoplastic oral appliance with mouth opening control to treat obstructive sleep apnea. In *Proceedings of the ACM International Conference Proceeding Series*; Association for Computing Machinery: New York, NY, USA, 2019; pp. 404–410.
14. Mulford, J.S.; Babazadeh, S.; Mackay, N. Three-dimensional printing in orthopaedic surgery: Review of current and future applications. *ANZ J. Surg.* **2016**, *86*, 648–653. [CrossRef] [PubMed]
15. Lunsford, C.; Grindle, G.; Salatin, B.; Dicianno, B.E. Innovations With 3-Dimensional Printing in Physical Medicine and Rehabilitation: A Review of the Literature. *PM R* **2016**, *8*, 1201–1212. [CrossRef] [PubMed]
16. Fitzpatrick, A.P. Design of a Patient Specific, 3D printed Arm Cast. *KnE Eng.* **2017**, *2*, 135. [CrossRef]
17. Cernohorsky, J.; Cadek, M. Smart rehabilitation splint. In *Advances in Mechanism Design II*; Springer: Cham, Switzerland, 2017.
18. Evill, J.; Evill, O. Cortex Evill. Available online: https://www.evilldesign.com/cortex (accessed on 8 April 2020).
19. Robin, O.; Claude, A.; Gehin, C.; Massot, B.; McAdams, E. Recording of bruxism events in sleeping humans at home with a smart instrumented splint. *J. Craniomandib. Sleep Pract.* **2020**. [CrossRef]
20. Goncu-Berk, G.; Topcuoglu, N. A Healthcare Wearable for Chronic Pain Management. Design of a Smart Glove for Rheumatoid Arthritis. *Des. J.* **2017**, *20*, S1978–S1988. [CrossRef]
21. Chiu, Y.H.; Chen, T.W.; Chen, Y.J.; Su, C.I.; Hwang, K.S.; Ho, W.H. Fuzzy logic-based mobile computing system for hand rehabilitation after neurological injury. *Technol. Health Care* **2018**, *26*, 17–27. [CrossRef]
22. Dimitrov, D.V. Medical internet of things and big data in healthcare. *Healthc. Inf. Res.* **2016**, *22*, 156–163. [CrossRef]
23. Yin, Y.; Zeng, Y.; Chen, X.; Fan, Y. The internet of things in healthcare: An overview. *J. Ind. Inf. Integr.* **2016**, *1*, 3–13. [CrossRef]
24. Zanella, A.; Bui, N.; Castellani, A.; Vangelista, L.; Zorzi, M. Internet of things for smart cities. *IEEE Internet Things J.* **2014**, *1*, 22–32. [CrossRef]
25. Fan, Y.J.; Yin, Y.H.; Xu, L.D.; Zeng, Y.; Wu, F. IoT-based smart rehabilitation system. *IEEE Trans. Ind. Inform.* **2014**, *10*, 1568–1577. [CrossRef]
26. Blaya, F.; Pedro, P.S.; Pedro, A.B.S.; Lopez-Silva, J.; Juanes, J.A.; D'Amato, R. Design of a Functional Splint for Rehabilitation of Achilles Tendon Injury Using Advanced Manufacturing (AM) Techniques. Implementation Study. *J. Med. Syst.* **2019**, *43*, 122. [CrossRef] [PubMed]
27. Ju, X.; Nebel, J.-C.; Siebert, J.P. 3D thermography imaging standardization technique for inflammation diagnosis. In *Proceedings of the Infrared Components and Their Applications*; Gong, H., Cai, Y., Chatard, J.-P., Eds.; SPIE: Bellingham, WA, USA, 2005.
28. Schlereth, T.; Drummond, P.D.; Birklein, F. Inflammation in CRPS: Role of the sympathetic supply. *Auton. Neurosci. Basic Clin.* **2014**, *182*, 102–107. [CrossRef] [PubMed]
29. Dallas Semiconductor. *Programmable Resolution 1-Wire®Digital Thermometer*; Dallas Semiconductor: Dallas, TX, USA, 2002.

30. Liu, T. *Digital-Output Relative Humidity & Temperature Sensor/Module DHT22 (DHT22 Also Named as AM2302)*; Aosong Electronics Co.: Guangzhou, China, 2015.
31. Datasheet Film Pressure Sensor DF9-40@10kg V2.0. Available online: https://www.winsen-sensor.com/d/files/df9-40%4010kg.pdf (accessed on 2 May 2020).
32. Reflective Optical Sensor with Transistor Output. Available online: https://www.tme.eu/Document/5c845fc67f29d9b4e8f31810ed773b0f/cny70.pdf (accessed on 2 May 2020).
33. Arduino Arduino Uno Rev3|Arduino Official Store. Available online: https://store.arduino.cc/arduino-uno-rev3 (accessed on 19 April 2020).
34. Haro, F.B.; de Agustín del Burgo, J.M.; D'Amato, R.; Islán, M.; Heras, E.S.; Alonso, J.M.G.; Mendez, J.A.J. Monitoring an Analysis of Perturbations in Fusion Deposition Modelling (FDM) Processes for the Use of Biomaterials. *J. Med. Syst.* **2019**, *43*, 109. [CrossRef]
35. Haro, F.B.; de Agustín del Burgo, J.M.; D'Amato, R.; Marcos, M.I.; Heras, E.; Alonso, J.M.G. Monitoring of the additive manufacturing process for the use of biomaterials in medical field. In Proceedings of the Sixth International Conference on Technological Ecosystems for Enhancing Multiculturality-TEEM'18, Salamanca, Spain, 24–26 October 2018; ACM Press: New York, NY, USA, 2018; pp. 428–432.
36. Soriano Heras, E.; Blaya Haro, F.; de Agustín del Burgo, J.M.; Islán Marcos, M.; D'Amato, R. Filament advance detection sensor for fused deposition modelling 3D printers. *Sensors* **2018**, *18*, 1495. [CrossRef]
37. Del Burgo, J.M.D.A.; D'Amato, R.; Méndez, J.A.J.; Ramírez, A.S.; Haro, F.B.; Heras, E.S. Real time analysis of the filament for FDM 3D printers. In *ACM International Conference Proceeding Series*; ACM Press: New York, NY, USA, 2019.
38. Lawson, R. Implications of surface temperatures in the diagnosis of breast cancer. *Can. Med. Assoc. J.* **1956**, *75*, 309–311. [PubMed]
39. Ströberg, B. The Use of Thermography in Equine Orthopedics. *Vet. Radiol.* **1974**, *15*, 94–97. [CrossRef]
40. Wang, L.; Guo, T.Z.; Wei, T.; Li, W.W.; Shi, X.; Clark, J.D.; Kingery, W.S. Bisphosphonates Inhibit Pain, Bone Loss, and Inflammation in a Rat Tibia Fracture Model of Complex Regional Pain Syndrome. *Anesthesia Analg.* **2016**, *123*, 1033–1045. [CrossRef]
41. Rundle, C.H.; Wang, H.; Yu, H.; Chadwick, R.B.; Davis, E.I.; Wergedal, J.E.; Lau, K.H.W.; Mohan, S.; Ryaby, J.T.; Baylink, D.J. Microarray analysis of gene expression during the inflammation and endochondral bone formation stages of rat femur fracture repair. *Bone* **2006**, *38*, 521–529. [CrossRef]

ANEXO VI:

DEVELOPMENT OF A SMART LEG SPLINT BY USING NEW SENSORS TECHNOLOGIES AND NEW THERAPY POSSIBILITIES

Hoy en día, tras sufrir una fractura en un miembro superior o inferior siendo necesario inmovilizarlo, se coloca un yeso en el miembro afectado. Es un dispositivo muy antiguo y eficaz para recuperarse de una lesión. Se sabe que esta técnica fue utilizada por los persas en el siglo X y todavía se usa en el siglo XXI.

Desde el origen, este tipo de férulas no han tenido cambios significativos. Este proyecto tiene como objetivo desarrollar un nuevo concepto de férula impresa en 3D inteligente mediante el uso de nuevas técnicas de detección. Se utilizarán dos tecnologías de fabricación avanzada (AM) en rápida evolución: escaneo 3D e impresión 3D, combinando así la ingeniería, la medicina y la evolución de los materiales. La férula se obtendrá para un área en particular y se diseñará específicamente para cada tipo de lesión con el apoyo de herramientas CAD. Además de esto, se incluirán nuevos sensores pequeños y livianos para detectar cualquier problema durante el proceso de tratamiento. Existen estudios previos que ya han incorporado este tipo de sensores con fines médicos. Sin embargo, en este estudio se implementa con otro concepto novedoso: la posibilidad de aplicar tratamientos durante el proceso de inmovilización y la retroalimentación que se obtiene de los sensores para modificar el tratamiento en tiempo real. Debido a esto, durante el tratamiento se pueden aplicar tratamientos como infrarrojos, ultrasonidos, electroshock, etc., y los sensores podrán detectar cómo estas terapias pueden afectar el proceso de rehabilitación. Los datos se enviarán a un dispositivo móvil para que puedan ser consultados de forma remota por un especialista. Además, sería posible incluir estos datos en el movimiento de Internet de las cosas. De esta forma, todos los datos recopilados podrían compararse y estudiarse para encontrar el mejor tratamiento para cada tipo de lesión.

Gracias a la impresión 3D, su fabricación será más rápida y sencilla, mediante el uso de un material biocompatible y degradable, sumergible y apto para el contacto con la piel. El uso de materiales biocompatibles hace necesario controlar las condiciones en las que se produce la férula, para asegurar que se mantengan las propiedades. Será posible diseñar un nuevo producto muy estético que ayudará a tener un tratamiento más rápido y sencillo.

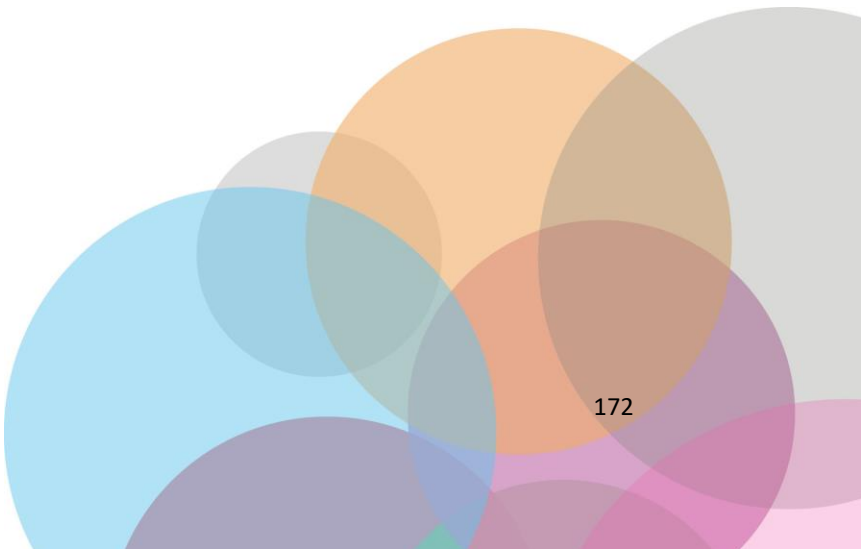

sensors

MDPI

Article

Development of a Smart Leg Splint by Using New Sensor Technologies and New Therapy Possibilities

José María De Agustín Del Burgo [1], Fernando Blaya Haro [2], Roberto D'Amato [2,*], Alonso Blaya [3] and Juan Antonio Juanes Méndez [1]

[1] Campus Miguel de Unamuno, Universidad de Salamanca, 37007 Salamanca, Spain; id00792219@usal.es (J.M.D.A.D.B.); jajm@usal.es (J.A.J.M.)
[2] ETSIDI-Departamento de Ingeniería Mecánica, Química y Diseño Industrial, Universidad Politécnica de Madrid (UPM), Ronda de Valencia 3, 28012 Madrid, Spain; fernando.blaya@upm.es
[3] Departamento de Fisioterapía de la, Universidad Europea de Madrid, 28670 Madrid, Spain; alonso.blaya.sp@gmail.com
* Correspondence: r.damato@upm.es; Tel.: +34-91-067-7654

Abstract: Nowadays, after suffering a fracture in an upper or lower limb, a plaster cast is placed on the affected limb. It is a very old and efficient technique for recovery from an injury that has not had significant changes since its origin. This project aims to develop a new low-cost smart 3D printed splint concept by using new sensing techniques. Two rapidly evolving Advanced Manufacturing (AM) technologies will be used: 3D scanning and 3D printing, thus combining engineering, medicine and materials evolution. The splint will include new small and lightweight sensors to detect any problem during the treatment process. Previous studies have already incorporated this kind of sensor for medical purposes. However, in this study it is implemented with a new concept: the possibility of applying treatments during the immobilization process and obtaining information from the sensors to modify the treatment. Due to this, rehabilitation treatments like infrared, ultrasounds or electroshock may be applied during the treatment, and the sensors (as it is showed in the study) will be able to detect changes during the rehabilitation process. Data of the pressure, temperature, humidity and colour of the skin will be collected in real time and sent to a mobile device so that they can be consulted remotely by a specialist. Moreover, it would be possible to include these data into the Internet of Things movement. This way, all the collected data might be compared and studied in order to find the best treatment for each kind of injury. It will be necessary to use a biocompatible material, submersible and suitable for contact with skin. These materials make it necessary to control the conditions in which the splint is produced, to assure that the properties are maintained. This development, makes it possible to design a new methodology that will help to provide faster and easier treatment.

Keywords: smart splint; rehabilitation therapy; IoT; AM technique; customized medicine; health monitoring

Citation: De Agustín Del Burgo, J.M.; Blaya Haro, F.; D'Amato, R.; Blaya, A.; Juanes Méndez, J.A. Development of a Smart Leg Splint by Using New Sensor Technologies and New Therapy Possibilities. *Sensors* **2021**, *21*, 5252. https://doi.org/10.3390/s21155252

Academic Editor: Gregory P. Nordin

Received: 13 June 2021
Accepted: 31 July 2021
Published: 3 August 2021

1. Introduction

Currently, 3D technology with biocompatible materials is being used for many applications [1] such as in dental reconstruction, by using the Selective laser fusion technique (SLM) [2]; or the manufacture of orthopedic prostheses [3,4] by using Fusion Deposition Modelling (FDM). In both cases, the process consists of scanning the patient's teeth or limb and after the corresponding processing, it is possible to manufacture a custom piece [5]. Moreover, in recent years, many studies have shown that 3D printing techniques make it possible to engineer anatomical parts of the human body such as tissues and organs [6–8].

The advantages offered by 3D technology applied to health science are of fundamental importance for the patient's recovery, especially for people with injuries whose only therapy is the immobilization of a part of the body. Furthermore, the digitalization and

3D prototyping of medical artifacts for immobilization, allows during the design phase, to create a solid product with non-continuous surfaces, while maintaining rigidity and resistance [5]. It also ensures a level of hygiene that cannot be attained with conventional immobilization techniques, thanks to the use of bio-plastic materials compatible with humid environments [9,10].

In addition, there is another great advantage of using new splints instead of tradition-al ones. These new splints allow the design of dedicated therapeutic windows (material-free areas) to apply treatments that must be applied directly to the skin, and therefore, cannot be applied otherwise. A simple window will allow cures for the case of wounds, dermatological pathologies or surgeries. The generation of windows on the splint, also allows for periodic visual medical inspection during the immobilization phase and rapid decisions on the evolution of the lesions.

This project focuses on the development and prototyping of an immobilization smart splint for a leg using a 3D scanner, processed from the obtained file, and its subsequent printing with biocompatible material. Taking advantage of new manufacturing techniques and novel technologies in sensors and electronics, it is proposed to bring the reinterpretation of this technique from the 10th century to our present time, by using new sensing and electronic technologies [11,12], and the use of the Internet of Things [13,14], applied in medical applications. It will be possible to develop intelligent splints designed according to the lesion and morphology of the patient.

The splint will be designed exclusively for each individual, and it may be possible to have splints prepared prior to injury, especially in high-level athletes. This would make it possible to modify the rehabilitation treatments with the data acquired by the sensors during the process [15]. In this study, the steps to manufacture a smart splint with AM technology starting from the digitalization of the leg to immobilization will be presented.

The sensing technologies will be presented for data acquisition in the IoT-based healthcare system. Based on the previous study [16] the parameters that will be monitored are temperature, humidity, pressure and skin colour. The combination of these, can indicate different problems that the patients may be suffering [17,18], such as inflammation. In order to obtain the prototype of the splint, the windows for the accommodation of the rehabilitation therapies and the type of treatment will be considered. In fact, the application of treatments in the immobilization phase has a substantial influence on the evolution of the injury and on mobility rehabilitation of the limb. Moreover, the splint will allow visual access through windows and direct contact with the skin.

There are different considered treatments for the case under study. Lymph drainage uses Combined Decongestive Physiotherapy (CDP) for lymphedema which is recognized and reimbursed by insurance companies [19]. The basis of lymph drainage is to create different pathways through which lymph can flow. Electrodes may be used for this purpose [20,21]. Iontophoresis is one of the most used during rehabilitation treatment for delivery of anti-inflammatory and painkiller medication in the parts of the human body affected by inflammatory processes of the musculoskeletal system [22–24]. This way, some medications are able to pass through the skin and produce their effect, circumventing the digestive tract and without the need to have them administered by injection [25–27]. The Therapeutic Ultrasound technique is used in rehabilitation therapies for its mechanical, analgesic and circulatory effects and it should be applied in an aqueous medium (gel or immersion), something impossible with traditional splints [28]. It also improves the elasticity of the tissues [29]. It reduces the symptoms of inflammation and promotes tissue regeneration [30,31]. Normally the bones and the tendon connection area have low absorption capacity, so the frequency will depend on the injury [32,33]. Laser therapy accelerates energy metabolism and tissue synthesis as reported by several studies, [34–36]. Low-level laser stimulates the cells and modulates inflammatory processes [37–39], produces an increment of collagen production in the tendons structure [30,40–42] and reduces the levels of inflammation [43,44]. Electrostimulation for neuromuscular-skeletal mild to moderate pain is based on transcutaneous electrical nerve stimulation (TENS) and

percutaneous electrical nerve stimulation (PENS) [45]. There are also different studies about the effects of electrostimulation on muscular strength and functional capacity in patients with osteoarthritis of the knee [46].

These techniques are only some examples considered in this study, that may for instance be applied to injuries or lesions in arms [47], knees [48], elbows [49] or Achilles tendons [50]. However, by using 3D splints, it could also be possible to apply other therapies, considered by a specialist [51].

As part of the process, objectives that will be considered are:

- Development of the protocol for scanning, meshing, designing and producing the splint.
- Development of mobile application for sensor monitoring.
- Implementation of an algorithm to detect inflammation through changes in pressure, temperature or colour of the affected area.
- Study on the measurement of humidity on the internal face of the splint, according to the discussion of convenience that will be done later in the article.

The full process will include obtaining the 3D scanning model using a 3Dscanner first, as well as the verification of the data obtained. After this, the file provided by the scanner will be modified using CAD Software to obtain a final model. This model will incorporate the sensors windows to apply the different treatments. Finally, the model will be produced and the software and electronics will be integrated.

2. Materials and Methods

The steps to model, design, manufacture and assemble the 3D smart and functional leg splint are presented and detailed below. The leg of a 29-year-old healthy volunteer was used as a model. The same proposed methodology could be applied to other parts of the body [10]. In fact, it is analogous to others lesions that may require immobilization of the upper limb articulations, such as the wrist [16].

Furthermore, the different rehabilitation treatments and sensors are detailed, to be implemented on the design of the splint.

2.1. Sensing Technologies

For this study, the parameters that will be monitored are temperature, humidity, pressure and skin color. The information recorded by these sensors is combined to determine if there is any kind of unexpected evolution of the treatment. In total, the implemented sensors are: two temperature sensors DS18B20 [52] in contact with the skin, one temperature and humidity sensor between the skin and the splint (DHT22) [53], two pressure sensors DF9-40 [54] placed in two different axes of the splint (X, Y), and one color sensor TCS34725 [55]. The shocks and vibrations that may be produced by the human body are not critical to the performance and durability of these sensors. Moreover, when an injury of these characteristics is being treated, it is due to the requirement of immobilization. Therefore, the shock and vibrations are controlled. In addition, some of these sensors have been tested in a previous study, where it is detailed that accuracy of the selected sensors is enough for the purpose [16]. Details of these sensors are shown in Table 1.

The electronic design and configuration of the temperature, humidity and pressure sensors are explained in a previous study [16]. However, the color sensor has been incorporated for the first time in this study.

During the healing process, a bruise will usually go through different colors. It often starts red because fresh, oxygen-rich blood has newly pooled underneath the skin. After around 1–2 days, the blood begins to lose oxygen and change color. A bruise that is a few days old will often appear blue, purple or even black. In about 5–10 days, it turns a yellow or green color. These colors come from compounds called biliverdin and bilirubin that the body produces when it breaks down hemoglobin. After 10–14 days, it will turn to a shade of yellowish-brown or light brown [56,57].

Table 1. Technical specifications of the sensors.

Sensor Serial Number	DS18B20	DHT22	DF9-40	TCS34725
Dimensions (mm)	6 × 6 × 50	15 × 7.7 × 20	40 × 20 × 0.25	25 × 20 × 1.5
Power voltage (V)	3.0–5.5	3.3–6	5	5
Working range	−55 °C to 125 °C	−40 °C to 80 °C 0 to 100% RH	0–500 g	-
Resolution	±0.0625 °C	0.1 °C, 0.1% RH	14.5 g	-

The TCS3472 sensor provides a digital return value of three components of the light (red, green and blue), and it also clears the light detection values. It includes an IR blocking filter, which minimizes the IR spectral component of the light, allowing for accurate color measurements over the skin, where there is not external light. Figure 1 shows graphs of the specific response from this sensor to the light. As Figure 1a shows, the sensor is able to detect different wavelengths by using a spectral photodiode. In this way, it comprises the amount of light of each wavelength that bounces off a surface. Figure 1b illustrates that the highest responsivity of the sensor is in the perpendicular direction of the photodiode surface. This must be considered when the housing of the sensor is designed. This sensor is an ideal solution for varying lighting conditions and materials, due to its sensitivity, the wide dynamic range and the IR blocking filter. The data are transferred via an I2C bus, using the SDA and SCL contacts.

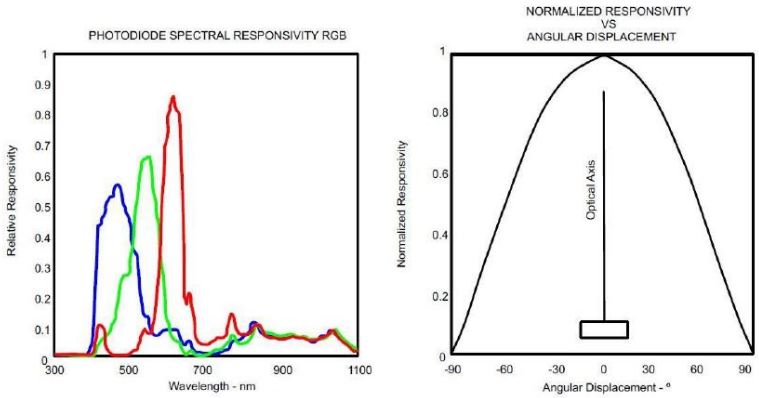

Figure 1. TCS3472 sensor responsivity graphs (**a**,**b**) [55].

Previous studies show the suitability of different RGB channels and their differences for detection of hematomas or ecchymosis [58,59]. The color sensor detects changing colors of the skin, during the initial inflammation stage, due to ecchymosis [60], which occurs around approximately the first six days [61,62]. The main purpose of using an RGB sensor, is to detect the variation in red, green and blue components of the light. The device incorporates an emitter of white light that bounces off the skin and goes back to the receiver. The sensor reads the variation of the three components, in comparison to the original white light. This way it is possible to know what component is absorbed, and therefore, the color of the skin. It is not necessary to modify the gain value or other parameters, as the sensor is already configured. Moreover, as the initial stage of the lesion that must be monitored has a duration of one week, the durability is not a critical parameter. The sensor reads the values in terms of RGB (red, green and blue) between 0 and 255.

2.2. Considered Therapies during the Design Process

According to the previous study [10], the treatment programming is shown in black color in Figure 2. Traditional splints do not allow the application of physiotherapy techniques until the device is removed. However, by using new smart splints, it is possible to apply the treatments as soon as the injury occurs. It is possible to see the new timing possibilities in blue color in Figure 2.

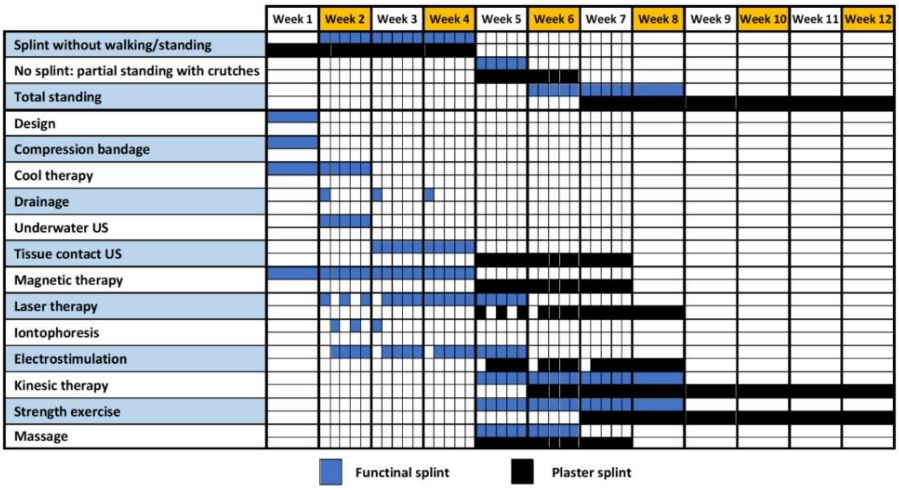

Figure 2. Chronogram of rehabilitation with new techniques applied [10].

This reduction involves at least 30% of the treatment period. Moreover, the application of physiotherapy techniques during the immobilization phase contributes to the prevention of joint, muscular and vascular complications, derived from the application of retention devices in the initial phase of the treatment.

2.3. 3D Model and Design

The first step for the design of the leg splint is the full scan of the injured limb in order to achieve the shape that perfectly suits the patient. In this case, the 3D Systems Sense® scanner is used to perform different sweeps of the leg. The leg to be immobilized must be kept suspended during this process so that a detailed scan of the bottom surface can also be made. The digitalization of this part is a fast step, but it is vital to getting a correct model later, so it is critical to the rest of the process. Table 2 shows the technical specifications of the scanner.

Table 2. Technical specifications of Sense™ 3D scanner.

Maximum Scan Volume	2 × 2 × 2 [m]
Minimum Scan Volume	0.2 × 0.2 × 0.2 [m]
Working Distance	0.2–1.6 [m]
Number of Cameras n	2
Class Certified Laser Product	1
Resolution at 0.5 m	1 [mm]

After this process, a points cloud is obtained and sent to the 3D CAD Geomagic Freeform Software (3D Systems, Inc., Rock Hill, SC, USA). This program, designed to manipulate no-geometric models, eliminates outlier data points from the points cloud [63,64].

These points are normally created during the scanning process due to disturbances from the light. After this, the software transforms the points cloud into a mesh surface. This surface will be the basis for the creation of the solid that will constitute the final splint (Figure 3a). Once the mesh is created, it is possible to manipulate it, creating offsets or cuts. It is necessary to create an offset of 0.5mm from the obtained surface. This way there will be slight free space between the limb and the splint. It is also at this point when the area of the limb that will be covered with the splint is decided (Figure 3b,c). Finally, a new mesh is generated with an offset of 3.7mm, which will be the thickness of the splint. That thickness will allow the different sensors to be fixed and a splint ruggedized enough to be built, based on previous studies about splints produced by fused deposition modeling and PLA mechanical properties [16,65].

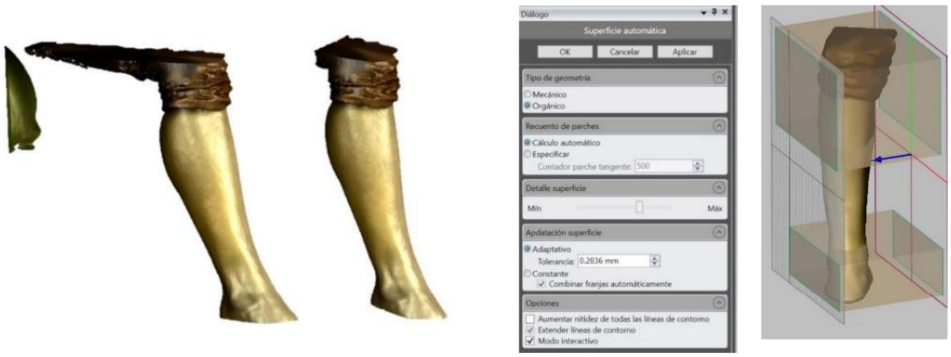

(**a**) (**b**) (**c**)

Figure 3. (**a**) Original and treated points cloud in Geomagic Software; (**b**) Mesh surface creation parameters; (**c**) Mesh manipulation.

It is possible to see the generated mesh of the splint and the splint over the original model in Figure 4. However, at this point, it is just a mesh. To be able to easily design the modifications for the treatments and sensors, it is necessary to create a solid body from this mesh surface. This way, it will be possible to import the digital model to a parametric CAD program to manipulate it correctly. This goal is not trivial, as the methodology of parametric modeling and non-parametric modelling programs (organic modelling programs) are complete opposites. Parametric modeling is an approach to 3D CAD in which you capture design intent using features and constraints, which allows users to automate repetitive changes, such as those found in families of product parts. These capabilities, are a great fit for design tasks that involve precise requirements and manufacturing criteria. For example, this is normally used when making families of products that include slight variations of a core design. This supports designs that will need to be modified or iterated on a regular basis and creates models with individual features, such as holes and chamfers, that can be modified or changed. First, the mesh is reduced to be able to manipulate it easily. It is important to reduce the number of triangles, but also to keep the original dimensions and forms. Then, the mesh is sent to 3D CAD Geomagic Design X™ Software (3D Systems, Inc., Rock Hill, SC, USA). With this program it is possible to complete the mesh and to reduce the number of surfaces. Figure 5 shows a total of 67,376 triangles, and after applying the tool, these triangles are reduced to 10,820. This 84% reduction of the mesh maintains the original design with a much smaller file size.

(**a**) (**b**)

Figure 4. Mesh of the splint (**a**) and mesh over the original 3D model (**b**).

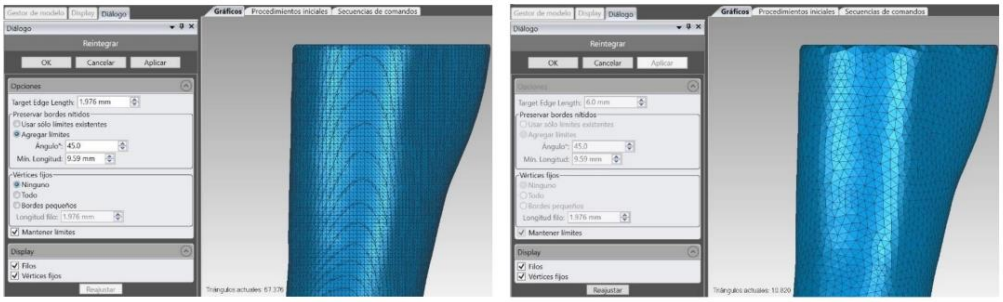

(**a**) (**b**)

Figure 5. Original mesh (**a**) and reduced mesh (**b**).

There are different steps to be followed using CATIA™ 3DEXPERIENCE® 3D Software (Dassault Systèmes®, France). The reduced mesh is imported by using the Assembly Design module. After that, the mesh is converted to an old extension "model" file using the DMU Optimizer module with the tool of applying a 0 offset to the mesh (Figure 6). The generated file is opened and the tree of the design must be copied and pasted to a new part in the Generative Shape Design module. Using this module, it is possible to use the "Joint" tool to create a unique and complex mesh. Finally, this mesh is opened using the Part Design module and the tool "Close Surface" is applied to create the solid body of the splint. After this procedure, the original mesh is converted to a solid body.

Thanks to this process, now it is possible to open the file with a parametric modeling software. In this case, Inventor Professional 2020 (Autodesk, Inc, Mill Valley, CA, USA) will be used. If the thickness is correct, this indicates the process has not modified the dimensions in comparison to the original offset that was set (Figure 7), so the process is valid and has not modified the original morphology and dimensions.

Once the model is included in this parametric design software, the procedure to modify the splint accordingly to the necessities begins.

The splint is divided in two parts so that the patient can correctly fix the real model later, joining these parts with a mechanical closure. In this case, twelve magnets of 3mm diameter and 3 mm high are set in each part. However, other fixing systems could be used. Figure 8 shows this process.

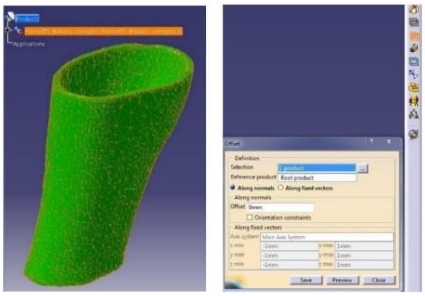

(**a**) (**b**)

Figure 6. Catia Software. Reduced mesh (**a**) and offset tool (**b**).

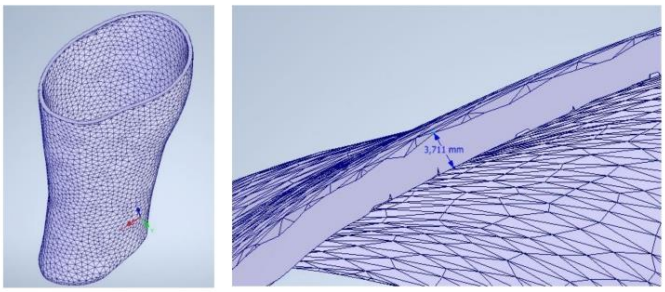

(**a**) (**b**)

Figure 7. Splint imported from Inventor Autodesk Software (**a**) and dimensional check (**b**).

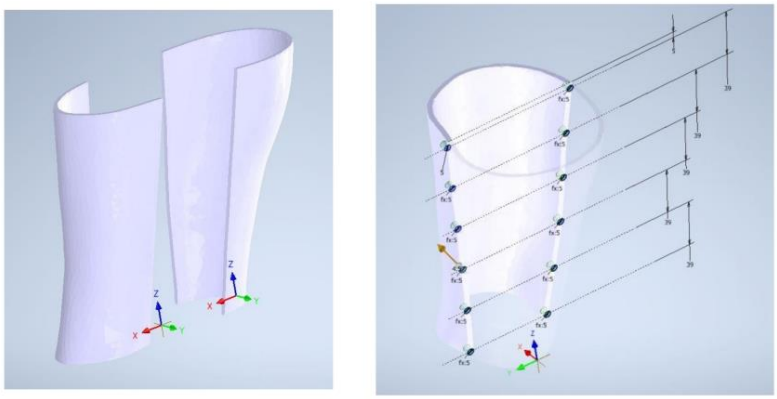

(**a**) (**b**)

Figure 8. Division of the splint (**a**) and magnet housing design (**b**).

At this point, it is necessary to introduce in the splint the different housings for the sensors as well as the windows for the different treatments proposed in Section 2.2.

Figure 9 shows the areas where the rehabilitation therapy treatments will be applied, according to the morphology of the limb to be immobilized and previous studies [25,30].

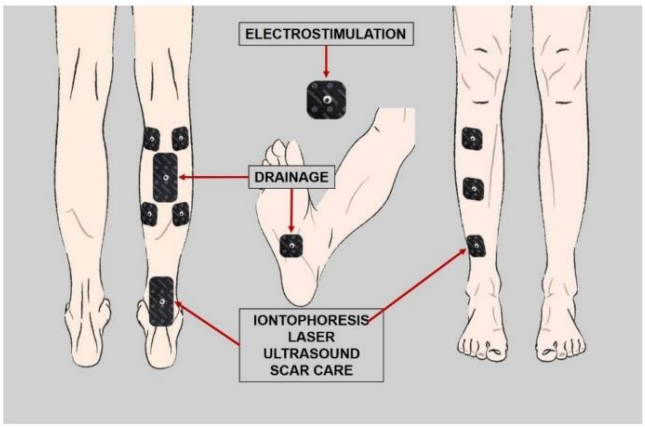

Figure 9. Therapeutic windows to be made in the splint.

Considering these factors, different windows are designed. For electrostimulation, 30 × 30 mm windows are made, whereas for drainage, iontophoresis, laser and ultrasound, the windows have a size of 30 × 40 mm. Furthermore, different housings for the sensors and wiring are considered. Figure 10a–c show both the back and front part after the designing process. Finally, the designed model is opened over the original mesh of the leg, obtained at the beginning of this process, to confirm it fits perfectly (Figure 10d).

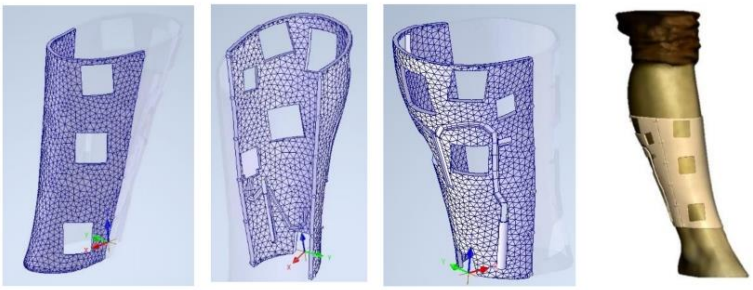

Figure 10. View of the splint: front part (**a**), inside (**b**) outside (**c**) from the back part of the splint. (**d**) designed splint over the scanned model.

2.4. Additive Manufacturing

After the 3D scanning and design process, a *.stl* file is obtained that can be processed by a slicer software that prepares the model to be produced by using AM processing (Figure 11). In this case, a FDM 3D printer "TotalPrinter" machine was used. This printer was designed, developed, and manufactured in the Aditive Manufacturing and Rapid Prototype Laboratory of the Escuela Tecnica Superior de Ingenieria y Diseño Industrial at Technical University of Madrid (Spain). This printer allows controlled and continuous

monitoring of printing parameters such as the thickness of the extruded thermoplastic filament [66], the humidity and temperature of the printing chamber and the temperature of the extruder [67] in order to optimize the printing process and to obtain a homogeneous model in terms of adhesion between the printed layers and mechanical characteristics [68].

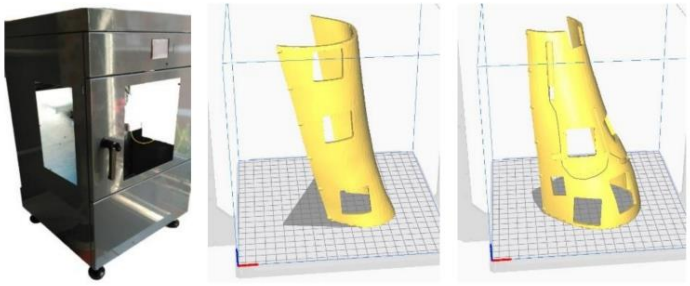

(a) (b) (c)

Figure 11. Total-Printer machine (**a**) and the two parts of the splint ready for printing (**b**,**c**).

For producing the splint, PLA filament (see Table 3 for mechanical properties) with a diameter of 1.75 mm was chosen. The material and process should be followed carefully in order to avoid biocompatibility issues [69–71]. The vertical position for printing was chosen as shown in Figure 11, taking into account the volume chamber of this machine (200 mm × 200 mm × 400 mm). In Table 4, it is possible to see the printing parameters set in the manufacturing process, following the material manufacturer's recommendations to obtain a quality and structure rigid enough.

Table 3. Mechanical properties [65].

Properties	Units	PLA
ϱ (Polymer density)	g/cm^3	1.21–1.25
σ (tensile strength)	MPa	21.0–60.0
E (tensile modulus)	GPa	0.35–3.50
ε (ultimate strain)	%	2.50–6.00
σ_s (specific tensile strength)	Nm/g	16.8–48.0
E_s (specific tensile modulus)	kNm/g	0.28–2.80
Tg (glass transition temperature)	°C	45–60
Tm (melting temperature)	°C	150–162

Table 4. Different parameters used for the manufacturing of the leg splint.

Layer height [mm]	0.2
Extruder [mm]	0.4
Density [%]	40
Thickness perimeter each layer [mm]	1
Print speed [mm/s]	60
Temperature [°C]	220

2.5. Sensing Technologies

In order to correctly detect the data from the sensors, it is necessary to develop an electronic board for connecting everything easily. It is important to focus on a durable design, with low weight and dimensions. By focusing on these main purposes, a board that will be installed directly to the TTGO OLED Display and Battery Board is designed, shown in Point 2.2 of this study. This board has two analog-to-digital converters (ADC1 and ADC2). The resolution of these converters is 12 bits. A 12 bits ADC means that is able

to read 2^{12} values between 0 and 5 V. This is 4096 values, so it detects changes of 1.22mv, which is enough for what is required by the selected sensors. ADC1 is used for the sensors, whilst ADC2 is used for the communication between the microprocessor and the Wi-Fi module, which is used to create the web server [72].

It is necessary to install different contacts and resistors to properly connect to each sensor. It is possible to see the design and assembly in Figure 12a,b. The final electronic assembly is showed in Figure 12c.

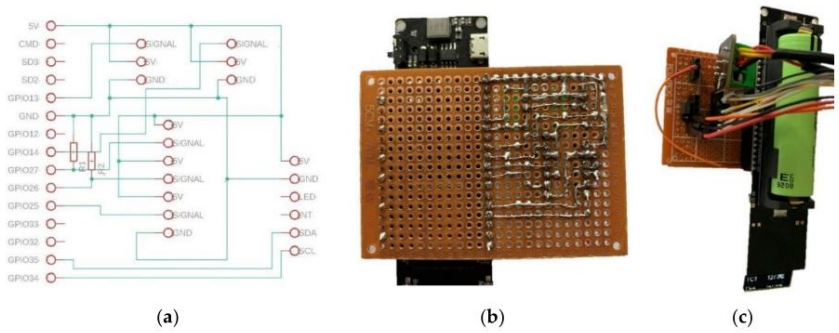

(**a**) (**b**) (**c**)

Figure 12. Schematic design of the electronic board for the sensors (**a**), soldering process (**b**) and electronic assembly (**c**).

The chosen board, as explained before, can be accessed from other devices through different ways and protocols. It has an OLED display that may show the acquired data (pressures, temperatures, humidity and color change detection). Furthermore, it is possible to create a Bluetooth connection with a mobile phone or similar device. However, in this case, the option of creating a web server is selected. This way, the information may be consulted from any device connected to the internet, anywhere in the world. The great benefit of this, is that a doctor can see the data and follow the treatment in real time from their place of work.

The total real consumption of the electronic board and sensing system is 84.66 mA. Due to the battery has a capacity of 12,210 mAh, the autonomy of the system is around 144 h. This means that the system is able to collect data during six days without charging the battery, what is very significant because the first week after occurring the lesion is the most important period to be analyzed [56,57]. After that, it is possible to replace or charge the battery.

3. Results

This section presents the different results obtained after the 3D printing process of the designed model. In addition, the electronic devices are assembled and the sensors are placed in their housings and connected to the electronic board. Finally, the configuration of the ESP32 microprocessor is presented as well as the acquisition of data and results.

Figure 13a shows the splint prototype obtained with the wiring and sensors fully assembled. In Figure 13b it is possible to see the interior of the splint with the housing for the sensors.

To test the fully assembled leg splint on a real leg, the splint was fixed to a healthy volunteer for 1.5 h (Figure 14). The volunteer was placed in seated position for the tests. However, this new "smart splint" is capable of obtaining data in a continuous way, so the patient does not need to adopt particular positions during the data acquisition. The main purpose of this test, was to collect data so that it could be analyzed if the sensors were able to acquire information correctly. The data collected by the sensors were treated with ESP32

micro and sent to a computer every 3 s by using the serial monitor of the Arduino platform. In the following sections the acquired data will be explained.

(**a**) (**b**)

Figure 13. Real splint assembled with the sensors (**a**) and interior view (**b**).

Figure 14. Real model over the leg.

3.1. Temperatures and Humidity

Two temperature sensors in contact with the skin were placed in two different zones. Moreover, a third sensor not in direct contact with the skin, read the temperature and humidity. The mean temperature of the first two sensors is shown in the color orange, whereas the internal temperature is shown in the color blue (Figure 15). The graph shows that the registered temperature by the sensor is slightly lower than 36 °C. This occurs because the exterior area of the sensor surface is not in real contact with the skin, and this produces a gradient of temperature between the environment and the body. However, what the authors are looking for in this study, is to detect an increment or decrement of the temperature of the located area of the skin, compared with the historical. It is perfectly possible to detect an increase or decrease of the registered temperature, in comparison with the historical data.

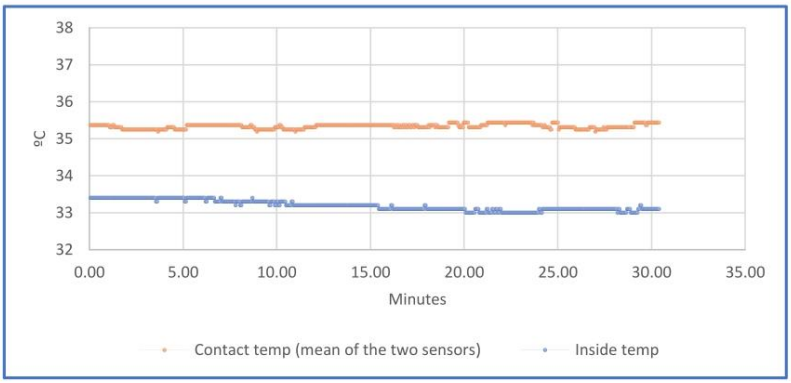

Figure 15. Temperature's graph.

Monitoring the humidity inside the splint and its fluctuations allows us to know if the injured area is in a healthy environment and unsuitable for the proliferation of bacteria, especially in cases of surgery or injury. Furthermore, some physiological events that can occur following a trauma have been shown to include changes in skin color due to edema, changes in temperature and an increase in sweating in the area affected by the lesion [73]. In fact, a change in the sudomotor function of the injured part implies central disturbances of thermoregulation [17,74]. Figure 16 shows the percentage of humidity that was registered during the test inside the splint (in orange color) and outside the splint (in blue color).

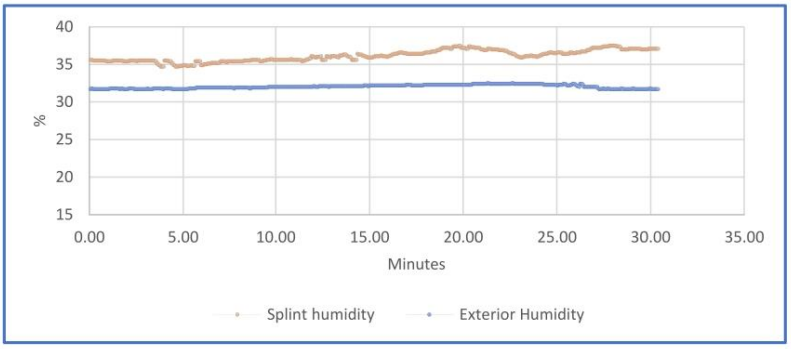

Figure 16. Humidity graph.

3.2. Pressure

Two sensors for reading pressure are placed. One is placed on the "X" axis and the second on the "Y" axis (Figure 17). The sensors have been placed on these positions for the tests, and the data are collected with the leg in vertical position and weightlessly. However, the potential of these kinds of 3D techniques makes it possible for other medical requirements to also be considered and included during the design process, according to specialist dictated requirements.

Figure 17. Pressure sensors on the "X" and "Y" axis.

The surface of the pressure sensor during the limb immobilization phase is 1 cm^2, according to 1 N = 1 Kg/s^2 the pressure values read by the sensor will have the dimensions of gf/cm^2. Figure 18 shows the detected mean pressure. As illustrated, during the normal state, the value of the pressure is constant and is equal to 60 gf/cm^2. However, when a slight pressure is produced due to an inflammatory process, the sensors are able to perfectly detect an increment of this pressure. In order to simulate what occurs in an inflammatory process, a force over the splint was applied between minutes 7 and 10. This variation was detected by the sensors, reading a pressure that rose from 60 gf/cm^2 to 100 gf/cm^2. Therefore, when the pressure was increased due to the inflammation of the area, the sensors perfectly detected the increment of the mass inside the splint [16]. The graph shows the actual and historical pressure. Real-time monitoring and the collection of historical data on the pressure variation of the injured area during the immobilization period allows the specialist to control inflammatory phenomena.

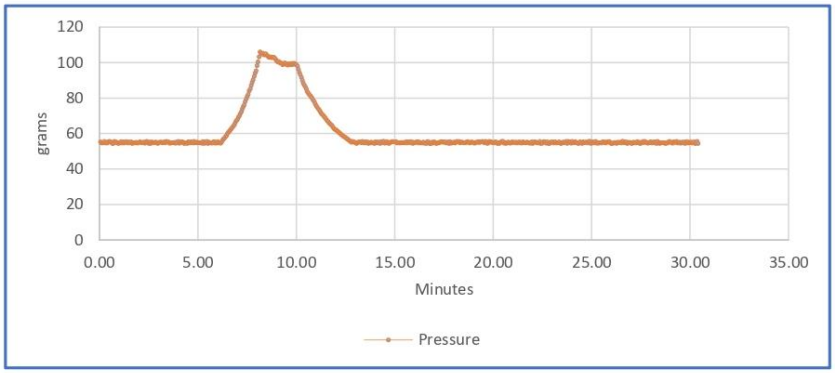

Figure 18. Pressure graph.

3.3. Colour

The test was done on the skin of a volunteer that had a hematoma, and was compared to another part of his body, that had no signs of hematoma. The sampling of the test was carried out with a frequency of 10 s. It is possible to see in Figure 19 that the sensor is capable of detecting a color change in the skin. In Figure 19a, the skin has a normal color with no signs of hematoma, whilst in Figure 19b the sensor detects an increment in the RGB

values due to the signs of hematoma. Due to this, it will be possible to check the evolution of the color during the very initial stages of the treatment, but also during posterior stages. It is possible to see that the three values are incremented, but it is specifically the 38% increment of the red value that makes it possible to detect the hematoma.

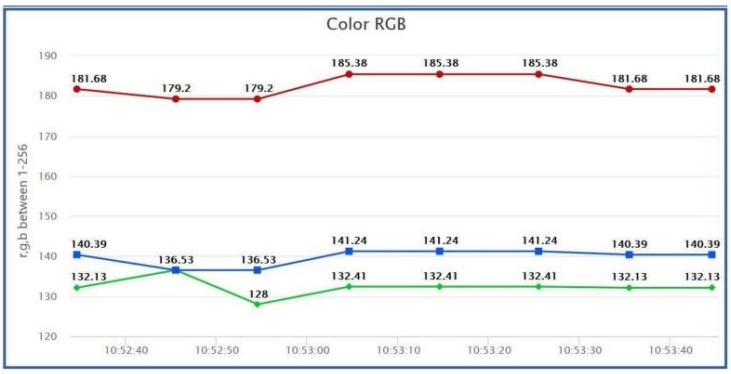

(**a**)

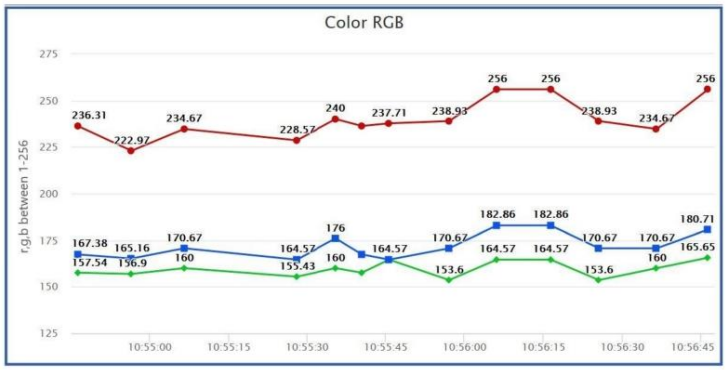

(**b**)

Figure 19. Color RGB sensor lectures without hematoma (**a**) and with hematoma (**b**).

3.4. Diagnostic

The knowledge of these data makes it possible to identify temperature, humidity, pressure or skin color changes. Combining them, makes it possible to identify signs of inflammation and detect possible problems during the treatment.

To accomplish this, an algorithm that can be configured to consider temperature and pressure changes during a period of time was programmed, to consider these data to be produced by an inflammation process but not by a position of the limb over a specific object. The considered parameters are showed in Table 5. However, these parameters are showed as an example of the possibilities of the system, with no real medical considerations in this case. The timing would be the necessary to distinguish a value due to inflammation from a collision or resting state position. Moreover, to avoid a wrong measure of the pressure sensors, it may be considered to add a third sensor in opposite position. An inflammation process will produce an increment volume inside the splint, and an increment of the

pressure in all the sensors, in a simultaneous and cotemporary way. About the range, it is proposed a 5%–10% change of the value due to the acquired data during the tests.

Table 5. Algorithm configuration to detect inflammation.

Temperature increment	1.5 °C
Pressure increment	60 gf/cm^2
Time during temperature increment	60 m
Time during pressure increment	60 m

Moreover, the combination of this information with color and humidity that can also be consulted remotely by a specialist will result in a complete diagnosis.

4. Discussions

This study shows the combination of traditional immobilization techniques with new 3D modelling and prototyping techniques. This new system allows us to follow the evolution of the injured part in a very detailed way. Moreover, it is possible to apply treatments that improve not only the timing but also the quality of the rehabilitation. As previously explained, in this study electrostimulation, drainage, iontophoresis, laser and ultrasound have been considered as treatments. However, the potential of these kinds of 3D techniques makes it possible for other medical therapies to also be considered and included during the design process, according specialist dictated requirements.

These treatment possibilities are combined with the acquired data to even improve the treatment. Adding sensors to these splints, makes it possible to analyze in real time how the therapy is functioning and new steps to get the most progress.

Furthermore, the vast capacities that remote monitoring allows would simplify the revisions that must be carried out by a specialist. This allows doctors to follow the progress of more patients, by using objective data. These data may be collected into a database, in order to compare different evolutions of different treatments in similar injuries.

For this study, the use of ruggedized sensors was not considered, as the main purpose of the study is to show the new possibilities of using sensors in splints, and the benefits of using new technologies in this kind of treatment. The performance and resolution of the implemented sensors, were correct for the tests, as it is possible to see in the different figures. Humidity sensor DHT22 has an error due to hysteresis of +-0.3%. The sensor is looking for an increment of the internal humidity in comparison with the external humidity. The value will be around 3%–5% higher when a sweating process is produced. Due to this, the error is not significant and will not interfere in the correct detection of a sweating process. In this case, it is completely functional.

From a medical point of view, there is no necessity to know the absolute value, or trying to get an optimal value, as this will depend on the patient and lesion. This is why the main focus of the study is to analyze the new capabilities by detecting the variations on the acquired data.

The design of the different windows includes round edges to avoid any kind of chafing or similar. In no case the design of these windows may cause injury to the affected limb or by edge effect since the additive manufacturing design allows smoothing all the edges in contact with the patient, nor by suction effect on the skin [75] as the splint is not indicated for support in load nor produce its own vacuum because it is an open design. Furthermore, it is mandatory to use biocompatible materials [76,77] to avoid any kind of irritation, eschar or ulcer.

The design of the splint is made according to the affected anatomic area of each patient. The design includes an offset to suit perfectly over the area. The design and the position of the windows must be supervised by a medical specialist, according to the lesion. These windows allow a visual control of the treatment, what is especially critical in the initial stages. However, the windows do not intervene in the treatment. In cases where the use of splints indicated for support and gait of the lower limb is required, the corresponding

structural study would be carried out, and accessible windows should be generated only at the time of use through the design of a closure. Moreover, this kind of module would allow us to take off the splint to clean the skin if needed, something not possible with traditional splints.

5. Conclusions

The main objective of this study is to show an evolution of traditional inmobilization methods. It is not possible to apply any kind of rehabilitation before removing the splint using a traditional inmobilization splint. Moreover, it is not possible to know what is happening under the splint.

This study shows the possibilities of using individualized immobilization splints by Advanced Manufacturing techniques scanning and prototyping. It is possible to fabricate a splint that fits perfectly on each limb. Moreover, it creates some areas for applying different treatments that produces at least a 30% decrease in the treatment period compared to plaster splints.

On the other hand, it is possible to incorporate some sensors for real time acquisition of data from inside the splint. This will allow health practitioners/doctors to anticipate treatment for different issues that may appear.

The electronic device that gets the data from the different sensors is able to combine and analyze the information received from the data. After that, it may send alerts when detecting inflammatory processes, skin color changes, or high humidity values. These alerts are shown on a display or a mobile device or may also be consulted remotely.

For future studies, the creation of a database where different smart splints send the acquired data is proposed as an improvement. This way, by using the new Big Data concept and Data Science, the device would be able to learn from the different symptoms to avoid problems before they happen and also to design specific treatments for each lesion and patient.

Author Contributions: Conceptualization, F.B.H.; J.M.D.A.D.B.; J.A.J.M. and F.B.H.; software J.M.D.A.D.B.; validation, R.D., J.A.J.M. and F.B.H.; formal analysis, A.B.; investigation, J.M.D.A.D.B., A.B. and R.D.; data curation, software J.M.D.A.D.B. and R.D.; writing—original draft preparation, J.M.D.A.D.B.; writing—review and editing, R.D. All authors have read and agreed to the published version of the manuscript.

Funding: This research received no external funding.

Institutional Review Board Statement: For this study, both for the scanning process and test of the model, have been carried out using the arm of the author José María de Agustín, who is completely informed about the use of this data for the article. Therefore, no Ethics Committee has been cited as there are no other patients involved.

Informed Consent Statement: Informed consent was obtained from the co-author involved in the study. This article does not contain any studies with human participants performed by any of the authors. This article does not contain any studies with animals performed by any of the authors.

Conflicts of Interest: The authors declare no conflict of interest.

References

1. Miravete, A.L.C.-T. De Disseny, and Undefined 2002, "Materiales Compuestos," Raco.Cat. Available online: https://www.raco.cat/index.php/Temes/article/view/29774 (accessed on 27 April 2020).
2. Gebhardt, A.; Schmidt, F.-M.; Hötter, J.-S.; Sokalla, W.; Sokalla, P. Additive Manufacturing by selective laser melting the realizer desktop machine and its application for the dental industry. *Phys. Procedia* **2010**, *5*, 543–549. [CrossRef]
3. Scholz, M.; Blanchfield, J.; Bloom, L.; Coburn, B.; Elkington, M.; Fuller, J.; Gilbert, M.; Muflahi, S.; Pernice, M.F.; Rae, S.; et al. The use of composite materials in modern orthopaedic medicine and prosthetic devices: A review. *Compos. Sci. Technol.* **2011**, *71*, 1791–1803. [CrossRef]
4. Saringer, W.; Nöbauer-Huhmann, I.; Knosp, E. Cranioplasty with Individual Carbon Fibre Reinforced Polymere (CFRP) Medical Grade Implants Based on CAD/CAM Technique. *Acta Neurochir.* **2002**, *144*, 1193–1203. [CrossRef]

5. Blaya, F.; Pedro, P.S.; Silva, J.L.; D'Amato, R.; Heras, E.S.; A Juanes, J. Design of an Orthopedic Product by Using Additive Manufacturing Technology: The Arm Splint. *J. Med. Syst.* **2018**, *42*, 54. [CrossRef] [PubMed]
6. Melchels, F.; Domingos, M.; Klein, T.; Malda, J.; Bartolo, P.; Hutmacher, D.W. Additive manufacturing of tissues and organs. *Prog. Polym. Sci.* **2012**, *37*, 1079–1104. [CrossRef]
7. Chia, H.N.; Wu, B.M. Recent advances in 3D printing of biomaterials. *J. Biol. Eng.* **2015**, *9*, 1–14. [CrossRef]
8. Jose, R.R.; Rodriguez, M.J.; Dixon, T.A.; Omenetto, F.; Kaplan, D.L. Evolution of Bioinks and Additive Manufacturing Technologies for 3D Bioprinting. *ACS Biomater. Sci. Eng.* **2016**, *2*, 1662–1678. [CrossRef] [PubMed]
9. Ambu, R.; Motta, A.; Calì, M. Design of a Customized Neck Orthosis for FDM Manufacturing with a New Sustainable Biocomposite. In Proceedings of the International Conference on Design, Simulation, Manufacturing: The Innovation Exchange, Modena, Italy, 9–10 September 2019; Springer: Berlin/Heidelberg, Germany, 2019; pp. 707–718.
10. Blaya, F.; Pedro, P.S.; Pedro, A.B.S.; Lopez-Silva, J.; A Juanes, J.; D'Amato, R. Design of a Functional Splint for Rehabilitation of Achilles Tendon Injury Using Advanced Manufacturing (AM) Techniques. Implementation Study. *J. Med. Syst.* **2019**, *43*, 122. [CrossRef]
11. McAuliffe, P.; Kim, J.H.; Diamond, D.; Lau, K.T.; O'Connell, B.C. A sleep bruxism detection system based on sensors in a splint—Pilot clinical data. *J. Oral Rehabil.* **2014**, *42*, 34–39. [CrossRef]
12. Gao, J.; Liu, L.; Gao, P.; Zheng, Y.; Hou, W.; Wang, J. Intelligent Occlusion Stabilization Splint with Stress-Sensor System for Bruxism Diagnosis and Treatment. *Sensors* **2019**, *20*, 89. [CrossRef]
13. Yin, Y.; Zeng, Y.; Chen, X.; Fan, Y. The internet of things in healthcare: An overview. *J. Ind. Inf. Integr.* **2016**, *1*, 3–13. [CrossRef]
14. Dimitrov, D.V. Medical Internet of Things and Big Data in Healthcare. *Healthc. Inform. Res.* **2016**, *22*, 156–163. [CrossRef]
15. Fan, Y.J.; Yin, Y.H.; Da Xu, L.; Zeng, Y.; Wu, F. IoT-Based Smart Rehabilitation System. *IEEE Trans. Ind. Inform.* **2014**, *10*, 1568–1577. [CrossRef]
16. De Agustín Del Burgo, J.M.; Blaya Haro, F.; D'Amato, R.; Juanes Méndez, J.A. Development of a Smart Splint to Monitor Different Parameters during the Treatment Process. *Sensors* **2020**, *20*, 4207. [CrossRef]
17. Ju, X.; Nebel, J.-C.; Siebert, J.P. 3D thermography imaging standardization technique for inflammation diagnosis. In *Infrared Components and Their Applications*; SPIE: Washington, DC, USA, 2005; Volume 5640, pp. 266–273.
18. Schlereth, T.; Drummond, P.D.; Birklein, F. Inflammation in CRPS: Role of the sympathetic supply. *Auton. Neurosci.* **2014**, *182*, 102–107. [CrossRef] [PubMed]
19. International Society of Lymphology. The diagnosis and treatment of peripheral lymphedema: 2016 consensus document of the International Society of Lymphology. *Lymphology* **2016**, *49*, 170–184.
20. Chikly, B.; Quaghebeur, J.; Wytryol, W. A Controlled Comparison between Manual Lymphatic Mapping (MLM) of Plantar Lymph Flow and Standard Physiologic Maps Using Lymph Drainage Therapy (LDT)/Osteopathic Lymphatic Technique (OLT). *Qual. Prim. Care* **2015**, *23*, 46–50. [CrossRef]
21. Wei, Y.; Yang, K.; Browne, M.; Bostan, L.; Worsley, P. Wearable Electrical Stimulation to Improve Lymphatic Function. *IEEE Sens. Lett.* **2019**, *3*, 1–4. [CrossRef]
22. Hamann, H.; Hodges, M.; Evans, B. Effectiveness of iontophoresis of anti-inflammatory medications in the treatment of common musculoskeletal inflammatory conditions: A systematic review. *Phys. Ther. Rev.* **2006**, *11*, 190–194. [CrossRef]
23. Costello, C.T.; Jeske, A.H. Iontophoresis: Applications in Transdermal Medication Delivery. *Phys. Ther.* **1995**, *75*, 554–563. [CrossRef] [PubMed]
24. Rigby, J.H.; Mortensen, B.B.; Draper, D.O. Wireless Versus Wired Iontophoresis for Treating Patellar Tendinopathy: A Randomized Clinical Trial. *J. Athl. Train.* **2015**, *50*, 1165–1173. [CrossRef]
25. Hao, J. Topical iontophoresis for local therapeutic effects. *J. Drug Deliv. Sci. Technol.* **2014**, *24*, 255–258. [CrossRef]
26. Taskaynatan, M.A.; Özgül, A.; Ozdemir, A.; Tan, A.K.; Kalyon, T.A. Effects of Steroid Iontophoresis and Electrotherapy on Bicipital Tendonitis. *J. Musculoskelet. Pain* **2007**, *15*, 47–54. [CrossRef]
27. Neeter, C.; Thomee, R.; Silbernagel, K.G.; Thomee, P.; Karlsson, J. Iontophoresis with or without dexamethazone in the treatment of acute Achilles tendon pain. *Scand. J. Med. Sci. Sports* **2003**, *13*, 376–382. [CrossRef] [PubMed]
28. Baker, K.G.; Robertson, V.J.; Duck, F.A. A Review of Therapeutic Ultrasound: Biophysical Effects. *Phys. Ther.* **2001**, *81*, 1351–1358. [CrossRef] [PubMed]
29. Robertson, V.J.; Baker, K.G. A Review of Therapeutic Ultrasound: Effectiveness Studies. *Phys. Ther.* **2001**, *81*, 1339–1350. [CrossRef] [PubMed]
30. Bjordal, J.M.; Iversen, V.; Lopes-Martins, R.A.B. Low level laser therapy reduces inflammation in activated Achilles tendinitis. In *Mechanisms for Low-Light Therapy*; SPIE: Washington, DC, USA, 2006; Volume 6140.
31. Ebenbichler, G.R.; Erdogmus, C.B.; Resch, K.L.; Funovics, M.A.; Kainberger, F.; Barisani, G.; Aringer, M.; Nicolakis, P.; Wiesinger, G.F.; Baghestanian, M.; et al. Ultrasound Therapy for Calcific Tendinitis of the Shoulder. *N. Engl. J. Med.* **1999**, *340*, 1533–1538. [CrossRef]
32. Rigby, J.H.; Taggart, R.M.; Stratton, K.L.; Lewis, G.K.; Draper, D.O. Intramuscular Heating Characteristics of Multihour Low-Intensity Therapeutic Ultrasound. *J. Athl. Train.* **2015**, *50*, 1158–1164. [CrossRef]
33. Mitragotri, S. Healing sound: The use of ultrasound in drug delivery and other therapeutic applications. *Nat. Rev. Drug Discov.* **2005**, *4*, 255–260. [CrossRef]

34. Kneebone, W. The Treatment of Achilles Tendonitis Using Therapeutic Laser. 2010. Available online: http://orthopedics.about.com/cs/ankleproblems/a/ (accessed on 27 April 2020).
35. Tumilty, S.; Munn, J.; McDonough, S.; Hurley, D.A.; Basford, J.R.; Baxter, G.D. Low Level Laser Treatment of Tendinopathy: A Systematic Review with Meta-Analysis. *Photomed. Laser Surg.* **2010**, *28*, 3–16. [CrossRef]
36. Bjordal, J.M.; Lopes-Martins, R.; Álvaro, B.; Joensen, J.; Iversen, V.V. The anti-inflammatory mechanism of low level laser therapy and its relevance for clinical use in physiotherapy. *Phys. Ther. Rev.* **2010**, *15*, 286–293. [CrossRef]
37. Karu, T.I. Mitochondrial Signaling in Mammalian Cells Activated by Red and Near-IR Radiation. *Photochem. Photobiol.* **2008**, *84*, 1091–1099. [CrossRef]
38. Moriyama, Y.; Nguyen, J.; Akens, M.; Moriyama, E.H.; Lilge, L. In vivo effects of low level laser therapy on inducible nitric oxide synthase. *Lasers Surg. Med.* **2009**, *41*, 227–231. [CrossRef]
39. Gao, X.; Xing, D. Molecular mechanisms of cell proliferation induced by low power laser irradiation. *J. Biomed. Sci.* **2009**, *16*, 4. [CrossRef] [PubMed]
40. Reddy, G.K.; Stehno-Bittel, L.; Enwemeka, C.S. Laser photostimulation of collagen production in healing rabbit achilles tendons. *Lasers Surg. Med.* **1998**, *22*, 281–287. [CrossRef]
41. Ng, G.Y.; Fung, D.T. The Combined Treatment Effects of Therapeutic Laser and Exercise on Tendon Repair. *Photomed. Laser Surg.* **2008**, *26*, 137–141. [CrossRef] [PubMed]
42. Msc, L.I.F.; Mauriz, J.L.; Vedovelli, K.; Msc, A.J.M.; Zettler, C.G.; Lech, O.; Marroni, N.P.; González-Gallego, J. Low-level laser therapy (LLLT) prevents oxidative stress and reduces fibrosis in rat traumatized Achilles tendon. *Lasers Surg. Med.* **2005**, *37*, 293–300. [CrossRef]
43. Aimbire, F.; Albertini, R.; Pacheco, M.T.T.; Castro-Faria-Neto, H.; Leonardo, P.; Iversen, V.; Lopes-Martins, R.; Bjordal, J. Low-Level Laser Therapy Induces Dose-Dependent Reduction of TNFα Levels in Acute Inflammation. *Photomed. Laser Surg.* **2006**, *24*, 33–37. [CrossRef] [PubMed]
44. Joensen, J.; Gjerdet, N.R.; Hummelsund, S.; Iversen, V.; Lopes-Martins, R.A.; Bjordal, J.M. An experimental study of low-level laser therapy in rat Achilles tendon injury. *Lasers Med. Sci.* **2012**, *27*, 103–111. [CrossRef]
45. Heidland, A.; Fazeli, G.; Klassen, A.; Sebekova, K.; Hennemann, H.; Bahner, U.; Di Iorio, B. Neuromuscular electrostimulation techniques: Historical aspects and current possibilities in treatment of pain and muscle waisting. *Clin. Nephrol.* **2012**, *79*. [CrossRef]
46. Rosemffet, M.G.; Schneeberger, E.E.; Citera, G.; Sgobba, M.E.; Laiz, C.; Schmulevich, H.; Artçanuturry, P.; Gagliardi, S.; Cocco, J.A.M. Effects of Functional Electrostimulation on Pain, Muscular Strength, and Functional Capacity in Patients with Osteoarthritis of the Knee. *JCR J. Clin. Rheumatol.* **2004**, *10*, 246–249. [CrossRef]
47. Johansson, K.; Albertsson, M.; Ingvar, C.; Ekdahl, C. Effects of compression bandaging with or without manual lymph drainage treatment in patients with postoperative arm lymphedema. *Lymphology* **1999**, *32*, 103–110.
48. Aiyejusunle, C.B.; Kola-Korolo, T.A.; Ajiboye, O.A. Comparison of the effects of tens and sodium salicylate iontophoresis in the management of osteoarthritits of the knee. *Niger. Q. J. Hosp. Med.* **2007**, *17*, 30–34. [CrossRef] [PubMed]
49. Stasinopoulos, D.I.; Johnson, M.I. Effectiveness of Low-Level Laser Therapy for Lateral Elbow Tendinopathy. *Photomed. Laser Surg.* **2005**, *23*, 425–430. [CrossRef]
50. Kaplan, K.; Olivencia, O.; Dreger, M.; Hanney, W.J.; Kolber, M.J. Achilles Tendinopathy: An Evidence-Based Overview for the Sports Medicine Professional. *Strength Cond. J.* **2019**, *41*, 24–40. [CrossRef]
51. Moein, H.; Jhalli, R.; Blaber, A.P.; Claydon, V.E.; Menon, C. Evaluating the efficacy of an active compression brace on orthostatic cardiovascular responses. *PLoS ONE* **2017**, *12*, e0187885. [CrossRef]
52. Dallas Semiconductor. Programmable Resolution 1-Wire® Digital Thermometer with 4-Bit ID. 2002. Available online: http://ee-classes.usc.edu/ee459/library/datasheets/DS18B20.pdf (accessed on 19 March 2021).
53. Aosong Electronics Co., Ltd. Digital-Output Relative Humidity & Temperature Sensor/Module DHT22 (DHT22 Also Named as AM2302). 2015. Available online: https://www.sparkfun.com/datasheets/Sensors/Temperature/DHT22.pdf (accessed on 6 June 2021).
54. Film Pressure Sensor DF9-40@10 kg V2.0. Available online: https://www.winsen-sensor.com/d/files/df9-40%4010kg.pdf (accessed on 6 June 2021).
55. TCS3472 Color Light-to-Digital Converter with IR Filter. Available online: https://cdn-shop.adafruit.com/datasheets/TCS34725.pdf (accessed on 30 April 2020).
56. Bruise Colors: Causes, Timescale, and When to See a Doctor. Available online: https://www.medicalnewstoday.com/articles/322742#bruise-colors-over-time-and-their-causes (accessed on 13 July 2021).
57. Tell-Tale Color Changes: Camera Can Find Age of a Bruise | Features | Oct 2012 | BioPhotonics. Available online: https://www.photonics.com/Articles/TellTale_Color_Changes_Camera_Can_Find_Age_of_a/a52130 (accessed on 13 July 2021).
58. Patašius, M.; Marozas, V.; Jegelevičius, D.; Lukoševičius, A.; Data Exploration for Hematoma Image Analysis. February 2016. Available online: http://biomed.ktu.lt/index.php/BME/article/view/2481 (accessed on 13 May 2021).
59. Al Ghozali, H.K.; Setiawardhana; Sigit, R. Vein detection system using infrared camera. In Proceedings of the 2016 International Electronics Symposium (IES), Denpasar, Indonesia, 29–30 September 2016; pp. 122–127. [CrossRef]

60. Automatización de la Datación de Equimosis en el Peritaje Médico Legal Peruano Mediante Redes Neuronales Artificiales y Procesamiento de Imágenes. Available online: http://cybertesis.unmsm.edu.pe/handle/20.500.12672/1071 (accessed on 26 May 2021).
61. Pourlak, T.; Ghavimi, M.A.; Nezafati, S.; Yazdani, J.; Amini, M.; Pourlak, T.; Ghoreishizadeh, A.; Negahdari, R. Comparison of edema and ecchymosis in rhinoplasty candidates after lateral nasal osteotomy using piezosurgery and external osteotomy. *J. Adv. Pharm. Technol. Res.* **2018**, *9*, 73–79. [CrossRef]
62. Gurlek, A.; Fariz, A.; Aydogan, H.; Ersoz-Ozturk, A.; Eren, A.T. Effects of Different Corticosteroids on Edema and Ecchymosis in Open Rhinoplasty. *Aesthet. Plast. Surg.* **2006**, *30*, 150–154. [CrossRef] [PubMed]
63. Nurunnabi, A.; West, G.; Belton, D. Outlier detection and robust normal-curvature estimation in mobile laser scanning 3D point cloud data. *Pattern Recognit.* **2015**, *48*, 1404–1419. [CrossRef]
64. Rakotosaona, M.; La Barbera, V.; Guerrero, P.; Mitra, N.J.; Ovsjanikov, M. PointCleanNet: Learning to Denoise and Remove Outliers from Dense Point Clouds. *Comput. Graph. Forum* **2020**, *39*, 185–203. [CrossRef]
65. Farah, S.; Anderson, D.G.; Langer, R. Physical and mechanical properties of PLA, and their functions in widespread applications—A comprehensive review. *Adv. Drug Deliv. Rev.* **2016**, *107*, 367–392. [CrossRef]
66. Heras, E.S.; Haro, F.B.; De Agustin del Burgo, J.M.; Marcos, M.I.; D'Amato, R. Filament Advance Detection Sensor for Fused Deposition Modelling 3D Printers. *Sensors* **2018**, *18*, 1495. [CrossRef] [PubMed]
67. Haro, F.B.; De Agustin del Burgo, J.M.; D'Amato, R.; Islán, M.; Heras, E.S.; Alonso, J.M.G.; Mendez, J.A.J. Monitoring an Analysis of Perturbations in Fusion Deposition Modelling (FDM) Processes for the Use of Biomaterials. *J. Med. Syst.* **2019**, *43*, 109. [CrossRef] [PubMed]
68. Haro, F.B.; De Agustin del Burgo, J.M.; D'Amato, R.; Marcos, M.I.; Heras, E.S.; Alonso, J.M.G. Monitoring of the additive manufacturing process for the use of biomaterials in medical field. In Proceedings of the Sixth International Conference on Technological Ecosystems for Enhancing Multiculturality, Salamanca, Spain, 24–26 October 2018; Association for Computing Machinery (ACM): New York, NY, USA, 2018; pp. 428–432.
69. De Agustin del Burgo, J.M.; D'Amato, R.; Méndez, J.A.J.; Ramírez, A.S.; Haro, F.B.; Heras, E.S. Real time analysis of the filament for FDM 3D printers. In Proceedings of the Seventh International Conference on Technological Ecosystems for Enhancing Multiculturality, León, Spain, 16–18 October 2019; pp. 354–360.
70. Vladescu, A.; Braic, M.; Azem, F.A.; Titorencu, I.; Braic, V.; Pruna, V.; Kiss, A.; Parau, A.C.; Birlik, I. Effect of the deposition temperature on corrosion resistance and biocompatibility of the hydroxyapatite coatings. *Appl. Surf. Sci.* **2015**, *354*, 373–379. [CrossRef]
71. Salentijn, G.; Oomen, P.E.; Grajewski, M.; Verpoorte, E. Fused Deposition Modeling 3D Printing for (Bio)analytical Device Fabrication: Procedures, Materials, and Applications. *Anal. Chem.* **2017**, *89*, 7053–7061. [CrossRef]
72. ESP32 Series Datasheet Including. 2020. Available online: https://www.espressif.com/en/support/download/documents (accessed on 28 April 2020).
73. Birklein, F.; Künzel, W.; Sieweke, N. Despite clinical similarities there are significant differences between acute limb trauma and complex regional pain syndrome I (CRPS I). *Pain* **2001**, *93*, 165–171. [CrossRef]
74. Jänig, W. *Functions of the Sympathetic Innervation of the Skin*; Loewy, A.D., Spyer, K.M., Eds.; Central Regulation of Autonomic Functions, Oxford University Press: New York, NY, USA, 1990; pp. 334–348.
75. Lowe, D.T. Cupping therapy: An analysis of the effects of suction on skin and the possible influence on human health. *Complement. Ther. Clin. Pract.* **2017**, *29*, 162–168. [CrossRef]
76. Kim, Y.; Son, S.; Chun, C.; Kim, J.-T.; Lee, D.Y.; Choi, H.J.; Kim, T.-H.; Cha, E.-J. Effect of PEG addition on pore morphology and biocompatibility of PLLA scaffolds prepared by freeze drying. *Biomed. Eng. Lett.* **2016**, *6*, 287–295. [CrossRef]
77. Hernández, J.A.J.; Vicente, E.J.G.; Sánchez, F.R.; Sánchez, F.M.; Rodríguez, M.P.C.; Morote, J.P. Prevención de úlceras iatrogénicas por inmovilización terapéutica en niños con férula. Ensayo clínico. *Enferm. Glob.* **2020**, *19*, 135–154. [CrossRef]

CAPÍTULOS EN LIBROS

ANEXO VII:

Technological Adoption and Trends in Health Sciences Teaching, Learning, and Practice

Samuel Marcos-Pablos (University of Salamanca, Spain) and Juan Antonio Juanes-Méndez (University of Salamanca, Spain)

Projected Release Date: February, 2022|Copyright: © 2022 |Pages: 330

DOI: 10.4018/978-1-7998-8871-0

ISBN13: 9781799888710|ISBN10: 1799888711|EISBN13: 9781799888727

ANEXO VII:

SMART SPLINTS DEVELOPMENT: NEW TECHNOLOGIES FOR DIAGNOSIS DURING INITIAL STAGES OF THE TREATMENT APPLIED TO SPLINTS. NEW THERAPIES POSSIBILITIES.

Hoy en día tras sufrir una fractura en un miembro superior o inferior, se coloca un yeso en el miembro afectado. Es una técnica muy antigua y eficaz para la recuperación de una lesión, que no ha tenido cambios significativos desde su origen. Este proyecto tiene como objetivo desarrollar un nuevo concepto de férula impresa en 3D inteligente de bajo costo mediante el uso de nuevas técnicas de detección. Se utilizarán dos tecnologías de fabricación avanzada (am) de rápida evolución: el escaneado 3d y la impresión 3d, esto es posible gracias a la aplicación de la ingeniería en técnicas de fabricación aditiva y al uso de materiales biocompatibles disponibles en el mercado. Este estudio propone el uso de estos materiales y técnicas, incluida la integración de sensores dentro de las férulas. Los principales parámetros considerados a estudiar son la presión, la humedad, el color de la piel y la temperatura. Estos aspectos se combinan y analizan para determinar cualquier tipo de evolución inesperada del tratamiento. El objetivo de este estudio es generar una férula inteligente mediante el uso de biomateriales y técnicas de ingeniería basadas en el sistema avanzado de fabricación y sensores, para fines clínicos. Los resultados muestran que el prototipo de la férula inteligente permite obtener datos cuando se coloca sobre el brazo de un paciente. Será necesario utilizar un material biocompatible, sumergible y apto para el contacto con la piel. Estos materiales hacen necesario controlar las condiciones en las que se produce la férula, para asegurar que se mantengan las propiedades. Este desarrollo, permite diseñar una nueva metodología que ayudará a brindar un tratamiento más rápido y sencillo.

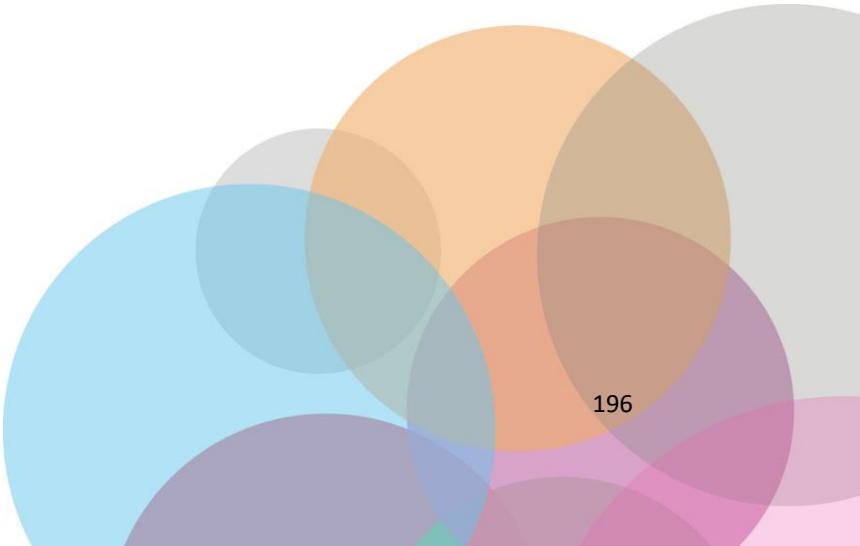

IGI Global
PUBLISHER of TIMELY KNOWLEDGE

www.igi-global.com

Smart Splints Development:

New technologies for diagnosis during initial stages of the treatment applied to Splints. New therapies possibilities.

José María de Agustín del Burgo
Campus Miguel de Unamuno, Universidad de Salamanca, 37007 Salamanca, Spain; id00792219@usal.es;

ABSTRACT

Nowadays after suffering a fracture in an upper or lower limb, a plaster cast is placed on the affected limb. It is a very old and efficient technique for recovery from an injury, that has not had significant changes since its origin. This project aims to develop a new low-cost smart 3d printed splint concept by using new sensing techniques. Two rapidly evolving advanced manufacturing (am) technologies will be used: 3d scanning and 3d printing, this is possible thanks to the application of engineering on additive manufacturing techniques and the use of biocompatible materials available in the market. This study proposes the use of these materials and techniques, including sensor integration inside the splints. The main parameters considered to be studied are pressure, humidity, skin colour and temperature. These aspects are combined and analyzed to determine any kind of unexpected evolution of the treatment. The goal of this study is to generate a smart splint by using biomaterials and engineering techniques based on the advanced manufacturing and sensor system, for clinical purposes. The results show that the prototype of the smart splint allows to get data when it is placed over the arm of a patient. It will be necessary to use a biocompatible material, submersible and suitable for contact with skin. These materials make it necessary to control the conditions in which the splint is produced, to assure that the properties are maintained. This development, makes it possible to design a new methodology that will help to provide faster and easier treatment.

Keywords: Smart Splint; Biomedical Sensor; IOT; Additive Manufacturing; Personalized Medicine; Health Monitoring

INTRODUCTION

Currently, 3D technology with biocompatible materials is being used for many applications (Miravete et al., n.d.) such as in dental reconstruction, by using the Selective laser fusion technique (SLM) (Gebhardt et

al., n.d.; Scholz et al., n.d.); or the manufacture of orthopedic prostheses (Bandyopadhyay et al., 2015; Chia & Wu, 2015b) by using Fu-sion Deposition Modelling (FDM). In both cases, the process consists of scanning the patient's teeth or limb and after the corresponding processing, it is possible to manu-facture a custom piece (Fernando Blaya et al., 2019). Moreover, in recent years, many studies have shown that 3D printing techniques make it possible to engineer anatomical parts of the human body such as tissues and organs (Fernando Blaya et al., 2018; Chia & Wu, 2015a; Melchels et al., 2012). The advantages offered by 3D technology applied to health science are of funda-mental importance for the patient's recovery. Especially for people with injuries whose only therapy is the immobilization of a part of the body. Furthermore, the digitalization and 3D prototyping of medical artifacts for immobilization, allows during the design phase, to create a solid product with non-continuous surfaces, while maintaining ri-gidity and resistance. It also ensures a level of hygiene that cannot be attained with conventional immobilization techniques, thanks to the use of bio-plastic materials compatible with humid environments (Ambu et al., 2020; Ugidos Lozano et al., 2018, 2019).

In addition, there is another great advantage of using new splints instead of tradi-tion-al ones. These new splints allow the design of dedicated therapeutic windows (material-free areas) to apply treatments that must be applied directly to the skin, and therefore, cannot be applied otherwise. A simple window will allow cures for the case of wounds, dermatological pathologies or surgeries. The generation of windows on the splint, also allows for periodic visual medical inspection during the immobilization phase and rapid decisions on the evolution of the lesions.

This project focuses on the development and prototyping of an immobilization smart splint for a leg using a 3D scanner, processed from the obtained file, and its subsequent printing with biocompatible material. Taking advantage of new manufac-turing techniques and novel technologies in sensors and electronics, it is proposed to bring the reinterpretation of this technique from the 10th century to our present time, by using new sensing and electronic technologies (Lozano et al., 2017; Mcauliffe et al., 2015) and the use of the Internet of Things (Dimitrov, 2016; YIN et al., 2016), applied in medical applications. It will be possible to develop intelli-gent splints designed according to the lesion and morphology of the patient.

The splint will be designed exclusively for each individual, and it may be possible to have splints prepared prior to injury, especially in high-level athletes. This would make it possible to modify the rehabilitation treatments with the data acquired by the sensors during the process (Fan et al., 2014). In this study, the steps to manufacture a smart splint with AM technology starting from the digitalization of the leg to immobilization will be presented.

The sensing technologies will be presented for data acquisition in the IoT-based healthcare system. The parameters that will be moni-tored are temperature, humidity, pressure and skin colour. The combination of these, can indicate different problems that the patients may be suffering (Ju et al., 2005; Schlereth et al., 2014), such as in-flammation. In order to obtain the prototype of the splint, the windows for the ac-commodation of the rehabilitation therapies and the type of treatment will be consid-ered. In fact, the application of treatments in the immobilization phase has a substantial influence on the evolution of the injury and on mobility rehabilitation of the limb. Moreover, the splint will allow visual access through windows and direct contact with the skin.

The full process will be to obtain the 3D scanning model using a 3Dscanner first, as well as the verification of the data obtained. After this, the file provided by the scanner will be modified using a CAD Software to obtain a final model. This model will incorporate the sensors holes and windows to apply the different treatments. Finally, the model will be produced and the Software and electronics will be integrated.

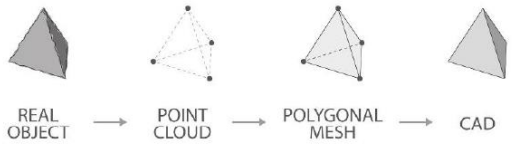

Figure 1. Reverse engineering methodology(Hire Freelance Point Cloud Modeling Services for Your Company | Cad Crowd, n.d.)

As part of the process, objectives that will be considered are:

- Development of the protocol for scanning, meshing, designing and producing the splint.
- Development of mobile application for sensor monitoring.
- Implementation of an algorithm to detect inflammation through changes in pres-sure, temperature or colour of the affected area.
- Study on the measurement of humidity on the internal face of the splint, according to the discussion of convenience that will be done later in the article.

The full process will include obtaining the 3D scanning model using a 3Dscanner first, as well as the verification of the data obtained. After this, the file provided by the scanner will be modified using CAD Software to obtain a final model. This model will incorporate the sensors windows to apply the different treatments. Finally, the model will be produced and the software and electronics will be integrated.

BACKGROUND

The new industry is experiencing an enormous growth, thanks to the use of techniques that include advanced manufacturing and industrial design. Moreover, the optimization of the process (Bandyopadhyay et al., 2015; Jammalamadaka & Tappa, 2018; Tappa & Jammalamadaka, 2018), the development of new materials by manufacturers (Chia & Wu, 2015a; Guvendiren et al., 2016; Valášek et al., 2018), or the decrease of environmental costs (Affatato et al., 2016) are some achievements that make it possible to expand these technics further than the industrial area. Nowadays, these techniques are being transferred to

medicine areas, by applications known as bioengineering (Affatato et al., 2016). Among all emerging technologies in the area of bioengineering, the implementation of additive manufacturing (AM) in the healthcare industry has led to several benefits. The design freedom allows customization of surgical equipment, medical devices, and implants. In fact, anatomy for pedagogical objectives (Ugidos Lozano et al., 2018, 2019), craniomaxillofacial surgery (Lozano et al., 2017), oral appliance therapy for snoring and obstructive sleep apnea (OSA) (Ghai et al., 2018; Montesdeoca et al., 2019), orthopedics surgery (Montesdeoca et al., 2019), and rehabilitation (Mulford et al., 2016) are some examples in which the benefits of fused filament fabrication (FFF) technology could improve the clinical course of patients. These new techniques allow to improve wearing comfort and better hygiene due to the bio-compatible and sterilizable properties (Lunsford et al., 2016). Over this fields, many developments have been carried out in recent years, like exoskeletons (P Fitzpatrick, 2017), prosthesis, or assistive devices. These specialties are in demand in developed countries (Cernohorsky & Cadek, 2017), but a level of maturity and technological development is necessary to promote a change in the actual model. Moreover, both orthopedics and rehabilitation are specialties of medicine very conducive and receptive to all kinds of technological developments or applications in the field of research, development, and innovation (R&D&I).

Thanks to the use of different methods of industrial three-dimensional digitization and reverse engineering, advanced manufacturing has generated a recent emergence of solutions. Based on additive manufacturing it has allowed a great advance in products of mass use such as splints, braces, prostheses, or assistive devices (Evill & Evill, 2013). Moreover, these techniques, combined with new sensors and actuators, have revolutionized the applications of exoskeletons by the hand of robotics (Robin et al., 2020). Products such as splints made by additive manufacturing offer great advantages over classical methods of permanent and splinting (splinting) or commercial immobilization (braces, corsets, etc.). Some of these advantages are adaptation, personalization, hygiene, materials used, or environmental impact, among others. The incursion of these new 3D techniques in medical processes allows to include smart systems to analyze different states of the medical evolution process (Goncu-Berk & Topcuoglu, 2017). This study proposes to combine 3D techniques with electronic systems to develop a new era of splints that have not been achieved before. The use of these kind of systems, which include small electronic boards, programming systems, and data communication, would make possible to monitor parameters as temperature and pressure. These parameters would be sent to an application running on a portable device and compared in a database with other similar treatments data or sent to the doctor to see if the process is evolving correctly. This way, it is possible to include the smart splints into the use of big data in healthcare and the Internet of Things (IoT) movement (Chiu et al., 2018; Dimitrov, 2016). In fact, it has been shown that the use of the IoT, allows data exchange through network connectivity and devices integrated with hardware, software, and sensors (YIN et al., 2016). This, applied to medicine, will lead to a reduction in costs and inefficiencies and better patient satisfaction in terms of medical care. One of the factors for the use of IoT in medicine and in rehabilitation (Zanella et al., 2014) are medical devices (things) integrated with a detection technology for the continuous acquisition of physiological data from patients. For these reasons, the purpose of this study is to present how to design and manufacture a smart and functional splint in order to monitor different physiological parameters of the patient and of the device (skin temperature, humidity, pressure, and color changes on the skin). In this manner, it is possible to have a continuous data acquisition that allows to improve the treatment outcomes and to reduce recovery times and healthcare costs.

DEVELOPMENT OF THE SMART SPLINT

Considered therapies during the design process

- Lymph drainage

The lymphatic system has been identified late in history. This is probably because of it is not possible to see it with the naked eye. However, manual techniques for the lymphatic system have been used since the end of the 19th century. Therapist Emil Vodder, developed an innovative approach that allowed manually enhance lymph flow of the body. Today, manual therapists, use Combined Decongestive Physiotherapy for lymphedema. CDP is one of the non-invasive treatments that are chosen for lymphedema, and it is recognized and reimbursed by insurance companies (Society et al., 2017). CDP consists of many components as hands-on, skin care, manual lymph drainage therapy (MLDT), external compressions, etc. The basis of MLDT is to create different pathways through which lymph can flow (Chikly et al., 2014; Wei et al., 2019).

- Iontophoresis

Iontophoresis is one of the most used during rehabilitation treatment for delivery of anti-inflammatory and painkiller medication in the parts of the human body affected by inflammatory processes of the musculoskeletal system (Costello & Jeske, 1995; Hamann et al., 2006; Rigby, Mortensen, et al., 2015). This way, some medications are able to pass through the skin and produce their effect, circumventing the digestive tract and without the need to have them adminis-tered by injection (Hao, 2014; Neeter et al., 2003; Taskaynatan et al., 2007). The explanation of the working mode is that ionic substances have an electric charge, so because of this, tend to move to the pole of the opposite sign. It is in that point where they are absorbed through the skin. This way, some medications are able to pass through the skin and have their effect, avoiding to go through the digestive tract and without the necessity of administering them by injection.

- Ultrasound

Therapeutic Ultrasound technique is considered an effective treatment for rehabilitating musculoskeletal conditions due to joint contracture, pain and muscle spasm or injuries. It improves the elasticity of tissues, and it has mechanical, antalgic and circulatory (Baker et al., 2001; Robertson & Baker, 2001). This treatment promotes the release of heat to tissues such as tendons, muscles and joints, reducing the symptoms of inflammation and promoting tissue regeneration(J. M. ; Bjordal et al., 2006; Ebenbichler et al., 1999). This treatment is not painful, has no side effects and is carried out by means of a transducer capable of generating alternating frequency electrical currents and capable of penetrating the tissue and stimulating blood flow in the area. Ultrasound can also be used in underwater mode or with gel.
The sound waves released through the transducer penetrate the tissue according to the type of medium used, that is, gel or lotion, quality of the transducer, treatment surface and the type of lesion to be treated. Normally the bones and the tendon connection area have low absorption capacity, being recommended to carry out another type of treatment or to use a lower frequency of ultrasound.(Mitragotri, 2005; Rigby, Taggart, et al., 2015)

- Laser

Laser therapy accelerates the metabolism energy and tissue synthesis. There are many studies that concluded that therapeutic laser can potentially be effective in treating tendinopathy when

recommended dosages are used. (J. M. Bjordal et al., 2010; Kneebone, 2010; Tumilty et al., 2010)

Low-level laser therapy is considered to act through light absorption by photoreceptors, that stimulate the cells and modulates inflammatory processes (Gao & Xing, 2009; Karu, 2008; Moriyama et al., 2009). Different studies performed in a variety of pathological conditions as injured tendons and using LLLT. The tendons, were treated daily for 3 to 21 days. It was observed histopathological changes in tendons that were receiving LLLT as an increment of collagen production, improved collagen bundle organization, and also an increment of the number of small blood vessels (J. M. ; Bjordal et al., 2006; Fillipin et al., 2005; Ng & Fung, 2008; Reddy et al., 1998). Moreover, some studies have investigated the effect of Laser therapy within the first 24h after an acute inflammation. It was found that after inflammation followed by just three or four LLLT sessions, the concentrations of inflammatory markers and cells had been reduced compared to no-treatment controls (Aimbire et al., 2006; Joensen et al., 2012).

- Electrostimulation

The application of electricity for the treatment of pain dates back to thousands of years BC. The Ancient Egyptians and later the Greeks and Romans recognized that electrical fishes are capable of generating electric shocks for relief of pain (management & 2003, n.d.). The modern electrotherapy therapies for neuromuscular-skeletal from mild to moderate pain is based on transcutaneous electrical nerve stimulation (TENS) and percutaneous electrical nerve stimulation (PENS) (Heidland et al., n.d.). There are also different studies about the effects of electrostimulation on pain, muscular strength and functional capacity in patients with osteoarthritis of the knee (Rosemffet et al., 2004).

For the electrostimulation therapy a simple device having at least one circuit with a pair of electrodes is required. Different curves and frequencies may be selected. Muscular electrostimulation electrotherapy TENS in gastrocnemius muscle has antalgic and anti-inflammatory effect, low frequency analgesic currents and faradic currents produces retardation of muscle atrophy in calf muscle, and stimulating currents in gastrocnemius and intrinsic muscles of the sole produces motor responses, avoiding Subdeck processes (Martín, 2014).

These techniques are only some examples considered in this study, that may for instance be applied to injuries or lesions in arms (Johansson et al., 1999), knees (Aiyejusunle et al., 2007), elbows (Stasinopoulos & Johnson, 2005) or Achilles tendons (Kaplan et al., 2019). However, by using 3D splints, it could also be possible to apply other therapies, considered by a specialist (Moein et al., 2017).

According to the previous study (Fernando Blaya et al., 2019), the treatment programming is shown in black colour in Figure 2. Traditional splints do not allow the application of physiotherapy techniques until the device is removed. However, by using new smart splints, it is possible to apply the treatments as soon as the injury occurs. It is possible to see the new timing possibilities in blue colour in Figure 2.

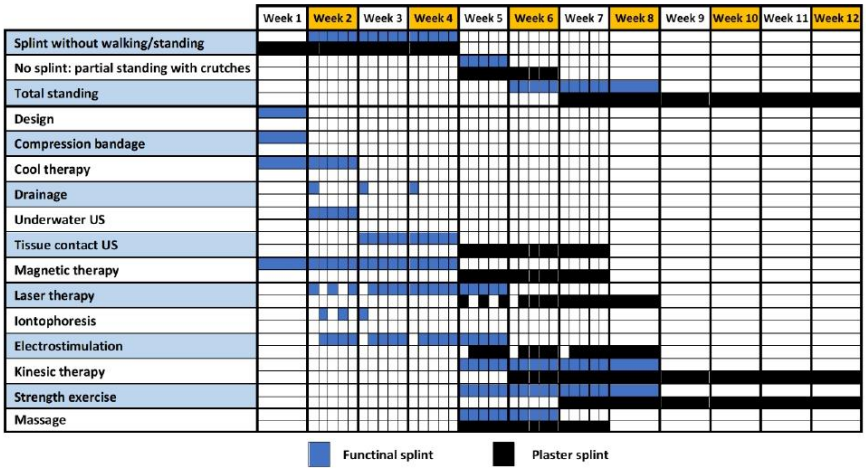

Figure 2: Chronogram of rehabilitation when new techniques are applied (Fernando Blaya et al., 2019)
This reduction involves at least 30% of the treatment period. Moreover, the appli-cation of physiotherapy techniques during the immobilization phase contributes to the prevention of joint, muscular and vascular complications, derived from the application of retention devices in the initial phase of the treatment.

Sensors

For this study, the parameters that will be monitored are temperature, humidity, pressure and skin colour. The information recorded by these sensors is combined to determine if there is any kind of unexpected evolution of the treatment. In total, the implemented sensors are: two temperature sensors DS18B20 (DallaDS18B20 Temperature Sensors Semiconductor, 2002) in contact with the skin, one temperature and humidity sensor between the skin and the splint (DHT22) (Aosong Electronics Co., 2015), two pressure sensors DF9-40 (*Film Pressure Sensor DF9-40@10kg V2.0*, n.d.) placed in two different axes of the splint (X, Y), and one colour sensor TCS34725 (*TCS3472 COLOR LIGHT-TO-DIGITAL CONVERTER with IR FILTER*, n.d.). The shocks and vibrations that may be produced by the human body are not critical to the performance and durability of these sensors. Moreover, when an injury of these characteristics is being treated, it is due to the re-quirement of immobilization. Therefore, the shock and vibrations are controlled. In addition, some of these sensors have been tested in a previous study, where it is detailed that accuracy of the selected sensors is enough for the purpose . Details of these sensors are shown in Table 1.

Table 1: Technical specifications of the sensors

Sensor Serial Number	DS18B20	DHT22	DF9-40	TCS34725
Dimensions (mm)	6 x 6 x 50	15 x 7.7 x 20	40 x 20 x 0.25	25 x 20 x 1.5
Power voltage (V)	3.0 – 5.5	3.3 – 6	5	5
Working range	-55°C to 125°C	-40°C to 80°C		
0 to 100% RH	0-500 g	-		
Resolution	± 0.0625°C	0.1°C, 0.1% RH	14.5 g	-

The DS18B20 sensors (Dallas Semiconductor™ Maxim Integrated Products, Inc., Dallas, TX, USA) are 1-Wire digital temperature sensor. It reports degrees in Celsius, with a precision of 9 to 12-bit. Each sensor

has a unique 64-Bit serial number etched into it, which allows a huge number of sensors to be used on one data bus. The DHT22 sensor (Aosong Electronics Co., Ltd., Guangzhou, China) utilizes exclusive digital-signal-collecting-technique and humidity sensing technology, its sensing elements is connected with 8-bit single-chip computer.

The DF9-40 sensor (Zhengzhou Winsen Electronics Technology Co., Ltd., Zhengzhou, China) is a film pressure based on flexible pressure sensing technology. In order to measure the applied force with an Arduino, it will be necessary to build a voltage divider circuit with a pull-down resistor. This circuit creates a variable voltage output that can be read by the ADC (analog to digital converter) input of the microcontroller. It means that for a simple force-to-voltage conversion, the force sensing resistor (RFSR) device is tied to a measuring resistor (RM) in a voltage divider. In this case, a 10kΩ resistor will be used. The output voltage (Vout) which is possible to measure with the Arduino is described by the following equation:
Vout = Vcc· RM RM + RFSR . (1)

Note that the output voltage measure is the voltage drop across the pull-down resistor. When no force is applied, the FSR resistance will be really high, for example, 10 MΩ. Using a 10 kΩ pull-down resistor and a VCC of 5 V, results in the following output when no force is applied VOUT = 0.005 V. When the FSR is pressed, the resistance goes down to roughly 200 Ω. This results in the following output voltage VOUT = 4.9. Similar developments have been carried out in other studies for other medical applications (Society et al., 2017).

During the healing process, a bruise will usually go through different colours. It often starts red because fresh, oxygen-rich blood has newly pooled underneath the skin. After around 1–2 days, the blood begins to lose oxygen and change color. A bruise that is a few days old will often appear blue, purple, or even black. In about 5–10 days, it turns a yellow or green color. These colors come from compounds called biliverdin and bilirubin that the body produces when it breaks down hemoglobin. After 10–14 days, it will turn to a shade of yellowish-brown or light brown (*Bruise Colors: Causes, Timescale, and When to See a Doctor*, n.d.; *Tell-Tale Color Changes: Camera Can Find Age of a Bruise | Features | Oct 2012 | BioPhotonics*, n.d.).
The TCS3472 sensor provides a digital return value of three components of the light (red, green and blue), and it also clears the light detection values. It includes an IR blocking filter, which minimizes the IR spectral component of the light, allowing for accurate colour measurements over the skin, where there is not external light. Figure 1 shows graphs of the specific response from this sensor to the light. As Figure 1a shows, the sensor is able to detect different wavelengths by using a spectral photodiode. In this way, it comprises the amount of light of each wavelength that bounces off a surface. Figure 1b illustrates that the highest responsivity of the sensor is in the perpendicular direction of the photodiode surface. This must be considered when the housing of the sensor is designed. This sensor is an ideal solution for varying lighting conditions and materials, due to its sensitivity, the wide dynamic range, and the IR blocking filter. The data is transferred via an I2C bus, using the SDA and SCL contacts.

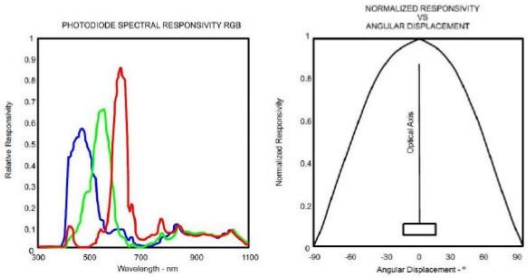

(a) (b)

Figure 1. TCS3472 sensor responsivity graphs (a), (b) (*TCS3472 COLOR LIGHT-TO-DIGITAL CONVERTER with IR FILTER*, n.d.)

Previous studies show the suitability of different RGB channels and their differ-ences for detection of hematomas or ecchymosis (Al Ghozali et al., 2017; Patašius et al., 2016). The colour sensor detects changing colours of the skin, during the initial inflammation stage, due to ecchymosis (*Automatización de La Datación de Equimosis En El Peritaje Médico Legal Peruano Mediante Redes Neuronales Artificiales y Procesamiento de Imágenes*, n.d.), which occurs around approximately the first six days (Ghavimi et al., 2018; Gurlek et al., 2006). The main purpose of using an RGB sensor, is to detect the variation in red, green and blue components of the light. The device, incorporates an emitter of white light, that bounces off the skin, and goes back to the receiver. The sensor reads the variation of the three components, in comparison to the original white light. This way it is possible to know what component is absorbed, and therefore, the colour of the skin. It is not necessary to modify the gain value or other parameters, as the sensor is already configured. Moreover, as the initial stage of the lesion that must be monitored has a duration of one week, the durability is not a critical parameter. The sensor reads the values in terms of RGB (red, green and blue) between 0 and 255.

3D Model and Design

As reported in other previous studies, the first step was to get the 3D model of the injured part (Fernando Blaya et al., 2019).

From that point, the splint is modeled over this part, considering the areas where the sensors are placed. A commercial scanner (Sense™ 3D scanner, 3D Systems Inc., Rock Hill, SC, USA) was used for the digitalization of the arm at a distance of 40 cm according to the manufacturer's instructions.

The technical specifications of the scanner are shown in Table 1

Table 1. Technical specifications of the Sense™ 3D scanner

Maximum Scan Volume	2 × 2 × 2 (m)
Minimum Scan Volume	0.2 × 0.2 × 0.2 (m)
Working Distance	0.2–1.6 (m)
Number of Cameras	2
Resolution at 0.5 m	1mm

It is possible to scan the entire area, at once or in several times if necessary due to limitations produced by a possible injury. Later, the software joins the points cloud. Figure 1 shows the scan process, and the 3D point cloud obtained the total time for the scanning process is 6 min.

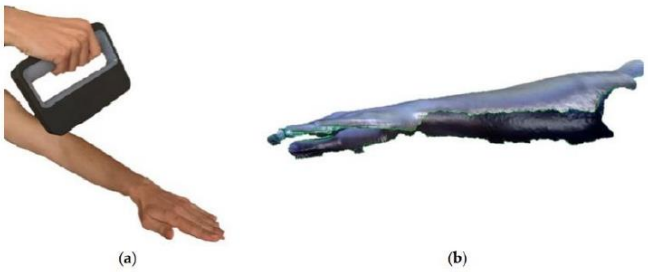

Figure 2. Scanning process of the arm to get the digital model (a) and points cloud (b)

Once the 3D point cloud is obtained post-processing has been carried out by using a 3D CAD software Geomagic FreeForm (3D Systems, Inc., United States). The 3D scanned models are shown in figure 2.

Figure 3. 3D model of the arm obtained after the scanning process: top side (a) and bottom side (b)

With this software it was possible to clean the point cloud by filling the holes due to noise appears during the scanning process and by correcting with a smoothing algorithm any minor anomalies due to misplaced of some points of the cloud or due to surfacing process. With this procedure it was possible to obtain a simpler mesh of the arm by limiting the area of the interest started from a point cloud. Starting from this mesh and creating an offset of 0.5mm, it is created the solid which will be the basis of the splint. Figure 3 shows the mesh of the scanned arm and the solid digital model obtained.

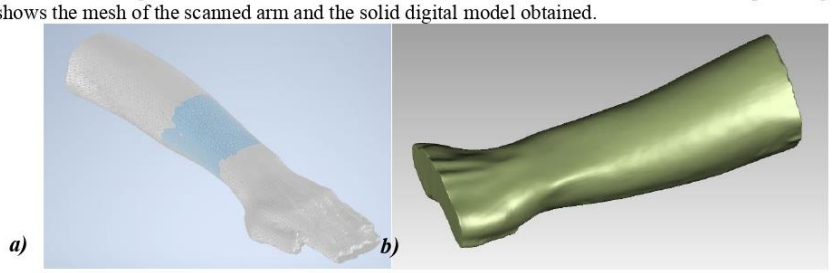

Figure 4. Post processed: mesh of the scanned arm (a) and solid digital model obtained from the clean mesh (b).

The solid digital model shown in the figure 3b represents the first step of the design of the splint. In fact, the solid surface created represents the internal face of the splint in direct contact with the skin of the patient's arm. Once this reference surface of the splint has been created a 5 mm thickness solid has been generated as shown in figure 4.

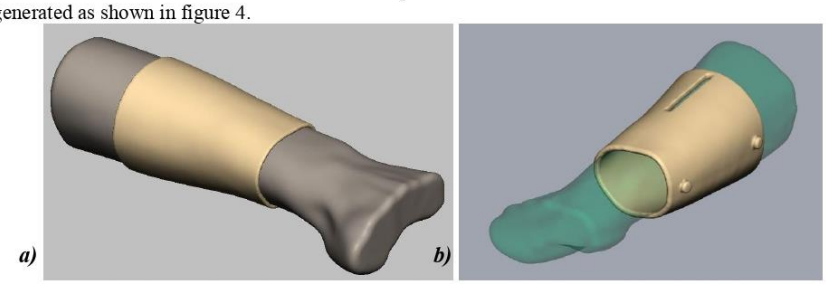

Figure 5. Initial solid obtained from the points cloud (a) and initial stage of the design, including the hole for the temperature sensor and closing buttons (b)

Once the body of the splint has been created, it was be necessary to divide it in two parts to make the mounting possible, that will be later joined with a mechanical closure (figure 5a). Also, the places for the sensors are designed and some holes are introduced as shown in the figures 5b and 5c. The function of these holes and windows is manifold. In fact, they allow, on the one hand, direct medical inspection of the injured part, aeration of the skin in contact with the splint and, on the other, the possibility of using electromedical devices for rehabilitation during immobilization of the limb. Figure 6 shows the final modelled splint over the initial 3d model.

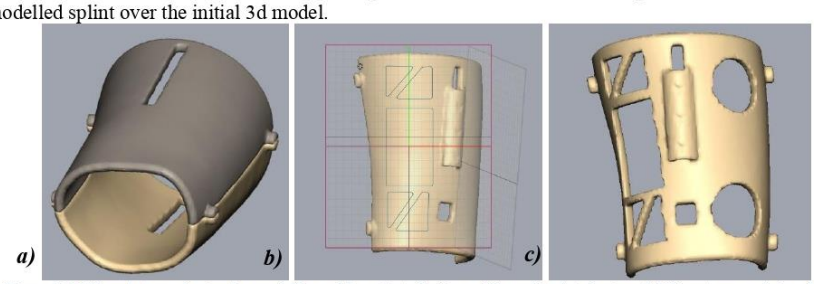

Figure 6. Different steps during the modelling of the splint: division of the splint (a), design of different sensor holes (b) and final top side splint (c)

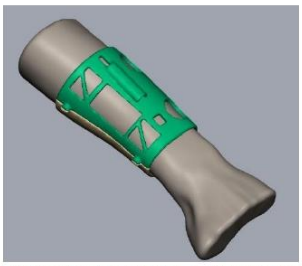

Figure 7. Final result of the modelled splint over the patient arm

This process may be also applied to other limbs:

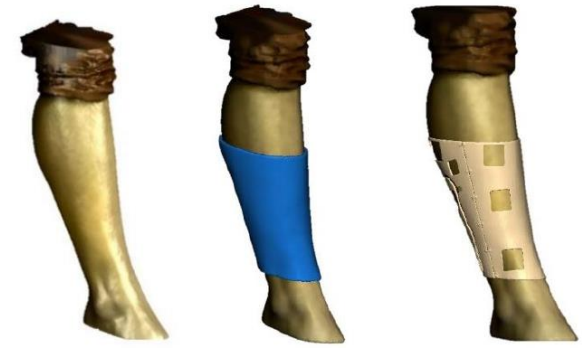

Additive manufacturing

After the digital modeling and design process, the file obtained is sent to a slicer that prepares the part to be produced by using the additive manufacturing process (Figure 7). The splint was manufactured by using a fusion deposition modeling (FDM) 3D printer "TotalPrinter" machine (Figure 7a). This 3D printer was designed, developed, and manufactured in the Additive Manufacturing and Rapid Prototype Laboratory of the Escuela Técnica Superior de Ingeniería y Diseño Industrial at Universidad Politécnica de Madrid. This 3D printer allows continuous temperature and humidity control of the printing chamber and of extruder temperature with the aim of optimizing the process and obtaining an homogeneous splint in terms of adhesion of the various printing layers, density of the material, and mechanical characteristics. In addition, this 3D printing machine allows continuous monitoring of the thickness of the PLA filament

used as reported in the study of Soriano et al. (2019) and in the study of J. M. D. A. Del Burgo et al. (2018) (Haro et al., 2019, 2018).

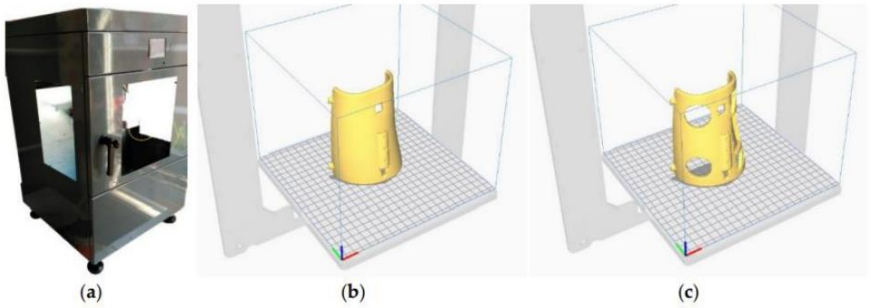

Figure 8.TotalPrinter machine developed to work with biomaterials (a). G-Code process generation

For producing the splint, PLA filament (see table 3 for mechanical properties) with a diameter of 1.75mm was chosen. The material and process should be followed carefully in order to avoid biocompatibility issues (Del Burgo et al., 2019; Salentijn et al., 2017; Vladescu et al., n.d.). The vertical position for printing was chosen as shown in Figure 11, taking into account the volume chamber of this machine (200mm x 200mm x 400 mm). In Table 4, it is possible to see the printing parameters set in the manufacturing process, following the material manufacturer's recommendations to obtain a quality and structure rigid enough.

Table 2: Mechanical properties (Farah et al., 2016)

Properties	Units	PLA
ϱ (Polymer density)	g/cm3	1.21–1.25
σ (tensile strength)	MPa	21.0–60.0
E (tensile modulus)	GPa	0.35–3.50
ε (ultimate strain)	%	2.50–6.00
σ* (specific tensile strength)	Nm/g	16.8–48.0
E* (specific tensile modulus)	kNm/g	0.28–2.80
Tg (glass transition temperature)	°C	45–60
Tm (melting temperature)	°C	150–162

Table 3: Different parameters used for the manufacturing of the leg splint.

Layer height [mm]	0.2
Extruder [mm]	0.4
Density [%]	40
Thickness perimeter each layer [mm]	1

Print speed [mm/s]	60
Temperature [°C]	220

Assembly of the real model

In order to correctly detect the data from the sensors, it is necessary to develop an electronic board for connecting everything easily. It is important to focus on a durable design, with low weight and dimensions. By focusing on these main purposes, a board that will be installed directly to the TTGO OLED Display and Battery Board is designed, shown in Point 2.2 of this study. This board has two analog to digital converters (ADC1 and ADC2). The resolution of these converters is 12 bits. A 12 bits ADC means that is able to read 2^{12} values between 0 and 5v. This is 4096 values, so it detects changes of 1.22mv, which is enough for what is required by the selected sensors. ADC1 is used for the sensors, whilst ADC2 is used for the communication between the microprocessor and the Wi-Fi module, which is used to create the web server (*ESP32 Series Datasheet Including*, 2020).

The chosen board, as explained before, can be accessed from other devices through different ways and protocols. It has an OLED display that may show the acquired data (pressures, temperatures, humidity and colour change detection). Also, it is possible to create a Bluetooth connection with a mobile phone or similar device. However, in this case, the option of creating a web server is selected. This way, the information may be consulted from any device connected to the internet, anywhere in the world. The great benefit of this, is that a doctor can see the data and follow the treatment in real time from their place of work.

The total real consumption of the electronic board and sensing system is 84.66mA. Due to the battery has a capacity of 12210mAH, the autonomy of the system is around 144h. This means that the system is able to collect data during six days without charging the battery, what is very significant because the first week after occurring the lesion is the most important period to be analyzed (*Bruise Colors: Causes, Timescale, and When to See a Doctor*, n.d.; *Tell-Tale Color Changes: Camera Can Find Age of a Bruise | Features | Oct 2012 | BioPhotonics*, n.d.). After that, it is possible to replace or charge the battery.

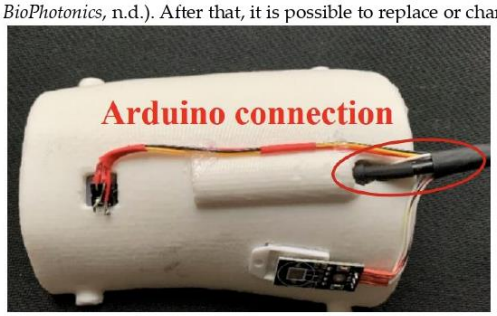

Figure 13a shows the splint prototype obtained with the wiring and sensors fully assembled. In Figure 13b it is possible to see the interior of the splint with the housing for the sensors.

(a) (b)

Figure 9: Real splint assembled with the sensors (a) and interior view (b)

To test the fully assembled leg splint on a real leg, the splint was fixed to a healthy volunteer for 1.5h (Figure 14). The volunteer was placed in seated position for the tests. However, this new "smart splint" is capable of obtaining data in a continuous way, so the patient does not need to adopt particular positions during the data acquisition. The main purpose of this test, was to collect data so that it could be analyzed if the sensors were able to acquire information correctly. The data collected by the sensors were treated with ESP32 micro and sent to a computer every 3 seconds by using the serial monitor of the Arduino platform. In the following sections the acquired data will be explained.

(a)

Figure 10: Real model over the leg

3.1 Temperatures and humidity

Two temperature sensors in contact with the skin were placed in two different zones. Moreover, a third sensor not in direct contact with the skin, read the temperature and humidity. The mean temperature of the first two sensors is shown in the colour orange, whereas the internal temperature is shown in the colour blue (Figure 15). The graph shows that the registered temperature by the sensor is slightly lower than 36ºC. This occurs because the exterior area of the sensor surface is not in real contact with the skin,

and this produces a gradient of temperature between the environment and the body. However, what the authors are looking for in this study, is to detect an increment or decrement of the temperature of the located area of the skin, compared with the historical. It is perfectly possible to detect an increase or decrease of the registered temperature, in comparison with the historical data.

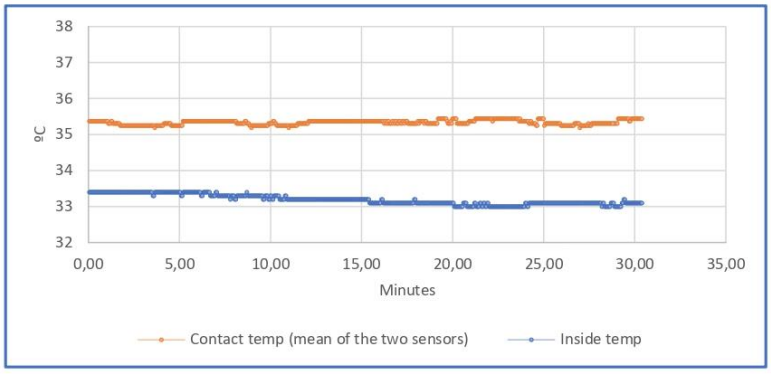

Figure 11: Temperature's graph

Monitoring the humidity inside the splint and its fluctuations allows us to know if the injured area is in a healthy environment and unsuitable for the proliferation of bacteria, especially in cases of surgery or injury. Furthermore, some physiological events that can occur following a trauma have been shown to include changes in skin colour due to edema, changes in temperature and an increase in sweating in the area affected by the lesion (Birklein et al., 2001). In fact, a change in the sudomotor function of the injured part implies central disturbances of thermoregulation (Jänig, 1990; Ju et al., 2005). Figure 16 shows the percentage of humidity that was registered during the test inside the splint (in orange colour) and outside the splint (in blue colour).

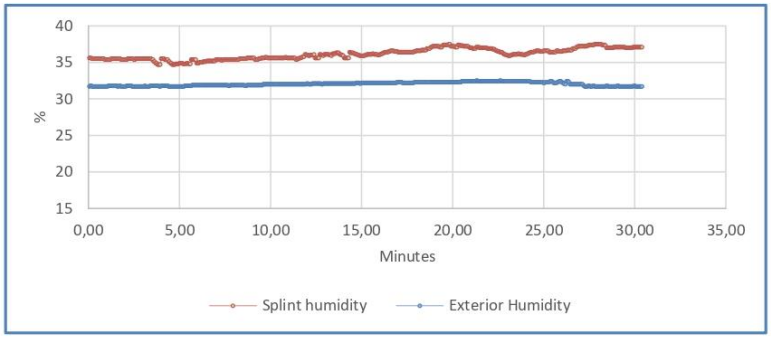

Figure 12: Humidity graph

3.2 Pressure

Two sensors for reading pressure are placed. One is placed on the "X" axis and the second on the "Y" axis (Figure 17). The sensors have been placed on these positions for the tests, and the data are collected with the leg in vertical position and weightlessly. However, the potential of these kinds of 3D techniques makes it possible for other medical requirements to also be considered and included during the design process, according specialist dictated requirements.

Figure 13: Pressure sensors on the "X" and "Y" axis.

The surface of the pressure sensor during the limb immobilization phase is 1 cm^2, according to $1N=1Kg/s^2$ the pressure values read by the sensor will have the dimensions of gf/cm^2. Figure 18 shows the detected mean pressure. As illustrated, during the normal state, the value of the pressure is constant and is equal to 60 gf/cm^2. However, when a slight pressure is produced due to an inflammatory process, the sensors are able to perfectly detect an increment of this pressure. In order to simulate what occurs in an inflammatory process, a force over the splint was applied between minutes 7 and 10. This variation was detected by the sensors, reading a pressure that rose from 60 gf/cm^2 to 100 gf/cm^2. Therefore, when the pressure was increased due to the inflammation of the area, the sensors perfectly detected the increment of the mass inside the splint (De Agustín Del Burgo et al., 2020). The graph shows the actual and historical pressure. Real-time monitoring and the collection of historical data on the pressure variation of the injured area during the immobilization period allows the specialist to control inflammatory phenomena.

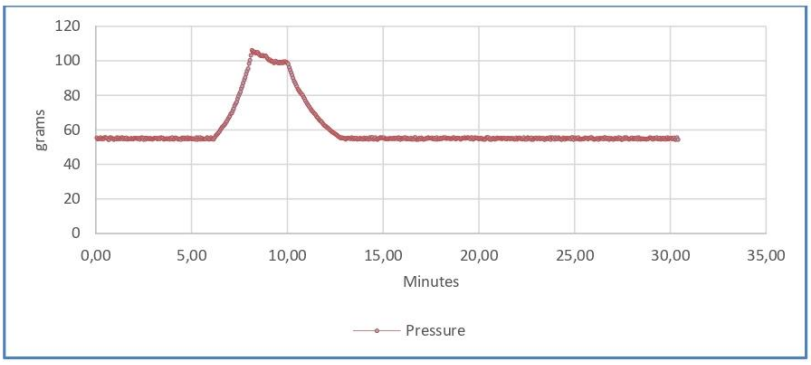

Figure 14: Pressure graph

3.3. Colour

The test was done on the skin of a volunteer that had a hematoma, and was compared to another part of his body, that had no signs of hematoma. The sampling of the test was carried out with a frequency of 10 seconds. It is possible to see in Figure 19 that the sensor is capable of detecting a colour change in the skin. In Figure 19a, the skin has a normal colour with no signs of hematoma, whilst in Figure 19b the sensor detects an increment in the RGB values due to the signs of hematoma. Due to this, it will be possible to check the evolution of the colour during the very initial stages of the treatment, but also during posterior stages. It is possible to see that the three values are incremented, but it is specifically the 38% increment of the red value that makes it possible to detect the hematoma.

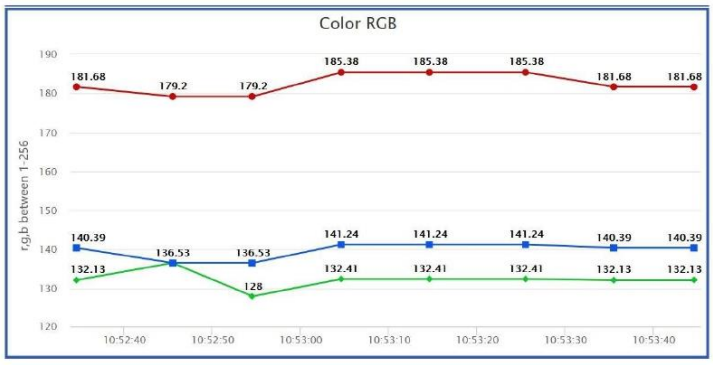

(a)

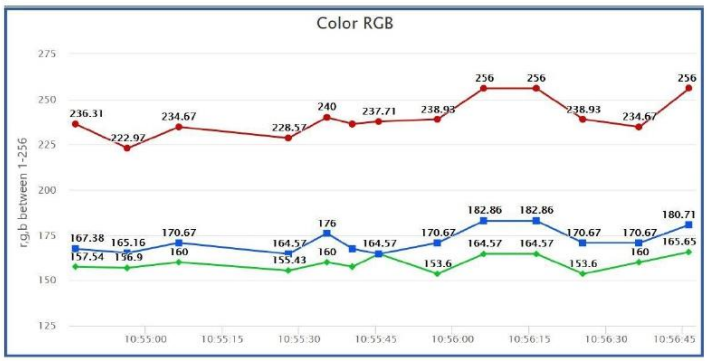

(b)

Figure 15: Colour RGB sensor lectures without hematoma (a) and with hematoma (b)

3.4. Diagnostic

The knowledge of these data makes it possible to identify temperature, humidity, pressure or skin colour changes. Combining them, makes it possible to identify signs of inflammation and detect possible problems during the treatment.

To accomplish this, an algorithm that can be configured to consider temperature and pressure changes during a period of time was programmed, to consider these data to be produced by an inflammation process but not by a position of the limb over a specific object. The considered parameters are showed in Table 5. However, these parameters are showed as an example of the possibilities of the system, with no real medical considerations in this case. The timing would be the necessary to distinguish a value due to inflammation from a collision or resting state position. Moreover, to avoid a wrong measure of the pressure sensors, it may be considered to add a third sensor in opposite position. An inflammation process will produce an increment volume inside the splint, and an increment of the pressure in all the sensors, in a simultaneous and cotemporally way. About the range, it is proposed a 5-10% change of the value due to the acquired data during the tests.

Table 4. Algorithm configuration to detect inflammation.

Temperature increment	1.5 ºC
Pressure increment	60 gf/cm^2
Time during temperature increment	60 *m*
Time during pressure increment	60 *m*

Moreover, the combination of this information with colour and humidity that can also be consulted remotely by a specialist will result in a complete diagnosis.

SOLUTIONS AND RECOMMENDATIONS (Subhead 1: Arial, Size 12, UPPERCASE, Bold)

This study shows the combination of traditional immobilization techniques with new 3D modelling and prototyping techniques. This new system allows us to follow the evolution of the injured part in a very detailed way. Moreover, it is possible to apply treatments that improve not only the timing but also the

quality of the rehabilitation. As previously explained, in this study electrostimulation, drainage, iontophoresis, laser and ultrasound have been considered as treatments. However, the potential of these kinds of 3D techniques makes it possible for other medical therapies to also be considered and included during the design process, according specialist dictated requirements.

These treatment possibilities are combined with the acquired data to even improve the treatment. Adding sensors to these splints, makes it possible to analyze in real time how the therapy is functioning and new steps to get the most progress.

Also, the vast capacities that remote monitoring allows would simplify the revisions that must be carried out by a specialist. This allows doctors to follow the progress of more patients, by using objective data. These data may be collected into a database, in order to compare different evolutions of different treatments in similar injuries.

For this study, the use of ruggedized sensors was not considered, as the main purpose of the study is to show the new possibilities of using sensors in splints, and the benefits of using new technologies in this kind of treatment. The performance and resolution of the implemented sensors, were correct for the tests, as it is possible to see in the different figures. Humidity sensor DHT22 has an error due to hysteresis of +-0.3%. The sensor is looking for an increment of the internal humidity in comparation with the external humidity. The value will be around 3-5% higher when a sweating process is produced. Due to this, the error is not significant and will not interfere in the correct detection of a sweating process. In this case, it is completely functional.

From a medical point of view, there is no necessity to know the absolute value, or trying to get an optimal value, as this will depend on the patient and lesion. This is why the main focus of the study is to analyze the new capabilities by detecting the variations on the acquired data.

The design of the different windows includes round edges to avoid any kind of chafing or similar. In no case the design of these windows may cause injury to the affected limb or by edge effect since the additive manufacturing design allows smoothing all the edges in contact with the patient, nor by suction effect on the skin (Lowe, 2017) as the splint is not indicated for support in load nor produce its own vacuum because it is an open design. Also, it is mandatory to use biocompatible materials (Hernández et al., 2020; Kim et al., 2016) to avoid any kind of irritation, eschar or ulcer.

The design of the splint is made according to the affected anatomic area of each patient. The design includes an offset to suit perfectly over the area. The design and the position of the windows must be supervised by a medical specialist, according to the lesion. These windows allow a visual control of the treatment, what is especially critical in the initial stages. However, the windows do not intervene in the treatment. In cases where the use of splints indicated for support and gait of the lower limb is required, the corresponding structural study would be carried out, and accessible windows should be generated only at the time of use through the design of a closure. Moreover, this kind of modules would allow to take off the splint to clean the skin if needed, something no possible with traditional splints.

For nearly half a century research has been conducted on humans (LAWSON, 1956) and animals (Ströberg, 1974; Wang et al., 2016) showing the correlation between temperature patterns and medical conditions. The temperature variation of an area of the body is produced by cell metabolism and local blood flow. The increments in temperature are normally the result of an increase of these factors, although it is true that blood flow plays the most important role. Moreover, with some disease processes or during the different bone formation stages and fractures repair, it may occur a reduction in blood flow to the affected areas (Rundle et al., 2006). This will also produce some alterations in surface temperature.

In the case of using a conventional arm splint, the weight of the material may produce pain in the neck. Also, the lack of ventilation and the difficulty of bathing could produce allergies and itching due to the poor hygiene of the skin and the device. Another negative point of traditional

cast implants is the difficulty of handling it in some daily activities by patients (F. Blaya et al., 2018).
This study proposes the implementation of a series of sensors to detect possible problems during the whole time of the treatment. The duration of the treatment does not interfere with the data collection and interpretation. In fact, the collection may be carried out periodically, depending on the specialized doctor necessities and on the injury evolution. For this reason, the data collection is carried out as a sign that the system works.
As it is possible to see in the charts obtained from the sensors, it is perfectly possible to detect temperature variations, pressure increment and humidity inside the splint. Besides, if more temperature sensors are situated in the splint, it would be possible to create a digital mapping of the different areas under the splint. This information to quantify temperature changes in skin surface indicates both hot and cold responses which may co-exist if the pain associate with an inflammatory focus excites an increase in sympathetic activity (Ju et al., 2005). Continuous monitoring of these parameters allows to know the progression of area at any time of the treatment. This allows early detection of possible vascular, muscular or joint complications that are difficult to observe without the removal of the immobilization splint or through severe symptoms caused by often irreparable damage.
The temperature registered by the sensor in contact with the skin, is slightly lower than the normal temperature. this is due to the temperature gradient that occurs on the sensor surface. The sensor surface in contact with the skin is about a 40%. The rest of the surface is covered by the splint but not in contact with the skin. This fact produces a difference of temperature between different points of the sensor. The metallic surface tends to get an equilibrium due to thermal conductivity (Horai & Shankland, 1987). The sensor gets a final temperature that is not the real skin temperature. However, this fact does not interfere with the main purpose of this sensor, which is to detect incremental temperature changes.
Temperature, humidity and pressure are correctly detected by the sensors. Also, the presence sensor detects perfectly whereas the splint is correctly fixed. However, the presence sensor cannot be used for its second propose, detecting colour changes by the variations of the reflection due to the skin colour. This sensor has not enough sensibility to detect so light variations. Moreover, it does not include an RGB sensor to detect different wavelengths, making it really difficult to use the sensor for this purpose. Therefore, the use of such a sensor for the proposed purpose is not estimated.

FUTURE RESEARCH DIRECTIONS (Subhead 1: Arial, Size 12, UPPERCASE, Bold)

Discuss future and emerging trends. Provide insight about the future of the book's theme from the perspective of the chapter focus. Viability of a paradigm, model, implementation issues of proposed programs, etc., may be included in this section. If appropriate, suggest future research opportunities within the domain of the topic.

CONCLUSION (Subhead 1: Arial, Size 12, UPPERCASE, Bold)

The main objective of this work was the study, design and manufacture of a smart and immobilization splint to monitor different parameters about the real evolution of an injury. This makes it possible to have real time data to diagnostic any kind of problems that are not possible to detect with traditional splints. The current state of the technology allows the realization of particular and individualized immobilization splints by using Advanced Manufacturing, based on

fused deposition modelling, 3D digitalization and reverse engineering. Moreover, the knowledge of these parameters, might reduce the curing time as some treatments can be applied in this kind of splints but not in traditional splints.
In this study it is shown an interesting and really possible evolution of the traditional splints, to provide them with the term "intelligent". The great possibilities that it is offered by this kind of splints, is fully demonstrated. However, there are some improvements that are proposed to be carried out in future studies:

- Implementation of a sensor to detect colour changes of the skin: This would make it possible to detect bruising and redness, that would allow to get more data for the diagnostic.
- Sending these data to a Bluetooth device that allows remote medical monitoring of the treatment applied and the application of an alarm system in the event of complications, as well as the generation of the data dump in a database for study.
- Integration into functional splints based on rehabilitation techniques in the immobilization phase. This would make necessary to incorporate a battery to get a full autonomous system.

To finish this study, the main objective is considered to have been achieved, by the incorporation of these sensors and demonstrated that it is possible to detect complications in the treatment of injuries using immobilization splints.

The main objective of this study is to show an evolution of traditional inmobilization methods. It is not possible to apply any kind of rehabilitation before removing the splint using a traditional inmobilization splint. Moreover, it is not possible to know what is happening under the splint.

This study shows the possibilities of using individualized immobilization splints by Advanced Manufacturing techniques scanning and prototyping. It is possible to fabricate a splint that fits perfectly on each limb. Moreover, it creates some areas for applying different treatments that produces at least a 30% decrease in the treatment period compared to plaster splints.

On the other hand, it is possible to incorporate some sensors for real time acquisition of data from inside the splint. This will allow health practitioners/doctors to anticipate treatment for different issues that may appear.

The electronic device that gets the data from the different sensors is able to combine and analyze the information received from the data. After that, it may send alerts when detecting inflammatory processes, skin colour changes, or high humidity values. These alerts are shown on a display, a mobile device, or may also be consulted remotely.

For future studies, the creation of a database where different smart splints send the acquired data is proposed as an improvement. This way, by using the new Big Data concept and Data Science, the device would be able to learn from the different symptoms to avoid problems before they happen and also to design specific treatments for each lesion and patient.

REFERENCES (Subhead 1: Arial, Size 12, UPPERCASE, Bold)

Affatato, S., Ruggiero, A., De Mattia, J. S., & Taddei, P. (2016). Does metal transfer affect the tribological behaviour of femoral heads? Roughness and phase transformation analyses on retrieved zirconia and Biolox® Delta composites. *Composites Part B: Engineering*, *92*, 290–298. https://doi.org/10.1016/j.compositesb.2016.02.020

Aimbire, F., Albertini, R., Pacheco, M. T. T., Castro-Faria-Neto, H. C., Leonardo, P. S. L. M., Iversen, V. V., Lopes-Martins, R. A. B., & Bjordal, J. M. (2006). Low-level laser therapy induces dose-dependent reduction of TNFα levels in acute inflammation. *Photomedicine and Laser Surgery*. https://doi.org/10.1089/pho.2006.24.33

Aiyejusunle, C. B., Kola-Korolo, T. A., & Ajiboye, O. A. (2007). Comparison of the effects of tens and sodium salicylate iontophoresis in the management of osteoarthritis of the knee. *Nigerian Quarterly Journal of Hospital Medicine*, *17*(1), 30–34. https://doi.org/10.4314/nqjhm.v17i1.12539

Al Ghozali, H. K., Setiawardhana, & Sigit, R. (2017). Vein detection system using infrared camera. *Proceedings - 2016 International Electronics Symposium, IES 2016*, 122–127. https://doi.org/10.1109/ELECSYM.2016.7860987

Ambu, R., Motta, A., & Cali, M. (2020). Design of a Customized Neck Orthosis for FDM Manufacturing with a New Sustainable Bio-composite. *Lecture Notes in Mechanical Engineering*, 707–718. https://doi.org/10.1007/978-3-030-31154-4_60

Aosong Electronics Co., L. (2015). *Digital-output relative humidity & temperature sensor/module DHT22 (DHT22 also named as AM2302)*.

Automatización de la Datación de Equimosis en el Peritaje Médico Legal Peruano mediante Redes Neuronales Artificiales y Procesamiento de Imágenes. (n.d.). Retrieved May 26, 2021, from http://cybertesis.unmsm.edu.pe/handle/20.500.12672/1071

Baker, K. G., Robertson, V. J., & Duck, F. A. (2001). A Review of Therapeutic Ultrasound: Biophysical Effects. *Physical Therapy*. https://doi.org/10.1093/ptj/81.7.1351

Bandyopadhyay, A., Bose, S., & Das, S. (2015). 3D printing of biomaterials. *MRS Bulletin*. https://doi.org/10.1557/mrs.2015.3

Birklein, F., Künzel, W., & Sieweke, N. (2001). Despite clinical similarities there are significant differences between acute limb trauma and complex regional pain syndrome I (CRPS I). *Pain*, *93*(2), 165–171. https://doi.org/10.1016/S0304-3959(01)00309-8

Bjordal, J. M. ;, Iversen, V. ;, Lopes-Martins, R., Alvaro, B., Huang, P., Gupta, Y.-Y., Vecchio, A., De Arce, D. ;, Bil, V. J., Huang, S.-F., Xuan, W. ;, & Hamblin, M. R. (2006). Low level laser therapy reduces inflammation in activated Achilles tendinitis NASA Astrophysics Data System (ADS). *NASA Astrophysics Data System (ADS)*.

Bjordal, J. M., Lopes-Martins, R. A. B., Joensen, J., & Iversen, V. V. (2010). The anti-inflammatory mechanism of low level laser therapy and its relevance for clinical use in physiotherapy. *Physical Therapy Reviews*, *15*(4), 286–293. https://doi.org/10.1179/1743288X10Y.0000000001

Blaya, F., Pedro, P. S., Silva, J. L., D'Amato, R., Heras, E. S., & Juanes, J. A. (2018). Design of an Orthopedic Product by Using Additive Manufacturing Technology: The Arm Splint. *Journal of Medical Systems*, *42*(3). https://doi.org/10.1007/s10916-018-0909-6

Blaya, Fernando, Pedro, P. S., Pedro, A. B. S., Lopez-Silva, J., Juanes, J. A., & D'Amato, R. (2019). Design of a Functional Splint for Rehabilitation of Achilles Tendon Injury Using Advanced Manufacturing (AM) Techniques. Implementation Study. *Journal of Medical Systems*, *43*(5). https://doi.org/10.1007/s10916-019-1247-z

Blaya, Fernando, San Pedro Orozco Bioingeniería Postura Salud, P. S., Lopez-Silva, J., San Pedro, P., López Silva, J., Soriano Heras, E., & Antonio Juanes, J. (2018). Design of an Orthopedic Product by Using Additive Manufacturing Technology: The Arm Splint Analytical models for lubricated journal bearings View project 3D Printing of Anatomical Pieces View project Design of an Orthopedic Product by Using Additive Manufacturing Technology: The Arm Splint. *Springer*, *42*(3). https://doi.org/10.1007/s10916-018-0909-6

Bruise colors: Causes, timescale, and when to see a doctor. (n.d.). Retrieved July 13, 2021, from https://www.medicalnewstoday.com/articles/322742#bruise-colors-over-time-and-their-causes

Cernohorsky, J., & Cadek, M. (2017). Smart rehabilitation splint. *Mechanisms and Machine Science*. https://doi.org/10.1007/978-3-319-44087-3_50

Chia, H. N., & Wu, B. M. (2015a). Recent advances in 3D printing of biomaterials. *Journal of Biological Engineering*. https://doi.org/10.1186/s13036-015-0001-4

Chia, H. N., & Wu, B. M. (2015b). Recent advances in 3D printing of biomaterials. *Journal of Biological Engineering*, *9*(1). https://doi.org/10.1186/s13036-015-0001-4

Chikly, B., Quaghebeur, J., & Witryol, W. (2014). A Controlled Comparison between Manual Lymphatic Mapping (MLM) of Plantar Lymph Flow and Standard Physiologic Maps Using Lymph Drainage Therapy (LDT)/Osteopathic Lymphatic Technique (OLT). *J Yoga Phys Ther*, *4*, 173. https://doi.org/10.4172/2157-7595.1000173

Chiu, Y. H., Chen, T. W., Chen, Y. J., Su, C. I., Hwang, K. S., & Ho, W. H. (2018). Fuzzy logic-based mobile computing system for hand rehabilitation after neurological injury. *Technology and Health Care : Official Journal of the European Society for Engineering and Medicine*. https://doi.org/10.3233/THC-171403

Costello, C. T., & Jeske, A. H. (1995). Iontophoresis: Applications in transdermal medication delivery. In *Physical Therapy* (Vol. 75, Issue 6, pp. 554–563). American Physical Therapy Association. https://doi.org/10.1093/ptj/75.6.554

DallaDS18B20 Temperature Sensors Semiconductor. (2002). DS18B20 Temperature Sensor. *Dallas Semiconductor Datasheets*.

De Agustín Del Burgo, J. M., Blaya Haro, F., D'Amato, R., & Juanes Méndez, J. A. (2020). Development of a Smart Splint to Monitor Different Parameters during the Treatment Process. *Sensors*, *20*(15), 4207. https://doi.org/10.3390/s20154207

Del Burgo, J. M. D. A., D'Amato, R., Méndez, J. A. J., Ramírez, A. S., Haro, F. B., & Heras, E. S. (2019). Real time analysis of the filament for FDM 3D printers. *ACM International Conference Proceeding Series*. https://doi.org/10.1145/3362789.3362818

Dimitrov, D. V. (2016). Medical internet of things and big data in healthcare. In *Healthcare Informatics Research* (Vol. 22, Issue 3, pp. 156–163). Korean Society of Medical Informatics. https://doi.org/10.4258/hir.2016.22.3.156

Ebenbichler, G. R., Erdogmus, C. B., Resch, K. L., Funovics, M. A., Kainberger, F., Barisani, G., Aringer, M., Nicolakis, P., Wiesinger, G. F., Baghestanian, M., Preisinger, E., Fialka-Moser, V., & Weinstabl, R. (1999). Ultrasound therapy for calcific tendinitis of the shoulder. *New England Journal of Medicine*. https://doi.org/10.1056/NEJM199905203402002

ESP32 Series Datasheet Including. (2020). https://www.espressif.com/en/support/download/documents.

Evill, J., & Evill, O. (2013). *Cortex Evill*.

Fan, Y. J., Yin, Y. H., Xu, L. Da, Zeng, Y., & Wu, F. (2014). IoT-based smart rehabilitation system. *IEEE Transactions on Industrial Informatics*, *10*(2), 1568–1577. https://doi.org/10.1109/TII.2014.2302583

Farah, S., Anderson, D. G., & Langer, R. (2016). Physical and mechanical properties of PLA, and their functions in widespread applications — A comprehensive review. In *Advanced Drug Delivery Reviews* (Vol. 107, pp. 367–392). Elsevier B.V. https://doi.org/10.1016/j.addr.2016.06.012

Fillipin, L. I., Mauriz, J. L., Vedovelli, K., Moreira, A. J., Zettler, C. G., Lech, O., Marroni, N. P., & González-Gallego, J. (2005). Low-level laser therapy (LLLT) prevents oxidative stress and reduces fibrosis in rat traumatized Achilles tendon. *Lasers in Surgery and Medicine*. https://doi.org/10.1002/lsm.20225

Film Pressure Sensor DF9-40@10kg V2.0. (n.d.).

Gao, X., & Xing, D. (2009). Molecular mechanisms of cell proliferation induced by low power laser irradiation. *Journal of Biomedical Science*. https://doi.org/10.1186/1423-0127-16-4

Gebhardt, A., Schmidt, F., Hötter, J., Procedia, W. S.-P., & 2010, undefined. (n.d.). Additive manufacturing by selective laser melting the realizer desktop machine and its application for the dental industry. *Elsevier*. Retrieved April 27, 2020, from https://www.sciencedirect.com/science/article/pii/S1875389210005080

Ghai, S., Sharma, Y., Jain, N., Satpathy, M., & Pillai, A. K. (2018). Use of 3-D printing technologies in craniomaxillofacial surgery: a review. In *Oral and Maxillofacial Surgery* (Vol. 22, Issue 3, pp. 249–259). Springer Verlag. https://doi.org/10.1007/s10006-018-0704-z

Ghavimi, M. A., Nezafati, S., Yazdani, J., Pourlak, T., Amini, M., Pourlak, T., Ghoreishizadeh, A., & Negahdari, R. (2018). Comparison of edema and ecchymosis in rhinoplasty candidates after lateral nasal osteotomy using piezosurgery and external osteotomy. *Journal of Advanced Pharmaceutical Technology and Research*, *9*(3), 87–93. https://doi.org/10.4103/japtr.JAPTR_294_18

Goncu-Berk, G., & Topcuoglu, N. (2017). A Healthcare Wearable for Chronic Pain Management. Design of a Smart Glove for Rheumatoid Arthritis. *The Design Journal*. https://doi.org/10.1080/14606925.2017.1352717

Gurlek, A., Fariz, A., Aydogan, H., Ersoz-Ozturk, A., & Eren, A. T. (2006). Effects of different corticosteroids on edema and ecchymosis in open rhinoplasty. *Aesthetic Plastic Surgery*, *30*(2), 150–154. https://doi.org/10.1007/s00266-005-0158-1

Guvendiren, M., Molde, J., Soares, R. M. D., & Kohn, J. (2016). Designing Biomaterials for 3D Printing. In *ACS Biomaterials Science and Engineering*. https://doi.org/10.1021/acsbiomaterials.6b00121

Hamann, H., Hodges, M., & Evans, B. (2006). Effectiveness of iontophoresis of anti-inflammatory medications in the treatment of common musculoskeletal inflammatory conditions: a systematic review. *Physical Therapy Reviews*, *11*(3), 190–194. https://doi.org/10.1179/108331906X144082

Hao, J. (2014). Topical iontophoresis for local therapeutic effects. In *Journal of Drug Delivery Science and Technology* (Vol. 24, Issue 3, pp. 255–258). Editions de Sante. https://doi.org/10.1016/S1773-2247(14)50043-3

Haro, F. B., de Agustín del Burgo, J. M., D'Amato, R., Islán, M., Heras, E. S., Alonso, J. M. G., & Mendez, J. A. J. (2019). Monitoring an Analysis of Perturbations in Fusion Deposition Modelling (FDM) Processes for the Use of Biomaterials. *Journal of Medical Systems*, *43*(5), 109. https://doi.org/10.1007/s10916-019-1236-2

Haro, F. B., de Agustín del Burgo, J. M., D'Amato, R., Marcos, M. I., Heras, E. S., & Alonso, J. M. G. (2018). Monitoring of the additive manufacturing process for the use of biomaterials in medical field. *Proceedings of the Sixth International Conference on Technological Ecosystems for Enhancing Multiculturality - TEEM'18*, 428–432. https://doi.org/10.1145/3284179.3284252

Heidland, A., Fazeli, G., Klassen, A., Sebekova, K., Hennemann, H., Bahner, U., & Iorio, B. Di. (n.d.). *Neuromuscular electrostimulation techniques: historical aspects and current possibilities in treatment of pain and muscle waisting*. https://doi.org/10.5414/CNX77S106

Hernández, J. A. J., Vicente, E. J. G., Sánchez, F. R., Sanchez, F. M., Rodríguez, M. P. C., & Morote, J. P. (2020). Prevention of iatrogenic ulcers produced by therapeutic immobilization with a lower limb splint in children. Clinical trial. *Enfermeria Global*, *19*(3), 135–154. https://doi.org/10.6018/eglobal.393911

Hire Freelance Point Cloud Modeling Services for Your Company | Cad Crowd. (n.d.). Retrieved April 27, 2020, from https://www.cadcrowd.com/architectural-design/point-cloud-modeling-services

Horai, K., & Shankland, T. (1987). Thermal conductivity of rocks and minerals. *Methods in Experimental Physics*. https://doi.org/10.1016/S0076-695X(08)60589-X

Jammalamadaka, U., & Tappa, K. (2018). Recent advances in biomaterials for 3D printing and tissue engineering. In *Journal of Functional Biomaterials*. https://doi.org/10.3390/jfb9010022

Jänig, W. (1990). Functions of the sympathetic innervation of the skin . *A.D. Loewy, K.M. Spyer (Eds.), Central Regulation of Autonomic Functions, Oxford University Press, New York.*, 334–348.

Joensen, J., Gjerdet, N. R., Hummelsund, S., Iversen, V., Lopes-Martins, R. A. B., & Bjordal, J. M. (2012). An experimental study of low-level laser therapy in rat Achilles tendon injury. *Lasers in Medical Science*, *27*(1), 103–111. https://doi.org/10.1007/s10103-011-0925-y

Johansson, K., Albertsson, M., Ingvar, C., & Ekdahl, C. (1999). EFFECTS OF COMPRESSION BANDAGING WITH OR WITHOUT MANUAL LYMPH DRAINAGE TREATMENT IN PATIENTS WITH POSTOPERATIVE ARM LYMPHEDEMA. In *Lymphology* (Vol. 32, Issue 3). https://journals.uair.arizona.edu/index.php/lymph/article/view/17363

Ju, X., Nebel, J.-C., & Siebert, J. P. (2005). 3D thermography imaging standardization technique for inflammation diagnosis. In H. Gong, Y. Cai, & J.-P. Chatard (Eds.), *Infrared Components and Their Applications* (Vol. 5640, p. 266). SPIE. https://doi.org/10.1117/12.577055

Kaplan, K., Olivencia, O., Dreger, M., Hanney, W. J., & Kolber, M. J. (2019). Achilles Tendinopathy: An Evidence-Based Overview for the Sports Medicine Professional. *Strength & Conditioning Journal*, *41*(5), 24–40. https://doi.org/10.1519/ssc.0000000000000485

Karu, T. I. (2008). Mitochondrial signaling in mammalian cells activated by red and near-IR radiation. In *Photochemistry and Photobiology*. https://doi.org/10.1111/j.1751-1097.2008.00394.x

Kim, Y., Son, S., Chun, C., Kim, J.-T., Lee, D. Y., Choi, H. J., Kim, T.-H., & Cha, E.-J. (2016). Effect of PEG addition on pore morphology and biocompatibility of PLLA scaffolds prepared by freeze drying. *Biomedical Engineering Letters 2016 6:4*, *6*(4), 287–295. https://doi.org/10.1007/S13534-016-0241-3

Kneebone, W. (2010). *The Treatment of Achilles Tendonitis Using Therapeutic Laser*. http://orthopedics.about.com/cs/ankleproblems/a/

LAWSON, R. (1956). Implications of surface temperatures in the diagnosis of breast cancer. *Canadian Medical Association Journal*, *75*(4), 309–311.

Lowe, D. T. (2017). Cupping therapy: An analysis of the effects of suction on skin and the possible influence on human health. *Complementary Therapies in Clinical Practice*, *29*, 162–168. https://doi.org/10.1016/J.CTCP.2017.09.008

Lozano, M. T. U., Haro, F. B., Ruggiero, A., & Mendez, J. A. J. (2017). Systems of digitalization and processing of anatomical pieces for their three-dimensional reconstruction. *Proceedings of the 5th International Conference on Technological Ecosystems for Enhancing Multiculturality - TEEM 2017*, 1–5. https://doi.org/10.1145/3144826.3145402

Lunsford, C., Grindle, G., Salatin, B., & Dicianno, B. E. (2016). Innovations With 3-Dimensional Printing in Physical Medicine and Rehabilitation: A Review of the Literature. In *PM and R* (Vol. 8, Issue 12, pp. 1201–1212). Elsevier Inc. https://doi.org/10.1016/j.pmrj.2016.07.003

management, U. R.-P. research and clinical, & 2003, undefined. (n.d.). *The history of electrical stimulation of the nervous system for the control of pain*.

Martín, J. M. R. (2014). *Electroterapia en fisioterapia*. Médica Panamericana. https://books.google.es/books?hl=en&lr=&id=TMR-DzWvieMC&oi=fnd&pg=PA17&dq=Rodríguez+Martín,+J.+M.,+Electroterapia+en+fisioterapia.+Editorial+Médica+Panamericana,+2014.&ots=z5bqoyeBU8&sig=RBsR9BawzcTgGx3ObCL_GxVBA48&redir_esc=y#v=onepage&q&f=false

Mcauliffe, P., Kim, J. H., Diamond, D., Lau, K. T., & O'Connell, B. C. (2015). A sleep bruxism detection system based on sensors in a splint - pilot clinical data. *Journal of Oral Rehabilitation*. https://doi.org/10.1111/joor.12223

Melchels, Marco, Klein, Travis, P., & Hutmacher, &. (2012). Additive manufacturing of tissues and organs. *Elsevier*. https://doi.org/10.1016/j.progpolymsci.2011.11.007

Miravete, A., disseny, L. C.-T. de, & 2002, undefined. (n.d.). Materiales compuestos. *Raco.Cat*. Retrieved April 27, 2020, from https://www.raco.cat/index.php/Temes/article/view/29774

Mitragotri, S. (2005). Healing sound: The use of ultrasound in drug delivery and other therapeutic applications. *Nature Reviews Drug Discovery*. https://doi.org/10.1038/nrd1662

Moein, H., Jhalli, R., Blaber, A. P., Claydon, V. E., & Menon, C. (2017). Evaluating the efficacy of an active compression brace on orthostatic cardiovascular responses. *PLOS ONE*, *12*(11), e0187885. https://doi.org/10.1371/JOURNAL.PONE.0187885

Montesdeoca, N., Lechosa, E., Haro, F. B., D'Amato, R., & Juanes, J. A. (2019). Design of thermoplastic oral appliance with mouth opening control to treat obstructive sleep apnea. *ACM International Conference Proceeding Series*, 404–410. https://doi.org/10.1145/3362789.3362864

Moriyama, Y., Nguyen, J., Akens, M., Moriyama, E. H., & Lilge, L. (2009). In vivo effects of low level laser therapy on inducible nitric oxide synthase. *Lasers in Surgery and Medicine*. https://doi.org/10.1002/lsm.20745

Mulford, J. S., Babazadeh, S., & Mackay, N. (2016). Three-dimensional printing in orthopaedic surgery: review of current and future applications. In *ANZ journal of surgery* (Vol. 86, Issue 9, pp. 648–653). Blackwell Publishing. https://doi.org/10.1111/ans.13533

Neeter, C., Thomee, R., Silbernagel, K. G., Thomee, P., & Karlsson, J. (2003). Iontophoresis with or without dexamethazone in the treatment of acute Achilles tendon pain. *Scandinavian Journal of Medicine and Science in Sports*, *13*(6), 376–382. https://doi.org/10.1046/j.1600-0838.2003.00305.x

Ng, G. Y. F., & Fung, D. T. C. (2008). The combined treatment effects of therapeutic laser and exercise on tendon repair. *Photomedicine and Laser Surgery*. https://doi.org/10.1089/pho.2007.2145

P Fitzpatrick, A. (2017). Design of a Patient Specific, 3D printed Arm Cast. *KnE Engineering*, *2*(2), 135. https://doi.org/10.18502/keg.v2i2.607

Patašius, M., Marozas, V., Jegelevičius, D., & Lukoševičius, A. (2016). Data Exploration for Hematoma Image Analysis. In *BIOMEDICAL ENGINEERING 2016* (Vol. 19, Issue 1). http://biomed.ktu.lt/index.php/BME/article/view/2481

Reddy, G. K., Stehno-Bittel, L., & Enwemeka, C. S. (1998). Laser photostimulation of collagen production in healing rabbit Achilles tendons. *Lasers in Surgery and Medicine*. https://doi.org/10.1002/(SICI)1096-9101(1998)22:5<281::AID-LSM4>3.0.CO;2-L

Rigby, J. H., Mortensen, B. B., & Draper, D. O. (2015). Wireless versus wired iontophoresis for treating patellar tendinopathy: A randomized clinical trial. *Journal of Athletic Training*, *50*(11), 1165–1173. https://doi.org/10.4085/1062-6050-50.11.04

Rigby, J. H., Taggart, R. M., Stratton, K. L., Lewis, G. K., & Draper, D. O. (2015). Intramuscular heating characteristics of multihour low-intensity therapeutic ultrasound. *Journal of Athletic Training*, *50*(11), 1158–1164. https://doi.org/10.4085/1062-6050-50.11.03

Robertson, V. J., & Baker, K. G. (2001). A Review of Therapeutic Ultrasound: Effectiveness Studies. *Physical Therapy*. https://doi.org/10.1093/ptj/81.7.1339

Robin, O., Claude, A., Gehin, C., Massot, B., & McAdams, E. (2020). Recording of bruxism events in sleeping humans at home with a smart instrumented splint. *Cranio - Journal of Craniomandibular Practice*. https://doi.org/10.1080/08869634.2019.1708608

Rosemffet, M. G., Schneeberger, E. E., Citera, G., Sgobba, M. E., Laiz, C., Schmulevich, H., Art??anuturry, P., Gagliardi, S., & Maldonado Cocco, J. A. (2004). Effects of Functional Electrostimulation on Pain, Muscular Strength, and Functional Capacity in Patients With Osteoarthritis of the Knee. *JCR: Journal of Clinical Rheumatology*, *10*(5), 246–249. https://doi.org/10.1097/01.rhu.0000141831.40350.91

Rundle, C. H., Wang, H., Yu, H., Chadwick, R. B., Davis, E. I., Wergedal, J. E., Lau, K. H. W., Mohan, S., Ryaby, J. T., & Baylink, D. J. (2006). Microarray analysis of gene expression during the inflammation and endochondral bone formation stages of rat femur fracture repair. *Bone*, *38*(4), 521–529. https://doi.org/10.1016/j.bone.2005.09.015

Salentijn, G. I. J., Oomen, P. E., Grajewski, M., & Verpoorte, E. (2017). Fused Deposition Modeling 3D Printing for (Bio)analytical Device Fabrication: Procedures, Materials, and Applications. *Analytical Chemistry*, *89*(13), 7053–7061. https://doi.org/10.1021/acs.analchem.7b00828

Schlereth, T., Drummond, P. D., & Birklein, F. (2014). Inflammation in CRPS: Role of the sympathetic supply. *Autonomic Neuroscience: Basic and Clinical*, *182*, 102–107. https://doi.org/10.1016/j.autneu.2013.12.011

Scholz, M., Blanchfield, J., Technology, L. B.-… S. and, & 2011, undefined. (n.d.). The use of composite materials in modern orthopaedic medicine and prosthetic devices: A review. *Elsevier*. Retrieved April 27, 2020, from https://www.sciencedirect.com/science/article/pii/S0266353811003071

Society, T. I., Document, C., Congress, X. V. I. I., Icl, X., Committee, E., Icl, X., Committee, I. S. L. E., Icl, X. X., Icl, X. X. I., Committee, E., Icl, X., Icl, X., Meetings, E. C., Icl, X., Icl, X. X. V, Francisco, S., Committee, E., & Society, T. (2017). The diagnosis and treatment of peripheral lymphedema: 2016 consensus document of the International Society of Lymphology. *Acta Angiologica*, *23*(4), 171–182.

Stasinopoulos, D. I., & Johnson, M. I. (2005). Effectiveness of low-level laser therapy for lateral elbow tendinopathy. In *Photomedicine and Laser Surgery* (Vol. 23, Issue 4, pp. 425–430). Mary Ann Liebert, Inc. 2 Madison Avenue Larchmont, NY 10538 USA . https://doi.org/10.1089/pho.2005.23.425

Ströberg, B. (1974). The Use of Thermography in Equine Orthopedics. *Veterinary Radiology*, *15*(1), 94–97. https://doi.org/10.1111/j.1740-8261.1974.tb00676.x

Tappa, K., & Jammalamadaka, U. (2018). Novel biomaterials used in medical 3D printing techniques. In *Journal of Functional Biomaterials*. https://doi.org/10.3390/jfb9010017

Taskaynatan, M. A., Ozgul, A., Ozdemir, A., Tan, A. K., & Kalyon, T. A. (2007). Effects of steroid iontophoresis and electrotherapy on bicipital tendonitis. *Journal of Musculoskeletal Pain*, *15*(4), 47–54. https://doi.org/10.1300/J094v15n04_06

TCS3472 COLOR LIGHT-TO-DIGITAL CONVERTER with IR FILTER. (n.d.). Retrieved April 30, 2020, from https://cdn-shop.adafruit.com/datasheets/TCS34725.pdf

Tell-Tale Color Changes: Camera Can Find Age of a Bruise | Features | Oct 2012 | BioPhotonics. (n.d.). Retrieved July 13, 2021, from https://www.photonics.com/Articles/TellTale_Color_Changes_Camera_Can_Find_Age_of_a/a52130

Tumilty, S., Munn, J., McDonough, S., Hurley, D. A., Basford, J. R., & Baxter, G. D. (2010). Low level laser treatment of tendinopathy: a systematic review with meta-analysis. In *Photomedicine and laser surgery* (Vol. 28, Issue 1, pp. 3–16). https://doi.org/10.1089/pho.2008.2470

Ugidos Lozano, M. T., Blaya Haro, F., Ruggiero, A., Manzoor, S., Nuere Menendez-Pidal, S., & Juanes Méndez, J. A. (2018). Different Digitalization Techniques for 3D Printing of Anatomical Pieces. *Journal of Medical Systems*, *42*(3), 46. https://doi.org/10.1007/s10916-018-0903-z

Ugidos Lozano, M. T., Haro, F. B., Ruggiero, A., Manzoor, S., & Juanes Méndez, J. A. (2019). Evaluation of the Applicability of 3d Models as Perceived by the Students of Health Sciences. *Journal of Medical Systems*, *43*(5), 108. https://doi.org/10.1007/s10916-019-1238-0

Valášek, P., D 'amato, R., Müller, M., & Ruggiero, A. (2018). Musa textilis Cellulose Fibres in Biocomposites – An Investigation of Mechanical Properties and Microstructure. *BioResources*, *13*(2), 3177–3194.

Vladescu, A., Braic, M., Azem, F., Titorencu, I., … V. B.-A. S., & 2015, undefined. (n.d.). Effect of the deposition temperature on corrosion resistance and biocompatibility of the hydroxyapatite coatings. *Elsevier*. Retrieved April 27, 2020, from https://www.sciencedirect.com/science/article/pii/S0169433215011770

Wang, L., Guo, T. Z., Wei, T., Li, W. W., Shi, X., Clark, J. D., & Kingery, W. S. (2016). Bisphosphonates Inhibit Pain, Bone Loss, and Inflammation in a Rat Tibia Fracture Model of Complex Regional Pain Syndrome. *Anesthesia and Analgesia*, *123*(4), 1033–1045. https://doi.org/10.1213/ANE.0000000000001518

Wei, Y., Yang, K., Browne, M., Bostan, L., & Worsley, P. (2019). Wearable Electrical Stimulation to Improve Lymphatic Function. *IEEE Sensors Letters*, *3*(2). https://doi.org/10.1109/LSENS.2019.2893478

YIN, Y., Zeng, Y., Chen, X., & Fan, Y. (2016). The internet of things in healthcare: An overview. In *Journal of Industrial Information Integration* (Vol. 1, pp. 3–13). Elsevier B.V. https://doi.org/10.1016/j.jii.2016.03.004

Zanella, A., Bui, N., Castellani, A., Vangelista, L., & Zorzi, M. (2014). Internet of things for smart cities. *IEEE Internet of Things Journal*, *1*(1), 22–32. https://doi.org/10.1109/JIOT.2014.2306328